Anion and Neutral Molecule Recognition by Electron Deficient Boranes

Rémi Tirfoin
St Cross College
Oxford
Hilary term 2015

A thesis submitted in partial fulfilment of the requirements for the degree of Doctor of Philosophy in Inorganic chemistry

DOCTOR OF PHILOSOPHY SCHOOL OF CHEMISTRY

DECLARATION OF AUTHORSHIP

Name: REMI ANTOINE CAMILLE TIRFOIN **Candidate number: 584224**

College: ST CROSS COLLEGE **Supervisor: PROF. SIMON ALDRIDGE**

Title of thesis: ANION AND NEUTRAL MOLECULE RECOGNITION BY ELECTRON DEFICIENT BORANES

Word count: ~ 60,500

Please tick to confirm the following:

I have read and understood the University's disciplinary regulations concerning conduct in examinations and, in particular, the regulations on plagiarism (*Essential Information for Students. The Proctors' and Assessor's Memorandum*, Section 9.6; also available at www.admin.ox.ac.uk/proctors/info/pam/section9.shtml). ☐

I have read and understood the Education Committee's information and guidance on academic good practice and plagiarism at www.admin.ox.ac.uk/edc/goodpractice. ☐

The thesis I am submitting is entirely my own work except where otherwise indicated. ☐

It has not been submitted, either partially or in full, for another Honour School or qualification of this University (except where the Special Regulations for the subject permit this), or for a qualification at any other institution. ☐

I have clearly indicated the presence of all material I have quoted from other sources, including any diagrams, charts, tables or graphs. ☐

I have clearly indicated the presence of all paraphrased material with appropriate references. ☐

I have acknowledged appropriately any assistance I have received in addition to that provided by my supervisor. ☐

I have not copied from the work of any other candidate. ☐

I have not used the services of any agency providing specimen, model or ghostwritten work in the preparation of this thesis. (See: http://www.admin.ox.ac.uk/statutes/352-051a.shtml#_Toc28142348.) ☐

I agree to retain an electronic copy of this work until the publication of my final examination result, except where submission in hand-written format is permitted. ☐

I agree to make any such electronic copy available to the examiners should it be necessary to confirm my word count or to check for plagiarism. ☐

Candidate's signature: …….. Date: ……..

Acknowledgements

First and foremost, I would like to thank my supervisor Prof. Simon Aldridge for the endless hours he has dedicated to mentoring and supporting me in my research. Always full of enthusiasm, advice and encouragement; he made this experience rich and exciting and for that I am eternally grateful.

I am very grateful to all the members of the Aldridge group past and present, for making these past few years memorable. In particular, my gratitude goes to Mr. Joseph Abdalla, Dr. Mike Kelly, Dr. Nicholas Phillips, Dr. Ian Riddlestone, and Dr. Josh Bates for their contributions and hours of helpful discussion. Valuable contributions to the discussion were made by past Part IIs from the group; Ms. Jessica Gilbert and Ms. Gaya Sri Navaneetha.

Many thanks go out to Dr. Amber Thompson and Dr. Richard Cooper for teaching me the secrets of X-ray crystallography, with the help of Dr. Mike Kelly, Dr. Ian Riddlestone and Dr. Nicholas Phillips. The collection and processing of Raman data was very kindly performed by Dr. Narayana Sirimuthu from the University of Strathclyde in Glasgow.

Thank you to Mr Joseph Abdalla, who conducted all the DFT calculations of my complexes with the support of Prof. John McGrady.

Thanks to all my friends in Oxford who made this experience so British. In particular I would like to thank Tim, Sean, Tom, Matteo and Stuart. Thank you also to Neil, Sofia, Stephany, Achim, Andy, and all the members of the Wolfson College boat club.

Cette expérience en Angleterre n'aurait pas été possible aussi sans l'appui d'amis proche, Kevin, Fanny, Heni, Esther et Elias merci pour les virées dans Paris et votre soutien moral au cours de ces années. Un petit clin d'œil à Elodie mais aussi à mes amis de fac, de prépa et à mes camarades d'enfance retrouvés. Merci à tous d'avoir été là.

Enfin j'aimerais remercier toute ma famille, tout particulièrement ma mère, mon père et ma grand-mère pour leur soutien inconditionnel, mais aussi mon frère Guillaume et sa femme Andréa. Ils m'ont félicité pour mes réussites et m'ont toujours encouragé aux moments les plus durs. Je leurs dédie ce travail en témoignage de mon amour profond.

Abstract

This thesis reports on the synthesis of a series of Lewis acidic boranes used as detectors for the cyanide or fluoride ion, and for the activation of molecular oxygen.

Chapter III focuses on the formation of monodentate boranes featuring a pendant ferrocenyl moiety. A systematic study of the fluoride and cyanide binding capabilities of isomeric ferrocenyl-functionalized phenyl boranes was conducted *via* spectroscopic, crystallographic and voltammetric techniques. The synthesis of receptors supported by an indenyl scaffold was also investigated and the binding properties of such systems studied in details. All receptors proved to be competent at binding both cyanide and fluoride in dry solvents; moreover one such indenyl receptor can selectively bind cyanide in aqueous media and signal the binding event by a green-to-red colour change.

Chapter IV constitutes an extension of the previous chapter targeting bidentate receptors with an (indenyl)(cyclopentadienyl)iron(II) back bone. A principle objective was the development of systems offering the chelation of fluoride, and hence a measure of selectivity over the more strongly basic cyanide ion. While *bis*(dimesitylborane) receptors proved to be synthetically inaccessible, a series of phosphine- and phosphonium-borane species was prepared and their comparative F^-/CN^- binding abilities determined.. Thus, while cationic phosphonium boranes favour fluoride binding by employing a bifunctional binding motif, the neutral phosphine boranes exclusively bind cyanide.

Chapter V details the activation of molecular oxygen by pentafluorophenyl-boranes in presence of weak reductants featuring a ferrocene unit. The highly Lewis acidic ferrocenyl bis(pentafluorophenyl)borane was initially studied, and its reaction with dry dioxygen shown to generate a (fully characterized) ferrocenium peroxoborate. Similar reactivity was observed for simple metallocenes such as cobaltocene and ferrocene (or even organic reductants) in presence of a strong Lewis acid, with the trapping of the O_2^{2-} ion by the borane thought to be a key thermodynamic driving force for the O_2 reduction.

Abreviations

K	binding constant
Ant	anthracene
aq.	aqueous
B3LYP	Becke-3 Lee-Yang Parr
b	broad
calc.	calculated
CT	Charge Transfer
CV	cyclic voltammetry
d	doublet
δ	NMR chemical shift
DCM	dichloromethane
DFT	density functional theory
DMAP	4-(N,N-dimethylamino)pyridine
DMSO	dimethylsulfoxide
DNA	Deoxyribonucleic Acid
EI	Electron Impact
ESI	electrospray ionisation
f	oscillator
FIA	Fluoride Ion Affinity
g	gram
h	hour
HOMO	Highest occupied molecular orbital
J	coupling constant
λ	wavelength
LC	ligand centred
LLCT	ligand-ligand charge transfer
lp	Lone Pair
LUMO	Lowest Unoccupied Molecular Orbital
m	multiplet
Me	methyl
meas.	measured

Mes	mesityl
mg	milligram
mL	millilitre
MLCT	metal-ligand charge transfer
MS	mass spectrometry
Naph	naphthalene
NBO	natural bond order
nm	nanometre
NMR	nuclear magnetic resonance
OTf	trifluoro methylsulfonate
PET	photoinduced electron transfer
Ph	phenyl
ppb	parts per billion
ppm	parts per million
s	singlet
TBACN	tetrabutylammonium cyanide
TBAF	tetrabutylammonium fluoride
TD-DFT	time dependent density functional theory
thf	tetrahydrofuran
TSAF	tris(dimethylamino)sulfonium difluorotrimethylsilicate
UV-Vis	Ultraviolet-visible light spectroscopy
VdW	Van der Waals

List of Publications

(1) Remi Tirfoin and Simon Aldridge, *Dalton Transactions,* **2015**, (submitted).

(2) Remi Tirfoin, Gayathri Srinavaneetha, Joseph A. B. Abdalla, and Simon Aldridge, *Chemistry - A European Journal,* **2015**, (submitted).

(3) Remi Tirfoin, Jessica Gilbert, Gregory Wildgoose, Narayana Sirimuthu and Simon Aldridge, *Inorganic chemistry,* **2015**, (submitted).

(4) Michael J. Kelly, Jessica Gilbert, Remi Tirfoin and Simon Aldridge, *Angewandte Chemie, International Edition*, **2013**, 52, 14094.

(5) Michael J. Kelly, Remi Tirfoin, Jessica Gilbert and Simon Aldridge, *Journal of Organometallic Chemistry*, **2014**, 769, 11.

(6) Remi Tirfoin and Simon Aldridge, *Dalton Transactions,* **2013**, 42, 12836.

(7) Remi Tirfoin, Lise-Marie Chamoreau, Yanling Li, Benoit Fleury, Laurent Lisnard and Yves Journaux, *Dalton Transactions*, **2014**, 43, 16805. (Master of Science)

Crystallography contributions

(1) René Frank, James Howell, Remi Tirfoin, Stefan Zahn, D. Michael P. Mingos and Simon Aldridge, *Angewandte Chemie, International Edition*, **2015**, (*submitted*).

(2) Joseph A. B. Abdalla, Ian R. Riddlestone, Remi Tirfoin and Simon Aldridge, *Angewandte Chemie, International Edition*, **2015**, 54, (*published*).

(3) Joseph A. B. Abdalla, Ian M. Riddlestone, Joshua Turner, Paul A. Kaufman, Remi Tirfoin, Nicholas Phillips and Simon Aldridge, *Chemistry - A European Journal*, **2014**, 20, 17624.

(4) Nicholas Phillips, Tristan Dodson, Remi Tirfoin, Joshua I. Bates and Simon Aldridge, *Chemistry - A European Journal*, **2014**, 20, 16721.

(5) Rene Frank, James Howell, Remi Tirfoin, Deepak Dange, Cameron Jones, D. Michael P. Mingos and Simon Aldridge, *Journal of the American Chemical Society*, **2014**, 136, 15730.

(6) Nicholas Phillips, Remi Tirfoin and Simon Aldridge, *Dalton Transactions*, **2014**, 43, 15279.

(7) Nicholas Phillips, Lucinda Treasure, Nicholas H. Rees, Remi Tirfoin, John E. McGrady, Simon Aldridge, *European Journal of Inorganic Chemistry*, **2014**, 2014, 4877.

(8) Nicholas Phillips, Christina Y. Tang, Remi Tirfoin, Michael J. Kelly, Amber L. Thompson, Matthias J. Gutmann and Simon Aldridge, *Dalton Transactions*, **2014**, 43, 12288.

(9) Nicholas Phillips, Remi Tirfoin and Simon Aldridge, *Chemistry - A European Journal*, **2014**, 20, 3825.

(10) Andrey V. Protchenko, Deepak Dange, Jeffrey R. Harmer, Christina Y. Tang, Andrew D. Schwarz, Michael J. Kelly, Nicholas Phillips, Remi Tirfoin, Krishna Hassomal Birjkumar, Cameron Jones, Nikolas Kaltsoyannis, Philip Mountford and Simon Aldridge, *Nature Chemistry*, **2014**, 6, 315.

(11) Joshua Turner, Joseph A. B.; Abdalla, Joshua I. Bates, Remi Tirfoin, Michael J. Kelly, Nicholas Phillips, Simon Aldridge, *Chemical Science*, **2013**, 4, 4245.

(12) Joseph A. B. Abdalla, Ian M.Riddlestone, Remi Tirfoin, Nicholas Phillips, Joshua I. Bates and Simon Aldridge, *Chemical Communications*, **2013**, 49, 5547.

Contents

CHAPTER 1: Introduction

The term 'anion' was coined by the English physicist and chemist Michael Faraday in 1834, when he observed unknown entities attracted by the anode in electrochemical experiments.[1] This empirical observation, followed by other scientific discoveries, revealed that anions are ubiquitous in our environment. Over the course of natural evolution, anions have become critical for a huge number of biochemical systems; the recognition, transport, and/or transformation of ions are key reactions for any metabolic pathway. For instance, the genetic mutations leading to cystic fibrosis cause an alteration of the CFTR chloride transport channel; in simple terms chloride, iodide and thiocyanate ions cannot cross the cytoplasmic membrane, causing chronic disability and reduced life expectancy.[2] Furthermore, human activities have skewed the balance of natural occurrence, and introduced new anions into the environment. Many anthropogenic anions represent major hazards for public health; these include pertechnetate, from nuclear fuel reprocessing, phosphate and nitrate from agriculture, chloride from road salts, fluoride from pesticides and dental products, cyanide from mining activities, *etc*.

The threat posed to the public health is a major driving force behind the design of receptors for the selective detection and reporting of anions, leading to a prolific field of research.[3] Within this field, certain characteristics must be considered carefully in order to design an effective sensor for a target analyte. Anions have a large range of geometries and size (Figure 1.1), for instance halides ions are spherical, azide and cyanide ions are linear, whereas carbonate and sulphate ions are respectively trigonal planar and tetrahedral.[3] Anions are also susceptible to pH, *i.e.* they can be protonated at low pH thus reducing their charge. The window of operation of a sensor must be compatible with its target anion, especially with protonated receptors.[3] Additionally, anions present relatively high hydration enthalpies (from -310 kJ mol^{-1} for the perchlorate anion to the sulphate anion with -1080 kJ mol^{-1}), and so the nature of the solvent also plays a key role.[4] When these factors are taken into account, the

design of a receptor can be optimised to enhance properties such as binding affinity and selectivity.

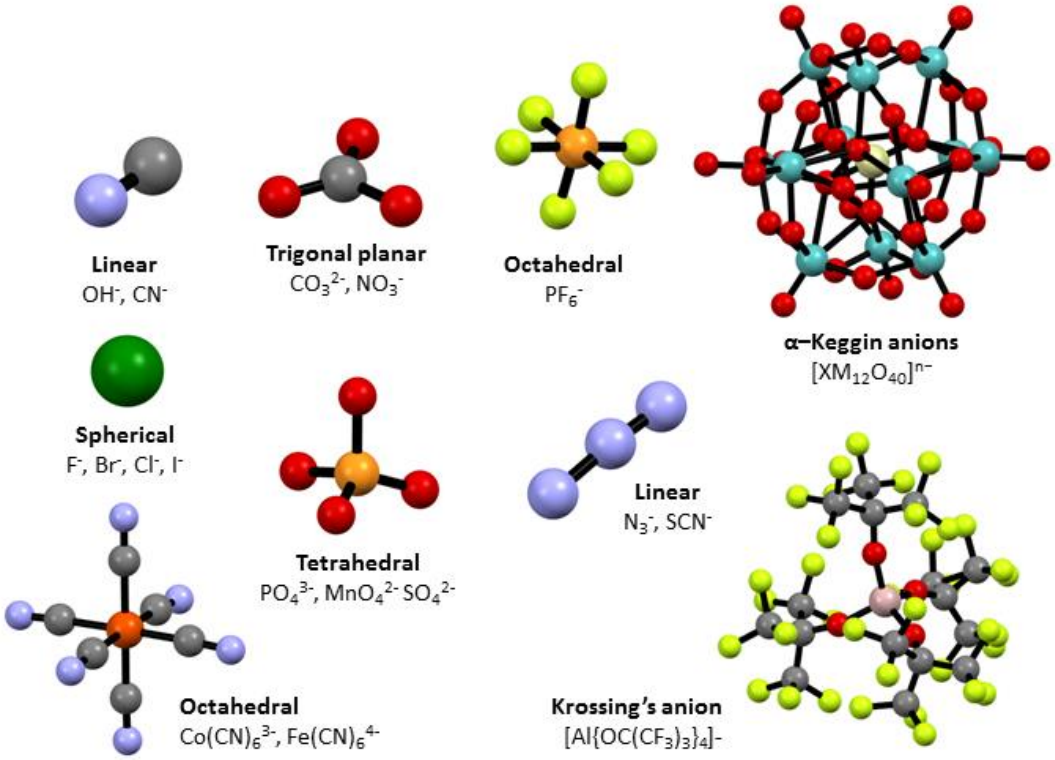

Figure 1.1: Selected anions of various charges, geometries and sizes.

Among others, the aqueous detection of fluoride and cyanide ions is of particular interest for industry in the control of waste effluent, and for government in the enforcement of environmental law. Fluoride is beneficial at low levels for dental hygiene,[5] and is the basis, therefore, of the government's programme of water fluoridation and the presence of fluoride in toothpaste. On the other hand, over exposure leads to skeletal fluorosis, a disease that is considered endemic by UNICEF and which affects tens of millions of people across 25 countries.[6] 4 mg L^{-1} of fluoride in drinking water is the current maximum contaminant level promulgated by the US Environmental Protection Agency.[7] One significant challenge for the aqueous detection of fluoride is its high hydration enthalpy ($\Delta H^{\ominus}_{\text{hydration}}$= -504 kJ mol^{-1}).[8] Cyanide, on the other hand, presents a higher level of toxicity, with an oral LD50 (lethal dose for 50 % of the sample) of only 3 mg kg^{-1} of body weight;[9] chronic exposure also leads to

nerve damage and thyroid problems.[10] The cyanide anion may be found in water from discharges from organic chemical production, iron and steel works and wastewater treatment facilities.[11] The use of nerve agents in the context of a terrorist threat or non-conventional warfare can be seen as another application for a cyanide and/or fluoride ion sensor. The G-series chemical warfare agents (CWAs) are organophosphonate nerve agents featuring a cyanide or fluoride group which is cleaved upon fixation with its target, the acetylcholine esterase enzyme.[12] Several variants have been synthesised (*e.g.* sarin, cyclosarin, tabun and soman), and differences in the group(s) bonded to the phosphorus centre lead to different physiochemical properties (*e.g.* vapour pressure, solubility, rate of hydrolysis, *etc.*) and to varying molecular geometries, both of which render detection challenging. Nonetheless, this group of CWAs each includes cyanide or fluoride as a leaving group that can be hydrolysed, thus offering a handle for detection. Herein are summarised two general approaches for the recognition of anions: the supramolecular approach and the Lewis acid strategy.

1.1. Supramolecular Chemistry: Beyond the Covalent Bond

Jean-Marie Lehn has defined supramolecular chemistry as the field that goes beyond molecular chemistry and its dependence on the covalent bond.[13] The main goal of supramolecular chemistry is to master the design of entities based mostly on intermolecular bonds, such as hydrogen bonding, halogen bonding, π-stacking, *etc.* Among the possible fields of application, anion recognition has yielded a large body of targeted supramolecular design, from molecular shuttles and machines to self-assembled cages.

A landmark in anion recognition is the work conducted by Simmon and Park at DuPont Central Research in the 1960's.[14] Their diazabicyclic systems that rely on two ammonium

units bridged by three alkyl chains have an affinity for chloride (K(Cl)= 4 M^{-1} in 50 % TFA solution). So while cation recognition founds its roots in the crown-ethers isolated by Pederson and the cryptands of Lehn, anion recognition was kick-started by Simmon and Park's contribution, which can be considered the first milestone of an extensive branch of supramolecular chemistry.[15]

1.1.1 Electrostatic Interactions

A large collection of receptors exploit the statement of the French physicist Coulomb: "*if two charged species have different sign, the electrostatic force between them is attractive*".[16] The magnitude of this force is directly proportional to the scalar multiplication of the charges and inversely proportional to the square of the distance between them. Several receptors based solely on electrostatics have been designed by maximising the positive charge and minimizing the distance between the receptor and the target anion.

A series of macrotricyclic ammonium receptors designed by Schmidtchen *et al.* are elegant examples of synthetic cationic hosts (Figure 1.2). Dipolar bonds positioned at the vertices of a tetrahedral cavity can form strong complexes with anions, and a certain level of selectivity can be achieved by the cavity size.[17] The formation of 1:1 host-guest complexes was observed by ^{1}H NMR, after the addition of an alkali metal halide to a solution of **1** or **2**.[17a-c] The stability constant for **1**·I suggests a strong interaction, consistent with the close contact observed in the crystal structure between the cationic vertices and the iodide ion.[17d] The larger intramolecular cavity in **2** can also accommodate the *p*-nitrophenolate ion which is too large to form complexes with receptor **1**. In order to counter-balance the positive charges of the tetrammonium **1** and **2,** the authors chose large partner anions (*e.g.* methyl *p*-toluenesulfonate, tetrafluoroborate or fluorosulfate), as a potential drawback is competition between the target iodide ion and the counter-anions associated with the "free" cage.[17a-b]

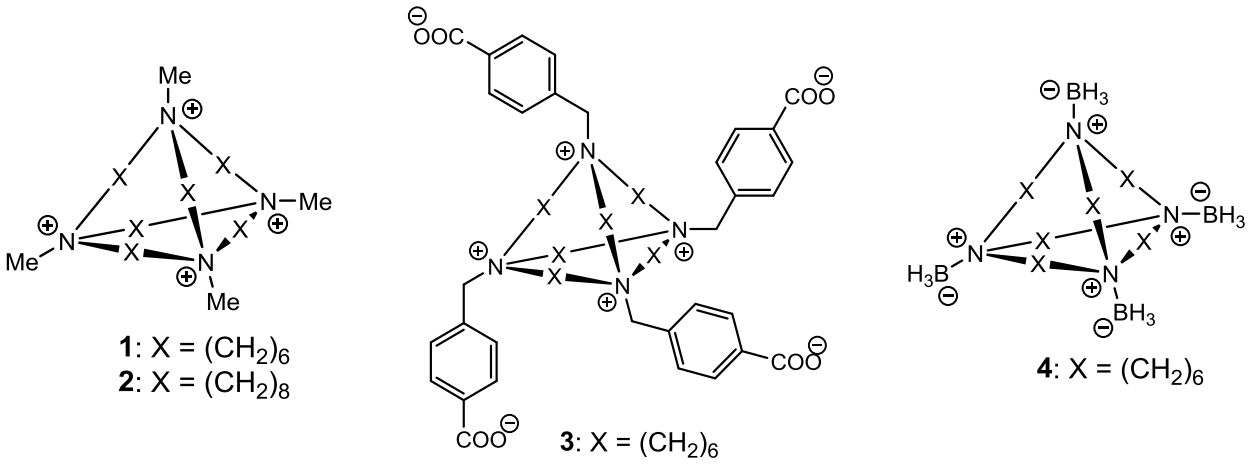

Figure 1.2: A series of cationic and zwitterionic macrocyclic quaternary ammonium cages reported by Schmidtchen and co-workers.[17]

To overcome this issue, Schmidtchen and co-workers subsequently synthesised zwitterionic cages such as **3** and **4**.[17e-f] As with the parent compounds, **3** and **4** form adducts with various anions, such as CN^-, Cl^-, Br^-, I^- and PF_6^-. However, through the use of ^1H NMR titrations, the authors demonstrated that zwitterionic **3** has stronger interactions with halides compared to formally tetra-cationic **1**.

On the same basis, Monzani designed a receptor that features a positively charged cavity suitable for anion detection.[18] The 1,3,5-trifunctionalised 2,4,6-trimethylbenzene core (**5**, Figure 1.3) with the three positive charges at its periphery, can fold onto the target anion, as shown by a molecular model of the adduct formed with chloride (Figure 1.3). Host **5** displays a high association constant with chloride in MeCN (K = 2.82(0.25) × 10^4 M^{-1}), however there is only a slight discrimination along the series $Cl^- > Br^- > I^-$.[18]

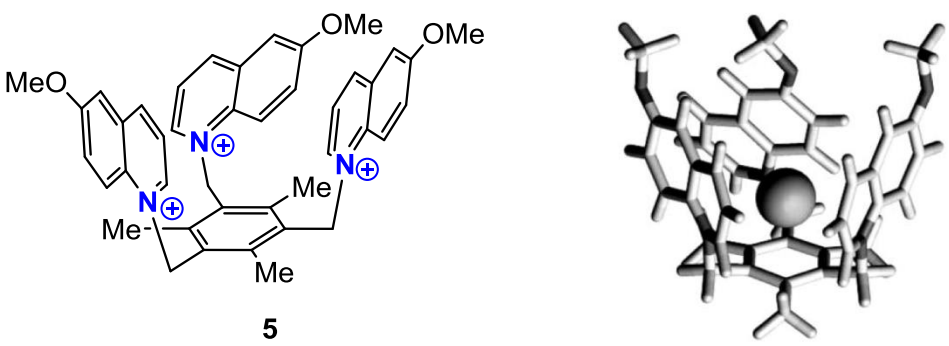

Figure 1.3: (left) Schematic representation of the free receptor **5** and (right) molecular model of the adduct [**5**·Cl]$^{2+}$ (reproduced from ref.18).

Anion recognition can also be achieved by weak interactions with the π-system of an electron deficient arene. Anion-π complexes involving halides have been widely modelled and a large collection of calculated structures for a variety of arenes has been reported in the literature (Figure 1.4).[19] In these structures, the halide is typically located directly over the centre of the arene ring along the pseudo C_6 symmetry axis. It has been established that this interaction is predominantly a non-covalent one, with affinities ranging from 41 to 83 kJ mol^{-1}, dominated by two components: (*i*) attraction between the negative charge of the anion and the electric field of the arene and (*ii*) anion-induced polarization.[20] Further studies have demonstrated that electron-deficient arenes can undergo charge transfer from the halide donor to the π–acceptor, as a result of displacing the halide from the centre to the periphery of the arene.[19]

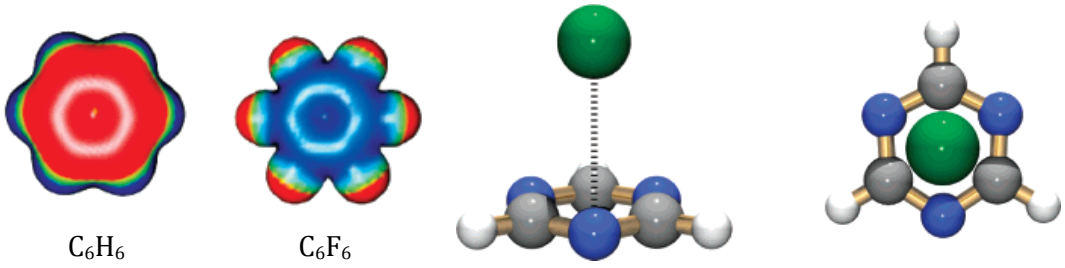

Figure 1.4: (*left*) Illustration of the electrostatic potential around C_6H_6 and C_6F_6 (calculated with Gaussian 03W, HF/3-21G* level[21]) (reproduced from ref. 19). (*right*) Initial theoretical observation of anion-π complexes occurred in a study of the interaction between Cl^- and triazine.

The one-pot syntheses of complexes **6** and **7** (*cf* Figure 1.5) reported by Dunbar *et al.* are textbook illustrations of applications of anion-π interactions.[22] These authors used 3,6-*bis*(2-pyridyl)-*s*-1,2,4,5-tetrazine and $[M(MeCN)_6]^{2+}$ (M = Ni, Co and Zn), with the counterion ($[BF_4]^-$ or $[SbF_6]^-$) as a template, in order to isolate a series of metallacyclophanes. In complex **6**, the fluoride of the tetrafluoroborate counterion engages in electrostatic interactions with the electron-deficient *s*-tetrazine component;[22a] in contrast the larger octahedral hexafluoroantimonate system yields the molecular pentagon **7**.[22b] Based on calculations

carried out by Garau and coworkers, the electrostatic binding contribution is estimated to be *ca.* -83 kJ mol^{-1} for one *s*-tetrazine molecule interacting with one fluoride ion.[23]

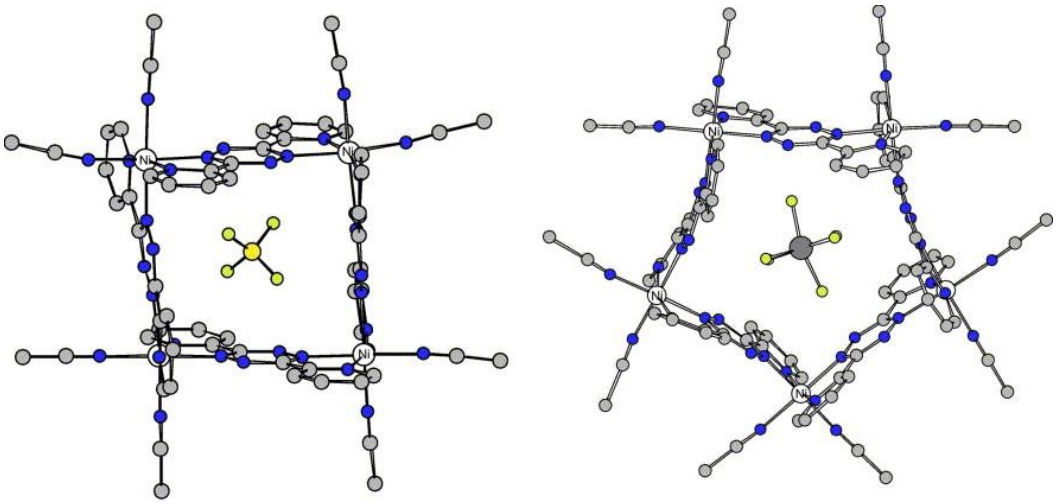

Figure 1.5: X-ray crystal structures of $[Ni_4(bptz)_4(CH_3CN)_8]^{8+}$ (**6**) with the encapsulated $[BF_4]^-$ ion (*left*) and $[Ni_5(bptz)_5(CH_3CN)_{10}]^{10+}$ (**7**) with the encapsulated $[SbF_6]^-$ ion (*right*) (reproduced from ref.23).

Electrostatic interactions have been widely used for the simple reason that they offer the advantage of being easily tuneable, and through clever assemblies a rudimentary screening of anions by size and/or shape is possible.[24] The intrinsic problem with Coulombic forces is their inherent lack of directionality, although in combination with other weaker forces (*e.g.* hydrogen or halogen bonding) it is possible to enhance the selectivity between species of the same charge and size.

1.1.2 Hydrogen Bonds

Like anions, hydrogen bonds are ubiquitous in Nature, and also play an important role in all living organisms, perhaps most obviously in the hydrogen bonds formed between the complementary purine (adenine and guanine) and pyrimidine (thymine and cytosine) bases that compose DNA. This property has been used to create nanoscale shapes and patterns by folding long strands of DNA like origami.[25] An undergraduate textbook will define hydrogen bonding as a X—H···Y system, where X and Y are electronegative elements and Y bears at least

one lone pair. The electrons from the lone pair are delocalised into the σ^* orbital of the X—H bond, thus weakening and lengthening the X—H bond.[26] Additionally the bond is strengthened due to some degree of charge transfer and electrostatic interaction, and is limited by exchange repulsion.[27,28]

Umeyama and Morokuma performed calculations to assess key parameters contributing to the association energies in hydrogen bonds.[28] As can be expected, these are a delicate balance between the nature of the atom in play, the geometries adopted and the environment. As with Coulombic forces, distance plays a major role as demonstrated by Kitaura and Morokuma. Considering the O—H···O interaction in H_2O_2 they calculated association energies of 54.0 kJ mol^{-1} and 27.7 kJ mol^{-1} for O···O distances of 2.78 Å and 3.18 Å respectively.[29] In addition, the angle of the X—H···Y unit is also crucial, as demonstrated by Dreyfus and Pullman in examining the N—H···OC moiety of peptide units and formamide dimers.[30] The total energy minimum is reached when the N—O—C angle is about 120°, although a large angular interval lies within 6.28 kJ mol^{-1} of the energetic minimum. This angle allows for maximum overlap between the σ^*(N—H) orbital and the HOMO of the C=O unit, a lone-pair with practically pure *p*-character perpendicular to the C=O bond. These parameters explain why the association energies for hydrogen bonds can range from virtually non-existent to very strong (*e.g.* 301 kJ mol^{-1} for FHI$^-$). For systems with X and Y = O or N, the usual range is between 13 and 63 kJ mol^{-1}.[27]

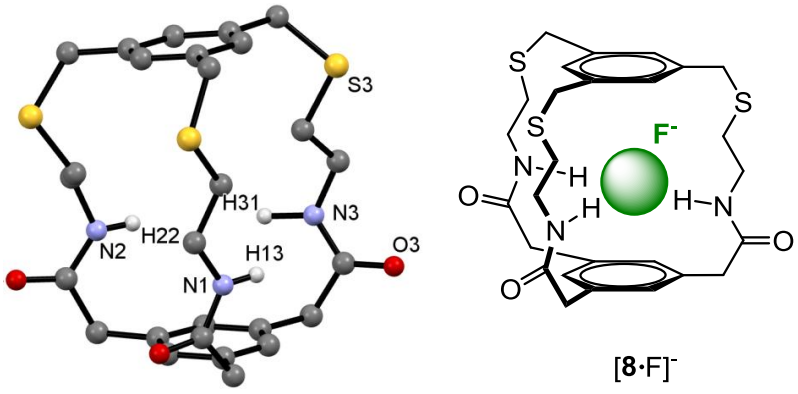

Figure 1.6: (*left*) Crystal structure of the free receptor **8**. (*right*) Schematic representation of the cyclophane **8** reported by Engbersen *et al.*[31]

The seminal research of Engbersen *et al.* is considered as introducing the first man-made receptors based solely on hydrogen-bonding.[31] These authors reported the synthesis of a cyclophane (**8**) bearing three amide groups oriented approximately inward towards the central cavity (Figure 1.6). The addition of tetrabutylammonium fluoride (TBAF) to a solution of the macrocycle was followed by ^{1}H and ^{19}F NMR spectroscopy suggesting that the fluoride anion is encapsulated within the void.

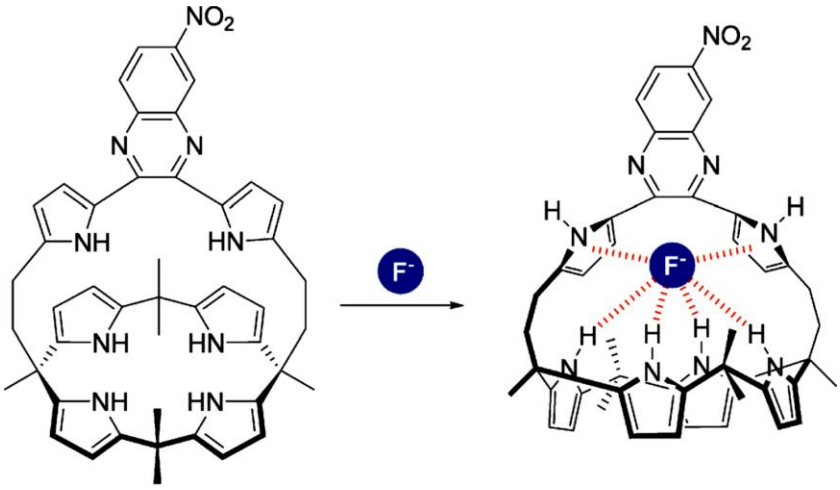

Figure 1.7: Schematic representation of the binding mode between receptor **9** and the F^- anion (reproduced from ref. 31).

Subsequent to this report, a large variety of macrocycles have followed, including work published by Sessler and co-workers involving a strapped calix-[4]-pyrrole.[32] The N—H bonds of the calix-[4]-pyrrole provide four accessible hydrogen bonds, and the pyrrole subunits on the strap potentially strengthen the anion association with some degree of anion-π interaction (Figure 1.7). The large shifts observed by ^{1}H NMR spectroscopy confirm this assessment, and the selectivity of the sensor for fluoride was additionally demonstrated by UV Vis titrations. Indeed, the binding constants for F^-, Cl^- and Br^- were estimated at 8.97×10^6 M^{-1}, 1.09×10^4 M^{-1} and 3.65×10^2 M^{-1} respectively, in a mixture of MeCN/DMSO (97:3). For comparison, the affinities of *meso*-octamethylcalix-[4]-pyrrole (*i.e.* **9** with no strap) for chloride and bromide are greater (1.02×10^5 M^{-1} and 1.05×10^3 M^{-1} respectively) but this system does not bind

fluoride under such conditions. This example demonstrates the importance of cooperative effects between weak forces; here the anion-π interaction and pre-organization provided by the strap seem to be a vital in the strong binding of the small fluoride anion.

Dreyfus and Pullman's calculations[30] demonstrated the importance of the X—H—Y angle between X—H···Y in hydrogen bonds, a good illustration of this effect comes from an amide-based cryptand developed by Bowman-James *et al.*[33] They report the synthesis of amide (**10**), isophthaloyl (**11**) and thioamide (**12**) based cryptands that can readily bind fluoride (Figure 1.8).

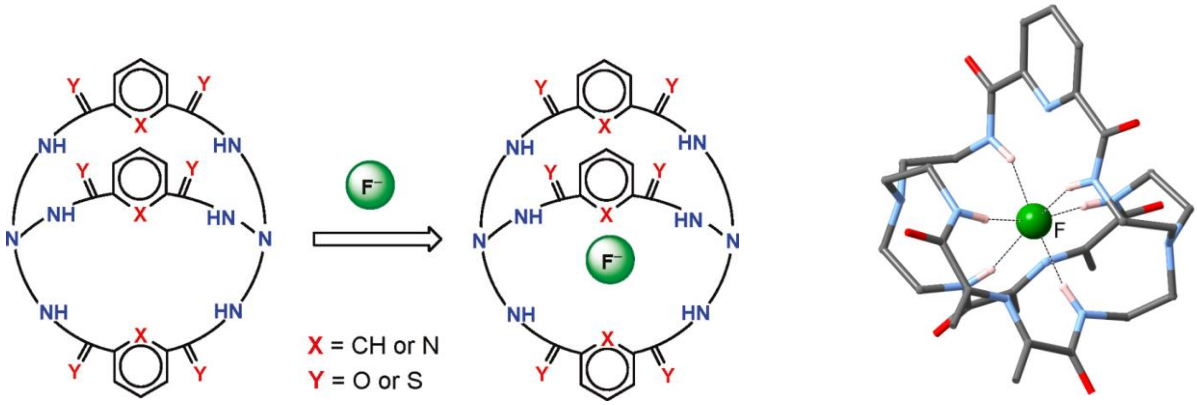

Figure 1.8: (left) Schematic representation of the association of **10** (X, Y = N, O), **11** (X, Y = CH, O) or **12** (X, Y = N, S) with fluoride (reproduced from ref.33) (right). X-ray crystal structure of the amide cryptand (**10**) with a fluoride ion encapsulated.

These authors monitored the addition of fluoride to the free receptors; all three give rise to similar shifts in the ^{1}H NMR spectrum, with a clear coupling also observed between the NH of the amide moiety and the fluoride (J_{HF} = 26 Hz for **10**). Moreover, in the ^{19}F NMR spectrum, the fluoride resonance shifts upfield from -96.7 ppm to -111.7 ppm and is observed as a septet, due to coupling with the six equivalent amide protons. Consistently, the crystal structure of [**10**·F]$^{-}$ pictured in Figure 1.8, reveals a fluoride atom encapsulated between six amides in a pseudo octahedral geometry. The N···F distances range from 2.822(2) to 2.889(2) Å and the N—F—N angle was on average 161°; similar values are observed in [**11**·F]$^{-}$. The geometry around the fluoride (*i.e.* close N···F contacts and angles approaching 180°) is almost

optimum for a strong hydrogen bonding, which then explains the high affinity of **10**-**12** for fluoride even in competitive solvents ($K_a \sim 10^4 - 10^5$ M^{-1} in DMSO).

The design of more complex architectures such as rotaxanes and catenanes, has also relied on weak interactions such as hydrogen bonding.[34] The Beer group has developed a large library of interlocked receptors for anions, such as [2]catenanes based on amides (**13**$^+$)[35] or triazoles (**14**$^+$)[36] (Figure 1.9).

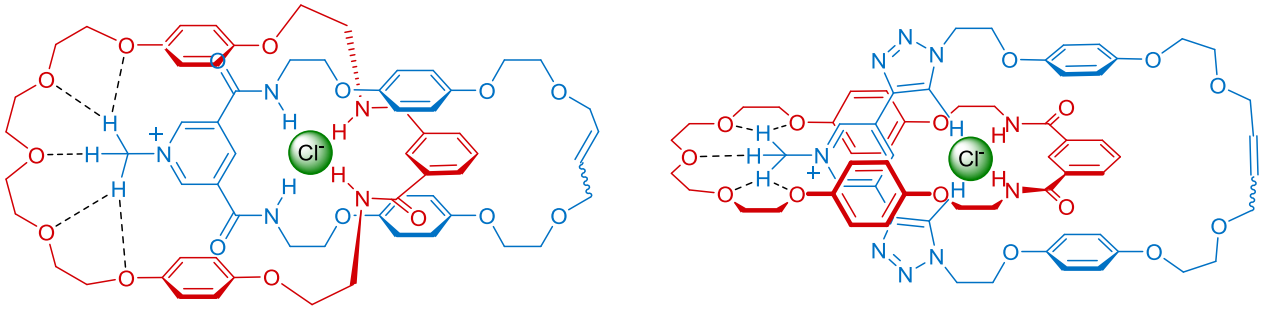

13·Cl **14**·Cl

Figure 1.9: Schematic representation of a chloride encapsulated in a amide-containing [2]-catenane (**13**$^+$)[35] or a triazole-containing [2]-catenane (**14**$^+$).[36]

Both systems were synthesised using the chloride anion as a template for a Grubbs'-catalyzed ring closing metathesis process. The interlocked structures are stabilized by several hydrogen bond interactions; for instance the chloride anion is in close contact with the amide or triazole cavity, additional stabilisation comes from the interaction between the pyridinium methyl group and the macrocycle polyether chain. The deshielding of the protons involved in hydrogen bonding can be monitored by ^{1}H NMR, with significant downfield shifts being observed for the triazole and amide signals.[35,36] The chloride ion can be removed by anion exchange, *e.g.* by washing several times with an aqueous solution of ammonium hexafluorophosphate, to yield the corresponding [**13**]PF_6 salt. The PF_6^- anion is too large to fit the cavity and leaves a free catenane specifically tailored for chloride (for **13**·PF_6:K_a = 730 M^{-1} for Cl^-; pyridinium thread precursor of **13**, K_a = 230 M^{-1} for Cl^-, both in d_4-MeOH/$CDCl_3$).[35]

Beer *et al.* also reported a [2]rotaxane with three anchor points, forming a complementary binding site design for the trigonal planar nitrate anion between the interlocked components.[37] This example demonstrates the versatile use of hydrogen bonding in supramolecular structures.

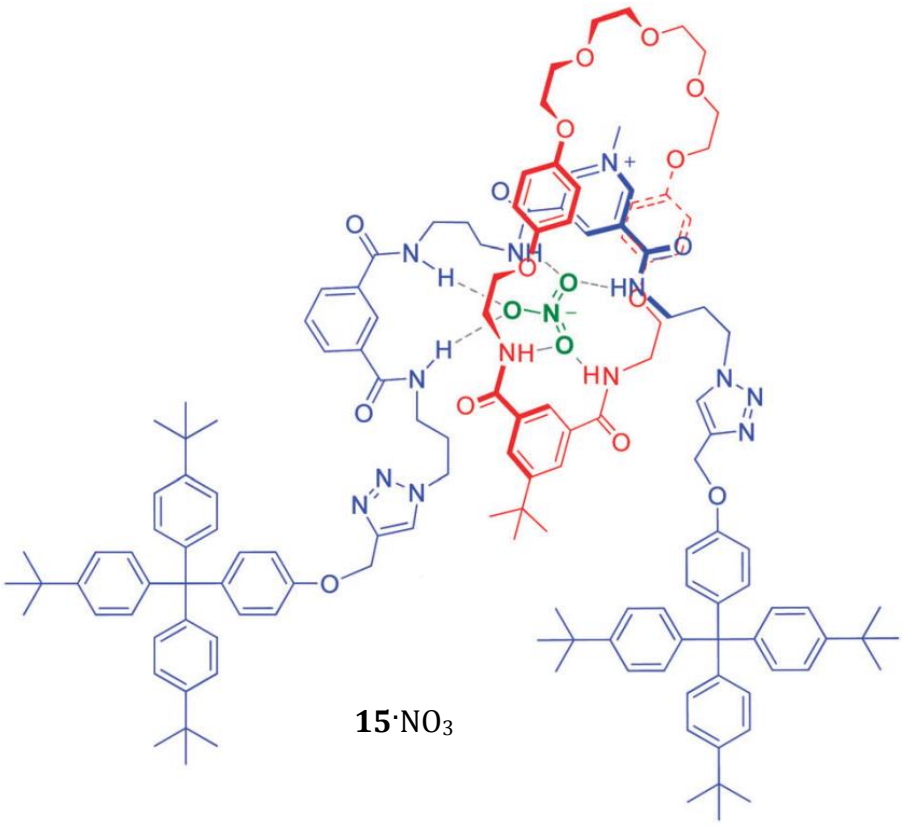

15·NO_3

Figure 1.10: Representation of a nitrate templated [2]rotaxane (**15**), with two hydrogen bonding recognition sites in the axle and one in the macrocycle (reproduced from ref. 37).

1.1.3 Halogen Bonds

Another weak interaction making a breakthrough in the field of anion recognition is halogen bonding. Hassel and Romming documented the existence of halogen bonding, by compiling crystallographic data on several halogen-bonded complexes featuring both inorganic and organic donors, *e.g.* chains of alternating halogens with either 1,4-dioxane molecules or acetone.[38] Moreover, under certain conditions halogen bonding can be competitive with hydrogen bonding in solution, as demonstrated by NMR studies conducted

by Sandorfy *et al.*[39] In addition, Murray-Rust and co-workers shed light on an interesting feature of halogen bonding in the solid state: for C—X bonds (where X = Cl, Br or I) electrophiles generally tend to approach the halogen perpendicular to the C—X bond or as they called "side-on". When it comes to nucleophiles the approach is along the C—X axis or "head-on".[40]

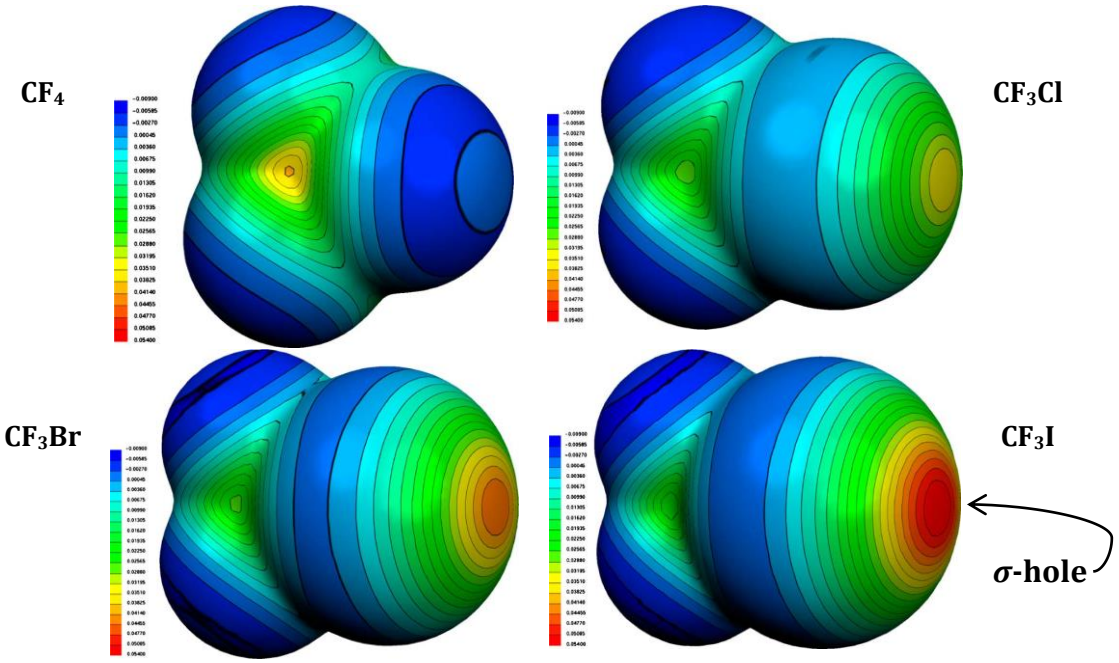

Figure 1.11: The molecular electrostatic potential, in Hartrees, at the 0.001 electrons Bohr^{-3} isodensity surface of CF_4, CF_3Cl, CF_3Br and CF_3I (reproduced from ref. 42b).

The electronic nature of halogen bonding was first postulated by Politzer[41] and further developments were illuminated by collaboration with Clark.[42] In a seminal paper, these authors used molecular electrostatic potentials (MEPs) to compare the electronic distribution on the molecular surface of CH_3X and CX_4 (X= F, Cl and Br). This work highlights the anisotropic distribution of the charge on the halogen in CH_3X where X is Br or Cl, *i.e.* the tip of the halogen is significantly more positively polarised than the side.[41]

Clark *et al.* also carried out further molecular electrostatic potential calculations on CF_3X (X= F, Cl, Br and I), and the results are shown in Figure 1.11.[42b] The outermost portion of the C—X bond gets more positive and large as the size of the halogen increases; the authors

termed this region the σ-hole (Figure 1.11). From the natural bond order (NBO) population analysis, they extrapolated the origin of the σ-hole; for instance, in CF_3Br the electronic configuration of the bromine atom is $[Ar]4s^2\ 4p_x^2 4p_y^2 4p_z^1$. The electron in the half filled p_z-orbital is involved in the F_3C—Br bond; that particular bond is strongly polarised and hence the electronic density in the outer lobe of the $4p_z$ will be depleted generating the σ-hole. An increase in the positive electrostatic potential is directly related to the polarizability of the atom bearing the σ-hole, together with the electron withdrawing properties of the rest of the molecule.[42c]

In the past decade the interest in halogen bonding has expanded, notably in molecular recognition, medicinal chemistry and catalysis.[43] The Beer group have been forerunners in anion recognition using halogen bonding, publishing the first macrocyclic halo-imidazolium receptor (Figure 1.12). Receptors **16** (X= Br) and **17** (X = I) can bind bromide with association constants of 2.88×10^4 M^{-1} and 9.55×10^5 M^{-1} respectively in MeOH/Water (9:1).[44]

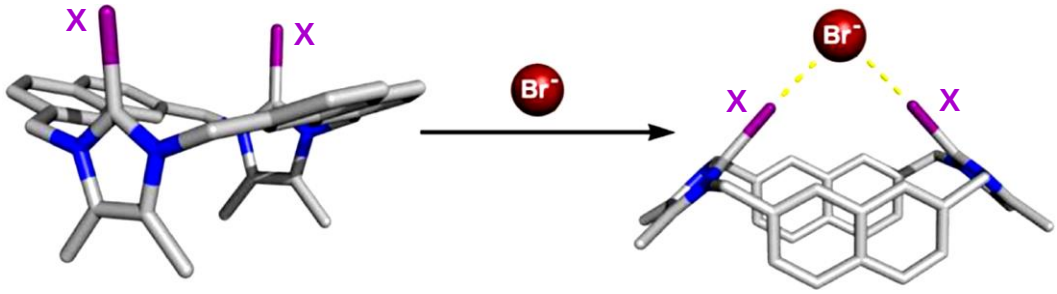

Figure 1.12: Representation of **16** (X = Br) and **17** (X = I) the halogen-bonding binding mode in solution (stoichiometry 1:1) (reproduced from ref. 44).

Beer and co-workers also published the first [2]-rotaxane (**18**) for anion sensing solely based on halogen bonding.[45] The axle and the macrocycle contain, respectively, two iodotrizoliums and two iodotriazoles (Figure 1.13) that can recognise chloride, bromide and iodide in aqueous media. The strength of the halogen bonding on the axle is enhanced by the presence of the triazolium unit which carries a positive charge. The crystal structure shown in Figure 1.13 reveals the strong interaction between one of the chloride anions and three

halogen bond donors. Moreover the "free" receptor **18**·2PF_6 can bind the halogens Cl^-, Br^- and I^- with the respective binding constants 513 M^{-1}, 5.7 × 10^3 M^{-1} and 2.4 × 10^4 M^{-1}.[45]

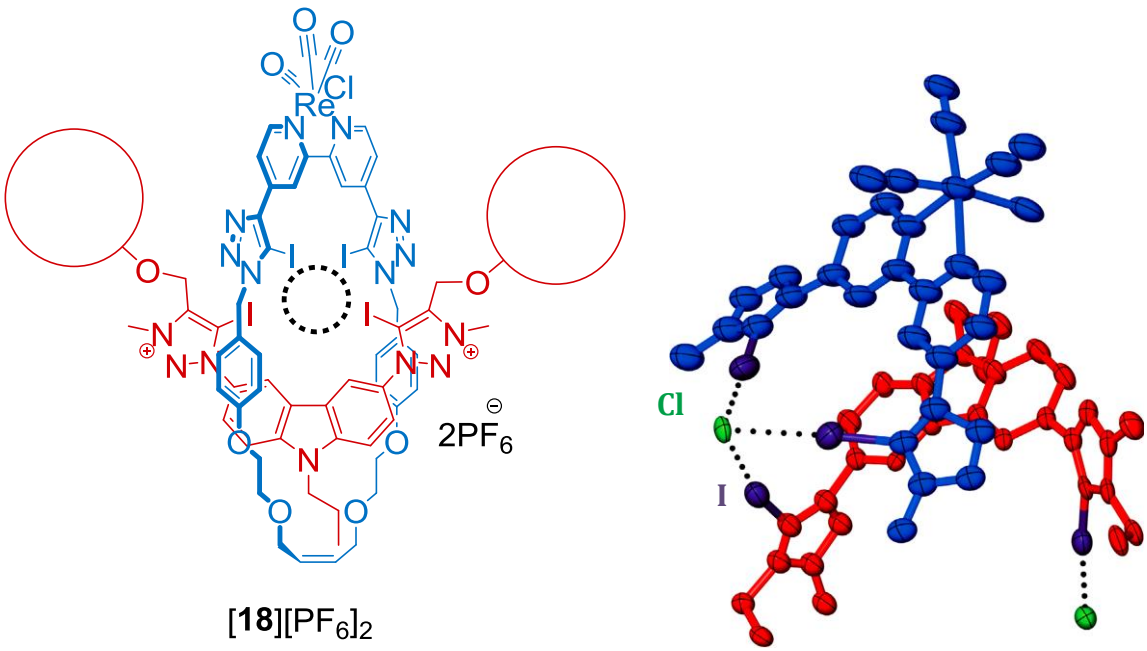

Figure 1.13: (left) Schematic representation of the [2]-rotaxane **18**·2PF_6, with the free cavity highlighted (dashed line) and the terphenyl stopper symbolised by red circles; (left) close-up of the receptor portions of the single-crystal structure of **18**·2Cl. Thermal ellipsoids are displayed at 30% probability and the hydrogen atoms are omitted for clarity (reproduced from ref. 45).

The design of receptors solely using supramolecular forces such as electrostatics, and/or hydrogen or halogen bonding, proves to be challenging in terms of selectively distinguishing one anion over others. One limitation of the supramolecular approach is the delicate balance between binding capabilities and selectivity; that is, maximising favourable interactions usually means more flexibility of the host at the cost of selectivity.

1.2. Anion Recognition: Lewis Acid-based Receptors

An alternative bonding interaction of use in anion recognition is the direct coordination of the anion to a Lewis acid. A Lewis base with an electron pair in its HOMO of

correct symmetry to overlap with the LUMO of a Lewis acid will usually form an adduct (provided steric hindrance does not dictate otherwise).[46] The large range of Lewis acid sources available offers the possibility for the design of receptors with a wide variety of properties. Beyond the different geometries accessible, selectivity for the target anion by the Lewis acid can be tuned by following Pearson's hard-soft acid base theory.[47] Competitive pathways can be designed based on the nature of the acid and the base targeted, since hard acids tend to bind hard bases and soft acids tend to bind soft bases.[47] This feature, in combination with cryptand-like design can drastically enhance the selectivity of anion receptors for a specific target analyte.

1.2.1 Cationic Transition Metals

Late-*d* transition metal cations such as Cu(II), Hg(II) and Zn(II), can be used for binding certain anions.[48] In aqueous media this method can be considered more advantageous with respect to hydrogen bonds: water is a poor Lewis base but forms strong hydrogen bonds, so potential interference with anion recognition by a metal cation is reduced compared to the systems described in section 1.1.2.[49]

Copper(II) has been used in several systems for anion detection, for example in Krämer's dicopper(II) macrocyclic sensor tailored for cyanide recognition.[50] In addition Ugozzoli *et al.* have isolated the bis(tren)dicopper(II) cryptand **19** and carried out a series of anion titrations (Figure 1.14),[51] revealing a preference for linear anions (*e.g.* azide and thiocyanate) and the chloride anion, with binding constants ranging from 5×10^5 M^{-1} for the linear azide anion to 245 M^{-1} for the spherical iodide. The effect of anion size/shape on selectivity is apparently attenuated by variation in the Cu···Cu distance through adjustment of the torsion angle of the spacer. This property can be highlighted by examining the structures of [**19**·OH]$^{3+}$ and [**19**·μ-Br]$^{3+}$, for which the Cu···Cu distances are respectively 3.87 Å and 4.866

Å.[51,52] The same cryptand **19** was used by Chen and Wolowska to bind cyanide. From IR spectroscopy and single X-ray crystallography the authors confirmed the presence of a bridging cyanide between the two copper(II) centres.[53] It can be noted that the flexibility of **19** is further underlined by the Cu···Cu distance which is stretched to 4.995 Å in [**19**·μ-CN]$^{3+}$.[53a]

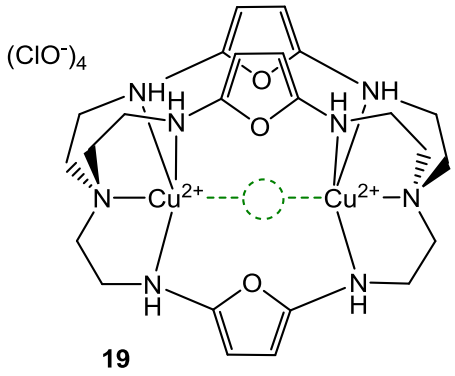

19

Anion	*K* in M^{-1}
N_3^-	$5.01(0.64) \times 10^4$
NCS^-	$1.9(0.12) \times 10^4$
F^-	1.580(70)
Cl^-	9550(430)
Br^-	1020(20)
I^-	246(12)

Figure 1.14: (*left*) Schematic diagram of the binding motif for the Cu(II) cryptate **19**[51,53] (*right*) binding constants of **19** for a series of halides in acid buffered solution (pH = 5.25).[51]

Hawthorne and co-workers offer an example of mercury-based recognition (Figure 1.15).[54] The macrocycle **24** consists of four cationic mercury(II) ions supported by four carboranes. The resulting tetramer **24** shown in Figure 1.15 was obtained only with mercury(II) *halide* precursors, while in absence of the templating halide (*e.g.* utilizing $Hg(OAc)_2$) the reaction yielded the trimeric macrocycle **23**.[55] The affinity of this system for halides can be monitored by $^{199}Hg\{^1H\}$ NMR spectroscopy: the resonance for the free sensor is found at -1230 ppm, which is shifted to -1184 ppm ($^1J_{HgF}$ = 698 Hz) with F^-, -1077 ppm with Cl^-, -1010 ppm with Br^- and -811 ppm with I^-.[54] The downfield shift of the ^{199}Hg signal increases as the halide becomes softer, and therefore as the magnitude of the interaction between the halide and the mercury centre increases. Moreover, the respective crystal structures provide insight into the interaction of the respective halides with the mercury centres. In Li[**24**·Br] the bromide ion sits in the centre of the macrocycle 0.95 Å above the least squares planes of the four Hg atoms,[54c] whereas the corresponding chloride deviates by 0.38 Å.[54b] On the other end, the fluoride adduct is perfectly aligned with the mercury plane,

but the carboranes alternate up and down.[54a] This torsional rotation of 82° allows the mercury centre to be drawn together to chelate the fluoride anion, with the Hg···Hg separations decreasing from an average 5.80 Å (for [**24**·Br]$^-$, [**24**·Cl]$^-$ and [**24**·I_2]$^{2-}$) to 5.309 Å and 5.114 Å for the encapsulated fluoride complex.

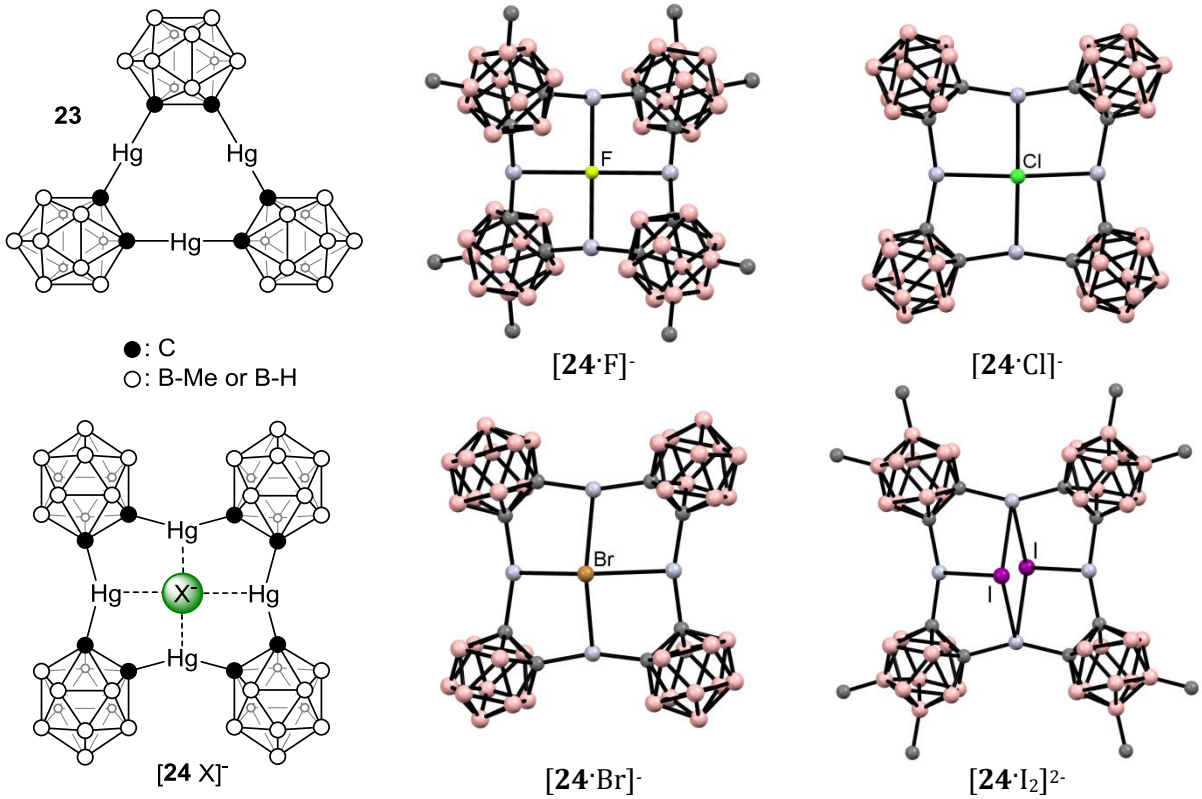

Figure 1.15: (*left*) Schematic representations of trimeric (**23**)[55] and tetrameric (**24**) mercuracaborands. (*right*) Structures of encapsulated halogen complexes: fluoride [NMe_4][**24**·F],[54a] chloride Li[**24**·Cl],[54b] bromide Li[**24**·Br][54c] and diiodide K_2[**24**·I_2].[54d] The counter-ions and solvate molecules have been omitted for clarity.

1.2.2 Lewis Acids from the Main Group (excluding Boron)

The *Octet Rule* outlined by Lewis-Langmuir has been a cornerstone of countless discussions on electronic structure, but has also stirred up significant debate on its validity, since initial publication in 1916.[56] Lewis observed that stable compounds are organised such that each atom has eight electrons in its valence shell. However, the list of exceptions to the rule has grown from the few examples already existing in Lewis' time. For instance PCl_5, SF_6 and IF_7 have individually five, six and seven pairs of electrons, and they are usually called

hypervalent. Early on, Pauling suggested a model, through a promotion of electrons into "low-lying" unfilled *d* orbitals, leading to a sp^3d hybridisation.[57] This model was disputed by several authors on the basis that the hybridisation process is *a priori* not energetically favoured according to calculations.[58] Moreover, suspicions were enhanced by the discovery of an increasing number of hypervalent species from the second row.[59] An alternative description *via* molecular orbital theory was presented by Robert Rundle[60] and George Pimentel:[61] a *3-centre-4-electron* (*i.e. 3c-4e*) molecular system.

The possibility for hypervalency in heavier Main Group elements has been widely exploited in anion recognition. Among the first examples were the cryptand-like tin macrocycles of Newcomb and co-workers.[62] These authors used different alkyl chains to bridge two or four tin centres, and followed halide binding by ^{119}Sn NMR spectroscopy. Similar cryptand systems were also isolated by Takeuchi *et al.* using germanium.[63]

Jurkschat *et al.* published a family of *ortho*-bis(halo-organostannyl)benzenes.[64] These "molecular tweezers" can easily chelate either chloride or fluoride between two tin centres. More recently Tamao *et al.* conducted a systematic binding study with related 1,2-disilyl benzenes (Figure 1.16).[65] Through ^{19}F NMR titrations and competitive binding experiments, the authors were able to estimate *K* for compounds **25** to **29**.

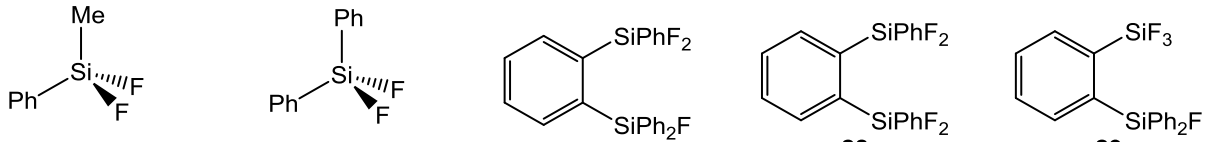

25 K= 2.00 x 10^3 M^{-1}, 291 K

26 K= 1.59 x 10^4 M^{-1}, 188 K

27 K= 6.30 x 10^5 M^{-1}, 183 K

28 K > 6.3 x 10^7 M^{-1}, 183 K

29 K > 10^9 M^{-1}, 193 K

Figure 1.16: Fluoride anion binding affinities of mono- and bifunctional silanes in d_6-acetone.

A general increase is observed from **25** to **29**, although most noticeably the binding affinity increases 40-fold from monodentate **26** (K= 1.59 × 10^4 M^{-1}) to bidentate **27** (K= 6.30 × 10^5 M^{-1}). This discrepancy is ascribed to the cooperative effect of the second silane in the *ortho* position, thus constituting a chelating binding domain (Figure 1.17). The incorporation

of the electron withdrawing fluorine atom in place of a phenyl ring at silicon increases the Lewis acidity of the silane, and has sweeping consequences on binding properties. From compound **27** bearing a difluoro(phenyl)silane the binding constant increases by at least 1500-fold for trifluorosilane (**29**) which has K_a in excess of 10^9 M^{-1}.

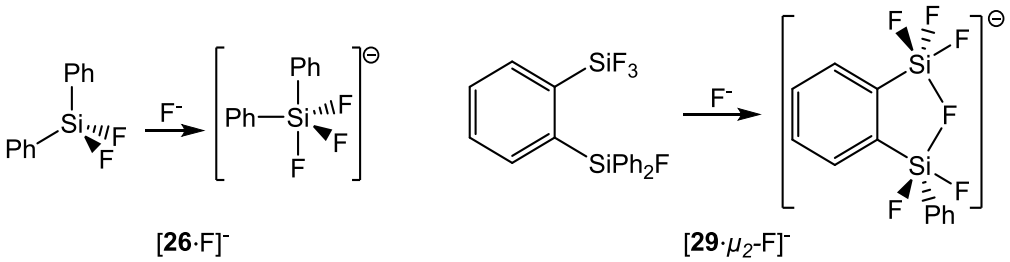

Figure 1.17: Schematic representation of fluoride binding by the monodentate silane **25** and the chelation of fluoride by bidentate silane **29**.

From another perspective, Lodeiro and coworkers have developed gallium(III) corrole systems, notably **30** and **31**, which can readily form a fluoride or cyanide adduct (Figure 1.18).[66] The Lewis acidity of gallium(III) is enhanced by its positioning in the middle of an extended π-conjugated system bearing several electron withdrawing groups (*e.g.* C_6F_5).

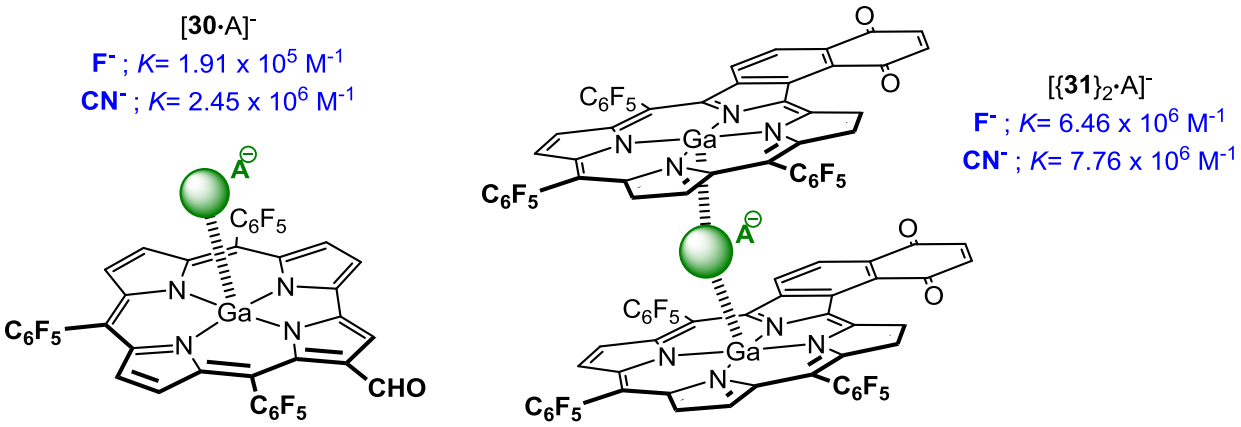

Figure 1.18: Postulated mode of interaction between the Ga(III) corrole complex **30** and **31** and the anion.

These authors carried out binding studies in toluene that highlight a number of interesting properties for **30** and **31**. A measurable spectroscopic response was observed on addition of the cyanide or fluoride ion, whereas titrations with the heavier halides did not seem to affect the free receptor. Additionally, the authors postulated a sensor/anion

stoichiometry of 1:1 for **30** and 2:1 for **31** (Figure 1.18). The fact that fluoride can easily be chelated between two gallium centres could account for the 34-fold increase in the binding constant. By contrast, the nitrogen atom of cyanide is a poor Lewis base, thus the association of **31**·CN^- with a second corrole system has little influence on the binding affinity (*c.f.* K= 2.45 × 10^6 M^{-1} for **30**; K= 7.76 × 10^6 M^{-1} for **31**).

Gabbaï's group have a long history in the design of sensors featuring Main Group elements, such as the pnictogen family.[67] This group started by assessing the binding capabilities of simple tetraphenylpnictonium cations (Pn: P, As and Sb) and demonstrated by UV-Vis or NMR titrations that only $[Ph_4Sb]^+$ was able to bind fluoride in acetonitrile (K_a > 10^6 M^{-1}). Lewis acidity rises as the group is descended (*i.e.* $[Ph_4P]^+$ ≈ $[Ph_4As]^+$ < $[Ph_4Sb]^+$), following increasing polarizability and electro-positivity from P to Sb.[67] The authors do not exclude steric effects, however, since as the element gets larger it should be easier to accommodate more ligands in its coordination sphere. Furthermore, according to DFT calculations, the fluoride affinity of $[Ph_4Sb]^+$ exceeds those of $[Ph_4P]^+$ (ΔFIA= +97 kJ mol^{-1}) and $[Ph_4As]^+$ (ΔFIA= +66.5 kJ mol^{-1}).[67] Elaborating on this study, Gabbaï *et al.* isolated the anthryltriphenyl-stibonium cation ([**32**]OTf) which incorporates the fluorescent anthracene reporter in place of a phenyl group.

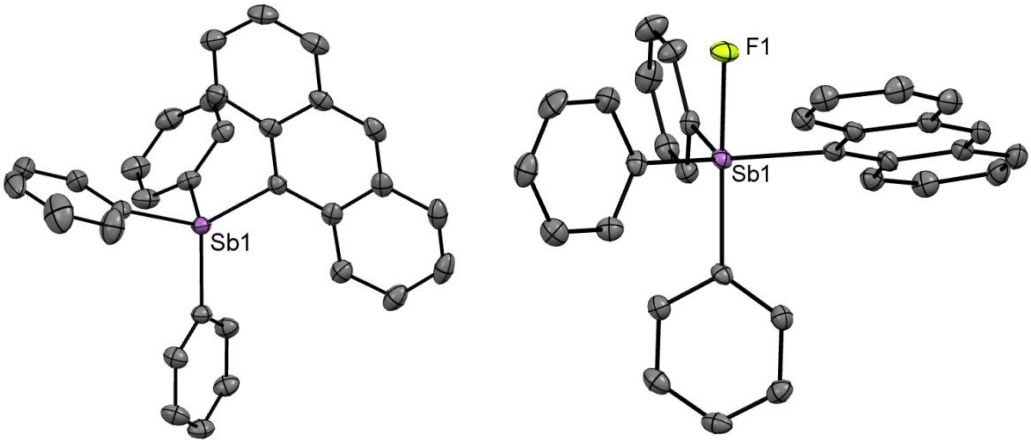

[**32**]$^+$ **32**·F

Figure 1.19: Crystal structures of the stibonium cation [**32**]$^+$ and the fluoride adduct from the reaction with KF in MeOH. Thermal ellipsoids drawn at the 50% probability level. The hydrogen atoms and the triflate counterion for [**32**]$^+$ are omitted for clarity.[67]

The stibonium centre adopts a tetrahedral structure, while the fluoride adduct is trigonal bipyramidal with the fluoride in the apical position and the sterically demanding anthryl group in the equatorial plane (Figure 1.19). The binding event can also be observed by ^{19}F NMR, with a peak at -75.8 ppm corresponding to the bound fluoride. Furthermore, receptor [**32**]$^+$ is compatible with water and also appears to selectively bind fluoride at ppm concentrations in a H_2O/DMSO mixture (9:1 vol.). Under such conditions, the binding constant was estimated at 12 000 ± 1100 M^{-1}, with no measurable interaction observed for Cl^-, Br^-, I^-, NO_3^-, N_3^-, HCO_3^- or HSO_4^- ions. In order to assess the effect of the strong Coulombic effect of cationic [**32**]$^+$ in anion binding, and as a point of comparison, Gabbaï *et al.* also synthesised a series of neutral receptors based on organoantimony(V) species.[68]

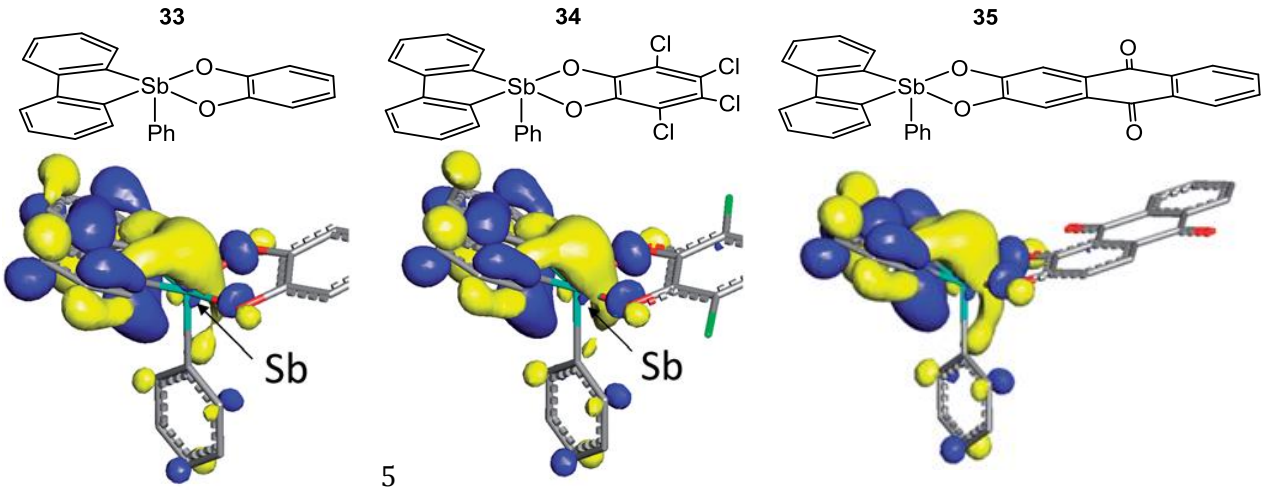

LUMO of **33** (-1.50 eV) LUMO of **34** (-1.73 eV) LUMO+1 of **35** (-1.61 eV)

Figure 1.20: (*top*) Schematic representation of compounds **33** to **35** (*bottom*) Contour plot and energy of the LUMOs centred on Sb in **33** to **35** (isodensity = 0.036)(reproduced from ref. 68).

Thus these authors isolated three stiborafluorene receptors **33** to **35** (Figure 1.20), with different Lewis acidities depending on the nature of the pendant catechol group. As verified by TD-DFT calculations, the incorporation of the very electron withdrawing perchlorinated catechol in **34** (Figure 1.20) lowers the energy of the LUMO to -1.73 eV (*cf.* -1.50 eV for compound **33**). The alizarin red unit in **35** engenders intermediate properties

with its LUMO+1 being found at -1.61 eV (note: the LUMO is largely centred on the alizarin red component). Yet in a THF/water mixture (1:7 vol.), receptor **35** (K_a = 1.61(0.11) × 10^4 M^{-1}) possess a similar if not higher binding constant for fluoride than **34** (K_a = 1.35(0.11) × 10^4 M^{-1}), whilst no discernible changes were observed with **33**. The crystal structures of the fluoride adducts of **34** and **35** have almost identical Sb–F bond lengths (respectively 1.973(4) Å and 1.978(2) Å), with a pseudo-octahedral geometry at the antimony centre in each case.

1.3. Borane Based Receptors

As outlined in the previous section, in the design of a Lewis acid a large variety of Main Group elements can be employed. Historically, however, group 13 systems have been widely employed and boron's versatility has made it a key component particularly for the detection of cyanide and fluoride.[8,69]

Boron trihalides BX_3 (X = F, Cl, Br) represent classic examples used in undergraduate textbooks to introduce the concept of a Lewis acid. The planar boron(III) centre is an exception to the *octet rule*, formally possessing 6 valence electrons and a vacant p_z-orbital, which can be quenched by a Lewis base. According to the HSAB theory, BX_3 and in general BR_3 systems (R = alkyl or aryl) are classified as hard acids, and they are prone to strong interactions with hard bases. Hence boron has been widely used in the design of receptors for hard bases, such as fluoride and cyanide. In part, boranes are attractive because their Lewis acidity can easily be tuned, thus allowing for high binding constants, whilst the selectivity for one anion over another can be optimised through peripheral steric hindrance. The influence of bulky aryl groups on the enthalpy of the addition reaction is due to the re-hybridisation of the boron centre from sp^2 to sp^3; pyramidalization increases the repulsive steric interaction between the substituents.

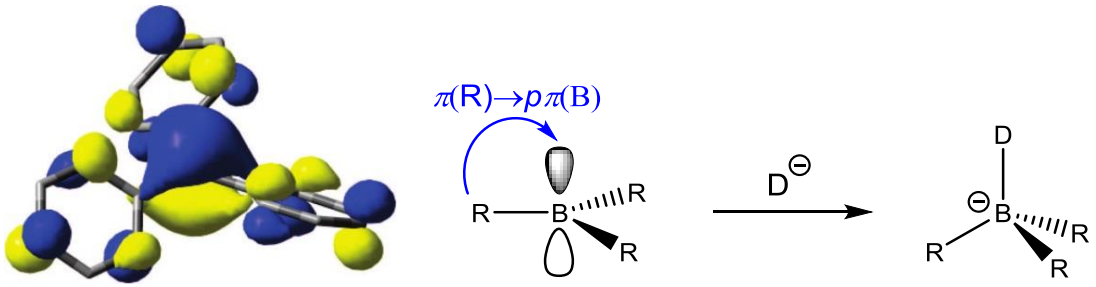

Figure 1.21: (*left*) Contour plot of the LUMO in BPh_3 (**63**) (B3LYP/6-31+G{d}) (reproduced from ref. 8). (*right*) re-hybridisation of the boron by reaction with a donor (D^-).

The Lewis acidity of boron trihalides is well known to be ordered $BF_3<BCl_3<BBr_3$,[70] *i.e.* opposite to the electronegativity scale of the halogen. This property arises from π-back-bonding from the halide into the boron empty p_z orbital; hence the B—F bond is very robust because the orbital overlap is the most efficient with the small fluorine atom (Figure 1.21). Conjugation of the π-system through boron can also be observed in arylboranes and exploited for sensing purposes. Although the disruption of the π interaction by addition of a base is not entropically favourable, a significant change in the conjugation network of the receptor can lead to quantifiable colorimetric or electrochemical alterations, thus offering the jump from anion recognition to molecular sensing.

1.3.1 Key Properties of Arylboranes: Lewis Acidity vs Sterics

The delicate balance between electronic properties and steric hindrance can be illustrated with several examples. Calculations on the simplest triaryl-borane, BPh_3, revealed that the gas-phase reaction with fluoride is more exothermic (ΔH = -342 kJ mol^{-1})[71] than with the more bulky Mes_2BPh (ΔH = -268.7 kJ mol^{-1}).[72] Even though these calculations relate to the gas phase (*i.e.* do not include solvation effects) they give a hint of steric effects. Another method to assess the Lewis acidity of the boron centre is by measuring its reduction potential. Electrochemistry provides a measurement of the electron affinity while neglecting the steric

implications of rehybridization: a low LUMO (*i.e.* strong Lewis acid) physically means a higher redox potential.

Entry	Compound	E° (V *vs* Fc/Fc$^+$)	*K* for F$^-$ (M^{-1})	*K* for CN$^-$ (M^{-1})
36	BPh_3	-2.13 (*a*)	-	-
37	$B(Ph)_2(Mes)$	-2.29 (*a*)	-	-
38	$B(Ph)(Mes)_2$	-2.35 (*a*)	$8.9(1.9) \times 10^4$ (*d*)	$1.9(0.5) \times 10^5$ (*d*)
39	$BMes_3$	-2.73 (*b*)	$3.3(0.4) \times 10^5$ (*e*)	4.3×10^4 (*g*)
40	$B(Mes)_2(Ant)$	-2.14 (*c*)	$2.9(0.3) \times 10^5$ (*f*)	-
41	$B(Mes)(Ant)_2$	-2.00 (*c*)	$2.6(0.2) \times 10^5$ (*f*)	-
42	$BAnt_3$	-1.83 (*c*)	$2.8(0.3) \times 10^5$ (*f*)	-

Table 1.1: Redox potential of a series of aryl boranes (Ant: anthracene)(*a*) 0.1 M [^{n}Bu$_4$N][ClO$_4$] in DMF.[73] (*b*) 0.1 M [^{n}Bu$_4$N][B(C$_6$F$_5$)$_4$] in THF.[74] (*c*) 0.1 M [^{n}Bu$_4$N][ClO$_4$] in MeCN/DCM (1:1).[75,76] (*d*),[77] (*e*),[78] (*f*),[79]and (*g*)[80] in thf.

Considering compounds **36** to **39** (Table 1.1), substitution of a phenyl group for the bulkier mesityl, means that steric hindrance is raised and the Lewis acidity drops.[73,74] Nonetheless, the association constants for either fluoride and cyanide ion are still within the range 10^5 – 10^6 M^{-1}.[77,80] The same pattern is observed for receptors **39** – **42**; the binding constants for fluoride ion are almost identical (log*K* ~ 5.4) even though the redox potentials increase sharply from -2.73 V to -1.83 V.[74-76] The data shown in Table 1.1 demonstrates how the steric hindrance can impede the pyramidalization of the boron, thus in effect weakening the B—F or B—CN bond.

The tetrahedralization of boron can be followed spectroscopically with a typical ^{11}B shift for a free arylborane being within the 60 to 80 ppm range, while borate species lie between +10 and -20 ppm. ^{11}B has a quadrupolar moment (I = 3/2) and is very sensitive to the symmetry at the boron nucleus; the switch from trigonal planar to tetrahedral boron thus notably sharpens the ^{11}B signal when the anion is bound.[8] Additionally the LUMO of

arylboranes is predominantly centred on the boron p_π-orbital (Figure 1.22) and quenching of the LUMO with a suitable base can therefore be followed by UV-vis absorption spectroscopy..

Crystallographically the length of the bond between the boron centre and the anion varies depending on the substituents at the boron, the nature of the anion and other intermolecular interactions (*e.g.* close contacts with counter-ion). Calculations on the B—F bond in [**36**·F]$^-$ give a distance of 1.465 Å (level of theory: RI-BP86/def2-TZVPP),[81] while the crystal structure of cyanide adduct reveals a B—C distance of 1.616(3) Å (Figure 1.22).[82] However the bond increases to 1.4809(19) Å and 1.631(3) Å for [**38**·F]$^-$ and [**38**·CN]$^-$ respectively; in both cases the introduction of two mesityl group significantly lengthens the B—X bond.[77] The large dissimilarity between the B—F and B—CN bond could be attributed to the close interaction of the nitrogen with the potassium cation (2.706(3) Å in [**36**·CN]$^-$; 2.758(2) Å in [**38**·CN]$^-$).[77,82] Finally the re-hybridization of the boron atom is marked by a decrease in the sum of the C—B—C angles, *e.g.* from 360.0° and 359.9° for receptors **36**[83] and **42**[76] to 335.3 and 345.2° for the respective adducts [**36**·CN]$^-$ and [**42**·F]$^-$ (Figure 1.22).[79,82] Once more, the enhanced steric interactions brought about by pyramidalization can account for the difference in the binding constant between [**36**·CN]$^-$ and [**42**·F]$^-$, considering the fact that an anthryl group is more bulky than a simple phenyl substituent.

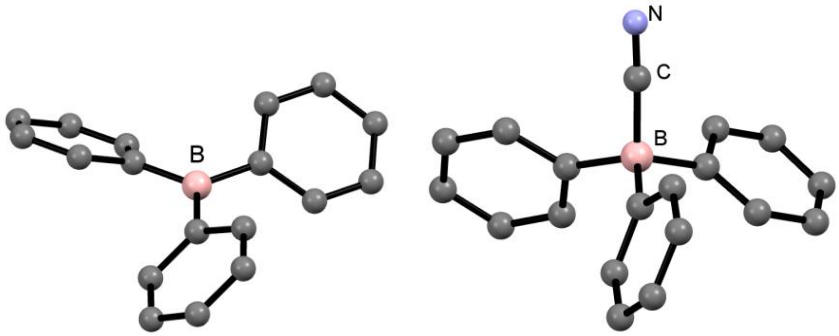

36 [**36**·CN]$^-$

Figure 1.22: Crystal structures of the free receptor **36** and the cyanide adduct [**36**·CN]$^-$.[82,83]

1.3.2 Variation in Lewis Acidity

As highlighted in the previous section, in order to have an efficient fluoride or cyanide receptor, the two key parameters to control are the steric hindrance and Lewis acidity. Steric hindrance can prevent interference by undesirable anions (*i.e.* other halides, hydroxide, azide, acetate, *etc.*), whilst a strong Lewis acid is essential to overcome the high solvation enthalpy (*e.g.* $\Delta H_{hydration}$ (F^-) = -504 kJ.mol^{-1}).[8] The latter effect can be clearly illustrated by the fluoride binding constants of $BMes_3$: with only 10% water in THF, K is about 1.0(3) M^{-1} while in dry thf this figure is elevated to $3.3(0.3) \times 10^5$ M^{-1}.[78]

1.3.2.1 Incorporation of Electron Withdrawing Groups

Several strategies can be adopted to increase the Lewis acidity at the boron centre, the use of electron withdrawing substituents being one. Ashley *et al.* performed a thorough study on a series of highly electron deficient boranes: $B(C_6Cl_5)_{3-n}(C_6F_5)_n$ (**43**: $B(C_6Cl_5)_3$; **44**: $B(C_6Cl_5)_2(C_6F_5)$; **45**: $B(C_6Cl_5)(C_6F_5)_2$; **46**: $B(C_6F_5)_3$).[84] The authors observed lower redox potentials with increasing n (**43**: -1.48(0.02) V; **44**: -1.55(0.05) V; **45**: -1.87(0.05) V; **46**: -1.97(0.01) V *vs* Fc/Fc^+ in dichloromethane). Comparison with the reduction potential of **39** (*i.e.* $E°(BMes_3)$ = -2.73 V *vs* Fc/Fc^+ in thf[74]), reveals the marked effects of halogenation of the aryl rings on the Lewis acidity of the boron centre. Another interesting factor is revealed here: the fluorine atom is more electronegative than chlorine, but it is the incorporation of the C_6Cl_5 group that lowers the LUMO. The authors point out that the C_6F_5 substituent is a σ-acid but also π-donor, that interacts with the p_π-orbital of boron, whereas C_6Cl_5 is essentially only a σ-acid.[84] Based on the redox potentials the Lewis acidity would therefore be expected to increase from **46** to **43**.

Despite this, Ashley[84] and Gabbaï[85] and their respective co-workers demonstrated that the Lewis acidity is reversed with respect to the electrophilicity, *i.e.* binding affinities increase with n. This apparent discrepancy rises from the fact that the chlorine atoms in the *ortho*

positions provide more steric hindrance than do the corresponding fluorines. This is apparent in bond lengths and C—B—C angles for various adducts (Figure 1.23). For instance in [**43**·F]$^-$ the B—F bond measures 1.482(13) Å while it is 1.434(5) Å in [**46**·F]$^-$. [85,86] As expected, the larger chloride sits further away with a B—Cl bond of 1.929(4) Å.[87] Through DFT calculations, Gabbaï *et al.* assessed the enthalpy of reaction with fluoride and found it to be far more exothermic for both halogenated arylboranes (ΔH(**43**) = -366 kJ mol^{-1} and ΔH(**46**) = -413 kJ mol^{-1}) compared to BPh_3 (ΔH(**36**) = -284 kJ mol^{-1}).[85]

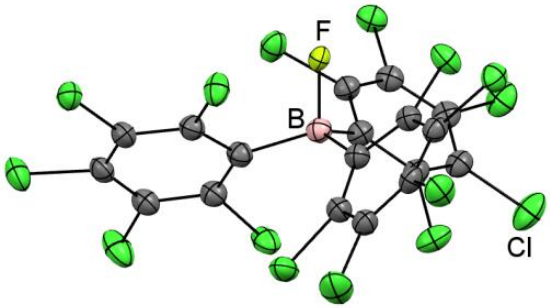

[**43**·F]$^-$
d(B—F)= 1.482(13) Å
$\sum_{C-B-C}$ = 346.7°

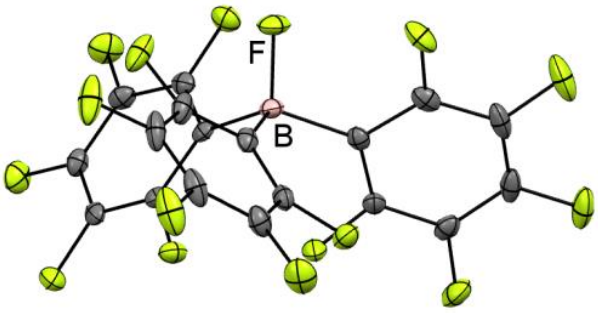

[**46**·F]$^-$
d(B—F)= 1.434(5) Å
$\sum_{C-B-C}$ = 335.1°

[**46**·Cl]$^-$
d(B—Cl)= 1.929(4) Å
$\sum_{C-B-C}$ = 337.8°

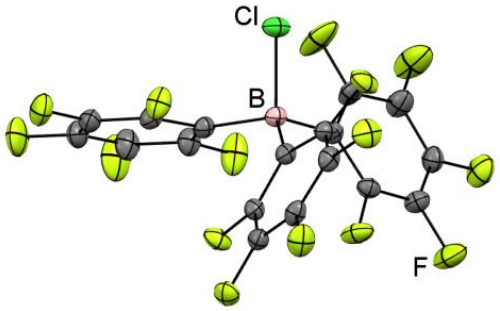

Figure 1.23: Crystal structures of fluoride and chloride adducts of **43** and **46**. Thermal ellipsoids are displayed at 30% probability and the counterion molecules are omitted for clarity.[85-87]

Strong Lewis acids such as $B(C_6Cl_5)_3$ form very robust adducts with fluoride and cyanide anions (K_a > 10^7 M^{-1} for either fluoride or cyanide). Unfortunately the steric hindrance is not sufficient to prevent the binding of chloride anions (K_a = 600(50) M^{-1}).[85] Lee and co-workers approached the matter in different way, by considering the effects of the substituents at the *para* position of the aryl group on the boron centre (Figure 1.24).[88] Throughout the

series **38** and **48** to **50**, the steric hindrance around the boron centre is virtually unchanged, while the Lewis acidity increases. UV Vis titrations reveal the expected trend in fluoride affinity which follows the Hammett parameter scale, from -0.17 for methyl to +0.172 for *ortho*-phenyl-carborane.[89] Receptor **50** is a strong fluorophile, as demonstrated by the binding constant of 5.0(0.3) × 10^3 M^{-1} measured with 10% water in thf at room temperature.[88]

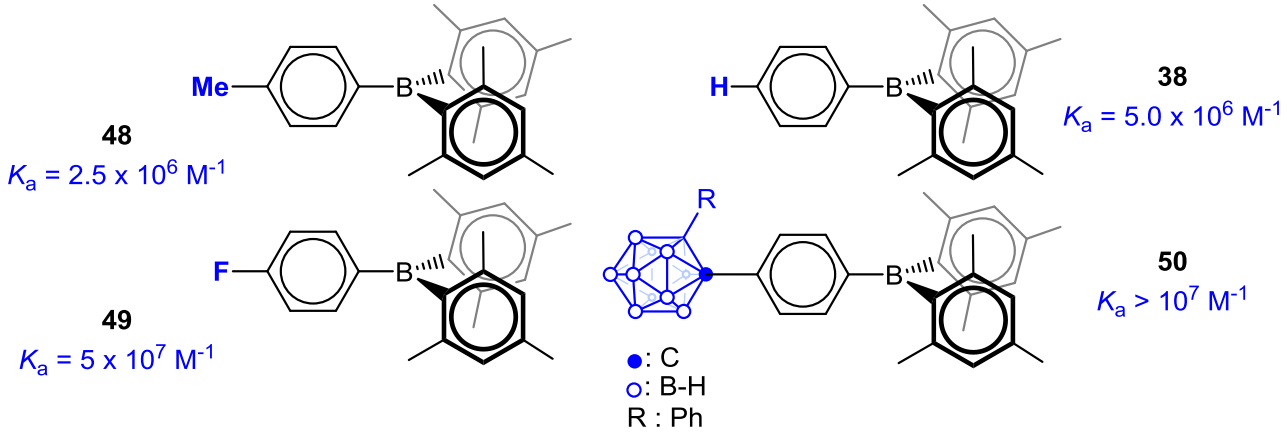

Figure 1.24: Schematic representation of different boranes receptor (**48**-**50**) with the associated binding constant for fluoride in THF, at room temperature.

1.3.2.2 Extension of the π-system

Increasing the Lewis acidity through the extension of the π-system conjugated through boron has already been introduced in section 1.3.1. The use of an anthryl substituent in place of mesityl or phenyl lowers the energy of the LUMO, although this modification also augments adverse steric factors due to repulsion upon pyramidalization.[76]

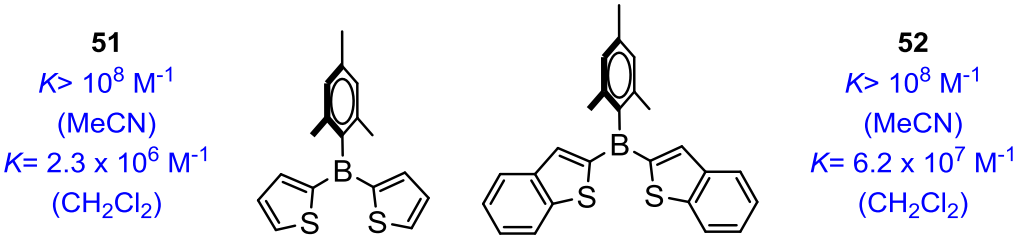

Figure 1.25: Schematic representation of **51** and **52** with their respective binding constant for fluoride ion in acetonitrile and dichloromethane.[90]

Kawashima *et al.* examined the effect of extending the conjugation of dithienylborane **51**, by using a benzothiophenone in system **52** (Figure 1.25).[90] A bathochromic shift in the absorbance from **51** (λ_{max}= 328 nm) to **52** (λ_{max}= 362 nm) is consistent with the extended π-conjugation brought about by the fused benzene ring linked through the formally empty p_π-orbital of the boron atom. This induces a decrease in the energy of the LUMO in **52**, which can be assessed through the respective binding constants for the fluoride ion in dichloromethane. Indeed, the fluoride affinity is enhanced at least 25-fold from K= 2.29 × 10^6 M^{-1} for **51** to K= 6.17 × 10^7 M^{-1} for **52** (Figure 1.25).

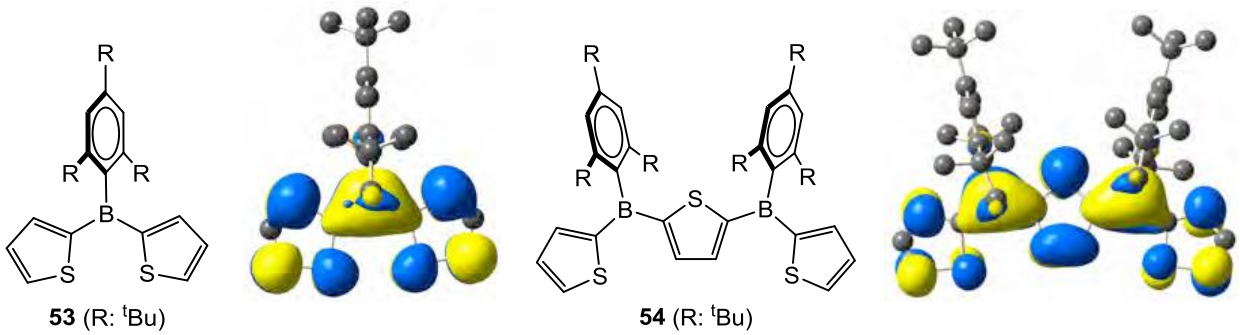

Figure 1.26: Schematic representation and contour plots of the LUMOs for **53** and **54** (Gaussian09-B3PW91/6-311+G*) (reproduced from ref. 91).

Jäkle and co-workers have carried out calculations and fluoride binding experiments on related thienylborane systems.[91] DFT calculations on both **53** and **54** reflect the conjugation of the aromatic thiophene ring with the p_π-orbital of the boron centre (Figure 1.26). Furthermore in **54**, the π-system is extended further, and is accompanied by a drop in the energy of the boron-centred LUMO, from -2.27 eV to -2.54 eV. These authors also isolated perfluorinated **55** and **56** (*i.e.* systems where R = CF_3) and compared their fluoride affinities.[91] For the mono-borane **55** the binding is about 1.59 × 10^7 M^{-1} whereas bis-borane **56** has an association constant of 6.31 × 10^7 M^{-1} for the first fluoride.

1.3.2.3 Coulombic Forces

Cationic substituents can exert a strong negative inductive effect which can be used to enhance the Lewis acidity at a three-coordinate boron centre. In modified $BMes_3$ receptors ($[\mathbf{57}]^{+}$, $[\mathbf{58}]^{2+}$ and $[\mathbf{59}]^{3+}$), the *para* methyl group of the mesityl substituent is formally replaced by a trimethylammonium substituent.[92] Since the cyclic voltammogram of $[\mathbf{59}]^{3+}$ is irreversible, the authors compared the peak potentials measured for $BMes_3$, $[\mathbf{57}]^{+}$, $[\mathbf{58}]^{2+}$ and $[\mathbf{59}]^{3+}$ (-2.63 V, -2.41 V, -2.16 V, and -1.86 V, respectively). Accordingly, the tricationic borane $[\mathbf{59}]^{3+}$ appears to be the most electron-deficient derivative in the series and is the only one that can irreversibly bind cyanide in pure water at pH 7 (δ_B -12.6 ppm).[8]

Alternatively, a positively charged group may be in direct contact with the target anion, as seen with receptor $\mathbf{61}^{+}$ (Figure 1.27).[93,94] The parent neutral amine-derivatized borane **60** does not show any affinity for fluoride by ^{1}H NMR spectroscopy, while methylated $\mathbf{61}^{+}$ can bind either cyanide or fluoride to form the corresponding B-bound adduct (Figure 1.27).

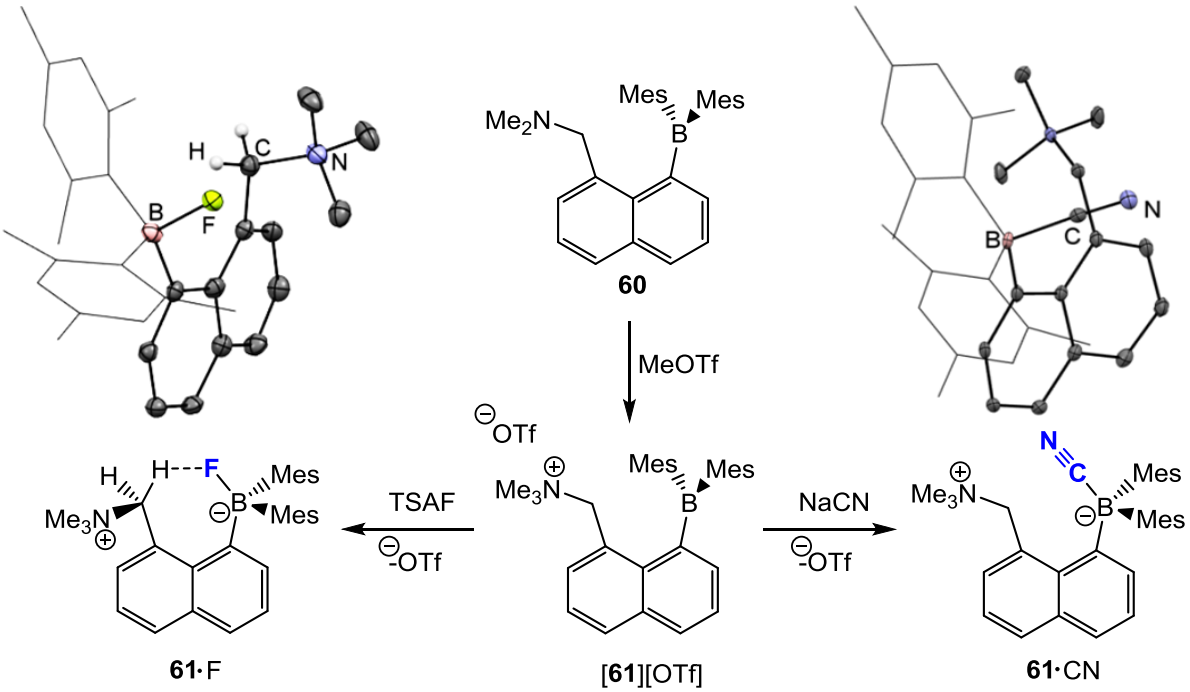

Figure 1.27: Schematic reactions of $\mathbf{61}^{+}$ with TSAF and NaCN. (*insets*) Crystal structures of **61**·F and **61**·CN. Thermal ellipsoids are displayed at 30% probability, the mesityl substituents are represented in wireframe format and hydrogens atoms not involved in the bonding are omitted for clarity.

Both products were fully characterised, notably by ^{11}B NMR spectroscopy with a resonance at +12.2 ppm and -12.2 ppm for **61**·F and **61**·CN, respectively.[93,94] Moreover in the solid state, the adduct **61**·F features an interaction between one hydrogen of the methylene bridge and the boron-bound fluoride. The C···F distance is 2.826(4) Å, *i.e.* within the range for a moderately strong hydrogen bond. This feature is maintained in solution, and the resonance for the F-bound hydrogen appears as a doublet of doublets in the ^{1}H NMR ($^{1}J_{F\text{-}H}$ = 9.2 Hz and $^{2}J_{H\text{-}H}$ = 12.9 Hz). The proximal cationic site also ensures high binding activity for cyanide (K(CN) = 8.0(0.5) × 10^{5} M^{-1} in thf)[94] but especially for fluoride (K(F) > 10^{8} M^{-1} in THF, K(F) = 5.0(0.5) × 10^{6} M^{-1} in mixture MeOH/thf (1:4 vol.)).[93] The binding affinities of **61**$^{+}$ are at least three orders of magnitude higher than those for the parent compound B(Mes)$_2$Ant (K(F) = 2.9(0.3) × 10^{5} M^{-1} in thf).[79]

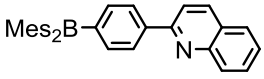

62

K(F)= 4.68 x 10^{4} M^{-1} *(a)*

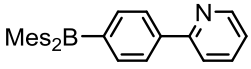

64

K(CN)= 3.98 x 10^{5} M^{-1} *(b)*

K(F)= 7.59 x 10^{2} M^{-1} *(b)*

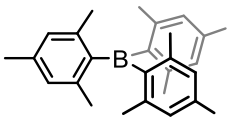

39

K(F)= 4.27 x 10^{4} M^{-1} *(c)*

K(CN)= 3.31 x 10^{5} M^{-1} *(c)*

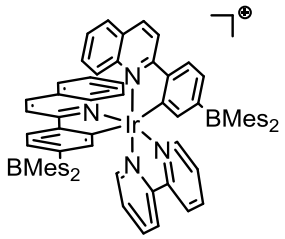

63^{+} : [Ir(**62**)$_2$(bpy)]$^{+}$

$K_{1:1}$(F)= 1.29 x 10^{6} M^{-1} *(a)*

$K_{1:2}$(F)= 4.27 x 10^{5} M^{-1} *(a)*

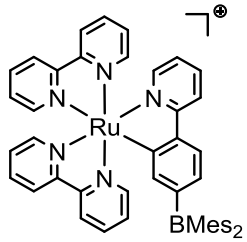

65^{+} : [Ru(**64**)(bpy)$_2$]$^{+}$

K(CN)= 3.02 x 10^{6} M^{-1} *(b)*

K(F)= 1.10 x 10^{4} M^{-1} *(b)*

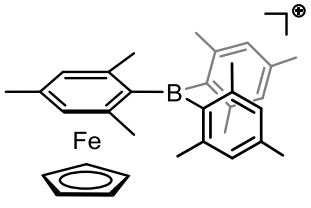

66^{+} : [CpFe(**39**)]$^{+}$

K(F)> 10^{7} M^{-1} *(c)*

K(CN)> 10^{7} M^{-1} *(c)*

Figure 1.28: Receptors **62**-**66**$^{+}$ and the related metal complexes. Binding constants are fitted to a 1:1 binding isotherm and 1:2 for a secondary boron binding site (*a*) in MeCN (*b*) $CHCl_3$/DMF (9:1 vol.) and (*c*) in thf.

In related fashion, a lower energy LUMO can also be achieved by the coordination of organoboranes to a cationic metal centre, such as iridium(III) (**63**$^+$),[95] ruthenium(II) (**65**$^+$),[96] or iron(II) (**66**$^+$)[97] (Figure 1.28). The transition metal bears a formal cationic charge, and is expected to affect the conjugation of the p_π-orbital at boron. Comparison of the binding constants measured for the neutral ligands **62**, **64** and **39** with the related metal complexes, shows an increase in binding by at least two orders of magnitude (Figure 1.28).[97] It should be noted that receptor **63**$^+$, after binding one fluoride ion, gives rise to a second binding constant which is still higher than the free ligand **62**.[95]

1.3.3 Bidentate Sensors: Teamwork

1.3.3.1.1 Diborane Systems

The early work of Schriver and Billias on bidentate Lewis acids, such as 1,2-bis(difluoroboryl)ethane, opened up the field of fluoride recognition using the chelate effect.[98] The geometry required of a preorganized bidentate site for fluoride binding is challenging, perhaps explaining why only a few examples of diborane receptors have been reported in the literature (*e.g.* 1,8-bis(boryl)naphthalene, **68**).[8] Similar in structure, to *proton sponge* developed by Winterman *et al.*,[99] **68** has been shown to chelate hydride, hydroxide and fluoride ions.[100] Evidence that the chelate effect is dominant comes from the complete abstraction of fluoride from mono-functional [**67**·F]$^-$ (Figure 1.29).

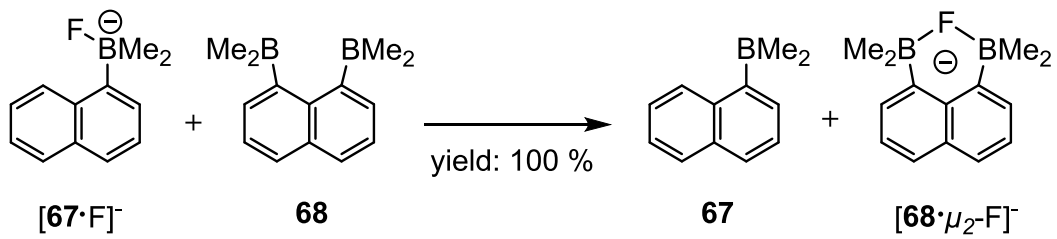

Figure 1.29: Competition reaction between monodentate receptor **67** and bidentate receptor **68**.[100]

Furthermore, selectivity can be enhanced by the introduction of more bulky groups, for example the mesityl substituents in **69**, while the incorporation of one borane in a secondary aromatic system, *c.f.* **70** to **72**$^+$ drastically increases the fluoride affinity (Figure 1.30).

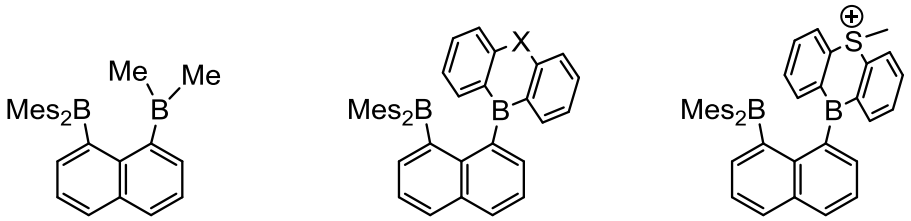

69
K> 5.0(0.2) x 10^5 M^{-1}
($CHCl_3$, rt)

70 (X: O)
71 (X: S)
K> 5 x 10^9 M^{-1}
(thf, rt)

72$^+$
K>> *K* of (**71**)

Figure 1.30: Receptors **69** - **72**$^+$ and their respective binding affinities for fluoride.[101-102]

Gabbaï's receptor **69** is found to bind fluoride equidistant from both boron atoms (1.600(5) Å and 1.606(5) Å).[101] Similarly, both **70** and **71** bind fluoride in the cavity between the two boron centres (Figure 1.31) with similar bond lengths to [**69**·μ_2-F]$^-$ (*e.g.* 1.634(5) Å and 1.636(6) Å for [**70**·μ_2-F]$^-$)[72,78] Additionally, the B···B distances in the adduct are altered compared to the free receptor *e.g.* 3.205 Å and 3.280 Å, respectively for **69** and **70** (*c.f.* 2.852 Å and 2.928 Å in the free receptors). Furthermore, methylation of the remote sulfur centre in **71** leads to the formation of a cationic site in the backbone of the anthryl group which enhances fluoride binding. Thus **72**-μ_2F displays a large asymmetry in the B—F bond distances (d(F—BMes_2)=1.822(4) Å, d(F—BAnthryl)=1.540(5) Å).[102]

Some disparity in the orbitals involved is uncovered by DFT calculations for **71** and **69**. In **71**, both boron p_z-orbitals are oriented toward one another in a transannular fashion and contribute significantly to the LUMO, while only the dimesitylboryl moiety participates in the LUMO of **69** (Figure 1.31). The high energy of the p_z-orbital of the BMe_2 unit — thought to be due to the inductive effect of the methyl group —precludes its significant involvement in the LUMO.[101b] The formation of all four adducts can also be monitored by ^{19}F NMR spectroscopy, with a shift within the -170 to -190 ppm range being associated with the product in each case

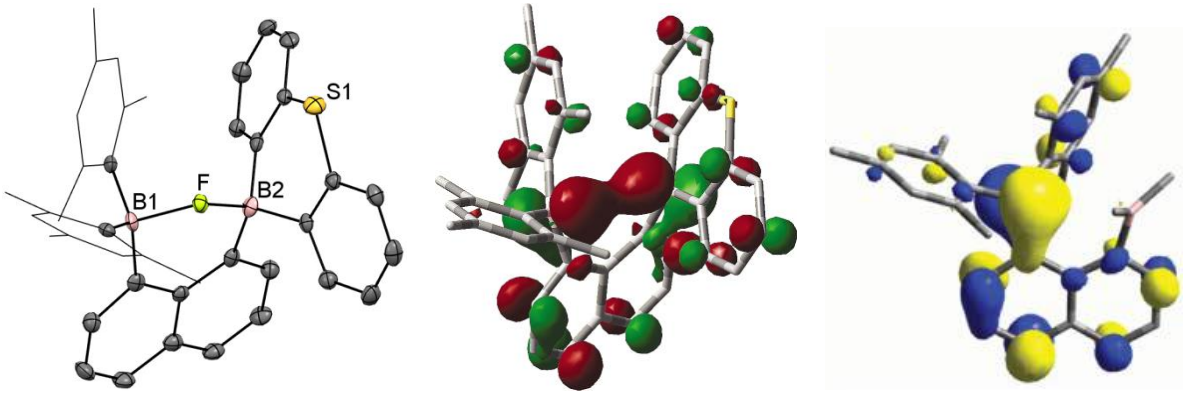

[**71**·μ_2-F]$^-$ **71** **69**

Figure 1.31: (*left*) Crystal structures of [**71**·μ_2-F]$^-$ and (*right*) contour plots of the LUMOs for **71** and **69** (B3LYP/6-31+G{d'} and 6-31+G) (reproduced from ref. 78 and 101b). Thermal ellipsoids are displayed at 50% probability. The mesityl groups are partially represented in wireframe format and the hydrogen atoms are omitted for clarity.

(*e.g.* δ_F -188 ppm for [**71**·μ_2-F]$^-$), ^{11}B NMR is also informative, with spectra typically featuring sharp signals centred around zero (*e.g.* δ_B -0.4 and 4.0 ppm for **72**·μ_2-F). Gabbaï and co-workers also assessed the corresponding fluoride binding constants (Figure 1.30); that for **69** is at least four magnitudes lower than those for **70** or **71**. This variation arises from cooperative interaction involving the two boryl units for efficient chelation of the fluoride ion. Competitive reactions reveal that cationic **72**$^+$ has a higher binding affinity than parent neutral **71**, which is consistent with the expected Coulombic effects. Finally, it is of note that the narrow size of the binding pocket in the napthalene systems allows for a selective binding fluoride rather than Cl^-, Br^-, I^-, AcO^- or NO_3^- anions.

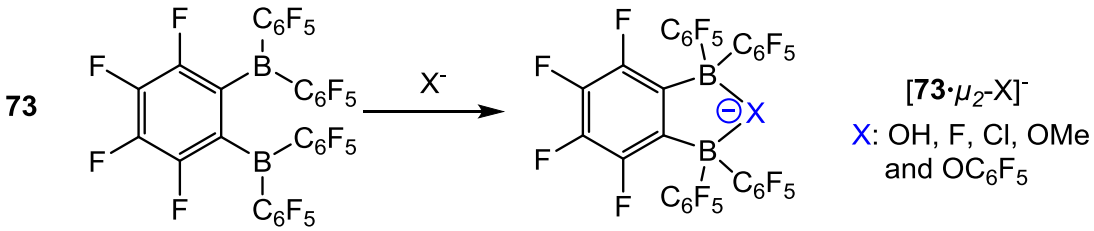

Figure 1.32: Chelation of different anions by **73**.

Piers and co-workers have developed several highly electron deficient systems based on an *ortho*-disubstituted benzene backbone, such as receptor **73** which features two

bis(pentafluorophenyl)boryl groups (Figure 1.32).[103] Diborane **73** has an intra-boron distance of 3.138(2) Å which should therefore only accommodate small anions.[103a] Moreover **73** is proven to be a strong Lewis acid, extracting fluoride from BF_4^- (FIA(BF_4^-)= 338 kJ mol^{-1}).[104] The peripheral pentafluoro-benzene substituents confer high Lewis acidity but no control over sterics, thus **73** exerts no discrimination between OH^-, Cl^-, F^-, MeO^- or $C_6F_5O^-$ ions.

The metallocene-derived Lewis acid bis(boryl)cobaltocenium published by Herberich *et al.* also demonstrates chelating abilities, as demonstrated by both NMR and X-ray structural studies.[105] Compound **74**, for example, is readily oxidized by $Cu(OH)_2$ to afford the adduct **74**·μ_2-OH, while C_2Cl_6 yields the adduct **74**·Cl. Treatment of **74** with [Fc][PF_6] on the other hand, yields the free cationic receptor as [**74**][PF_6].

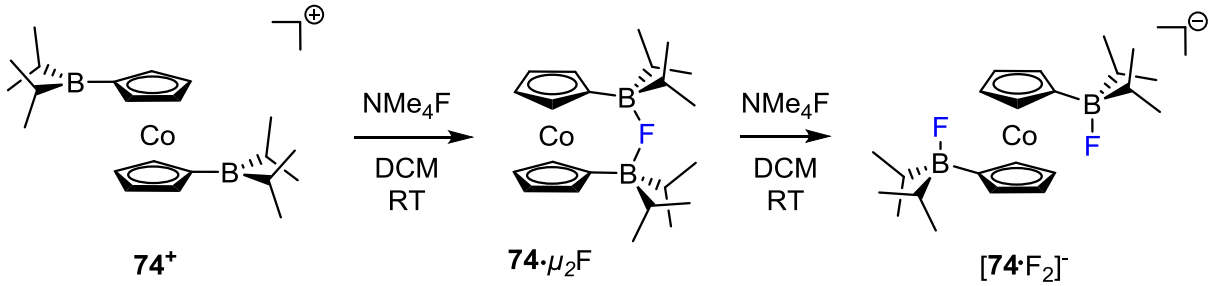

Figure 1.33: Sequential addition of a fluoride source (*i.e.* NMe_4F) to **74**$^+$.

The latter chelates one fluoride upon addition of [NMe_4]F with a ^{11}B NMR shift from 79 ppm to 26.4 ppm and a broad peak in the ^{19}F NMR at -158 ppm signalling the binding event and being consistent with a bridging fluoride (Figure 1.33).[105] The B···B distance is reduced from 3.543 Å for an eclipsed configuration to 3.157 Å when fluoride is bound in bridging fashion, with a B—F distance of 1.641(4) Å.[105] The addition of two equivalents of fluoride leads to the binding of one fluoride at each boron centre.

As with other modes of binding, selective and effective recognition is contingent on the geometry of the binding site, as well as on factors such as steric hindrance and the energy of the LUMO at the implicated boryl function. Anion chelation can also be realised with

heteronuclear systems, that is by employing a borane with another Lewis acid substituent as the auxiliary receptor site.

1.3.3.2 Bidentate Hybrids: Diversity in Bonds

Various receptors using a secondary Lewis acidic binding site contiguous to a boryl centre have been developed, relying on the cooperative effect of either hydrogen bonds or a proximal Lewis acid. This hybrid tactic offers two major advantages, (*i*) it should limit B—C cleavage in presence of water, and (*ii*) it imposes spatial constraints which can be mitigated if the secondary binding site is a softer Lewis acid, such as mercury or tin.

Related to the work on the 1,8-*bis*(boryl)-napthalenes, Gabbaï *et al.* developed boryl mercury systems such as **75**, **76** and cationic **77**$^+$ (Figure 1.34).[101,106,107] Study of the respective crystal structures reveals similar B···Hg distances in each case (*ca.* 3.30 to 3.47 Å), but the distribution of the LUMO is unsymmetrical. For instance, methylation leading to **77**$^+$ redistributes the LUMO with a lobe extending over the two Lewis acidic centres and a large contribution centred on the benzene ring; the LUMO in **76** by contrast is dominated by the boron atom. The presence of the cationic ammonium function lowers the energies of the Hg-centred vacant orbitals, thus the mix of molecular orbitals with the B atom is now more efficient, leading to a stronger chelating site.[106]

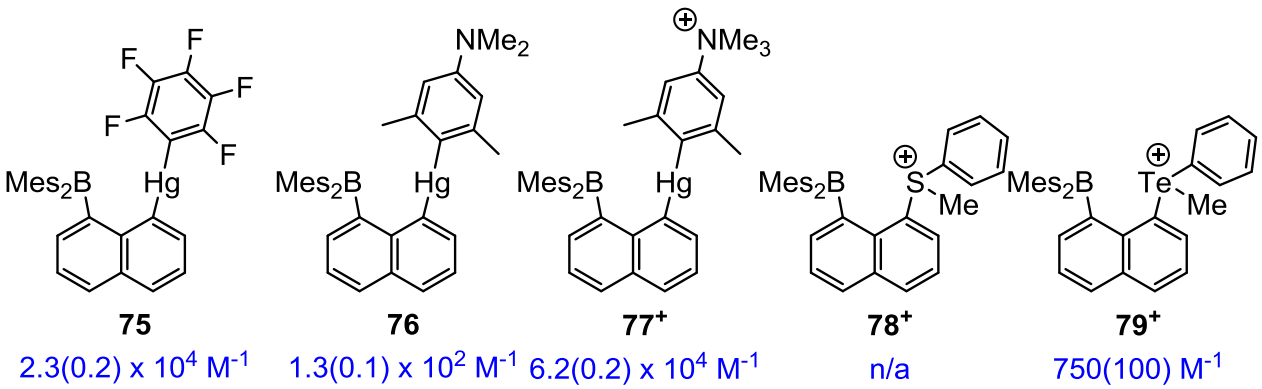

Figure 1.34: Schematic representation of **75** - **79**$^+$ with their respective fluoride binding constants in a thf/Water mixture (9:1 vol.) for **75** - **77**$^+$ and MeOH for **78**$^+$ and **79**$^+$.

This observation explains the two orders of magnitude disparity in the fluoride affinity between **77**$^+$ (K= 6.2(0.2) × 10^4 M^{-1}) and **76** (K= 1.3(0.1) × 10^2 M^{-1}). The binding constants of **75** (K= 2.3(0.2) × 10^4 M^{-1}) and **77**$^+$ are similar, and thus it appears that the electron withdrawing group (*i.e.* C_6F_5) has comparable effects on the Lewis acidity of the Hg centre, as does the $ArNMe_3^+$ group in **77**$^+$.[107] Nonetheless, chelation of the fluoride ion by all three receptors is evident from a large shift in the ^{11}B NMR spectra and from the coupling constants between the F and Hg, observed by NMR spectroscopy (*e.g.* **77**$^+$, ^{199}Hg NMR: -759.8 and $^1J_{Hg\text{-}F}$ = 122.0 Hz).[106]

Gabbai and co-workers also explored the use of the heavy elements of the group 16, such as sulphur and tellurium. Based again on the 1,8-napthalene scaffold, they designed the cationic receptors **78**$^+$ and **79**$^+$ (Figure 1.34).[108] Binding studies carried out in pure methanol reveal that **78**$^+$ has little or no affinity for fluoride, but **79**$^+$ is able to selectively chelate one fluoride under the same conditions (K= 750(100) M^{-1}). The tellurium atom being more polarisable and electropositive compared to sulfur, allows for a greater contribution of the σ^*(Te—C) molecular orbital in the LUMO+1 of **79**$^+$ (Figure 1.35). Thus, a donor-acceptor interaction between the lone pair of the fluoride and the σ^*(Ch—C) orbital is stronger with tellurium.[108]

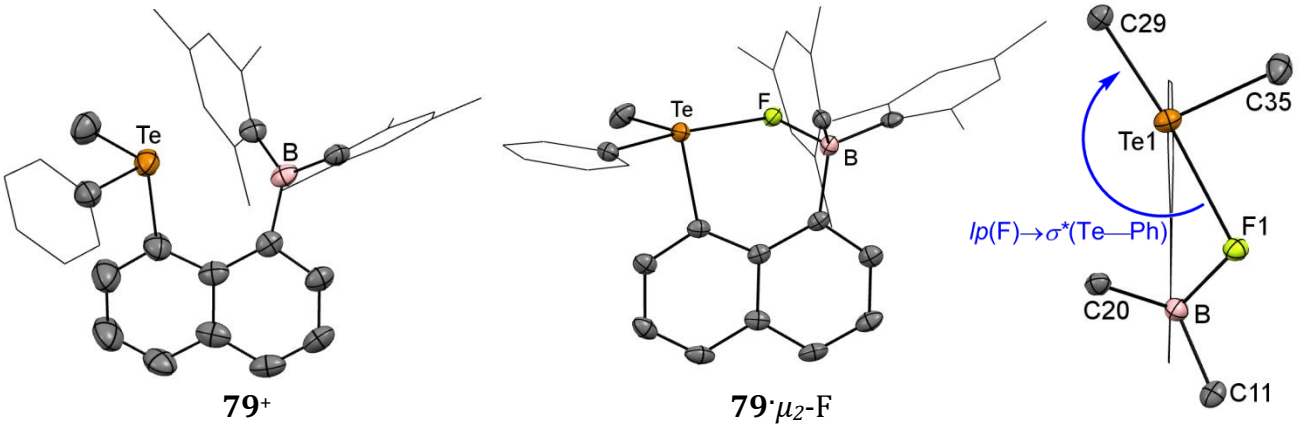

79$^+$ **79**·μ_2-F

Figure 1.35: (*left*) Crystal structures of the free cationic receptor **79**$^+$ and the fluoride adduct **79**·μ_2-F. Thermal ellipsoids are displayed at 50% probability. (*right*) top view of **79**·μ_2-F highlighting the atoms involved in the chelation of fluoride.

This interaction or lack thereof is apparent in the crystal structures of both fluoride adducts **78**·μ_2-F and **79**·μ_2-F (Figure 1.35). The weak interaction between sulfur and fluorine atoms is reflected in a shorter B—F bond in **78**·μ_2-F than in **79**·μ_2-F (respectively 1.481(2) Å and 1.514(4) Å), and a S—F bond (2.548(1) Å) which is somewhat longer than the Te—F bond (2.506(2) Å) in spite of larger the larger size of tellurium (S $_{VdW}$= 1.80 Å *vs* Te $_{VdW}$= 2.06 Å).[108,109] The fluoride contribution to the σ*(Ch—C) molecular orbital (Ch = S or Te) was evaluated to be 95 kJ mol^{-1} for **79**·μ_2-F and only 38.5 kJ mol^{-1} in the case of **78**·μ_2-F.

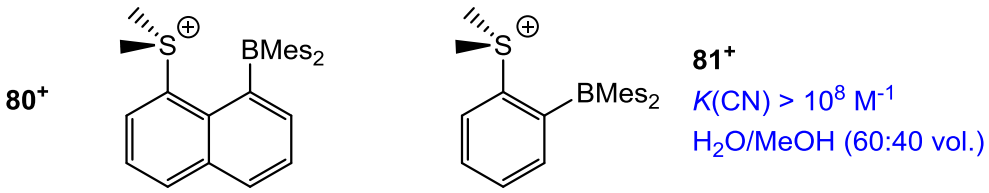

Figure 1.36: Schematic representation of sulfonium receptors **80**$^+$ and **81**$^+$.

Further work by Gabbaï on sulfonium boranes emphasizes the importance of the preorganization at the chelating site.[110] Changing from a 1,8-napthalene core for **80**$^+$ and a 1,2-benzene framework for **81**$^+$ (Figure 1.36), allows for the effects of different bite angles and distances between the two Lewis acidic centres to be investigated. Thus, for example, the energy associated to the donor-acceptor interaction from the lone pair of the sulfur into the empty p_z-orbital of the B is weaker for **81**$^+$ due to the divergent orientation of the orbitals involved (**80**$^+$: E = -28.5 kJ mol^{-1}; **81**$^+$: E = -9.6 kJ mol^{-1}).[110] Both receptors were tested for their propencity to recognise anions in a H_2O/MeOH mixture (95:5 vol.). Thus, formation of **81**·CN was observed, whereas addition of 15 equivalents of Cl^-, Br^-, I^-, NO_3^-, $H_2PO_4^-$, $MeCO_2^-$ or HSO_4^- did not result in anion fixation. From the crystal structure **81**·CN and further calculations, the authors explain that selectivity is enforced by a small but crucial interaction between the charged sulfonium centre and the CN bond (Figure 1.37).

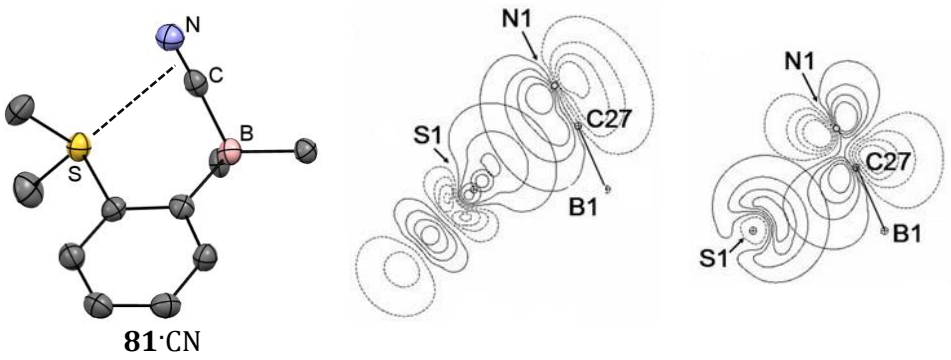

81·CN

Figure 1.37: (*left*) Crystal structure of the cyanide adduct **81**·CN. Thermal ellipsoids are displayed at 50% probability. The mesityl substituents and the hydrogen atoms are omitted for clarity. (*right*) NBO contour plots showing $\pi(C{\equiv}N){\rightarrow}\sigma^*(S{-}C)$ and $lp(S){\rightarrow}\pi^*(C{\equiv}N)$ interactions in **81**·CN (reproduced from ref.110).

1.4. Macroscopic Responses for Anion Binding

In the true sense of the term, a sensor is a receptor that includes a macroscopic response upon fixation of the targeted anion and is strictly reversible. The response can be multiple and varied in nature, either an optical (*i.e.* involving colour, phosphorescence or fluorescence) or electrochemical.[8,111] After initially focusing on binding motifs, the following sections will focus on possible responses associated with the binding event.

1.4.1 Colorimetric Response

The empty p_z-orbital of the boron is usually the main contributor to the LUMO in borane receptor systems, hence low energy electronic transitions are closely related to the fate of the tri-coordinate boron centre. The fact that electronic transitions are shifted to higher energies when the borane is quenched by an anion can be useful for colorimetric sensing. For instance, a boron centre involved in highly delocalised systems, such as Tamao's anthrylborane compounds, can absorb in the visible region of the spectrum (Figure 1.38).[76,112] Thus, on formation of the corresponding fluoroborate by fluoride uptake, receptors **40**-**42** undergo marked changes of colour, from yellow/orange to colourless. The result is

quantifiable by UV-visible spectroscopy measurements: the interruption of the π-conjugation leads to new absorption bands between 360 and 410 nm. This hypsochromic shift is also observed for sensor **82** which can be quenched stepwise with a progressive change from a red to an orange solution.

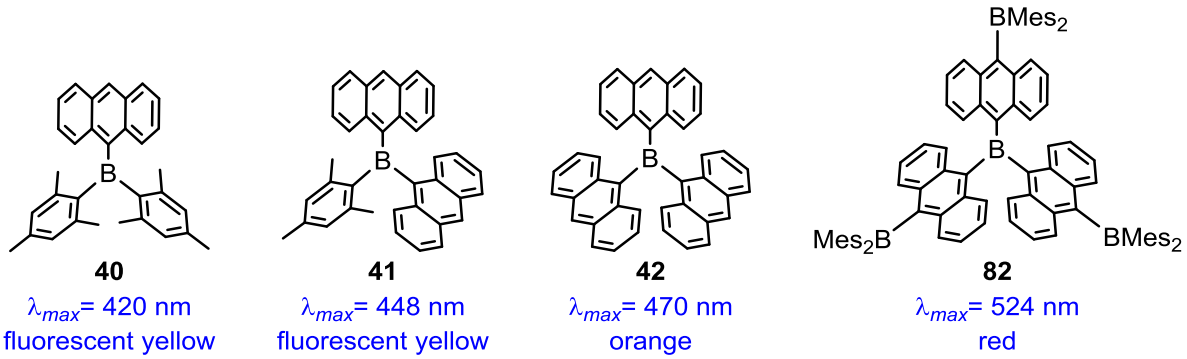

Figure 1.38: Schematic representation of receptors **40** - **42** and **82** with their respective λ_{max} values (measured in thf).

Even though the blue-shift from coloured to colourless is distinct, a "turn-on" response is more desirable in terms of applications for a sensor. With this in mind, Wang *et al.* developed a system in which the emission of an aryl amine is initially masked by the aryl borane substituent *via* a donor-acceptor electron transfer process.[113] Emission can then be triggered by simple quenching of the empty p_z-orbital at boron, giving a "turn-on" response to the addition of fluoride. Gabbaï and co-workers have also exploited the donor properties of the fluoroborate in connection with a pyridinium function as the electron deficient acceptor (Figure 1.39).[114]

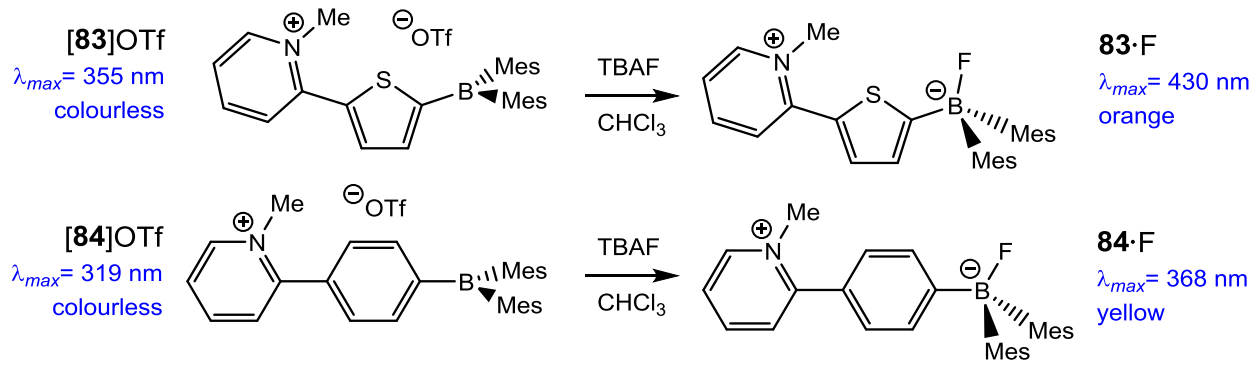

Figure 1.39: Reactions of **83**$^+$ and **84**$^+$ with TBAF and the associated photo-physical responses.

The formation of the zwitterionic fluoroborates **83**·F and **84**·F is accompanied by an intense colour change, from colourless to orange and yellow respectively. DFT calculations were carried out both on the free receptors and the fluoride adducts; for each receptor the LUMO is localised on the pyridinium moiety, whilst the HOMO is largely focused on the mesityl substituents. The electronic transitions are mainly from the HOMO to the LUMO, and thus can be regarded, in effect, as intramolecular charge transfer processes. On fixation of fluoride (*e.g.* from **83**$^+$ to **83**·F, or from **84**$^+$ to **84**·F), the energy gap diminishes between the frontier orbitals, and thus the fluoride adducts absorb in the visible region of the spectrum.[114]

1.4.2 Fluorescence

Gabbaï and co-workers published a series of onium borane salts bearing either an ammonium[115] or phosphonium substituent (Figure 1.40).[116] The cationic receptor **85**$^+$ gives rise to a strong green fluorescence (λ_{em}= 495 nm) attributed to an intramolecular charge transfer (ICT) from the mesityl components to the vacant p_z-orbital at boron.[116a] The formation of the zwitterionic system **85**·F, cuts off the pathway for ICT, which leads to a fluorescence quenching. This "turn-off" response is less desirable from an analytical point of view compared to a "turn-on" response.

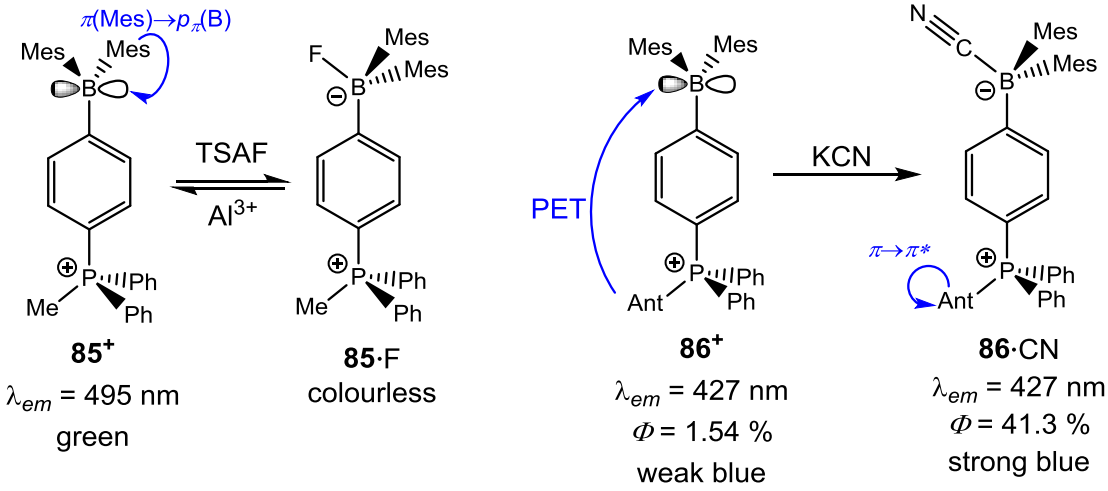

Figure 1.40: Luminescence response upon addition of fluoride to the cationic receptor **85**$^+$ and **86**$^+$ (blue: absorption processes involved in fluorescence).[116]

The simple introduction of a fluorophore, such as an anthracenyl moiety, in place of the methyl group on the phosphine component further redistributes the relevant frontier orbitals (Figure 1.40). Indeed receptor **86**$^+$ features a donor-acceptor interaction, between the electron-deficient phosphonium borane and the anthracene donor, *via* a photo-induced electron-transfer (PET) process. This leads to a weak blue fluorescence (Φ = 1.54 %), instead of the elevated quantum yield usually observed for the anthracene fluorophore. This observation is concordant with the increase in fluorescence intensity observed when the vacant *p* orbital is populated by cyanide coordination, as in **86**·CN (Φ = 41.3 %).

Arylboranes in close contact with a peripheral donor are usually characterised by emissive CT transitions, as observed by Wang *et al.* for **87** (Figure 1.41).[117] This "U-shaped" receptor gives rise to a white fluorescence due to a dual emission at λ_{em} = 407 and 532 nm. The high-energy peak corresponds to a Mes(π)→B—Ph(π^*) transition, while the low-energy peak relates to *lp*(P)→p_z(B) through space CT transition. Consistent with with the existence of a short B···P contact in the solid state (6.24 Å), the quenching of the low-energy CT emission is observed after addition of TBAF to **87**. The strong blue emission in the fluoride adduct [**87**·F]$^-$ rises from π→π^* transitions (*c.f.* Figure 1.41) with similar energy to that of **87**.[117]

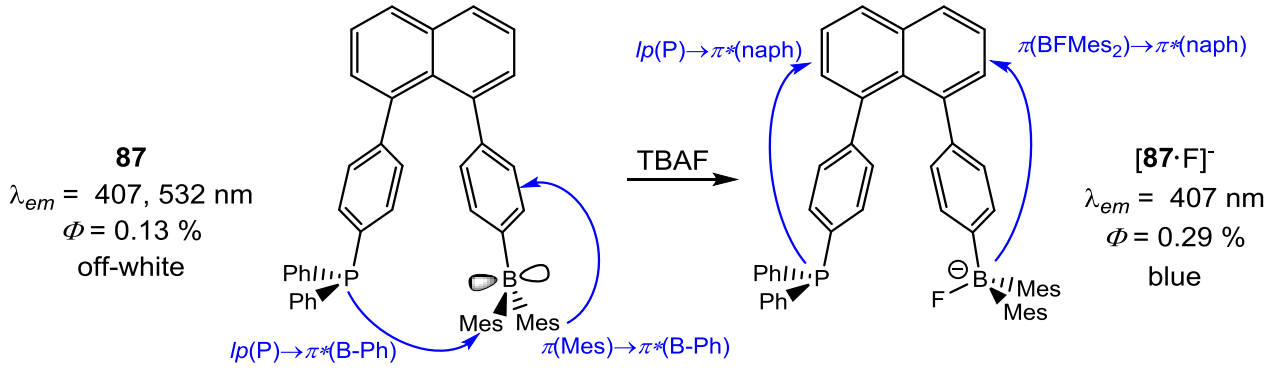

Figure 1.41: reaction of **87** with TBAF (blue: absorption processes involved in fluorescence).

A "turn-on" response can also be achieved by the re-emergence of a π→π^* transition after the coordination of the target anion, as demonstrated by Jäkle and co-workers with their

dimesitylboryl-functionalized quaterthiophene (**88**).[118] The blue fluorescence (λ_{em}= 560 nm) arises from the central bithiophene moiety, and the empty *p*-orbitals at boron in combination with a low energy $\pi \rightarrow \pi^*$ transition localized on the thiophene main chain (Figure 1.42).

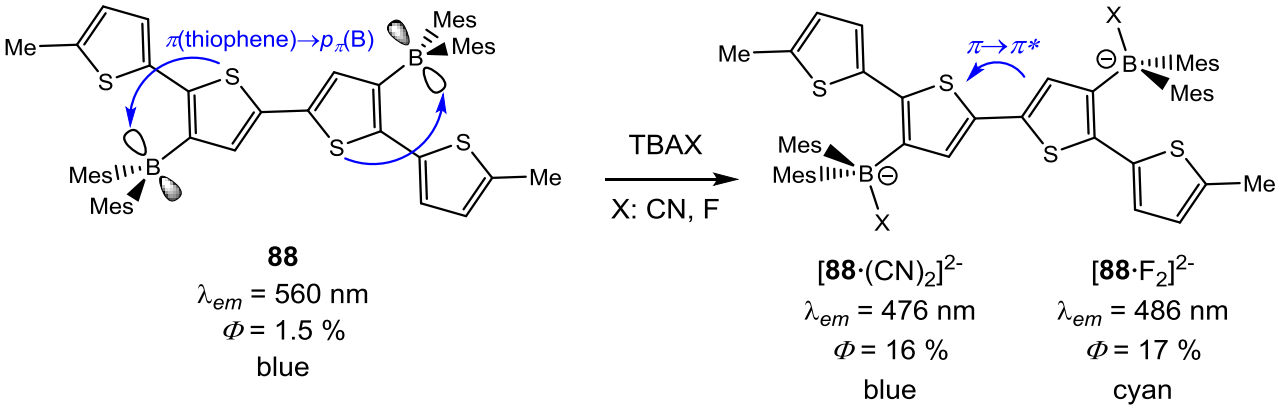

Figure 1.42: Formation of $[\mathbf{88}\cdot(CN)_2]^{2-}$ and $[\mathbf{88}\cdot F_2]^{2-}$ (blue: photo-physical processes involved in fluorescence).

Titrations with cyanide or fluoride ions lead to hypsochromic shifts from 560 nm to 476 nm and 486 nm respectively with a 10-fold increase of the fluorescence quantum yields (*c.f.* $\Phi_{88\cdot CN}$ = 17 % ; $\Phi_{88\cdot F}$ = 16 % ; Φ_{88} = 1.5 %). This increased fluorescence is due to a greater gap of the main chain-based $\pi \rightarrow \pi^*$ transition, along with increased oscillator strength. Moreover the difference between bis-cyanide and -fluoride adducts is attributed to the torsion angle between the thiophene rings; the more twisted $[\mathbf{88}\cdot(CN)_2]^{2-}$ (31.0°) leads to a larger energy gap and a blue shift in the absorption relative to $[\mathbf{88}\cdot(CN)_2]^{2-}$ (16.0°).

The last result demonstrates how the luminescence properties of a receptor are correlated with its three structural characteristics: π-conjugation length and rigidity, molecular symmetry and the donor/acceptor strength.[119] Wang's system based on a truxene (heptacyclic polyarene) maximizes the conjugation among a rigid and highly symmetric planar skeleton (Figure 1.43). The binding of fluoride disrupts the p_π(B)—π conjugation and is at the origin of a 100 nm blue-shift in the fluorescence emission. It reflects the transfer of the LUMO from the arylborane to the truxene-thiophene backbone with a HOMO-LUMO gap

increase of 0.78 eV. Furthermore, the oscillator strength of the first accessible excited state increases from **89** to [**89**·F]$^-$ (f= 0.0106 and 0.5702 respectively).[119]

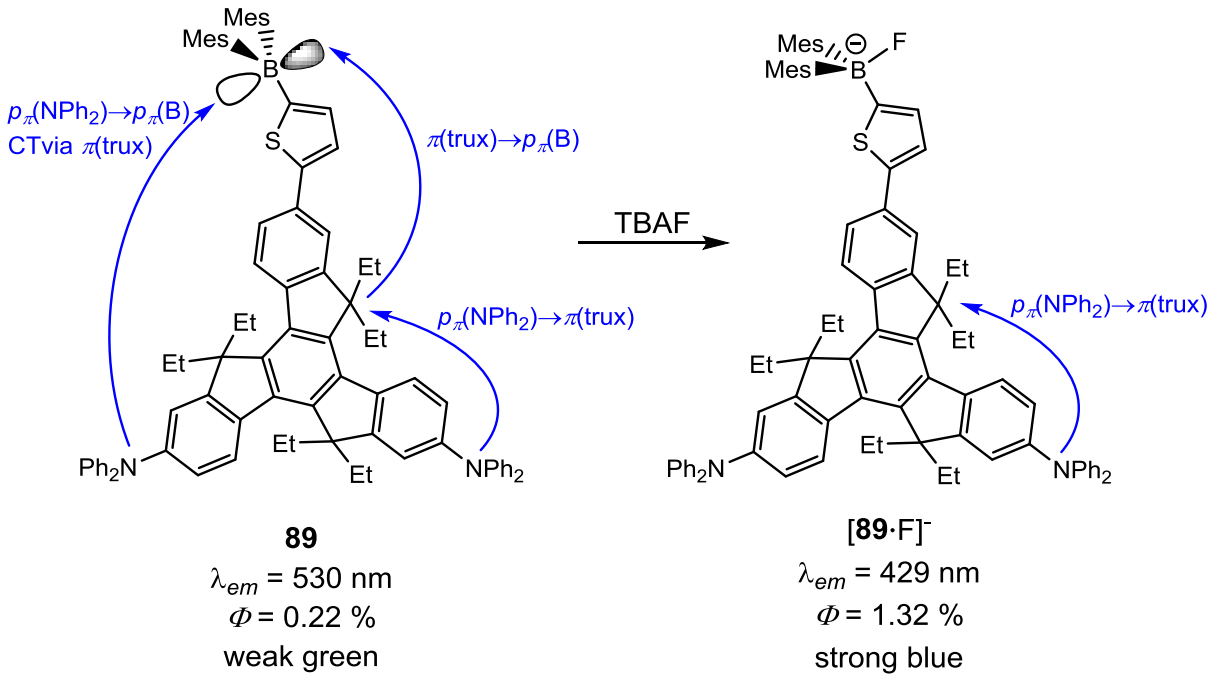

Figure 1.43: Reaction of **89** with TBAF (blue: photo-physical processes involved in fluorescence).

A rather elegant and efficient "turn-on" fluorescence system has been designed by Gabbaï *et al.* based on a simple BODIPY skeleton (Figure 1.44).[120] One fluoride of pyromethene-boron-difluoride was abstracted and replaced by the weakly coordinating dimethylaminopyridine (DMAP) to form the fluorescent [**90**·DMAP]$^+$ (λ_{em} = 525 nm).

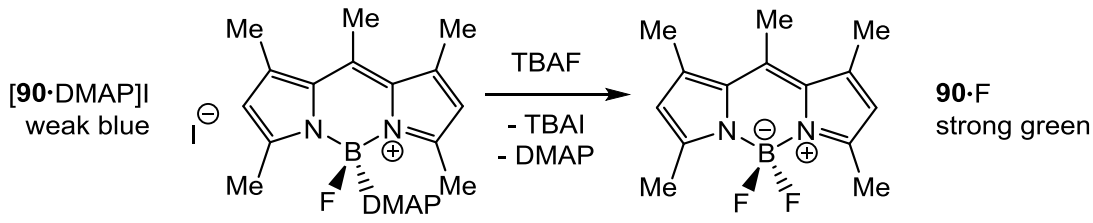

Figure 1.44: Formation of **90**·F by reaction of [**90**·DMAP]I with one equivalent of TBAF in $CHCl_3$.

The addition of 10 equivalents of iodide results in the quenching of the fluorescence, due to the external heavy atom effect. The recognition properties of [**90**·DMAP]$^+$ are not, however, impeded by ion pair formation. Hence addition of fluoride leads to the zwitterionic product **90**·F, and elimination of the iodide counter-ion thus gives a "turn-on" response, with an increase of the fluorescence by 500%.

1.4.3 Phosphorescence

Phosphorescence is formally a spin forbidden transition and is consistent with the rate of the intersystem crossing ($S_1 \rightarrow T_n$), a process that can be enhanced by a strong spin-orbit coupling from a heavy element (*e.g.* iridium, platinum or mercury). As with fluorescence, the luminescence properties of such systems can be tuned by disruption of the empty p_π-orbital of a conjugated tri-coordinate boron. Gabbaï *et al.* reported the first example of a phosphorescent anion sensor based on a heteronuclear B/Hg bidentate Lewis acid (Figure 1.45).[107]

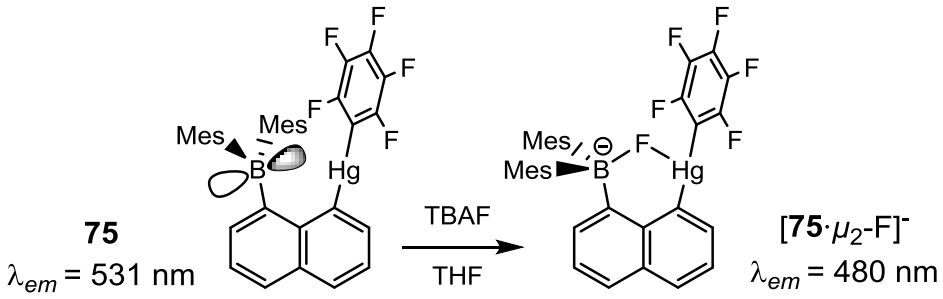

Figure 1.45: Reaction of the heteronuclear receptor **75** with TBAF.

In the solid state, receptor **75** give rises to a red phosphorescence (λ_{em}= 531 nm), but re-hybridisation of the boron on fluoride fixation blocks any $\pi \rightarrow \pi^*$ interactions between the mesityl and the naphthalene components. In the solid state the phosphorescence of the sequestered naphthalenediyl is shifted to a pale green color (λ_{em}= 480 nm).

1.4.4 Electrochemical Response

The empty p_π-orbital of the boron is amenable to one-electron reduction which can be probed by cyclic voltammetry (section 1.3.1). In the case of 1,8-bis(boryl)naphthalene systems, such as **69**, **70** and **71**, two distinct reduction waves are observed, while in the case of **76** a single reduction event is evident (Figure 1.46).[72,101]

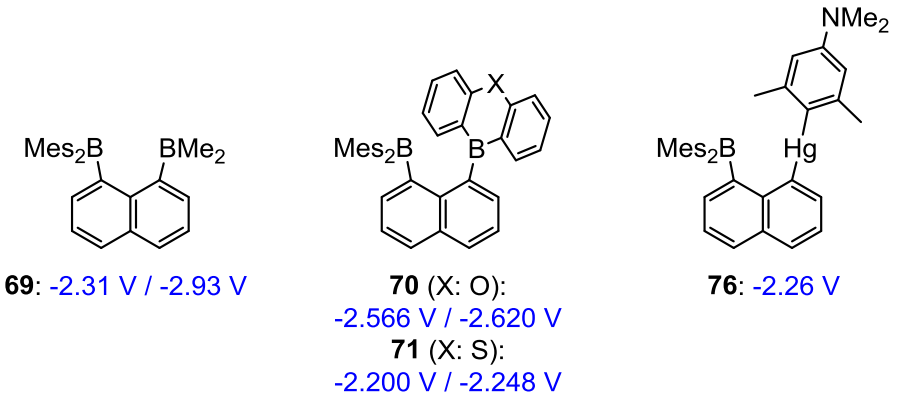

69: -2.31 V / -2.93 V

70 (X: O):
-2.566 V / -2.620 V
71 (X: S):
-2.200 V / -2.248 V

76: -2.26 V

Figure 1.46: Diboryl (**69** to **71**) and mercury-boryl (**76**) receptors with their respective half-cell reduction potentials. The redox potentials are given with respect to the Fc/Fc^+ couple.

The incremental addition of fluoride to **70** leads to the formation of the F-chelated product, a process which can be followed by cyclic or differential pulsed voltammetry, with parallel quenching of the two reduction waves in the homo-bidentate systems.

The redox potential of a pendant metal in close contact with the boryl substituent can also be used for monitoring the binding of cyanide or fluoride ions. Among others, ferrocene has been widely, *e.g.* in borylated metallocenes such as receptors **93** to **96** (Figure 1.47).[121,122] Addition of either fluoride or cyanide to the free receptors, shifts the Fe(II)/Fe(III) oxidation potential by roughly -550 mv (*e.g.* from +181 mV for **93** to -483 mV and -369 mV for [**93**·CN]$^-$ and [**93**·F]$^-$ respectively). The anodic shift of the free receptors with respect to ferrocene is due to the presence of the electron-withdrawing boryl binding site, and a major cathodic shift is measured once this unit is converted to the electron rich borate adduct.

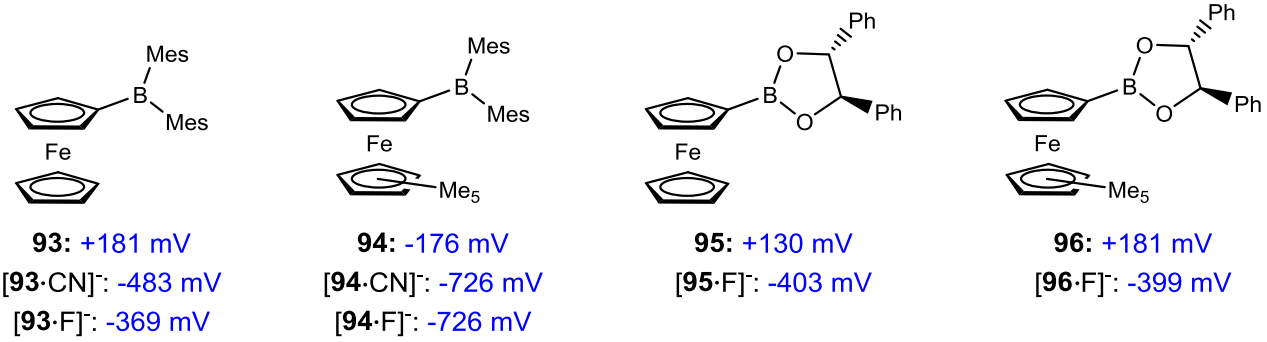

93: +181 mV
[**93**·CN]$^-$: -483 mV
[**93**·F]$^-$: -369 mV

94: -176 mV
[**94**·CN]$^-$: -726 mV
[**94**·F]$^-$: -726 mV

95: +130 mV
[**95**·F]$^-$: -403 mV

96: +181 mV
[**96**·F]$^-$: -399 mV

Figure 1.47: Receptors **93-96** with their respective anion adducts. The redox potentials are given against the FcH/FcH$^+$ couple.

Furthermore Shinkai *et al.* demonstrated how to exploit these dissociated redox potentials, by introducing a suitable redox active dye, thus the binding event can be signalled by an irreversible colour change.[123] This process relies on the fact that the more electron rich anionic adduct can reduce the dye while the free sensor cannot, as demonstrated by Broomsgrove and co-workers by combining the Lewis acid **94** with tetrazolium violet.[121] While **94** does not discriminate between cyanide and fluoride in MeCN/MeOH (>1000:1 vol.), the weaker Lewis acidic receptor **96** binds only fluoride under the same conditions, and use of the two systems in tandem thus gives a two-receptor logic gate.

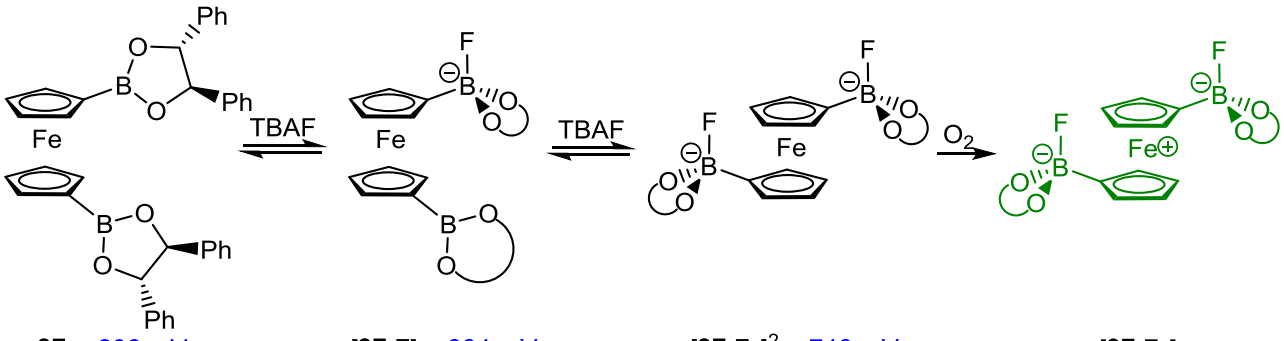

97: +206 mV
[**97**·F]$^-$: -384 mV
[**97**·F_2]$^{2-}$: -746 mV
[**97**·F_2]$^-$

Figure 1.48: Behaviour of ferrocenyl bis(boronic ester) (**97**) under incremental addition of fluoride. The redox potentials are given against the FcH/FcH$^+$ couple.

In some cases, the electrochemical shift of the iron centre is sufficient enough to be oxidised by molecular oxygen. For instance, ferrocenyl bis(boronic-ester) (**97**) sees its redox potential sequentially reduced from +206 mV for the free sensor, to -384 mV and -746 mV for

the mono and bis(fluoride) adducts in chloroform (Figure 1.48).[124] Once [**97**$^{\cdot}$$(F)_2]^{2-}$ is exposed to air the iron(II) centre is oxidised to iron(III) and the system undergoes an irreversible colour change from orange to green.

1.5. Outline Aims of DPhil project

The principal objective of this DPhil thesis at the outset was the synthesis of an air and moisture resistant system for the detection of either cyanide or fluoride in water. The two main influences were the work conducted by the Aldridge group at one end and the research directed by Gabbaï on the other. Ferrocenyl boranes have a long shelf life, and large changes in their photo and electrochemical properties upon binding cyanide or fluoride. Attempts to discriminate fluoride over cyanide by designing a chelating site met little success due to the inherent large angle offered by the cyclopentadienyl scaffold. But Gabbaï and co-workers were able to achieve fluoride chelation with system relying on a six membered ring scaffold. Hence the idea is to merge the two systems to obtain a series of receptors that combine the qualities of both approaches – *i.e.* the reporter output of a ferrocene-type system and the selectivity of a chelating framework based on a six-membered ring backbone.

The strategy, from a synthetic point of view, is to start with a simple ferrocenyl derivative with a pendant phenyl group bearing a boryl binding domain. Such a system would offer the possibility to appraise not only binding phenomena, but also the possibility for electronic communication between the borane and ferrocene centres (*e.g.* for electrochemical or colorimetric reporting). Once the scaffold properties is optimised with respect to communication with the reporter unit, the inclusion of a secondary binding site would be explored. The hypothesis is that the inclusion of a second proximal borane or other Lewis acid

centre should engender some degree of selectivity for fluoride, since fluoride can be readily chelated and cyanide cannot.

A secondary project area would be also develop utilising $FcB(C_6F_5)_2$ as the Lewis acidic borane. In combination with an appropriate Lewis base this system can be used for the detection of nitrous oxide and oxygen. The scope and outline mechanism of dioxygen capture by this and related systems would investigated by spectroscopic, electrochemical and crystallographic methods.

1.6. References

(1) W. E. Flood, *The Origins of Chemical Names* **1963**, London: Oldbourne Book Co.

(2) D. C. Gadsby, P. Vergani and L. Csanády, *Nature* **2006**, 440, 477.

(3) J. L Sessler, P. Gale, W.-S. Cho, "*Anion Receptor Chemistry: RSC (Monographs in Supramolecular Chemistry)*", **2006**, RSC Publishing 1edn, Cambridge (UK).

(4) D. W. Smith, *J. Chem. Ed.* **1977**, 54, 540.

(5) Centers for Disease Control and Prevention (CDC), *Morbidity and Mortality Weekly Report*, **August 17, 2001**, 50(RR14).

(6) The United Nations Children's Fund, *Water Front* **1999**, issue 13.

(7) (*a*) R. J Carton, *Fluoride* **July-September 2006**, 39, 163. (*b*) US Department of Health and Human Services: Agency for Toxic Substances and Disease Registry, **September 2003**, *Toxicological Profile for Fluorides, Hydrogen Fluoride and Fluorine.*

(8) C. R. Wade, A. E. J. Broomsgrove, S. Aldridge and F P Gabbaï, *Chem. Rev.* **2010**, 110, 3958.

(9) (*a*) F. J. Baud, *Human & Experimental Toxicology* **2007**, *26*, 191. (*b*) Centers for Disease Control: Agency for Toxic Substances and Disease Registry, Toxicological Profiles: Cyanide (PB2007-100674).

(10) M. A. Holland, L. M. Kozlowski, *Clin. Pharm.* **1986**, 5, 737.

(11) World Health Organisation, *Report on Chemical hazards in drinking-water,* WHO/HSE/WSH/09.01/3.

(12) F. R. Sidell, E. T. Takafuji D. R. Franz, *Medical Aspects of Chemical and biological warfare*, Office of The Surgeon General Department of the Army, United States of America, **1997**.

(13) J. M. Lehn, *Science* **1993**, 260, 1762.

(14) (*a*) H. E. Simmons and C. H. Park, *J. Am. Chem. Soc.* **1968**, 90, 2428. (*b*) C. H. Park and H. E. Simmons, *J. Am. Chem. Soc.* **1968**, 90, 2431.

(15) R. Custelcean, *Chem. Soc. Rev.* **2014**, 43, 1813.

(16) C. Augustin de Coulomb, "*mémoire sur l'électricité et le magnétisme*," *Histoire de l'Académie Royale des Sciences*, **1785**.

(17) (*a*) F. P. Schmidtchen, *Angew. Chem.* **1977**, 89, 751; *Angew. Chem. Int. Ed. Engl.* **1977**, 16, 720. (*b*) F. P. Schmidtchen, *Chem. Ber.* **1980**, 113, 864. (*c*) F. P. Schmidtchen, *Chem. Ber.* **1981**, 114, 597. (*d*) F. P. Schmidtchen and G. Muller, *J. Chem. Soc. Chem. Commun.* **1984**, 1115. (*e*) K. Worm, F. P. Schmidtchen, A. Schier, A. Schäfer and M. Hesse, *Angew. Chem.* **1994**, 106, 360; *Angew. Chem. Int. Ed. Engl.* **1994**, 33, 327. (*f*) K. Worm and F. P. Schmidtchen, *Angew. Chem.* **1995**, 107, 71; *Angew. Chem. Int. Ed. Engl.* **1995**, 34, 65.

(18) V. Amendola, L. Fabbrizzi, and E. Monzani *Chem. Eur. J.* **2004**, 10, 76.

(19) O. B. Berryman, V. S. Bryantsev, D. P. Stay, D. W. Johnson and B. P. Hay, *J. Am. Chem. Soc.* **2007**, 129, 48.

(20) (*a*) Y. S. Rosokha, S. V. Lindeman, S. V. Rosokha, J. K. Kochi, *Angew. Chem. Int. Ed.* **2004**, *43*, 4650. (*b*) S. Demeshko, S. Dechert, F. Meyer, *J. Am. Chem. Soc.* **2004**, *126*, 4508.

(21) Frisch *et al. Gaussian 03*, revision B.05; Gaussian, Inc.: Pittsburgh PA, **2003**.

(22) (*a*) C. S. Campos-Fernandez, R. Clerac, K. R. Dunbar, *Angew. Chem. Int. Ed.* **1999**, 38, 3477. (*b*) C. S. Campos-Fernandez, R. Clerac, J. M. Koomen, D. H. Russell, K. R. Dunbar, *J. Am. Chem. Soc.* **2001**, 123, 773.

(23) C. Garau, D. Quinonero, A. Frontera, A. Costa, P. Ballester, P. M. Deya, *Chem. Phys. Let.* **2003**, 370, 7.

(24) (*a*) D. Best, S. L. Tobey and E. V. Anslyn, *Coord. Chem. Rev.*, **2003**, 240, 3. (b) J. M. Llinares, D. Powell and K. Bowman-James, *Coord*. *Chem. Rev.*, **2003**, 240, 57. (*c*) K. A. Schug and W. Lindner, *Chem. Rev.*, **2005**, 105, 67. (*d*) J. Yoon, S. K. Kim, N. J. Singh and K. S. Kim, *Chem. Soc. Rev.*, **2006**, 35, 355. (*e*) P. Blondeau, M. Segura, R. Perez-Fernandez and J. de Mendoza, *Chem. Soc. Rev.*, **2007**, 36, 198. (*f*) Z. Xu, S. K. Kim and J. Yoon, *Chem. Soc. Rev.*, **2010**, 39, 1457. (*g*) E. Garcia-Espana, P. Diaz, J. M. Llinares and A. Bianchi, *Coord. Chem. Rev.* **2006**, 250, 2952. (*h*) Schmuck, *Coord. Chem. Rev.* **2006**, 250, 3053.

(25) (*a*) Paul W. K. Rothemund, *Nature* **2006**, 440, 297. (*b*) P. W. K. Rothemund, *J. Am. Chem. Soc.* **2004**, 26, 16344.

(26) A.E. Reed, L.A. Curtiss and F. Weinhold, *Chem. Rev.* **1988**, 88, 899.

(27) A. D. W. McNaught, A. *IUPAC. Compendium of Chemical Terminology, 2nd ed. (the "Gold Book")*; Blackwell Scientific Publications Oxford, **1997**.

(28) H. Umeyama and K. Morokuma, *J. Am. Chem. Soc.* **1977**, 99, 1316.

(29) K. Kitaura and K. Morokuma, *International Journal of Quantum Chemistry* **1976**, 10, 325.

(30) (*a*) M. Dreyfus and A. Pullman, *Theoret. Chim. Acta.* **1970**, 19, 20. (*b*) M. Dreyfus, B. Maigret, and A. Pullman, *Theoret. Chim. Acta.* **1970**, 17, 109.

(31) R. A. Pascal, J. Spergel, D. V. Engbersen, *Tetrahedron Lett.* **1986**, 27, 4099.

(32) J. Yoo, M.-S. Kim, S.-J. Hong, J. L. Sessler and C.-H. Lee, *J. Org. Chem.* **2009**, 74, 10655.

(33) S. Ok Kang, V. W. Day, and K. Bowman-James, *J. Org. Chem.* **2010**, 75, 277.

(34) (*a*) P. A. Gale, N. Busschaert, C. J. E. Haynes, L. E. Karagiannidis and Isabelle L. Kirby, *Chem. Soc. Rev.* **2014**, 43, 205. (*b*) L. E. Santos-Figueroa, M. E. Moragues, E. Climent, Alessandro Agostini, R. Martınez-Manez and F. Sancenon, *Chem. Soc. Rev.* **2013**, 42, 3489. (*c*) G. T. Spence and P. D. Beer, *Acc. Chem. Res.* **2013**, 46, 571. (*d*) L. Adriaenssensa and P. Ballester, *Chem. Soc. Rev.,* **2013**, 42, 3261. (*e*) M. E. Moragues, R. Martinez-Manez and F. Sancenon, *Chem. Soc. Rev.* **2011**, 40, 2593. (*f*) A. Caballero, F. Zapata and P. D. Beer, *Coord. Chem. Rev.* **2013**, 257, 2434. (*g*) M. J. Langton and P. D. Beer, *Acc. Chem. Res.* **2014**, 47, 1935.

(35) M. R. Sambrook, P. D. Beer, J. A. Wisner, R. L. Paul, A. R. Cowley, *J. Am. Chem. Soc.* **2004**, 126, 15364.

(36) N. G. White and P. D. Beer, *Chem. Commun.* **2012**, 48, 8499.

(37) Matthew J. Langton, Lucy C. Duckworth and Paul D. Beer, *Chem. Commun.* **2013**, 49, 8608.

(38) (*a*) O. Hassel and C. Romming, *Q. Rev. Chem. Soc.* **1962**, 16, 1. (*b*) O. Hassel, K. O. Stromme, *Nature* **1958**, 182, 1155. (*c*) O. Hassel, *Science* **1970**, 170, 497.

(39) (*a*) M.-C. Bernard-Houplain and C. Sandorfy, *Can. J. Chem.* **1973**, 51, 3640. (*b*) T. Di Paolo and C. Sandorfy, *Can. J. Chem.* **1974**, 52, 3612.

(40) (*a*) P. Murray-Rust and W. D. S. Motherwell, *J. Am. Chem. Soc.* **1979**, 101, 4374. (*b*) P. Murray-Rust, W. C. Stallings, C. T. Monti, R. K. Preston and J. P. Glusker, *J. Am. Chem. Soc.* **1983**, 105, 3206. (*c*) N. Ramasubbu, R. Parthasarathy and P. Murray-Rust, *J. Am. Chem. Soc.* **1986**, 108, 4308.

(41) T. Brinck, J. S. Murray and P. Politzer, *Int. J. Quantum Chem.: Quantum Biol. Symp.* **1992**, 19, 57.

(42) (*a*) P. Politzer,P. Lane,M. C. Concha, Y. Ma and J. S. Murray, *J. Mol. Model.* **2007**, 13, 305. (*b*) T. Clark, M. Hennemann, J. S. Murray and P. Politzer *J. Mol. Model.* **2007**, 13, 291. (*c*) T. Clark, *Comput. Mol. Sci.* **2013**, 3, 13. (*d*) P. Politzer, J. S. Murray and T. Clark *Phys. Chem. Chem. Phys.* **2013**, 15, 11178.

(43) T. M. Beale, M. G. Chudzinski, M. G. Sarwar and M. S. Taylor *Chem. Soc. Rev.* **2013**, 42, 1667.

(44) F. Zapata, A. Caballero, N. G. White, T. D. W. Claridge, P. J. Costa, V. Feĺix and P. D. Beer, *J. Am. Chem. Soc.* **2012**, 134, 11533.

(45) B. R. Mullaney, A. L. Thompson, and P. D. Beer, *Angew. Chem. Int. Ed.* **2014**, 53, 11458.

(46) G. N. Lewis, *Valence and the structure of atoms and molecules*; Chemical Catalogue Company: New York, **1923**.

(47) (*a*) R. Pearson, *J. Am. Chem. Soc.* **1963**, 85, 3533. (*b*) R. Pearson, *J. Chem. Educ.* **1968**, *45*, 581 (Part I) and *J. Chem. Educ.* **1968**, *45*, 643 (Part II).

(48) H. Tien Ngo, X. Liu and K. A. Jolliffe, *Chem. Soc. Rev.* **2012**, 41, 4928.

(49) E. J. O'Neil, B. D. Smith, *Coord. Chem. Rev.* **2006**, 250, 3068.

(50) B. Ahlers, K. Cammann, S. Warzeska and R. Krämer, *Angew. Chem. Int. Ed.* **1996**, *35*, 2141.

(51) V. Amendola, E. Bastianello, L. Fabbrizzi, C. Mangano, P. Pallavicini, A. Perotti, A. Mannotti Lanfredi and F. Ugozzoli, *Angew. Chem. Int. Ed.* **2000**, 39, 2917.

(52) C. J. Harding, V. McKee, J. Nelson and Q. Lu, *J. Chem. Soc., Chem. Commun.* **1993**, 1768.

(53) (*a*) D. Bond, S. Derossi, C. J. Harding, E. J. L. McInnes, V. McKee, C. J. McKenzie, J. Nelson and J. Wolowska, *Dalton Trans.* **2005**, 2403. (*b*) T. Lu, X. Zhuang, Y. Li, and S. Chen, *J. Am. Chem. Soc.* **2004**, 126, 4760.

(54) (*a*) [**24**·F]⁻: M. J. Bayer, Satish S. Jalisatgi, B. Smart, A. Herzog, C. B. Knobler and M. F. Hawthorne, *Angew. Chem. Int. Ed.* **2004**, 43, 1854. (*b*) [**24**·Cl]⁻: X. Yang, C. B. Knobler and M. F. Hawthorne, *Angew. Chem. Int. Ed.* **1991**, 30, 1507. (*c*) [**24**·Br]⁻: X. Yang, C. B. Knobler, Z. Zheng, M. F. Hawthorne, *J. Am. Chem. Soc.* **1994**, 116, 7142. (*d*) [**24**·I_2]$^{2-}$: Z. Zheng, C. B. Knobler, M. D. Mortimer , G. Kong , and M. F. Hawthorne, *Inorg. Chem.* **1996**, 35, 1235.

(55) X. Yang, Z. Zheng, C. B. Knobler and M. F. Hawthorne, *J. Am. Chem. Soc.* **1993**, 115, 193.

(56) (*a*) G. N. Lewis ,*J. Am. Chem. Soc.* **1916**, 38, 762. (*b*) I. Langmuir, *J. Am. Chem. Soc.* **1919**, 41, 868.

(57) L. Pauling, *The Nature of the Chemical Bond 2nd edition*, 145, Cornell Univ.Press, **1940**.

(58) (*a*) J. G. Malm, H. Selig, J. Jortner, and S. A. Rice, *Chem. Rev.* **1965**, 65, 199. (*b*) A. E. Reed and P. V. R. Schleyer, *J. Am. Chem. Soc.* **1990**, 112, 1434. (*c*) J. I. Musher, *Angew. Chem. Int. Ed.* **1969**, 8, 54.

(59) (*a*) J. C. Martin, *Science* **1983**, 221, 509. (*b*) M. Yamashita, Y. Yamamoto, K.-Y. Akiba, D. Hashizume, F. Iwasaki, N. Takagi and S. Nagase, *J. Am. Chem. Soc.* **2005**, 127, 4354.

(60) (*a*) R. E. Rundle, *J. Am. Chem. Soc.*, **1947**, *69*, 1327. (*b*) R. J. Hach, and R. E. Rundle, *J. Am. Chem. Soc.* **1951**, 73, 4321.

(61) G. Pimentel, *J. Chem. Phys.* **1951**, *19*, 446.

(62) (*a*) M. Newcomb, M. T. Wanda, Y. Azuma, and T. J. Delord, *J . Chem. Soc., Chem. Commun.* **1984**, 1159. (*b*) M. Newcomb, J. H. Horner, and M. T. Blanda, *J. Am. Chem.* Soc. **1987**, 109*,* 7878. (*c*) M. Newcomb and M. T. Blanda *Tetrahedron Letters* **1988**, 29, 4261.

(63) (*a*) S. Aoyagi, K. Tanaka, I. Zicmane and Y. Takeuchi, *J. Chem. Soc., Perkin Trans. 2* **1992**, 2217. (*b*) K. Ogawa, S. Aoyagi and Y. Takeuchi, *J. Chem. Soc., Perkin Trans. 2* **1993**, 2389.

(64) R. Altmann, K. Jurkschat, M. Schürmann, D. Dakternieks and A. Duthie, *Organometallics* **1998**, 17, 5858.

(65) K. Tamao, T. Hayashi and Y. Ito, *J Organomet. Chem.* **1996**, 506, 85.

(66) C. I. M. Santos, E. Oliveira, J. F. B. Barata, M. Amparo, F. Faustino, J. A. S. Cavaleiro, M. Graça, P. M. S. Neves and C. Lodeiro, *J. Mater. Chem.* **2012**, 22, 13811.

(67) I.-S. Ke, M. Myahkostupov, F. N. Castellano and F. P. Gabbaï, *J. Am. Chem. Soc.* **2012**, 134, 15309.

(68) M. Hirai and F. P. Gabbaï *Chem. Sci.* **2014**, 5, 1886.

(69) (*a*) Y. Zhou, J. Feng Zhang, and J. Yoon, *Chem. Rev.* **2014**, 114, 5511. (*b*) Z. Xu, X. Chen, H. Na Kim and J. Yoon, *Chem. Soc. Rev.* **2010**, 39, 127.

(70) See F. A. Cotton, G. Wilkinson, C. A. Murillo, M. Bochmann, *Advanced Inorganic Chemistry*, 6th edn., Wiley, New York, **1999**, 165 for examples.

(71) A. Timoshkin and G. Frenking, *Organometallics* **2008**, 27, 371.

(72) M. Melaïmi, S. Solé, C.-W. Chiu, H. Wang and F. P. Gabbaï, *Inorg. Chem.* **2006**, 45, 8136.

(73) A. Schulz und W. Kaim, *chem. Ber.* **1989**, 122, 1863.

(74) S. A. Cummings, M. Iimura, C. J. Harlan, R. J. Kwaan, I. Vu Trieu, J. R. Norton, B. M. Bridgewater, F. Jäkle, A. Sundararaman and M. Tilset, *Organometallics* **2006**, 25, 1565.

(75) J. F. Blount, P. Finocchiaro, D. Gust, K. Mislow, *J. Am. Chem. Soc.* **1973**, 95, 7019.

(76) S. Yamaguchi, S. Akiyama, and K. Tamao, *J. Am. Chem. Soc.* **2000**, 122, 6335.

(77) C. Bresner, C. J. E. Haynes, D. A. Addy, A. E. J. Broomsgrove, P. Fitzpatrick, D. Vidovic, A. L. Thompson, I. A. Fallis and S. Aldridge, *New J. Chem.* **2010**, 34, 1652.

(78) S. Solé and F. P. Gabbaï, *Chem. Commun.* **2004**, 1284.

(79) S. Yamaguchi, S. Akiyama and K. Tamao, *J. Am. Chem. Soc.* **2001**, 123, 11372.

(80) D. Cao, H. Zhao and F. P. Gabbaï, *New J. Chem.* **2011**, 35, 2299.

(81) A. Y. Timoshkin and G. Frenking, *Organometallics* **2008**, 27, 371.

(82) A. Y. Nazarenko and V. N. Nemykin, *Cryst. Eng. Comm.* **2011**, 13, 6352.

(83) F. Zettler, H. D. Hausen and H. Hess, *J. Organomet. Chem.* **1974**, 72, 157.

(84) A. E. Ashley, T. J. Herrington, G. G. Wildgoose, H. Zaher, A. L. Thompson, N. H. Rees, T. Krämer and D. O'Hare, *J. Am. Chem. Soc.* **2011**, 133, 14727.

(85) H. Zhao, J. H. Reibenspies and F. P. Gabbaï, *Dalton Trans.* **2013**, 42, 608.

(86) A. J. V. Marwitz, J. L. Dutton, L. G. Mercier and W. E. Piers, *J. Am. Chem. Soc.* **2011**, 133, 10026.

(87) J. Zhou, S. J. Lancaster, D. A. Walker, S. Beck, M. Thornton-Pett and M. Bochmann, *J. Am. Chem. Soc.* **2001**, 123, 223.

(88) J. Oh Huh, H. Kim, K. Mun Lee, Y. Sup Lee, Y. Do and M. Hyung Lee, *Chem. Commun.* **2010**, 46, 1138.

(89) (*a*) C. Hansch, A. Leo and R. W. Taft, *Chem. Rev.* **1991**, 91, 165. (*b*) V. I. Bregadze, *Chem. Rev.* **1992**, 92, 209.

(90) S. Miyasaka, J. Kobayashi and T. Kawashima, *Tet. Lett.* **2009**, 50, 3467.

(91) X. Yin, J. Chen, R. A. Lalancette, T. B. Marder, and F. Jäkle, *Angew. Chem. Int. Ed.* **2014**, 126, 9919.

(92) C.W. Chiu, Y. Kim and F. P Gabbaï, *J. Am. Chem. Soc.* **2009**, 131, 60.

(93) C.-W. Chiu and F. P. Gabbaï, *J. Am. Chem. Soc.* **2006**, 128, 14248.

(94) C.-W. Chiu and F. P. Gabbaï, *Dalton Trans.* **2008**, 814.

(95) Q. Zhao, F. Li, S. Liu, M. Yu, Z. Liu, T. Yi and C. Huang, *Inorg. Chem.* **2008**, 47, 9256.

(96) C. R. Wade and F. P. Gabbaï, *Inorg. Chem.* **2010**, 49, 714.

(97) D. Cao, H. Zhao and F. P. Gabbaï, *New J. Chem.,* **2011**, 35, 2299.

(98) D. F. Shriver and M. J. Biallas, *J. Am. Chem. Soc.* **1967**, 86, 1078.

(99) R. W. Alder, P. S. Bowman, W. R. S. Steele and D. R. Winterman, *Chem. Commun. (London)*, **1968**, 723.

(100) H. E. Katz, *J. Org. Chem.* **1985**, 50, 5027.

(101) (*a*) J. D. Hoefelmeyer and F. P. Gabbaï, *Organometallics* **2002**, 21, 982. (*b*) C. L. Dorsey, Pawel Jewula, T. W. Hudnall, J. D. Hoefelmeyer, T. J. Taylor, N. R. Honesty, C.-W. Chiu, M. Schulte and F. P. Gabbaï, *Dalton Trans.* **2008**, 4442.

(102) H. Zhao and F. P. Gabbaï, *Organometallics* **2012**, 31, 2327.

(103) (*a*) V. Clifford Williams, W. E. Piers, W. Clegg, M. R. J. Elsegood, S. Collins and T. B. Marder, *J. Am. Chem. Soc.* **1999**, *121,* 3244. (*b*) V. C. Williams, G. J. Irvine, W. E. Piers, Z. Li, S. Collins, W. Clegg, M. R. J. Elsegood and T. B. Marder, *Organometallics* **2000**, *19,* 1619. (*c*) S. P. Lewis, N. J. Taylor, W. E. Piers and S. Collins, *J. Am. Chem. Soc.* **2003**, 125, 14686. (*d*) P. A. Chase, L. D. Henderson, W. E. Piers, M. Parvez, W. Clegg and M. R. J. Elsegood, *Organometallics* **2006,** *25,* 349.

(104) I. Krossing, and I. Raabe, *Chem. Eur. J.* **2004**, 10, 5017.

(105) (*a*) G. E. Herberich, A. Fischer and D. Wielbelhaus, *Organometallics* **1996**, 15, 3106. (*b*) G. E. Herberich, U. Englert, A. Fischer and D. Wiebelhaus, *Eur. J. Inorg. Chem.* **2004**, 4011.

(106) M. Hyung Lee and F. P. Gabbaï, *Inorg. Chem.* **2007**, 46, 8132.

(107) M. Melaimi and F. P. Gabbaï, *J. Am. Chem. Soc.* **2005**, 127, 9680.

(108) H. Zhao and F. P. Gabbaï, *Nat. Chem.* **2010**, 2, 984.

(109) M. Mantina, A. C. Chamberlin, R. Valero, C. J. Cramer and D. G. Truhlar, *J. Phys. Chem. A* **2009**, 113, 5806.

(110) Y. Kim, H. Zhao and F. P. Gabbaï, *Angew. Chem. Int. Ed.* **2009**, 48, 4957.

(111) P. D. Beer and P. A. Gale, *Angew. Chem. Int. Ed.* **2001**, 40, 486.

(112) S. Yamaguchi, S. Akiyama and K. Tamao, *J. Am. Chem. Soc.* **2001**, 123, 11372.

(113) X. Y. Liu, D. R. Bai and S. Wang, *Angew. Chem. Int. Ed. Engl.* **2006**, 45, 5475.

(114) C. R. Wade and F. P. Gabbaï, *Dalton Trans.* **2009**, 9169.

(115) T. W. Hudnall and F. P Gabbaï, *J. Am. Chem. Soc.* **2007**, 129, 11978.

(116) (*a*) M. Hyung Lee, T. Agou, J. Kobayashi, T. Kawashima and F. P. Gabbaï, *Chem. Commun.* **2007**, 1133. (*b*) Y. Kim, H.-S. Huh, M. Hyung Lee, I. L. Lenov, H. Zhao, and F. P. Gabbaï, *Chem. Eur. J.* **2011**, 17, 2057.

(117) Y. Li, Y. Kang, J.-S. Lu, I. Wyman, S.-B. Ko, and S. Wang, *Organometallics* **2014**, 33, 964.

(118) H. Li, Roger, A. Lalancette and F. Jäkle, *Chem. Commun.* **2011**, 47, 9378.

(119) M.-A. Yuan, Q. Wang, D.-E. Wang, J. Wang and J. Wang, *Analyst* **2014**, 139, 1541.

(120) T. W. Hudnall and F. P. Gabbaï, *Chem. Commun.* **2008**, 4596.

(121) A. E. J. Broomsgrove, D. A. Addy, C. Bresner, I. A. Fallis, A. L. Thompson and S. Aldridge, *Chem. Eur. J.* **2008**, 14, 7525.

(122) C. Bresner, J. K. Day, N. D. Coombs, I. A. Fallis, S. Aldridge, S. J. Coles and M. B. Hursthouse, *Dalton Trans.* **2006**, 3660.

(123) H. Yamamoto, A. Ori, K. Ueda, C. Dusemund and S. Shinkai, *Chem. Commun.* **1996**, 407.

(124) J. K. Day, C. Bresner, N. D. Coombs, I. A. Fallis, L.-L. Ooi and S. Aldridge, *Inorg. Chem.* **2008**, 47, 793.

CHAPTER 2: Experimental techniques

2.1. General Remarks on Reaction Conditions

Some of the reagents/intermediates used in this thesis were highly sensitive to both air and moisture. So unless otherwise stated, it can be assumed that an inert atmosphere and high vacuum techniques were employed as an alternative to bench-top methods.

Handling and storage of air- and moisture-sensitive solids was accomplished within a glove box, while solution-phase manipulations were performed with a standard dual-manifold Schlenk line.[1] Both systems offer an inert atmosphere of anhydrous nitrogen gas in which to store and handle sensitive compounds. Schlenk line techniques have been used since the 19th Century and are used to lower the risk of oxidation or hydrolysis.[2] A typical Schlenk line consists of dual Pyrex glass manifold; one manifold is evacuated and maintained under high vacuum (10^{-3} mBar) provided by a Trivac® Rotary Vane, oil sealed pump, which was monitored by Edwards® Pirani gauge attached to a Edwards® digital gauge controller. The second manifold was under positive pressure of dry nitrogen gas and vented through a mercury bubbler allowing for pressure slightly greater than atmospheric. In order to create a dry and oxygen free environment successive "pump and purge" cycles were performed. The reaction vessel was subjected to three cycles of evacuation and filling with nitrogen, and thoroughly "flamed out" with a Bunsen burner on the first vacuum cycle. Liquids were transferred either *via* cannulae or syringes, preventing exposure to the atmosphere. For the handling of solids two types of glove boxes were used, a Saffron® Omega Scientific glove-box or a Vacuum Atmospheres® Dri-Lab. For both, the atmosphere was scrubbed by passing through activated copper metal and activated molecular sieves to remove oxygen and water, respectively. Reactants and apparatus were transferred into the box via a side port to which the standard "pump and purge" method was applied.

2.2. Physical Measurements

2.2.1. *Nuclear Magnetic Resonance (NMR) Spectroscopy*

NMR spectra were measured on a Varian® 'Mercury' or 'Venus' 300 MHz, a Varian® 'Unity' 500 FT-NMR or a Bruker® 400 MHz spectrometer. For ^{1}H and ^{13}C NMR spectra, signals were referenced to the residual solvent signal of the deuterated solvent;[3] ^{11}B, ^{19}F and ^{31}P NMR spectra were referenced against $BF_3{\cdot}OEt_2$, $CFCl_3$ and 85% H_3PO_4 in H_2O respectively. Air-sensitive solutions were prepared in Young's NMR tubes.

2.2.2. *X-ray crystallography*

All single X-ray crystal structures determinations were performed by the author. Diffraction data were collected using a Nonius Kappa® CCD or Oxford Diffraction (Agilent®) SuperNova diffractometer at 150 K;[4] data were reduced using either DENZO, SCALEPACK or CrysAlisPro.[5] The structures were solved with either SIR92[6] or SuperFlip[7] and refined with full-matrix least squares within CRYSTALS[8] as described in the CIF.

2.2.3. *Raman spectroscopy*

The Raman spectra were recorded on an inVia Raman Microscope by Renishaw, fitted with a 514 nm Flexible Laser Solutions Modu-Laser and a Leica DMLM microscope platform. Spectra were acquired for 10 s at 50 % of the laser intensity, resulting in 15 mW laser power. For solid-state acquisition, a Realtime Analyzers with a 1064 nm portable Raman system (~70 mW) with an exposure time of 80 seconds was generally used. All spectra were collected at 8 cm^{-1} resolution from 250 to 3311 cm^{-1}.

2.2.4. *Elemental analyses*

Elemental analyses were carried out by Stephen Boyer at London Metropolitan University using a Carlo Erba® CE1108 Elemental Analyser.

2.2.5. *Mass spectrometry (MS)*

Neutral samples were submitted to the EPSRC National Mass Spectrometry Service Centre, Swansea University and to Colin Sparrow, University of Oxford for EI measurements. Charged compounds were analysed using a Bruker® MicroTOF ESI mass spectrometer connected to a glove box via PEEK tubing.[9] These ESI mass spectrometry measurements were carried out by Mr Joe Abdalla of the Aldridge research group.

2.2.6. *pH titrations*

The pH titrations were recorded using a microprocessor pH meter, HANNA® pH 210 with a glass body pH Electrode and a temperature probe. The instrument was calibrated using three buffer solutions at pH = 4.01, 7.01 and 10.01.

2.2.7. *DFT and TD-DFT*

DFT calculations were performed by Mr Joe Abdalla of the Aldridge group. Calculations of the energy levels were carried out using the Amsterdam Density Functional (ADF 2012) Software Package.[10]

2.2.8. *Electrochemistry*

Electrochemical measurements were performed within a Saffron Omega Scientific glovebox under anhydrous Nitrogen on a PARAMETEK® VersaSTAT3 potentiostat. Cyclic voltammetry measurements were carried out as outlined in the literature, with a silver quasi-

reference electrode, a glassy-carbon working electrode and a platinum auxiliary electrode, all sourced from Bioanalytical Systems®. The supporting electrolyte for the measurements was a 0.1 M solution of tetrabutylammonium hexafluorophosphate in tetrahydrofuran. The quasi-reference electrode was immersed in the electrolyte solution for 48 h prior to the experiment and the nickelocene / nickelocenium couple was used as an internal reference. Redox potentials were subsequently re-calibrated to the ferrocene/ferrocenium (Fc/Fc^+) system (ΔE = -379 mV)[11] CV experiments were typically performed at three different scan rates of 0.05, 0.1 and 1.0 V s^{-1}.

2.2.9. *Ultra-violet and Visible Spectroscopy (UV-Vis)*

UV-Vis spectra were measured using a Scintio UV S-2100 UV-Vis spectrometer or a Perkin Elmer Lambda750S spectrometer using Spectrosil® or quartz cuvettes. Air-sensitive samples were prepared in a J. Young's tap-adapted Spectrosil® cuvette inside a glovebox or on a Schlenk line.

2.2.10. *UV/Vis binding constant determination*

Binding constants were determined by titration using UV/Vis spectra measured for a tetrahydrofuran solution. A stock solution of receptor was prepared (typically 20 mg in 20 mL), from which exactly 3 mL was transferred to a UV cuvette (Spectrosil® or quartz). A first absorption spectrum of the free receptor was measured and then aliquots of a TBAF or TBACN solution were added. Supplementary additions to the cuvette of these solutions of known concentration were accomplished until a total of at least 2.5 equivalents was reached. The binding constants were typically fitted to a 1:1 binding isotherm taking the dilution into account in the calculations, using the REACTLAB™ software package of Jplus Consulting®. The program uses 100 points from the UV-vis spectral data, centred on the maximum absorption

of the receptor, in order to minimize the margin of error. Furthermore the calculations were performed over four sets of measurements with different weights.

2.3. Preparation and Purification of Starting Materials

2.3.1 Purification of Solvents and Reagents

Commercially available materials used in chemical reactions described in this thesis are listed in Appendix A1, which also includes details of the commercial supplier, the purity of the material supplied and whether any further purification was required before use. All air- and/or moisture-sensitive reagents were stored under inert atmosphere, with liquids contained in ampoules and solids stored in a Saffron Omega Scientific glove-box. All solvents for inert-atmosphere chemistry were sparged with anhydrous nitrogen for 30 min and then stored in ampoules. Compounds already reported in the literature but prepared by a different procedure are described in this section; in most cases the adaptation led to better yields and/or easier scaling up processes.

2.3.2 Synthesis of Starting Materials

Tris(pentafluorobenzene)borane (BCF)

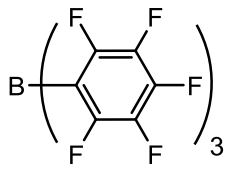

Following the work of Wang *et al.*[12]: a 1.6 M hexane solution of ^{n}BuLi (31.0 mL, 50.0 mmol) was added dropwise to a stirred solution of BrC_6F_5 (12.35 g, 50.0 mmol) in pentane at -78 °C.

The reaction mixture was stirred at -78 °C for 1 h being careful to keep the temperature low (LiC_6F_5 is explosive above -50 °C). A 1.0 M heptane solution of BCl_3 (16.7 mL, 16.7 mmol) was then added rapidly and the mixture was stirred at -78 °C for a further 3 h. The mixture was allowed to warm to room temperature over a period of 12 h. After filtration and concentration, the solution was cooled to -30 °C to a yield a white precipitate of $B(C_6F_5)_3$. ^{11}B and ^{19}F NMR spectra were in good agreement with literature data.[12]

Fluorodimesytilborane ($FBMes_2$)

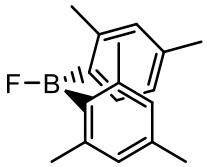

Following the work of Eisch *et al.*[13] 2-bromomesitylene (50.36 mL, 0.329 mol) in thf (300 mL) added onto magnesium turnings (8.0 g, 0.329 mol) over 1 h was then refluxed for a further 2h. The resulting solution was filtered, diluted with thf (250 mL) and cooled down to -78 °C. Boron trifluoride diethyl etherate (20.7 mL, 0.166 mol) was the added to the cold solution was warmed to room temperature over 12 h. The mixture was filtered and the solid extracted with hexane. The combined organic extracts were pumped down in vacuo yielding a white solid. The resulting solid was extracted with hexane which was subsequently removed under reduce pressure to yield a white solid. Yield: 32.13 g, 72%. ^1H, ^{19}F and ^{11}B NMR spectra were in agreement with literature data.[13]

(Naphthalene)cyclopentadienyliron(II) hexafluorophosphate ([FeCp(naph)][PF_6])

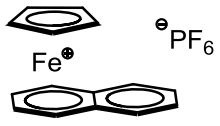

Following the work of Bernardinelli *et al.*,[14] naphthalene (51.2 g, 400 mmol), ferrocene (18.6 g, 100 mmol), aluminium chloride (14.7 g, 110 mmol) and aluminium powder (1.4 g, 52 mmol) were suspended in methylcyclohexane (180 mL). Titanium chloride (5.5 ml, 50 mmol) was added and the mixture heated to 90 °C for 3 h. The red solution was cooled to 0 °C was treated with HCl (37 ml) dissolved in degassed water (170 mL), followed by a solution of hydrogen peroxide. The resulting mixture was warmed to 50 °C for 30 min and then filtered; the aqueous phase was separated and treated with an aqueous solution of $K[PF_6]$ (18.4 g, 100 mmol). The resulting red precipitate was filtered off and dried under vacuum. Red crystals of the product were obtained from a solution in acetone cooled to -25° C. Yield: 19.82 g, 50%. The ^1H NMR spectrum was in agreement with literature data.[14]

*4-bromoindanone (**IIIa**)*

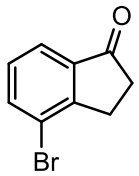

Following the work of Langhauser *et al.*[15] 3-(2-bromophenyl) propionic acid (25.0 g, 0.11 mol) was refluxed in an excess of thionyl chloride (24 mL, 0.33 mol) for 1 h. The excess thionyl chloride was pumped down in vacuo, yielding a brown oil. Aluminium chloride (21.83 g, 0.16 mol) was then added to the oil in dichloromethane (200 mL) at 0 °C. The reaction mixture was stirred for a further 2 h, and subsequently quenched with ice cold water. The aqueous layer was acidified, then extracted with dichloromethane. The combined organic fractions were washed with 2M HCl, water and dried over $MgSO_4$. Dichloromethane was removed under reduced pressure to yield a yellow solid. Yield: 20.35 g, 88%. The ^1H NMR spectrum was in agreement with literature data.[15]

*4-bromoindanol (**IIIb**)*

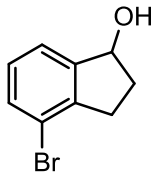

Following the work of Gibson *et al.*,[16] 4-bromoindanone (20.35 g, 96.42 mmol) in a dichloromethane /MeOH mixture (50:150 mL) was treated with sodium borohydride (9.12 g, 241.05 mmol) at -20 °C. The mixture was kept cold until the evolution of hydrogen had stopped and then stirred at room temperature for a further 2 h. The solvents were removed in vacuo and the resulting yellow residue was partitioned between dichloromethane and water. The aqueous fraction was extracted with dichloromethane, the combined organic layers dried over $MgSO_4$, and the solvent removed under reduce pressure yielding a yellow solid. White crystals were obtained from cold hexane (-25° C). Yield: 15.32 g, 75%. The ^1H NMR spectrum was in agreement with literature data.[16]

*7-bromoindene (**IIIc**)*

Following the work of Gibson *et al.*[16] a mixture of 4-bromoindanol (15.32 g, 71.9 mmol) and *p*-TsOH (cat.) in toluene (200 mL) was heated overnight at 110 °C and water removed via a Dean-Stark apparatus. After cooling, the organic layer was washed with water, dried over $MgSO_4$ and pumped down in vacuo yielding a yellow oil. The product was purified by flash chromatography column yielding a colourless oil. Yield: 13.61 g, 97%. The ^1H NMR spectrum was in agreement with literature data.[16]

*5-bromoindanone (**IVa**)*

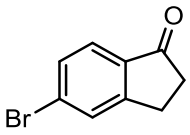

Following the work of Gorman *et al.*,[17] 3-(4-bromophenyl) propionic acid (5.00 g, 21.83 mmol) was added to a neat solution of chlorosulfonic acid (63.58 g, 546 mmol), the mixture cooled to 0 °C and stirred for 1 h. The reaction mixture was quenched with water (*ca.* 100 mL), and the mixture extracted with dichloromethane. The combined organic layers were washed with a saturated aqueous solution of $NaCO_3$, dried over $MgSO_4$ and the solvent was removed under reduced pressure to yield a yellow solid. Yield: 2.43 g, 53%. The ^{1}H NMR spectrum was in agreement with literature data.[17]

*5-bromoindanol (**IVb**)*

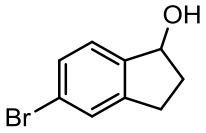

Following the work of Gibson *et al.*,[16] 4-bromoindanone (2.70 g, 12.80 mmol) in a dichloromethane /MeOH mixture (10:50 ml) was treated with sodium borohydride (1.21 g, 12.80 mmol) at -20 °C. The mixture was kept cold until the evolution of hydrogen had stopped and then stirred at room temperature for a further 2 h. The solvents were removed in vacuo and the resulting yellow residue was divided between dichloromethane and water. The aqueous fraction was extracted with dichloromethane, the combined organic layer dried over $MgSO_4$ and the solvent removed under reduced pressure yielding a yellow solid. White crystals were obtained from cold hexane (-25° C). Yield: 2.51 g, 92%. The ^{1}H NMR spectrum was in agreement with literature data.[16]

*6-bromoindene (**IVc**)*

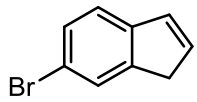

Following the work of Gibson *et al.*,[16] a mixture of 4-bromoindanol (2.50 g, 11.73 mmol) and *p*-TsOH (cat.) in toluene (100 mL) was heated overnight at 110 °C and water removed *via* a Dean-Stark apparatus. After cooling, the organic layer was washed with water, dried over $MgSO_4$ and pumped down in vacuo yielding a yellow oil. The product was purified by flash column chromatography yielding a colourless oil. Yield: 1.64 g, 72%. The ^{1}H NMR spectrum was in agreement with literature data.[16]

*(5-bromo-indenyl)cyclopentadienyliron(II) (**IVd**)*

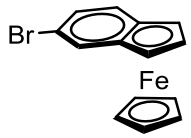

Following the work of Dötz *et al.*,[18] a solution of 6-bromoindene (1.81 g, 9.28 mmol) dissolved in dry thf (100 mL) was added to potassium hydride (392 mg, 9.75 mmol), and the reaction mixture stirred for 1 h. The brown solution was transfered onto [CpFe(naph)][PF_6] (3.84 g, 9.75 mmol) and the mixture stirred for a further 12 h. The solution was pumped down in vacuo yielding a purple residue which was extracted with hexane, and the solvent then removed under reduced pressure. The product was purified by an air-free column chromatography yielding a purple solid. Yield: 1.33 g, 46%. The ^{1}H NMR spectrum was in agreement with literature data.[18]

3-(2,3-dichlorophenyl) propanoic acid

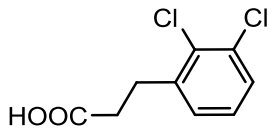

Following a preparation modified from the work of Vaidya *et al.*,[19] 2,3-dichloroaniline (29.16 g, 180 mmol) and hydrobromic acid (53 mL) in acetone (300 mL) was treated with sodium nitrite (18.66 g, 219.6 mmol) at -5 °C. Methyl acrylate (162 ml, 1.8 mol) then cuprous bromide (12.92 g, 90 mmol) were then added to the cold solution. The acetone was removed in vacuo and the crude mixture extracted with toluene. The combined organic fractions were dried over $MgSO_4$ and solvents removed under reduced pressure. The resulting methyl-2-bromo-3-(2,3-dichlorophenyl) propionate was dissolved in glacial acetic acid (200 mL) and treated with zinc powder (23.9 g, 360 mmol). Residual zinc was removed by filtration and the acetic acid removed under vacuum. The resulting oil was partitioned between a 1:1 mixture of water and chloroform. The organic fraction was isolated and the aqueous fraction extracted with further chloroform. The combined chloroform fractions were dried over $MgSO_4$ and the solvent then removed under reduced pressure. Subsequent deprotection was achieved by a 2 h reflux in an aqueous solution of 10% NaOH. The reaction mixture was then filtered, and the product was precipitated by addition of HCl, yielding a white powder. Yield: 28.97 g, 74%. The ^1H NMR spectrum was in agreement with literature data.[19]

3-(3,4-dichlorophenyl) propanoic acid

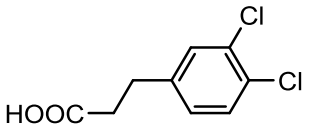

3-(3,4-dichlorophenyl) propanoic acid was prepared following a similar procedure as 3-(2,3-dichlorophenyl) propanoic acid. 3,4-dichloroaniline (29.16 g, 180 mmol) and hydrobromic acid (56 mL) in acetone (300 mL) was treated with sodium nitrite (18.66 g, 219.6 mmol) at -5 °C. Methyl acrylate (162 ml, 1.8 mol) then cuprous bromide (12.92 g, 90 mmol) were added to the cold solution. The methyl-2-bromo-3-(2,3-dichlorophenyl) propionate was dissolved in glacial acetic acid (200 mL) and treated with zinc powder (23.9 g, 360 mmol). Subsequent

deprotection yielded the target material as an off white powder. Yield: 28.19 g, 72%. The ^{1}H NMR spectrum was in agreement with literature data.[20]

3-(3,4-dibromophenyl) propanoic acid

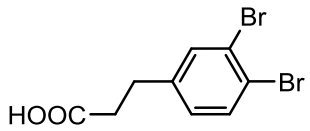

3-(3,4-dibromophenyl) propanoic acid was prepared following an analogous procedure to 3-(2,3-dichlorophenyl) propanoic acid. 3,4-dibromoaniline (34.10 g, 140.08 mmol) and hydrobromic acid (44 mL) in acetone (350 mL) was treated with sodium nitrite (17.07 g, 201 mmol) at -5 °C. Methyl acrylate (122 ml, 1.35 mol) then cuprous bromide (9.75 g, 67.95 mmol) were added to the cold solution. Methyl-2-bromo-3-(3,4-dibromophenyl) propionate was dissolved in glacial acetic acid (200 mL), and treated with zinc powder (18.04 g, 271.8 mmol). Subsequent deprotection by NaOH yielded the target material as an off white powder. Yield: 22.14 g, 50%. The ^{1}H NMR spectrum was in agreement with literature data.[21]

*4,5-dichloroindanone (**Va**)*

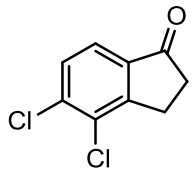

Following the work of Langhauser *et al.*,[15] 3-(2,3-dichlorophenyl) propionic acid (28.97 g, 132.24 mmol) was refluxed in an excess of thionyl chloride (40 mL) for 1 h. The excess thionyl chloride was pumped down in vacuo, yielding a brown oil. Aluminium chloride (26.45 g, 198.36 mmol) was added to the oil in dichloromethane (300 ml) at room temperature. The mixture was stirred for a further 2 h and subsequently quenched with ice cold water. The aqueous layer was acidified, then extracted with dichloromethane. The combined organic

fractions were washed with 2M HCl and water, and dried over $MgSO_4$. Dichloromethane was removed under reduced pressure to yield a brown solid. The solid was suspended in diethylether in order to separate the two possible isomers: the target material was insoluble in the ether component. The solid was filtered and dried under vacuum as a brown solid. Yield: 18.48 g, 72%. The ^{1}H NMR spectrum was in agreement with literature data.[22]

*5,6-dichloroindanone (**VIa**)*

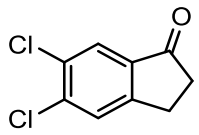

5,6-dichloroindanone was prepared using an analogous procedure as for 4,5-dichloroindanone: 3-(3,4-dichlorophenyl) propionic acid (28.19 g, 128.68 mmol) was treated with thionyl chloride (40 mL) then with aluminium chloride (25.73 g, 193.03 mmol). After work-up the product was isolated as a light brown solid. Yield: 22.59 g, 85%. The ^{1}H NMR spectrum was in agreement with literature data.[23]

*4,5-dichloroindanol (**Vb**)*

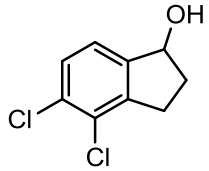

Following the work of Gibson *et al.*,[16] 4,5-dichloroindanone (18.48 g, 91.91 mmol) in a dichloromethane /MeOH mixture (10:50 ml) was treated with sodium borohydride (8.70 g, 230 mmol) at -20 °C. The mixture was kept cold until the evolution of hydrogen had stopped and then stirred at room temperature for a further 2 h. The solvents were removed in vacuo and the resulting yellow residue was divided between dichloromethane and water. The aqueous fraction was extracted with dichloromethane, the combined organic layers dried

over $MgSO_4$ and the solvent removed under reduced pressure yielding a yellow solid. Yield: 16.02 g, 86%. The ^1H NMR spectrum was in agreement with literature data.[22]

*5,6-dichloroindanol (**VIb**)*

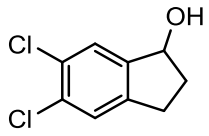

Following the work of Gibson *et al.*,[16] 5,6-dichloroindanone (22.59 g, 112.36 mmol) was treated with sodium borohydride (10.62 g, 281 mmol). The product was isolated as pale yellow solid. Yield: 21.06 g, 92%. The ^1H NMR spectrum was in agreement with literature data.[23]

*4,5-dichloroindene (**Vc**)*

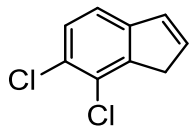

Following the work of Gibson *et al.*,[16] a mixture of 4,5-dichloroindanol (16.01 g, 78.84 mmol) and *p*-TsOH (cat.) in toluene (250 mL) was heated overnight at 110 °C. The product was purified by flash chromatography column yielding a white solid. Yield: 12.50 g, 86%. The ^1H NMR spectrum was in agreement with literature data.[24]

*5,6-dichloroindene (**VIc**)*

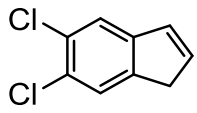

Following the work of Gibson *et al.*,[16] a mixture of 5,6-dichloroindanol (21.06 g, 103.71 mmol) and *p*-TsOH (cat.) in toluene (300 mL) was heated overnight at 110 °C. The product was

isolated as a colourless oil. Yield: 16.54 g, 86%. The ^{1}H NMR spectrum was in agreement with literature data.[25]

2.4. References

(1) R. E. Dodd and P. L. Robinson, "Experimental Inorganic Chemistry. A Guide to Laboratory Practice", *Elsevier Publishing Co.*, Amsterdam, **1954**. (b) R. J. Errington, "Advanced Practical Inorganic and Metalorganic Chemistry", *Blackie Academic & Professional*, London, **1997**.

(2) D. Shriver and M. Drezdon, "The Manipulation of Air-Sensitive Compounds", *Wiley-Interscience*, **1986**.

(3) H. E. Gottlieb, V. Kotlyar and A. Nudelman, *J. Org. Chem.* **1997**, 62, 7512.

(4) J. Cosier and A. M. Glazer, *J. Appl. Crystallogr.* **1986**, 19, 105.

(5) Z. Otwinowski and W. Minor, *Methods Enzymol.* **1997**, 276, 307.

(6) A. Altomare, G. Cascarano, C. Giacovazzo and A. Guagliardi, *J. Appl. Crystallogr.* **1994**, 27, 1045.

(7) L. Palatinus, and G. Chapuis, *J. Appl. Crystallogr.* **2007**, 40, 786.

(8) (*a*) P. W. Betteridge, J. R. Carruthers, R. I. Cooper, K. Prout, and D. J. Watkin, *J. Appl. Crystallogr.* **2003**, 36, 1487. (*b*) R. I. Cooper, A. L. Thompson and D. J. Watkin, *J. Appl. Crystallogr.* **2010**, 43, 1100. (*c*) A. L. Thompson and D. J. Watkin, *J. Appl. Crystallogr.* **2011**, 44, 1017.

(9) A. T. Lubben, J. S. Mc Indoe and A. S. Weller, *Organometallics* **2008**, 27, 3303.

(10) (*a*) C. F. Guerra, J. G. Snijders, G. te Velde and E. J. Baerends, *Theor. Chem. Acc.*, **1998**, 99, 391. (*b*) G. te Velde, F. M. Bickelhaupt, E. J. Baerends, C. F. Guerra, S. J. A. Van Gisbergen, J. G. Snijders and T. Ziegler, *J. Comput. Chem.*, **2001**, 22, 931.

(11) A. J. Bard, E. Garcia, S. Kukharenko and V. V Strelets, *Inorg. Chem.* **1993**, 32, 3528.

(12) C. Wang, G. Erker, G. Kehr, K. Wedeking and R. Fröhlich, *Organometallics* **2005**, 24, 4760.

(13) J. J. Eisch, B. Shafii, J. D. Odom and A. L. Rheingold, *J. Am. Chem. Soc.* **1990**, 112, 1847.

(14) E. P. Kündig, P. Jeger and G. Bernardinelli, *Inorganica Chimica Acta* **2004**, 357, 1909.

(15) T. Sell, A Winter, M. Thorn, A. Dimeska, F. Langhauser, "New metallocene compounds, catalysts comprising them, process for producing an olefin polymer by use of the catalysts and olefin homo and copolymers", *WO2010/077230*, 8th July **2010**.

(16) D. R. Boyd, N. D. Sharma, N. I. Bowers, R. Boyle J. S. Harrison, K. Lee, T. D. H. Bugg, D. T. Gibson, *Org. Biomol. Chem.* **2003**, 1, 1298.

(17) A. K. Sharma, A. V. Subramani, C. B. Gorman, *Tetrahedron* **2007**, 63, 389.

(18) J. Bennewitz, M. Nieger, B. Lewall, K. Heinz Dötz, *J. Organomet. Chem.* **2005**, 690, 5892.

(19) W. E. Bondinell, F. W. Chapin, G. R. Girard, C. Kaiser, A. J. Krog, A. M. Pavloff, M. S. Schwartz, J. S. Silvestri, P. D. Vaidya, *J. Med. Chem.* **1980**, 23, 506.

(20) W. K. Anderson, A. R. Heider, N. Raju, and J. A. Yucht, *J. Med. Chem.* **1988**, 31, 2097.

(21) P. K. Dubey, R. Kumar, J. S. Grossert and D. L. Hooper, *Indian J. Chem., Section B: Org. Chem. Including Medicinal Chemistry* **1998**, 37B, 288.

(22) A. Okano and M. Ohkouchi, "Novel 3-hydroxy-5-arylisoxazole derivative", *WO2010JP69380*, 29th October **2010**.

(23) N. Rackelmann; L. Bialy, H. Englert, K. Wirth, P. Arndt, J. Weston, U. Heinelt, M. Follmann, "Substituted aminoindanes and analogs thereof, and the pharmaceutical use thereof", *WO2009EP06135*, 25th August **2009**.

(24) W. E. Bondinell, R. G. Pendleton, "4- and 5-halo- substituted 2-indanamine compounds", *US 4128666*, 5th December **1978**.

(25) F. Clemence, M. Fortin, G. Hamon, O. Le Martret, A. M. Moura, "Preparation of (pyrrolidinylindanyl)benzeneacetamides as diuretics", *EP 374054 A1*, 20th June **1990**.

CHAPTER 3: Ferrocene/benzene monodentate systems

3.1. Introduction

Three-coordinate boranes have been known to bind cyanide even in the presence of water for more than 50 years;[1] they also have been exploited to bind fluoride. Thus, for instance, Aldridge *et al.* developed ambiphilic ferrocene derivatives for the selective electrochemical detection of hydrogen fluoride.[2] This system based on a ferrocenyl framework (**98** and **99**) with a pendant borane in close contact with an amine (Figure 3.1), exploits the cooperative effect between the Lewis acid and the Lewis base to cleave the H—F bond. NMR and electrochemical monitoring reveal that three equivalents of hydrogen fluoride are necessary to drive the reactions to completion. In both cases (*i.e.* **98** and **99**) the B—O bond was cleaved and substituted by fluorine atoms, thereby forming the anionic borate species shown in Figure 3.1. Despite the fact that the ferrocenyl unit proved to be an efficient reporter (*c.f.* **98**, $E_{1/2}$= -190.5 mV and $FcBF_3^-$, $E_{1/2}$= -320 mV both *vs* Fc/Fc^+), the use of a boronic ester or acid should be avoided in the design of *reversible* HF sensors.

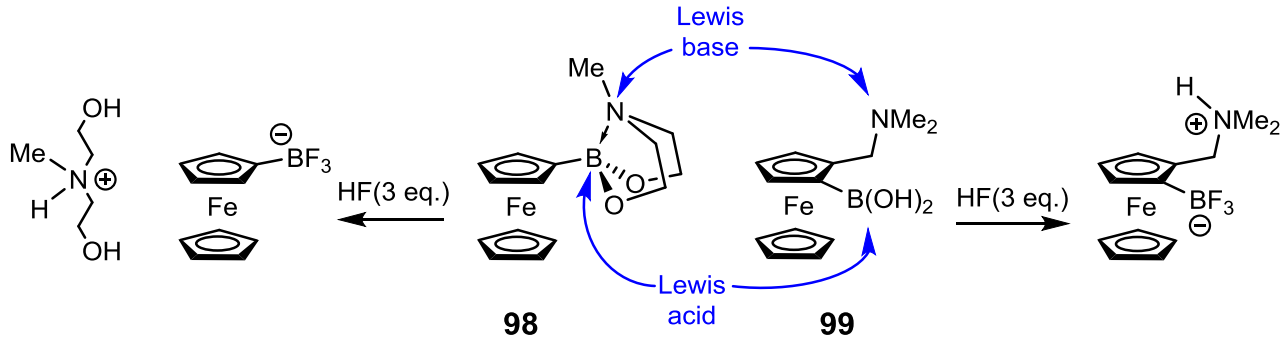

Figure 3.1: Reaction of the ferrocene boronic ester derivatives **98** and **99** with hydrogen fluoride.

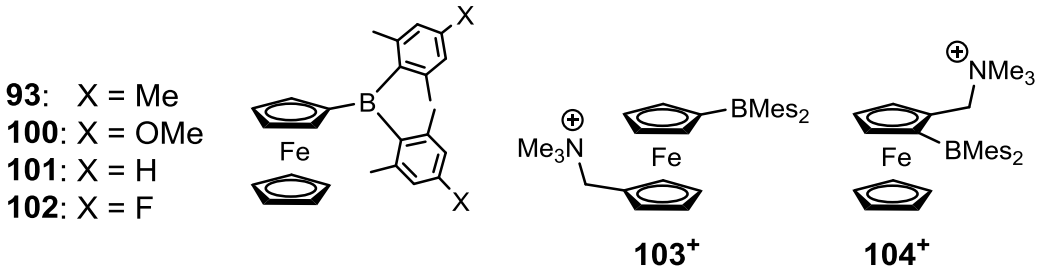

Figure 3.2: Arylborane substituted ferrocene receptors (**93**, **100**-**102**) and 1,1'- and 1,2-substituted ferrocene (**103**$^+$ and **104**$^+$).

When in contact with moisture, ferrocene boronic esters are prone to decomposition, whereas dimesitylborane ferrocene is air and moisture stable (Figure 3.2).[3] Thus Broomsgrove and co-workers were able to quantify the addition of cyanide and fluoride with the monodentate **100**; the binding affinities fitted to a 1:1 binding isotherm for both ions in dichloromethane gave K_F = 6.6(0.4) × 10^4 M^{-1} and K_{CN} = 1.5(0.2) × 10^5 M^{-1}, respectively. Besides a cathodic electrochemical shift ($\Delta E_{1/2}$=-560 mV, *c.f.* section 1.4.4), the fixation of the anion can also be demonstrated unequivocally by ^{11}B NMR spectroscopy, for instance with the cyanide ion giving a sharp signal at -16 ppm. In addition, quenching of the absorption band involving the boron-centred LUMO in the respective UV-vis spectra is typically observed on anion binding. Broomsgrove subsequently investigated the electronic effects of different substituents at the *para* position of the aryl rings with increasing Hammett parameters (*e.g.* OMe, Me, H, F: σ_{para}= 0.06, 0, -0.17 and -0.27).[4] The trend observed in the redox potential follows the electron donating/withdrawing properties of the *para* substituent, although the influence is only a minor one on the respective binding constants. Indeed the cyanide binding affinities differ only by a factor of two (Table 3.1).

Entry	Receptor	K(F) (M^{-1})	K(CN) (M^{-1})	$E_{1/2}$ (mV)
100	$FcBXyl_2^{OMe}$	6.6(0.4) × 10^4	1.5(0.2) × 10^5	+95
93	$FcBMes_2$	7.8(1.2) × 10^4	8.3(2.0) × 10^4	+131
101	$FcBXyl_2$	4.4(0.5) × 10^5	1.4(0.2) × 10^5	+153
102	$FcBXyl_2^F$	4.3(0.7) × 10^5	7.7(1.8) × 10^4	+184
103·I	[1,1'-$Fc(CH_2NMe_3)BMes_2$]I	9.4(3.6) × 10^5	5.8(1.7) × 10^5	+314
104·I	[1,2-$Fc(CH_2NMe_3)BMes_2$]$I^{(\star)}$	5.6(2.3) × 10^9	5.6(2.4) × 10^9	+367

Table 3.1: Binding constants of receptors **93** and **100**-**104**$^+$ in dichloromethane and the corresponding reduction potentials with respect to Fc/Fc^+. (⋆) Determined from competition experiments with $PhBMes_2$.

With the aim of enhancing the binding interaction, a pendant cationic group can readily be introduced either in a 1,1'- or 1,2- fashion thereby giving receptors **103**·I and **104**·I, respectively (Figure 3.2). The immediate consequence is an increase in the Fe(II)/Fe(III) redox potential, due to the additive electron withdrawing effects of the cationic group and the Lewis acid on the cyclopentadienyl rings. However, although the two disubstituted systems exhibit similar redox potentials $E_{1/2}$, the binding constant of **104**$^+$ is greater by at least 3 orders of magnitudes for both anions (*c.f.* Table 3.1). The net effect of the proximal cationic ammonium unit is not only a Coulombic contribution, but a potential source of hydrogen bonding, as has previously been observed in 1,8-naphthalene systems (*c.f.* section 1.3.2.3, **61**$^+$). Thus, in the case of **104**·F a downfield shifted resonance for one of the methylene protons of the $CH_2NMe_3^+$ unit is observed in the ^{1}H NMR spectrum, with a large coupling constant with the fluoride ($^1J_{FH}$= 6.6 Hz).[4]

An inherent problem with such monodentate receptors is the lack of discrimination between the cyanide and fluoride ions. One possible solution could take advantage of the fact that fluoride can readily be chelated between two boron centres, whereas attempts to chelate the cyanide entity have thus far met with little success, as illustrated by 2,2'-bis(dimesitylboryl)tolan **105**.[5] Bresner *et al.* observed the formation of the bis(cyanide) adduct even after addition of only one equivalent of the anion. Presumably a better pre-organised (but more synthetically challenging) receptor is required for cyanide chelation.

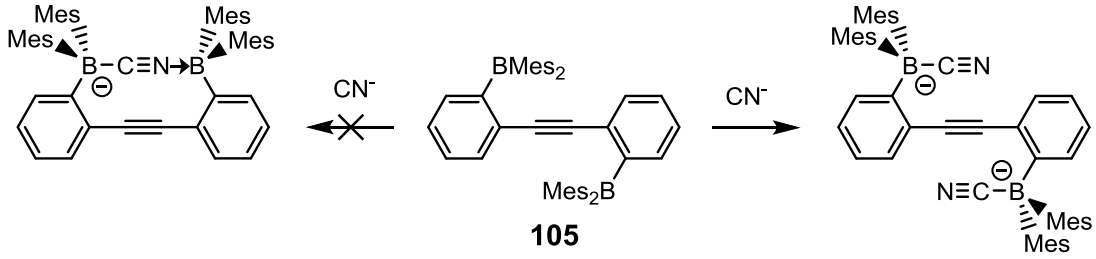

Figure 3.3: Cyanide binding properties of 2,2'-bis(dimesitylboryl)tolan (**105**).

In a complementary approach, Morgan and co-workers synthesized 1,2-dimesitylboryl ferrocene (**106**), which offers a smaller binding cavity potentially able to chelate monatomic anions.[6] However, the intra-boron distance of 3.702 Å (Figure 3.4), is significantly larger than that observed in Gabbaï's 1,8-naphthalene systems (*e.g.* 3.280 Å for **70**)[7] or in Herberich's bis-boryl-cobaltocenium system (*c.f.* 3.543 Å for **74**$^+$). As a consequence, **106** does not bind either cyanide or fluoride cooperatively. Cyanide binds to one $BMes_2$ moiety, outside of the B···B pocket to form *exo*-[**106**·CN]$^-$ (Figure 3.4). The formation of the $-BMes_2(CN)^-$ unit drastically increases the steric hindrance at the boryl units, leading to a sharp increase in the associated C—C—B angles (from 114.4(4)°, 120.6(4)° to 138.5(2)°, 137.2(2)°) as well as a wider B···B distance (3.887 Å). On the other hand, fluoride binds within the cavity to yield *endo*-[**106**·F]$^-$ (Figure 3.4), but the separation between the boryl units is too wide to allow for chelation (B31—F50 1.471(5) Å and B12—F50 3.441 Å; $\sum_{VdW}$(B—F)= 3.39 Å).[6]

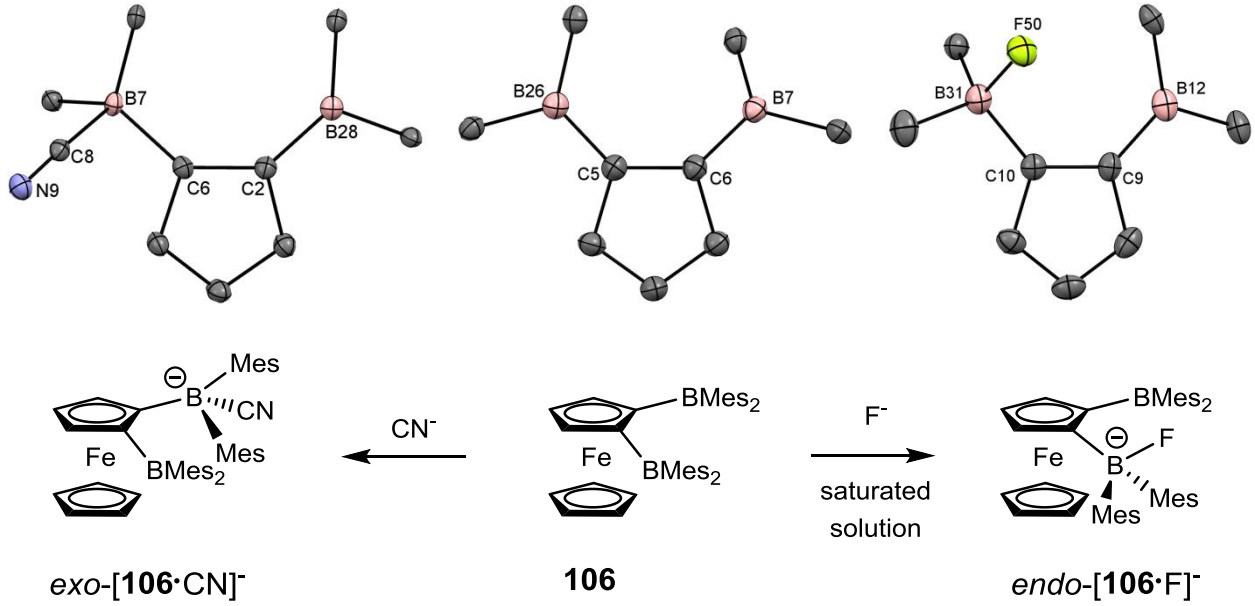

Figure 3.4: (*bottom*) Interaction of fluoride and cyanide ion with **106**. (*top*) Selected portions of the crystal structures showing the cyclopentadienyl ligand bearing the boryl constituents. Thermal ellipsoids set at the 50% probability level; the iron centre, cyclopentadienyl ligand and most of the mesityl moieties, counter-ion, solvent molecules and hydrogen atoms have been omitted for clarity.

As with cyanide, the binding of fluoride requires structural rearrangements: wider C—C—B angles, but a somewhat shorter B···B distance (3.602Å). **106** possesses a high binding affinity for cyanide (K= 3.7(06) × 10^4 M^{-1}) even though the fixation of the anion builds up steric hindrance, while binding of fluoride has as slow rate constant even in the presence of a 20 fold excess of the anion (k= 1.6 × 10^{-2} s^{-1}) due to the endo nature of the binding motif. Precise determination of K_F was thus difficult to obtain. However, competition experiments show that this receptor is actually selective for the cyanide over fluoride.[6]

3.2. Aims

The chemistry of 1,2 dimesitylboryl ferrocene highlights the structural problems inherent in the use of bifunctional receptors which result from the wide angle imposed by the five membered backbone ring (72°); systems based on the analogous 1,2-disubstituted framework benzene appear to be closer to optimal for a chelating site for fluoride. Thus, receptors **81**$^+$ and **73** respectively developed by both Gabbaï[8] and Piers,[9] could be combined with a CpFe-containing moiety to constitute a practical reporter that combines an electrochemical and colorimetric response (Figure 3.5).

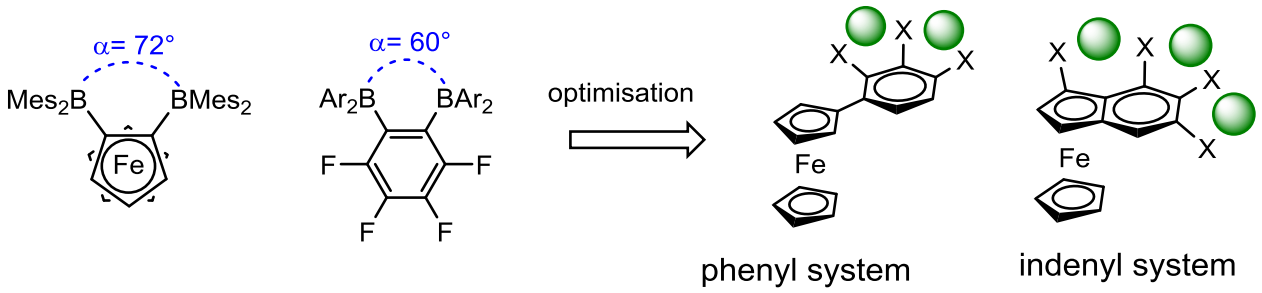

Figure 3.5: Schematic of potential anion chelating receptors targeted in this project. Green spheres highlight the possible chelating sites.

The objective of the research presented in this chapter is a systematic study of the electronic communication between the binding site and the iron centre for a range of possible systems. Starting with a ferrocene derivative with a pendant phenyl group (Figure 3.5); both the steric and electronic effects of incorporation of the binding sites at the *ortho*, *meta* and *para* positions will be investigated. A parallel study will be also conducted on a system in which the benzene ring is fused to one of the cyclopentadienyl unit of the ferrocene component. These indenyl systems (Figure 3.5) are thought to have a greater π-conjugation between the borane unit and the iron centre compared to ferrocene-phenyl systems, and therefore communication of the binding event to the reporter might be expected to be more efficient.

The criteria used to evaluate the practicality of the various receptors include not only the absolute anion binding constants, but issues of selectivity, stability to air and moisture and usefulness of reporter response (be it colorimetric or electrochemical).

3.3. Experimental

3.3.1 Syntheses of phenylferrocene receptors

The three (bromophenyl)ferrocene isomers (*ortho*, *meta* and *para*) were synthesised following a common procedure: A mixture of bromoaniline (2.0 equiv.), concentrated H_2SO_4 and water was cooled to -10 °C and treated with an aqueous solution of $NaNO_2$ (2.02 equiv.) over 20 min. The cold reaction mixture was added slowly to a cold solution (0 °C) of ferrocene (1.0 equiv.), H_2SO_4 and hexadecyltrimethylammonium bromide in diethyl ether. The mixture was stirred for 5h at -5 °C and warmed to room temperature overnight. After neutralization by the addition of NaOH (aq. 10%), the ether layer was separated and the aqueous fraction

extracted with ether. The combined organic fractions were dried over $MgSO_4$, filtered and pumped down to dryness under reduced pressure. The crude products were purified using an alumina column and eluted with hexane. The purity was assessed by ^1H NMR and elemental analysis. Crystals suitable for X-ray diffraction were obtained from hexane solutions cooled to -25^o C.

*(2-bromophenyl)ferrocene (**Ia**)*

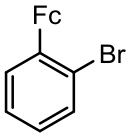

2-bromoaniline (10.67 g, 62.0 mmol), concentrated H_2SO_4 (10 mL) and water (20 mL) were treated with an aqueous solution (20 mL) of $NaNO_2$ (4.36 g, 63.2 mmol). The reaction mixture was then added to a mixture of ferrocene (5.82 g, 31.3 mmol) (250 mL), H_2SO_4 (1 mL) and hexadecyltrimethylammonium bromide (400 mg) in diethyl ether. Yield: 2.64 g, 25%.

^1H NMR (300 MHz, $CDCl_3$, 20 °C): δ_H 4.19 (*s*, 5H, Cp), 4.37 (*s*, 2H, C_5H_4 of Cp), 4.76 (*s*, 2H, C_5H_4 of Cp), 7.07 (*t*, $^3J_{HH}$ = 9.2 Hz, 1H, *para*-CH of Ph), 7.27 (*t*, $^3J_{HH}$ = 9.2 Hz, 1H, *meta*-CH of Ph), 7.54 (*d*, $^3J_{HH}$ = 9.1 Hz, 1H, *ortho*-CH of Ph), 7.73 (*d*, $^3J_{HH}$ = 9.3 Hz, 1H, *meta*-CH of Ph). ♦ $^{13}C\{^1H\}$ NMR (76 MHz, $CDCl_3$, 20 °C): δ_C 68.2 (C_5H_4), 69.7 (Cp), 70.3 (C_5H_4) 86.3 (quaternary C of C_5H_4), 122.5, 126.9, 127.4, 132.2, 133.5 and 139.0 (aromatic C of Ph). ♦ MS (EI+), *m/z* (%) 339.9 (100%) and 341.9 (90%), accurate mass (calc. for M^+, ^{79}Br isotopomer) 339.9550, (meas.) 339.9552, (calc. for M^+, ^{81}Br isotopomer) 341.9530, (meas.) 341.9547, isotopic pattern correct for $C_{16}H_{13}BrFe$.

*(3-bromophenyl)ferrocene (**Ib**)*

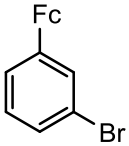

3-bromoaniline (6.6 g, 38.4 mmol), concentrated H_2SO_4 (6 mL) and water (20 mL) were treated with an aqueous solution (20 mL) of $NaNO_2$ (2.70 g, 39.1 mmol). The reaction mixture was then added to a mixture ferrocene (3.6 g, 19.4 mmol), H_2SO_4 (1 mL) and hexadecyltrimethylammonium bromide (360 mg) in diethyl ether (250 mL). Yield: 2.85 g, 43%.

^{1}H NMR (300 MHz, $CDCl_3$, 20 °C): δ_H 4.08 (*s*, 5H, Cp), 4.36 and 4.64 (*s*, each 2H, C_5H_4), 7.16 (*t*, $^3J_{HH}$ = 9.0 Hz, 1H, *meta*-CH of Ph), 7.32 (*d*, $^3J_{HH}$ = 9.3 Hz, 1H, *ortho*-CH of Ph), 7.40 (*d*, 1H, $^3J_{HH}$ = 9.3 Hz, *para*-CH of Mes), 7.61 (*b s*, 1H, *ortho*-CH of Ph). ♦ ^{13}C{^{1}H} NMR (76 MHz, $CDCl_3$, 20 °C): δ_C 66.6 (Cp), 69.3 and 69.7 (C_5H_4), 83.7 (quaternary C of C_5H_4), 122.5, 124.6, 128.7, 128.8, 129.8 and 141.9 (aromatic C of Ph). ♦ MS (EI+), *m/z* (%) 339.9 (100%) and 341.9 (90%), accurate mass (calc. for M+, ^{54}Fe isotopomer) 339.9550 and 341.9530, (meas.) 339.9557, and 341.9552, isotopic pattern correct for $C_{16}H_{13}BrFe$.

*(4-bromophenyl)ferrocene (**Ic**)*

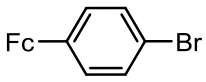

4-bromoaniline (13.2 g, 76.8 mmol), concentrated H_2SO_4 (13 mL) and water (20 mL) was treated with an aqueous solution (20 mL) of $NaNO_2$ (5.40 g, 78.2 mmol). The reaction mixture was then added to a mixture of ferrocene (7.2 g, 38.8 mmol), H_2SO_4 (1 mL) and hexadecyltrimethylammonium bromide (700 mg) in diethyl ether (250 mL). Yield: 6.45 g, 49%. The ^{1}H NMR spectrum of the product was in agreement with literature data.[10]

The three isomers of (dimesitylborylphenyl)ferrocene (*ortho*, *meta* and *para*) were synthesised following a common procedure: the respective (bromophenyl)ferrocene (1 equiv.) in thf was cooled to -78 °C and treated with ^{n}BuLi 1.6 M in hexane (1.1 equiv.). After 30 min, a solution of fluorodimesitylborane (1.0 equiv.) in diethyl ether was added to the cold reaction mixture, which was then was warmed to room temperature overnight. The excess

^{n}BuLi was quenched by addition of water, and the solution pumped down to dryness under reduced pressure. The resulting orange solid was extracted with dichloromethane, which was subsequently removed under vacuum yielding a red/orange solid.

*(2-(dimesitylboryl)phenyl)ferrocene (**IIa**)*

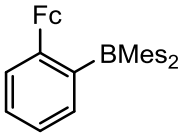

(2-bromophenyl)ferrocene (5.21 g, 15.28 mmol) was treated with ^{n}BuLi 1.6 M in hexane (10.50 mL, 16.80 mmol) and quenched with $FBMes_2$ (4.10 g, 15.28 mmol). Crystals suitable for X-ray crystallography were obtained from a dichloromethane solution cooled to -25° C. Yield: 2.74 g, 35%.

^{1}H NMR (300 MHz, $CDCl_3$, 20 °C): δ_H 1.94 (*b s*, 12H, *ortho*-Me of Mes), 2.24 (*s*, 6H, *para*-Me of Mes), 3.87 (*s*, 2H, CH of C_5H_4), 4.08 (*s*, 5H, Cp), 4.27 (*s*, 2H, CH of C_5H_4), 6.66 (*s*, 4H, *meta*-CH of Mes), 7.19 (*s*, 1H, *meta*-CH of Ph), 7.20 (*s*, 1H, *meta*-CH of Ph), 7.44 (*td*, $^{3}J_{HH}$ = 6.3 Hz and 3.1 Hz, 1H, *para*-CH of Ph), 7.83 (*d*, $^{3}J_{HH}$ = 3.0 Hz, 1H, *ortho*-CH of Ph). ♦ ^{13}C{^{1}H} NMR (76 MHz, $CDCl_3$, 20 °C): δ_C 21.14 (*para*-Me of Mes), 23.2 (*ortho*-Me of Mes), 67.4 (aromatic CH of C_5H_4), 69.2 (Cp), 70.0 (aromatic CH of C_5H_4), 90.1 (quaternary C of C_5H_4), 126.0 (*meta*-CH of Ph), 128.1 (*meta*-CH of of Mes), 130.24 (*para*-CH of Ph), 130.3 (*ortho*-CH of Ph), 134.1 (*meta*-CH of Ph), 138.3 (*ortho*-quaternary C of Mes), 140.5 (*para*-quaternary C of Mes), 143.0 (*b s*, *ipso*-quaternary C of Mes), 144.7 (quaternary C of Ph bound to Cp), 148.0 (*b s*, quaternary C of Ph bound to B). ♦ ^{11}B{^{1}H} NMR (96 MHz, $CDCl_3$, 20 °C): δ_B 78. ♦ Elemental microanalysis: calc. for $C_{34}H_{35}BFe{\cdot}H_2O$: C, 77.30%; H, 7.06%. Found: C, 77.56%; H, 6.93%. ♦ MS (EI+), *m/z* (%) 510.2 (100%), accurate mass (calc. for M+, ^{54}Fe and ^{10}B isotopomer) 510.2181, (meas.) 510.2183, isotopic pattern correct for $C_{34}H_{35}BFe$. ♦ $E_{1/2}$= +454 mV (Fe^{II}/Fe^{III}), -2024 mV ($B^{\cdot-}/B$) *vs* $NiCp_2$ / $NiCp_2^{+}$ couple with 0.1 M [$^{n}Bu_4N$][PF_6] in thf. ♦ Crystallographic data: $C_{34}H_{35}FeB$, M_r =

510.31, triclinic, *P-1*, *a* = 7.45110(10) Å, *b* = 11.4935(2) Å, *c* = 16.8162(3) Å, α = 71.4209(8)°, β = 83.5154(8)°, γ = 77.8551(8) °, *V* = 1332.88(4) Å^3, *Z* = 2, *T* = 150 K, λ = 0.71073 Å. 35607 reflections collected, 6037 independent [R(int) = 0.034] used in all calculations, with 371 refined parameters, GOF on F^2 = 0.9279. R_1 = 0.0454, wR_2 = 0.0934 for observed unique reflections [I>2σ(I)] and R_1 = 0.0659, wR_2 = 0.1126 for all unique reflections. Max. and min. residual electron densities 0.53 and -0.54 e Å^{-3}.

*(3-(dimesitylboryl)phenyl)ferrocene (**IIb**)*

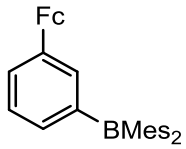

(3-bromophenyl)ferrocene (2.37 g, 6.95 mmol) was treated with ^{n}BuLi 1.6 M in hexane (4.78 mL, 7.65 mmol) and quenched with $FBMes_2$ (1.86 g, 6.95 mmol). Crystals suitable for X-ray crystallography were obtained from a hexane solution cooled to -25° C. Yield: 2.57 g, 73%.

^{1}H NMR (300 MHz, $CDCl_3$, 20 °C): δ_H 0.90 and 1.29 (hexane) 2.08 (*s*, 12H, *ortho*-Me of Mes), 2.30 (*s*, 6H, *para*-Me of Mes), 3.95 (*s*, 5H, Cp), 4.29 (*t*, $^3J_{HH}$ = 1.5 Hz, 2H, aromatic CH of C_5H_4), 4.60 (*t*, $^3J_{HH}$ = 1.5 Hz, 2H, aromatic CH of C_5H_4), 6.88 (*s*, 4H, *meta*-CH of Mes), 7.28 (*dt*, $^3J_{HH}$ = 6.0 Hz and $^4J_{HH}$ = 1.5 Hz, 2H, *ortho*-CH of Ph), 7.34 (*t*, 1H, $^3J_{HH}$ = 6.0 Hz, 1H, *meta*-CH of Ph), 7.66 (*s*, 1H, *ortho*-CH of Ph), 7.69 (*dt*, $^3J_{HH}$ = 6.1 Hz and 1.5 Hz, 1H, *para*-CH of Ph). ♦ ^{13}C{^{1}H} NMR (76 MHz, $CDCl_3$, 20 °C): δ_C 21.4 (*para*-Me of Mes), 23.7 (*ortho*-Me of Mes), 67.3 and 69.9 (aromatic CH of C_5H_4), 70.3 (Cp), 86.0 (quaternary C of C_5H_4), 129.1 (C5), 129.2 (aromatic CH of Mes), 130.5 (*para*-CH of Ph), 134.3 and 134.4 (*ortho*-CH of Ph), 139.6 (*para*-quaternary C of Mes), 140.0 (*ipso*-quaternary C of Ph bound to Cp), 141.5 (*ortho*-quaternary C of Mes), 142.7 (*b s*, *ipso*-quaternary C of Mes), 147.1 (*b s*, C of Ph bound to B). ♦ ^{11}B{^{1}H} NMR (96 MHz, $CDCl_3$, 20 °C): δ_B 80. ♦ MS (EI+), *m/z* (%) 510.2 (100%), exact mass (calc. for M+, ^{54}Fe and ^{10}B isotopomer) 510.2181, (meas.) 510.2188, isotopic pattern correct for $C_{34}H_{35}BFe$. ♦ Elemental

microanalysis: calc. for $C_{34}H_{35}BFe\cdot(hexane)_{0.5}$: C, 80.89%; H, 6.97%. Found: C, 80.81%; H, 7.20%. ♦ $E_{1/2}$=+519 mV (Fe^{II}/Fe^{III}), -1936 mV ($B^{\cdot-}/B$) *vs* $NiCp_2$ / $NiCp_2^+$ couple with 0.1 M [^{n}Bu$_4$N][PF_6] in thf. ♦ Crystallographic data: $C_{34}H_{35}FeB$, M_r = 510.31, triclinic, *P-1*, *a* = 14.1028(3) Å, *b* = 14.4095(3) Å, *c* = 15.1800(3) Å, α = 67.3715(9)°, β = 70.3692(8)°, γ = 82.3985(11)°, *V* = 2681.81(10) Å^3, *Z* = 4, *T* = 150 K, λ = 0.71073 Å. 17351 reflections collected, 10379 independent [R(int) = 0.029] used in all calculations, with 649 refined parameters, GOF on F^2 = 0.9344. R_1 = 0.0424, wR_2 = 0.0862 for observed unique reflections [I>2σ(I)] and R_1 = 0.0615, wR_2 = 0.1000 for all unique reflections. Max. and min. residual electron densities 0.58 and -0.59 e Å^{-3}.

*(4-(dimesitylboryl)phenyl) ferrocene (**IIc**)*

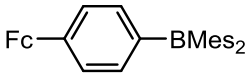

(4-bromophenyl)ferrocene (4.00 g, 11.72 mmol) was treated with ^{n}BuLi 1.6 M in hexane (8.1 mL, 12.90 mmol) and quenched with $FBMes_2$ (3.14 g, 11.72 mmol). Crystals suitable for X-ray crystallography were obtained from an acetonitrile solution at -25° C. Yield: 2.63 g; y= 44%. ^{1}H NMR (300 MHz, $CDCl_3$, 20 °C): δ_H 2.04 (*s*, 12H, *ortho*-Me of Mes), 2.29 (*s*, 6H, *para*-Me of Mes), 4.01 (*s*, 5H, Cp), 4.41 (*t*, $^3J_{HH}$ = 1.5 Hz, 2H, aromatic CH of C_5H_4), 4.84 (*t*, $^3J_{HH}$ = 1.5 Hz, 2H, aromatic CH of C_5H_4), 6.85 (*s*, 4H, aromatic CH of Mes), 7.39 (*d*, $^3J_{HH}$ = 6.2 Hz, 2H, *ortho*-CH of Ph), 7.58 (*d*, 1H, $^3J_{HH}$ = 6.1 Hz, 1H, *meta*-CH of Ph). ♦ $^{13}C\{^1H\}$ NMR (76 MHz, $CDCl_3$, 20 °C): δ_C 21.3 (*para*-Me of Mes), 23.7 (*ortho*-Me of Mes), 67.7 and 70.6 (aromatic CH of C_5H_4), 70.7 (Cp), 84.7 (quaternary C of C_5H_4), 126.3 (*meta*-CH of Ph), 129.1 (*meta*-CH of Mes), 137.4 (*ortho*-CH of Ph), 139.3 (*para*-quaternary C of Mes), 141.4 (*ortho*-quaternary C of Mes), 142.7 (*b s*, *ipso*-quaternary C of Mes), 144.3 (*b s*, C of Ph bound to B), 145.4 (*ipso*-quaternary C of Ph bound to Fc). ♦ $^{11}B\{^1H\}$ NMR (96 MHz, $CDCl_3$, 20 °C): δ_B 82. ♦ MS (EI+), *m/z* (%) 510.2 (100%), exact mass (calc. for M+, ^{54}Fe and ^{10}B isotopomer) 510.2183, (meas.) 510.2188, isotopic pattern

correct for $C_{34}H_{35}BFe$. ♦ Elemental microanalysis: calc. for $C_{34}H_{35}BFe\cdot(H_2O)_{0.4}(thf)_{0.1}$: C, 78.74%; H, 7.03%. Found: C, 78.77%; H, 7.02%. ♦ $E_{1/2}$= +628 mV (Fe^{II}/Fe^{III}), -2010 mV ($B^{\cdot-}/B$) *vs* $NiCp_2$ / $NiCp_2^+$ couple with 0.1 M [^{n}Bu$_4$N][PF_6] in thf. ♦ Crystallographic data: $C_{34}H_{35}FeB$, M_r = 510.31, monoclinic, *P2₁/c*, *a* = 8.11722(6) Å, *b* = 11.63718(10) Å, *c* = 28.9944(2) Å, α = 90°, β = 94.5040(7)°, γ = 90°, *V* = 2730.39(4) Å^3, *Z* = 4, *T* = 150 K, λ = 0.71073 Å. 24937 reflections collected, 5696 independent [R(int) = 0.025] used in all calculations, with 371 refined parameters, GOF on F^2 = 0.9140. R_1 = 0.0319, wR_2 = 0.0712 for observed unique reflections [I>2σ(I)] and R_1 = 0.0344, wR_2 = 0.0742 for all unique reflections. Max. and min. residual electron densities 0.29 and -0.33 e Å^{-3}.

3.3.2 Anion binding by phenylferrocene receptors

*[K(18-crown-6)][**IIb**·CN]*

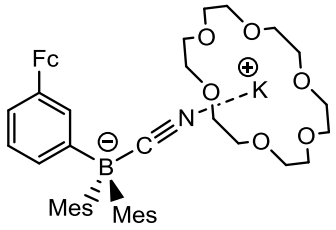

IIb (150 mg, 0.284 mmol), potassium cyanide (191.4 mg, 2.94 mmol) and 18-crown-6 (75 mg, 0.284 mmol) were dissolved in chloroform. The reaction mixture was stirred for 24 h, filtered and pumped down to dryness yielding an orange solid. Crystals suitable for X-ray crystallography were obtained from an acetonitrile solution cooled to -25° C.

^{1}H NMR (300 MHz, $CDCl_3$, 20 °C): δ_H 2.04 and 2.07 (*b s*, each 6H, *ortho*-Me of Mes), 2.07 (MeCN), 2.19 and 2.22 (*b s*, each 3H, *para*-Me of Mes), 3.52 (*b s*, 24H, 18-crown-6), 3.77 (*b s*, 5H, Cp), 4.05 and 4.42 (*b s*, each 2H, C_5H_4), 6.63 (*b s*,4H, *para*-CH of Mes), 7.26 ($CHCl_3$), 6.85, 7.06, 7.35 and 7.95 (*b s*, each 1H, aromatic CH of Ph). ♦ ^{13}C{^{1}H} NMR (76 MHz, $CDCl_3$, 20 °C): δ_C 20.8 (*para*-Me of Mes), 25.5 (*ortho*-Me of Mes), 67.7 (C_5H_4), 69.3 (Cp), 69.4 (C_5H_4), 69.9 (18-

crown-6), 87.9 (quaternary *ipso*-C of Cp), 120.8 and 128.1 (CH of Ph), 128.6 (*meta*-CH of Mes), 131.9 (quaternary C of Mes), 133.8 and 134.9 (CH of Ph), 140.7 and 142.0 (quaternary C of Mes), 142.3 (quaternary C of Ph bound to Cp), 146.2 (*b s*, quaternary C of Ph bound to B), 150.6 (*b s*, quaternary C of Mes bound to B), 157.0 (*b s*, CN bound to B). ♦ $^{11}B\{^{1}H\}$ NMR (96 MHz, $CDCl_3$, 20 °C): δ_B -13. ♦ Elemental microanalysis: calc. for $C_{47}H_{59}BFeKNO_6 \cdot (MeCN)_{1.15}(CHCl_3)_{0.4}$: C, 63.86%; H, 6.78%; N, 3.22%. Found: C, 64.21%; H, 6.32%; N, 3.66%. ♦ MS (ESI-), *m/z* (%): 536.2 (100%), accurate mass (calc. for M-, ^{56}Fe and ^{11}B isotopomer) 536.2223, (meas.) 536.2224, isotopic pattern correct for $[C_{35}H_{35}BNFe]^-$. ♦ $E_{1/2}$= + 340 mV (Fe^{II}/Fe^{III}) *vs* $NiCp_2$ / $NiCp_2^+$ couple with 0.1 M $[^nBu_4N][PF_6]$ in thf. ♦ Crystallographic data: $C_{49}H_{62}BFeKN_2O_6$, M_r = 880.80, triclinic, *P-1*, *a* = 13.0828(2) Å, *b* = 14.7366(2) Å, *c* = 14.9552(3) Å, α = 60.8147(7)°, β = 72.4211(7)°, γ = 69.3532(9)°, *V* = 2325.53(7) Å^3, *Z* = 2, *T* = 150 K, λ = 0.71073 Å. 111266 reflections collected, 10571 independent [R(int) = 0.029] used in all calculations, with 704 refined parameters, GOF on F^2 = 0.9555. R_1 = 0.0459, wR_2 = 0.0938 for observed unique reflections [I>2σ(I)] and R_1 = 0.0755, wR_2 = 0.1215 for all unique reflections. Max. and min. residual electron densities 0.67 and -0.60 e Å^{-3}.

*[K(18-crown-6)][**IIc**·CN]*

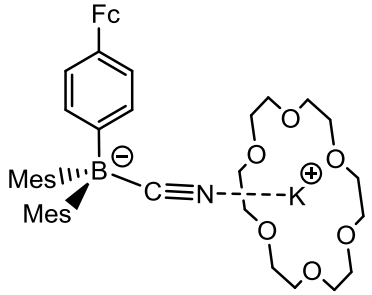

IIc (200 mg, 0.39 mmol), potassium cyanide (255.3 mg, 3.92 mmol) and 18-crown-6 (103.1 mg, 0.39 mmol) were dissolved in chloroform. The mixture was left to react for 24 h, the

solution filtered and pumped down to dryness yielding a light orange solid. Crystals suitable for X-ray crystallography were obtained from an acetonitrile solution cooled to -25° C.

^{1}H NMR (300 MHz, $CDCl_3$, 20 °C): δ_H 1.98 (*s*, 12H, *para*-Me of Mes), 2.03 (MeCN), 2.22 (*s*, 6H, *ortho*-Me of Mes), 3.54 (*s*, 24H, 18-crown-6), 3.99 (*s*, 5H, Cp), 4.23 (*t*, $^{3}J_{HH}$ = 1.5 Hz, 2H, aromatic CH of C_5H_4), 4.65(*t*, $^{3}J_{HH}$ = 1.5 Hz, 2H, aromatic CH of C_5H_4), 6.63 (*s*, 4H, aromatic CH of Mes), 7.05 (*d*, $^{3}J_{HH}$ = 3.1 Hz, 1H, *meta*-CH of Ph), 7.18 (*d*, $^{3}J_{HH}$ = 3.0 Hz, 1H, *ortho*-CH of Ph), 7.28 (*d*, $^{3}J_{HH}$ = 3.0 Hz, 1H, *ortho*-CH of Ph), 8.04 (*d*, $^{3}J_{HH}$ = 3.1 Hz, 1H, *meta*-CH of Ph). ♦ ^{13}C{^{1}H} NMR (76 MHz, $CDCl_3$, 20 °C): δ_C 20.8 (*para*-Me of Mes), 25.2 (*ortho*-Me of Mes), 65.8 and 68.0 (aromatic CH of C_5H_4), 69.5 (Cp), 70.0 (18-crown-6), 87.3 (quaternary C of C_5H_4), 123.5 and 124.4 (*ortho*-CH of Ph), 128.5 (aromatic CH of Mes), 131.8 (*para*-quaternary C of Mes), 132.7 (quaternary C of Ph), 135.5 and 135.6 (*meta*-CH of Ph), 142.2 (*ortho*-quaternary C of Mes), 146.5 (CN), 150.5 (*b s*, *ipso*-quaternary C of Mes), 155.4 (*b s*, *para*-quaternary C of Ph bound to B). ♦ ^{11}B{^{1}H} NMR (96 MHz, $CDCl_3$, 20 °C): δ_B -13. ♦ Elemental microanalysis: calc. for $C_{47}H_{59}BFeKNO_6$•$(MeCN)_2$: C, 66.45%; H, 7.11%; N, 2.82%. Found: C, 66.50%; H, 6.78%; N, 2.47%. ♦ MS (ESI-), *m/z* (%), *m/z* (%): 536.0 (100%), exact mass (calc. for M-, ^{56}Fe and ^{11}B isotopomer) 536.2223, (meas.) 536.2239, isotopic pattern correct for $[C_{35}H_{35}BNFe]^-$. ♦ $E_{1/2}$= + 345 mV (Fe^{II}/Fe^{III}) *vs* $NiCp_2$ / $NiCp_2^+$ couple with 0.1 M $[^nBu_4N][PF_6]$ in thf. ♦ Crystallographic data: $C_{100}H_{124}B_2Cl_{18}Fe_2K_2N_2O_{12}$, M_r = 2395.30, triclinic, *P-1*, *a* = 11.55760(10) Å, *b* = 12.45330(10) Å, *c* = 20.8917(3) Å, α = 103.3893(4)°, β = 90.8717(4)°, γ = 101.9001(4)°, *V* = 2856.08(5) Å^3, *Z* = 1, *T* = 150 K, λ = 0.71073 Å. 72790 reflections collected, 12945 independent [R(int) = 0.025] used in all calculations, with 784 refined parameters, GOF on F^2 = 0.9123. R_1 = 0.0683, wR_2 = 0.1473 for observed unique reflections [I>2σ(I)] and R_1 = 0.0918, wR_2 = 0.1720 for all unique reflections. Max. and min. residual electron densities 1.57 and -1.37 e Å^{-3}.

*[^{n}Bu$_4$N][**IIa**·F]*

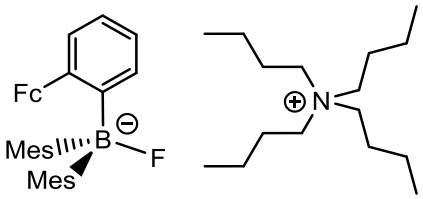

IIa (20 mg, 0.06 mmol) and [^{n}Bu$_4$N]F·4H$_2$O (23 mg, 0.07 mmol) were dissolved in dry thf-d$_8$ and analysed in situ by multinuclear NMR spectroscopy.

^{1}H NMR (300 MHz, thf-d$_8$, 20 °C): δ_H 0.94 (*t*, $^{3}J_{HH}$= 9.0 Hz, Me of [^{n}Bu$_4$N]), 1.32 (*sextet*, $^{3}J_{HH}$ = 6.0 Hz, CH$_2$ of [^{n}Bu$_4$N]), 1.59 (*m*, CH$_2$ of [^{n}Bu$_4$N]), 1.89 (*s*, 12H, *ortho*-Me of Mes), 2.13 (*s*, 6H, *para*-Me of Mes), 3.18 (*t*, $^{3}J_{HH}$ = 9.0 Hz, NCH$_2$ of [^{n}Bu$_4$N]), 3.81 (*s*, 2H, aromatic CH of C$_5$H$_4$), 3.85 (*s*, 5H, Cp), 4.60 (*s*, 2H, aromatic CH of C$_5$H$_4$), 6.42 (*s*, 4H, aromatic CH of Mes), 6.60 (*t*, $^{3}J_{HH}$ = 8.9 Hz, 1H, *meta*-CH of Ph), 6.80 (*td*, $^{3}J_{HH}$ = 6.1 Hz and $^{4}J_{HH}$ = 1.5 Hz, 1H, *para*-CH of Ph), 7.04 (*d*, $^{3}J_{HH}$ = 9.1 Hz, 1H, *ortho*-CH of Ph), 7.67 (*dd*, $^{3}J_{HH}$ = 6.1 Hz and 1.5 Hz, 1H, *meta*-CH of Ph). ♦ ^{13}C{^{1}H} NMR (76 MHz, thf-*d$_8$*, 20 °C): δ_C 14.2 (Me of [^{n}Bu$_4$N]), 20.6 (CH$_2$ of [^{n}Bu$_4$N]), 21.4 (*para*-Me of Mes), 24.7 (CH$_2$ of [^{n}Bu$_4$N]), 25.9 (*ortho*-Me of Mes), 59.1 (CH$_2$ of [^{n}Bu$_4$N]), 66.5 (aromatic CH of C$_5$H$_4$), 70.1 (Cp), 72.6 (aromatic CH of C$_5$H$_4$), 94.2 (quaternary C of C$_5$H$_4$), 122.8 (*para*-CH of Ph), 124.3 (*meta*-CH of Ph), 128.8 (aromatic CH of Mes), 130.6 (*meta*-CH of Ph), 131.1 (*para*-quaternary C of Mes), 137.1 (*ortho*-CH of Ph), 142.5 (quaternary C of C$_5$H$_4$), 142.6 (*ortho*-quaternary C of Mes), 157.9 (*b s*, *ipso*-quaternary C of Mes bound to B), 162.5 (*b s*, *ortho*-quaternary C of Ph bound to B). ♦ ^{11}B{^{1}H} NMR (96 MHz, thf-*d$_8$*, 20 °C): δ_B 8. ♦ ^{19}F NMR (282 MHz, thf-d$_8$, 20°C): δ_F -171.5. ♦ MS (ESI-), *m*/*z* (%): 529.2 (100%), accurate mass (calc. for M-, ^{56}Fe and ^{11}B isotopomer) 529.21708 (meas.) 529.21715, isotopic pattern correct for [C$_{34}$H$_{35}$BFFe]$^{-}$. ♦ Elemental microanalysis: calc. for C$_{50}$H$_{71}$BFFeN: C, 77.81%; H, 9.27%; N, 1.81%. Found: C, 77.56%; H, 8.80%; N, 1.89%. ♦ Crystallographic data: C$_{50}$H$_{69}$BFFeN, M_r = 769.76, trigonal, *P3$_2$*, *a* = 12.32960(10) Å, *b* = 12.32960(10) Å, *c* = 24.7600(3) Å, α = 90°, β = 90°, γ = 120°, *V* = 3259.71(5) Å^3, *Z* = 3, *T* = 150 K, λ = 1.54180 Å. 6661 reflections collected,

6661 independent [R(int) = 0.028] used in all calculations, with 533 refined parameters, GOF on F^2 = 0.9938. R_1 = 0.0341, wR_2 = 0.0885 for observed unique reflections [I>2σ(I)] and R_1 = 0.0354, wR_2 = 0.0926 for all unique reflections. Max. and min. residual electron densities 0.33 and -0.33 e $Å^{-3}$.

*[^{n}Bu$_4$N][**IIa**·CN]*

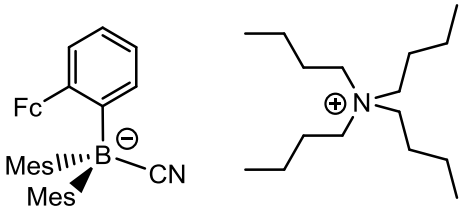

IIa (20 mg, 0.06 mmol) and [^{n}Bu$_4$N][CN]·3H$_2$O (22 mg, 0.07 mmol) were dissolved in dry thf-d$_8$ and analysed in situ by multinuclear NMR spectroscopy.

^{1}H NMR (300 MHz, thf-d$_8$, 20 °C): δ_H 0.92 (*t*, $^3J_{HH}$= 9.0 Hz, Me of [^{n}Bu$_4$N]), 1.29 (*sextet*, $^3J_{HH}$= 5.9 Hz, CH$_2$ of [^{n}Bu$_4$N]), 1.56 (*m*, CH$_2$ of [^{n}Bu$_4$N]), 1.92 (*s*, 12H, *ortho-Me* of Mes), 2.15 (*s*, 6H, *para-Me* of Mes), 3.15 (*t*, $^3J_{HH}$= 9.1 Hz, NCH$_2$ [^{n}Bu$_4$N]), 3.84 (*s*, 2H, aromatic CH of C$_5$H$_4$), 3.90 (*s*, 5H, Cp), 4.56 (*s*, 2H, aromatic CH of C$_5$H$_4$), 6.49 (*s*, 4H, *meta*-CH of Mes), 6.61 (*t*, $^3J_{HH}$= 9 Hz, 1H, C4H), 6.86 (*td*, $^3J_{HH}$= 6.2 Hz and $^4J_{HH}$ = 1.5 Hz, 1H, C5H), 7.01 (*d*, $^3J_{HH}$= 6.1 Hz, 1H, C3H), 7.79 (*d*, $^3J_{HH}$= 9.1 Hz, 1H, C6H). ♦ ^{13}C{^{1}H} NMR (76 MHz, thf-d$_8$, 20 °C): δ_C 14.1 (Me of [^{n}Bu$_4$N]), 20.6 (CH$_2$ of [^{n}Bu$_4$N]), 21.3 (*para*-Me of Mes), 24.9 (CH$_2$ of [^{n}Bu$_4$N]), 26.5 (*ortho*-Me of Mes), 59.2 (CH$_2$ of [^{n}Bu$_4$N]), 66.8 (aromatic CH of C$_5$H$_4$), 69.9 (Cp), 72.9 (aromatic CH of C$_5$H$_4$), 93.91 (quaternary C of C$_5$H$_4$), 123.2 (*para*-CH of Ph), 124.6 (*para*-CH of Ph), 129.5 (*meta*-CH of Mes), 131.4 (*para*-CH of Ph), 131.8 (*para*-quaternary C of Mes), 138.1 (*ortho*-CH of Ph), 143.6 (*ortho*-quaternary C of Mes), 143.8 (*ipso*-quaternary C of Ph bound to Fc), 154.0 (*b s*, *ipso*-quaternary C of Mes), 157.4 (*b s*, *ortho*-quaternary C of Ph bound to B). ♦ ^{11}B{^{1}H} NMR (96 MHz, thf-d$_8$, 20 °C): δ_B -13.

*[^{n}Bu$_4$N][**IIb**·F]*

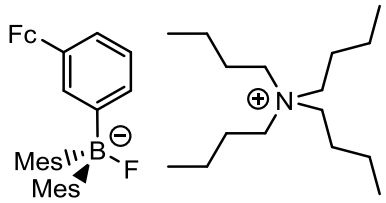

IIb (20 mg, 0.06 mmol) and [^{n}Bu$_4$N]F·4H$_2$O (23 mg, 0.07 mmol) were dissolved in dry thf-d$_8$ and analysed in situ by multinuclear NMR spectroscopy. Even though [^{n}Bu$_4$N]F·4H$_2$O was used in excess, both the ^{1}H and ^{13}C NMR spectra revealed the presence of free **IIb** (*ca.* 25%). The ^{1}H spectrum was re-measured at low temperature (-30° C) in order to slow down the exchange process and allow deconvolution of the peaks of the adduct and the free receptor. The resonances attributable to the adduct are reported below:

^{1}H NMR (300 MHz, thf-d$_8$,-30 °C): δ_H 0.97 (*t*, $^3J_{HH}$ = 6.2 Hz, Me of [^{n}Bu$_4$N]), 1.34 (*sextet*, $^3J_{HH}$ = 6.1 Hz, CH$_2$ of [^{n}Bu$_4$N]), 1.57 (*b s*,CH$_2$ of [^{n}Bu$_4$N]), 1.96 and 2.00 (*s*, each 6H, *ortho*-Me of Mes), 2.12 (*s*, 6H, *para*-Me of Mes), 3.19 (*b s*,NCH$_2$ of [^{n}Bu$_4$N]), 3.73 (*s*, 5H, Cp), 4.06 (*s*, 2H, C1), 4.40 (*s*, 2H, C2), 6.43 and 6.93 (*s*, each 2H, aromatic CH of Mes), 7.33, 7.59, 7.92 and 8.12 (*b s*,each 1H, aromatic CH of Ph). ♦ ^{13}C{^{1}H} NMR (76 MHz, thf-d$_8$, 20 °C): δ_C 18.6 (Me of [^{n}Bu$_4$N]), 25.0 (CH$_2$ of [^{n}Bu$_4$N]), 25.8 (*para*-Me of Mes), 29.2 (CH$_2$ of [^{n}Bu$_4$N]), 30.4 and 30.4 (*ortho*-Me of Mes), 63.5 (CH$_2$ [^{n}Bu$_4$N]), 71.2 and 72.8 (aromatic CH of C$_5$H$_4$), 74.5 (Cp), 94.3 (aromatic CH of C$_5$H$_4$), 125.6 and 130.4 (aromatic C of Ph), 133.4 (aromatic CH of Mes), 135.5 (*para*-quaternary C of Mes), 136.9, 138.5 and 140.0 (aromatic C of Ph), 146.7 (*ortho*-quaternary C of Mes), 161.0 (*ipso*-quaternary C of Mes), 168.81 (C of Ph bound to B). ♦ ^{11}B{^{1}H} NMR (96 MHz, thf-d$_8$, 20 °C): δ_B 6.98. ♦ ^{19}F NMR (282 MHz, thf-d$_8$, 20°C): δ_F -173.0. ♦ MS (ESI-), *m/z* (%): 529.2 (100%), accurate mass (calc. for M-, ^{56}Fe and ^{11}B isotopomer) 529.21708 (meas.) 529.21760, isotopic pattern correct for [C$_{34}$H$_{35}$BFFe]$^-$. ♦ Elemental microanalysis: calc. for C$_{50}$H$_{71}$BFFeN·(CHCl$_3$)$_{0.1}$: C, 77.29%; H, 9.21%; N, 1.80%. Found: C, 77.17%; H, 9.16%; N, 1.46%. ♦ Crystallographic data: C$_{50}$H$_{71}$BFFeN, M_r = 771.78, triclinic, *P1*, *a* = 11.3315(4) Å, *b* =

11.9625(3) Å, c = 18.7698(5) Å, α = 77.888(2)°, β = 74.092(3)°, γ = 64.932(3)°, V = 2203.53(13) Å^3, Z = 2, T = 150 K, λ = 1.54180 Å. 28111 reflections collected, 9133 independent [R(int) = 0.056] used in all calculations, with 1001 refined parameters, GOF on F^2 = 0.9838. R_1 = 0.0552, wR_2 = 0.1493 for observed unique reflections [I>2σ(I)] and R_1 = 0.0589, wR_2 = 0.1538 for all unique reflections. Max. and min. residual electron densities 0.64 and -0.79 e Å^{-3}.

[^{n}Bu$_4$N][Fc-2-C$_6$H$_4$(B(CN)Mes$_2$)]

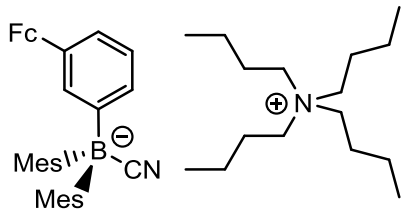

IIb (20 mg, 0.06 mmol) and [^{n}Bu$_4$N][CN]·3H$_2$O (22 mg, 0.07 mmol) were dissolved in dry thf-d$_8$ and analysed in situ by multinuclear NMR spectroscopy. Even though [^{n}Bu$_4$N][CN]·3H$_2$O was introduced in excess, both the ^{1}H and ^{13}C NMR spectra revealed the presence of free **IIb** (*ca.* 16%). The resonances attributable to the adduct are reported below:

^{1}H NMR (300 MHz, thf-d$_8$, 20 °C): δ$_H$ 0.97 (*t*, $^3J_{HH}$ = 5.9 Hz, Me of [^{n}Bu$_4$N]), 1.35 (*sextet*, $^3J_{HH}$ = 6.0 Hz, CH$_2$ of [^{n}Bu$_4$N]), 1.58 (*quintet*, $^3J_{HH}$ = 6.0 Hz, CH$_2$ of [^{n}Bu$_4$N]), 1.97 and 2.01 (*s*, each 6H, *ortho*-Me of Mes), 2.13 (*s*, 6H, *para*-Me of Mes), 3.13 (*t*, $^3J_{HH}$ = 9.2 Hz, NCH$_2$ of [^{n}Bu$_4$N]), 3.70 (*s*, 5H, Cp), 4.02 and 4.34 (*s*, each 2H, aromatic CH of C$_5$H$_4$), 6.50 (*s*, 4H, aromatic CH of Mes), 6.95 (*b s*, 2H, aromatic CH of Ph), 7.32 (*b s*, 1H, aromatic CH of Ph), 7.90 (*b s*, 1H, aromatic CH of Ph). ♦ ^{13}C{^{1}H} NMR (76 MHz, thf-d$_8$, 20 °C): δ$_C$ 14.8 (Me of [^{n}Bu$_4$N]), 20.7 (CH$_2$ of [^{n}Bu$_4$N]), 21.4 (*para*-Me of Mes), 24.8 (CH$_2$ of [^{n}Bu$_4$N]), 26.4 (*ortho*-Me of Mes), 59.0 (CH$_2$ of [^{n}Bu$_4$N]), 67.0 and 68.5 (aromatic CH of C$_5$H$_4$), 70.2 (Cp), 89.3 (quaternary C of C$_5$H$_4$), 121.7 and 126.3 (aromatic CH of Ph), 129.58 (aromatic CH of Mes), 131.9 (*ortho*-quaternary C of Mes), 135.4 and 135.7 (aromatic CH of Ph), 135.9 (quaternary C of Ph), 142.8 (*para*-quaternary C of Mes),

146.3 (*b s*, CN), 152.6 (*b s*, *ipso*-quaternary C of Mes), 158.5 (*b s*, C6, C of Ph bound to B). ♦ $^{11}B\{^1H\}$ NMR (96 MHz, thf-d_8, 20 °C): δ_B -11.

*[^{n}Bu$_4$N][**IIc**·F]*

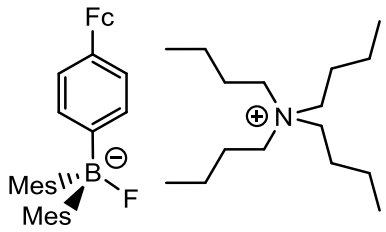

IIc (20 mg, 0.06 mmol) and [^{n}Bu$_4$N]F·4H$_2$O (23 mg, 0.07 mmol) were dissolved in dry thf-d_8 and analysed in situ by multinuclear NMR spectroscopy.

^1H NMR (300 MHz, thf-d_8, -20 °C): δ_H 0.97 (*b s*, Me of [^{n}Bu$_4$N]), 1.39 (*b s*, CH$_2$ of [^{n}Bu$_4$N]), 1.64 (*b s*, CH$_2$ of [^{n}Bu$_4$N]), 1.93 (*s*, 12H, *ortho-Me* of Mes), 2.11 (*s*, 6H, *para-Me* of Mes), 3.32 (*b s*, CH$_2$ of [^{n}Bu$_4$N]), 3.92 (*s*, 5H, Cp), 4.15 and 4.58 (*s*, each 2H, aromatic CH of C_5H_4), 6.41 (*s*, 6H, aromatic CH of Mes), 6.93 (*d*, $^3J_{HH}$ = 6.0 Hz, 1H, aromatic CH of Ph), 7.02 (*d*, $^3J_{HH}$ = 9.1 Hz, 1H, aromatic CH of Ph), 7.22 (*d*, $^3J_{HH}$ = 8.9 Hz, 1H, aromatic CH of Ph), 7.69 (*d*, $^3J_{HH}$ = 6.1 Hz, 1H, aromatic CH of Ph). ♦ $^{13}C\{^1H\}$ NMR (76 MHz, thf-d_8, -20 °C): δ_C 14.4 (Me of [^{n}Bu$_4$N]), 20.6 (CH$_2$ of [^{n}Bu$_4$N]), 21.4 (*para*-Me of Mes), 24.81 (CH$_2$ of [^{n}Bu$_4$N]), 25.7 and 25.8 (*ortho*-Me of Mes), 59.0 (NCH$_2$ of [^{n}Bu$_4$N]), 66.3 and 68.0 (aromatic CH of C_5H_4), 70.2 (Cp), 89.0 (quaternary C of C_5H_4), 124.08 and 124.35 (aromatic CH of Ph), 128.8 (aromatic CH of Mes), 130.9 (*para*-quaternary C of Mes), 132.7 (quaternary C of Ph), 134.0 and 135.1 (aromatic CH of Ph), 142.1 (*ortho*-quaternary C of Mes), 156.6 (*b s*, *ipso*-quaternary C of Mes), 162.9 (*b s*, C of Ph bound to B). ♦ $^{11}B\{^1H\}$ NMR (96 MHz, thf-d_8, 20 °C): δ_B 7. ♦ ^{19}F NMR (282 MHz, thf-d_8, -20°C): δ_F -171.6.

3.3.3 Syntheses of indenyl receptors

(4-bromo-indenyl)cyclopentadienyliron(II) ***(IIId)***

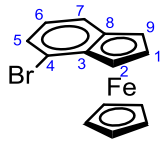

A solution of 7-bromoindene (2.75 g, 14.10 mmol) dissolved in dry thf (200 mL) was added to potassium hydride (594 mg, 14.80 mmol), and the reaction mixture stirred for 1 h at room temperature. The resulting brown solution was transferred onto [FeCp(naph)][PF_6] (5.83 g, 14.80 mmol) and the mixture allowed to react over 12 h. The solution was pumped to dryness, yielding a brown-purple residue which was extracted with hexane. The solvent was removed under reduced pressure yielding a solid that was purified by air-free column chromatography yielding a purple solid. Purple crystals suitable for X-ray crystallography were obtained from cold hexane (-25° C). Yield: 2.99 g, 67%.

^{1}H NMR (300 MHz, CD_2Cl_2, 20 °C): δ_H 3.87 (*s*, 5H, Cp), 4.18 (*t*, $^3J_{HH}$ = 3.0 Hz, 1H, C1H), 5.05 (*s*, 1H, C2H), 5.09 (*s*, 1H, C9H), 6.79 (*dd*, $^3J_{HH}$ = 9.1 Hz and 6 Hz, 1H, C6H), 7.18 (*d*, $^3J_{HH}$ = 5.9 Hz, 1H, C7H), 7.59 (*d*, $^3J_{HH}$ = 9.2 Hz, 1H, C5H). ♦ ^{13}C{^{1}H} NMR (76 MHz, CD_2Cl_2, 20 °C): δ_C 63.4 (C1), 64.0 (C8), 69.2 (Cp), 71.4 (C9), 89.0 (C2), 89.6 (C7), 124.1 (C4), 124.5 (C6), 125.6 (C3), 129.0 (C5). ♦ MS (EI+), *m/z* (%): 313.9 (100%), 315.9 (95%), isotopic pattern correct for $C_{14}H_{11}BrFe$. ♦ Elemental microanalysis: calc. for $C_{14}H_{11}BrFe$: C, 53.38%; H 3.52%. Found: C, 52.98%; H, 3.59%. ♦ Crystallographic data: $C_{14}H_{11}BrFe$, M_r = 314.99, monoclinic, $P2_1/c$, a = 9.4289 (1) Å, b = 10.1614 (1) Å, c = 12.1495 (2) Å, α = 90°, β = 105.3181 (6)°, γ = 90°, V = 1122.70 (2) Å^3, Z = 4, T = 150 K, λ = 0.71073 Å. 33225 reflections collected, 2553 independent [R(int) = 0.022] used in all calculations, with 145 refined parameters, GOF on F^2 = 0.9918. R_1 = 0.0333, wR_2 = 0.0715 for observed unique reflections [I>2σ(I)] and R_1 = 0.0425, wR_2 = 0.0756 for all unique reflections. Max. and min. residual electron densities 0.96 and -0.97 e Å^{-3}.

*(4-dimesitylboryl-indenyl)cyclopentadienyliron(II) (**IIIe**)*

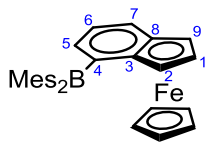

To a solution of **IIId** (1.15 g, 3.65 mmol) in thf (50 mL) at -78° C was added ^{n}BuLi (2.40 mL of a 1.6 M solution in hexane, 3.83 mmol). The red solution stirred for 30 min at the same temperature before a solution of $FBMes_2$ (1.03 g, 3.83 mmol) in thf (ca. 50 mL) was added. The reaction mixture was warmed to room temperature over 12 h, and the resulting green solution then pumped to dryness, yielding a dark green solid. The solid was extracted with hexane and the solvent removed under reduced pressure then purified by air-free column chromatography (silica, hexane then 50% Et_2O in hexane). Crystals suitable for X-ray were obtained from cold hexane (-25° C) Yield: 1.27 g, 68%.

^{1}H NMR (300 MHz, $CDCl_3$, 20 °C): δ_H 2.13 (*b s*, 12H, *ortho-Me* of Mes), 2.34 (*s*, 6H, *para-Me* of Mes), 3.82 (*s*, 5H, Cp), 3.96 (*t*, $^3J_{HH}$ = 3.5 Hz, 1H, C1H), 4.39 (*dd*, $^3J_{HH}$ = 3.5 Hz and 3.4 Hz, 1H, C2H), 4.89 (*dd*, $^3J_{HH}$ = 3.0 Hz and 3 Hz, 1H, C9H), 6.84 (*s*,4H, aromatic CH of Mes), 6.90 (*dd*, $^3J_{HH}$ = 9.2 Hz and 6.3 Hz, 1H, C6H), 7.27 (*dd*, $^3J_{HH}$ = 9.1 Hz and 3.0 Hz, 1H, C5H), 7.78 (*d*, $^3J_{HH}$ = 9.4 Hz, 1H, C7H). ♦ ^{1}H NMR (300 MHz, CD_2Cl_2, -80 °C): δ_H 1.48, 1.97, 2.25, 2.27, 2.28 and 2.40 (*s*, each 3H, Me of Mes), 3.74 (*s*, 5H, Cp), 3.88 (*t*, $^3J_{HH}$ = 3.5 Hz, 1H, C1H), 4.39 (*d*, $^3J_{HH}$ = 3.5 Hz, 1H, C2H), 4.87 (*d*, $^3J_{HH}$ = 3.4 Hz, 1H, C9H), 6.65 and 6.76 (*s*, each 1H, aromatic CH of Mes), 6.82 (*dd*, *J* = 9.0 Hz and 6.3 Hz, 1H, C6H), 6.88 and 6.91 (*s*, each 1H, aromatic CH of Mes), 7.12 (*d*, $^3J_{HH}$ = 6.2 Hz, 1H, C5H), 7.79 (*d*, *J* = 6.3 Hz, 1H, C7). ♦ ^{13}C{^{1}H} NMR (126 MHz, $CDCl_3$, 20 °C): δ_C 21.2 (*para*-Me of Mes), 23.1 (*ortho*-Me of Mes), 61.3 (C9), 63.8 (C2), 68.1 (Cp), 71.1 (C1), 86.2 (C8), 94.0 (C3), 122.7 (C6), 128.1 (aromatic CH of Mes), 136.6 (C7), 138.1 (C5), 138.2 (*para*-quaternary C of Mes), 140.4 (*ipso*-quaternary C of Mes), 142.5 (*ortho*-quaternary C of Mes), 147.3 (*b s*, C4 of Ind bound to B). ♦ ^{11}B{^{1}H} NMR (96 MHz, $CDCl_3$, 20 °C): δ_B 77. ♦ Elemental microanalysis: calc. for $C_{32}H_{33}BFe$: C, 79.37%; H 6.87%. Found: C, 79.28%; H, 6.83%. ♦ MS

(EI+), *m/z* (%): 484.2 (100%), accurate mass (calc. for M+, ^{54}Fe and ^{10}B isotopomer) 481.20667 (meas.) 481. 209505, isotopic pattern correct for $C_{32}H_{33}BFe$. ♦ $E_{1/2}$= +16 mV (Fe^{II}/Fe^{III}), -2356 mV ($B^{\cdot-}/B$) *vs* Fc / Fc^+ couple with 0.1 M [^{n}Bu$_4$N][PF_6] in thf. ♦ Crystallographic data: $C_{32}H_{33}BFe$, M_r = 484.27, monoclinic, P 1, *a* = 12.18666(5) Å, *b* = 14.62360(6) Å, *c* = 14.43211(6) Å, α = 90°, β = 91.0308(4)°, γ = 90°, *V* = 2571.570(18) Å^3, *Z* = 4, *T* = 150 K, λ = 0.71073 Å. 60968 reflections collected, 5397 independent [R(int) = 0.026] used in all calculations, with 599 refined parameters, GOF on F^2 = 0.9278. R_1 = 0.0460, wR_2 = 0.0892 for observed unique reflections [I>2σ(I)] and R_1 = 0.0475, wR_2 = 0.0897 for all unique reflections. Max. and min. residual electron densities 0.82 and -1.01 e Å^{-3}.

*(5-dimesitylboryl-indenyl)cyclopentadienyliron(II) (**IVe**)*

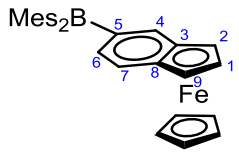

To a solution of **IVd** (1.33 g, 4.22 mmol) in thf (50 mL) at -78° C was added ^{n}BuLi (2.77 mL of a 1.6 M solution in hexane, 4.43 mmol). After stirring for 30 min, at the same temperature, a solution of $FBMes_2$ (1.19 g, 4.43 mmol) in thf (ca. 50 mL) was added to the cold solution. The reaction mixture was warmed to room temperature over 12 h and the resulting green solution then pumped to dryness, yielding a dark green solid. The crude product was purified by air-free column chromatography (silica, 10% Et_2O in hexane) then recrystallized from cold hexane. Yield: 1.33 g, 46%.

^{1}H NMR (300 MHz, $CDCl_3$, 20 °C): δ_H 0.90 and 1.30 (hexane), 2.09 (*s*, 12H, *ortho-Me* of Mes), 2.34 (*s*, 6H, *para-Me* of Mes), 3.88 (*s*, 5H, Cp), 4.22 (*t*, $^3J_{HH}$ = 2.9 Hz, 1H, C1H), 4.93 (*d*, $^3J_{HH}$ = 3.1 Hz, 1H, C2H), 5.04 (*d*, $^3J_{HH}$ = 3.0 Hz, 1H, C9H), 6.85 (*s*, 4H, aromatic CH of Mes), 7.01 (*d*, $^3J_{HH}$ = 6.0 Hz, 1H, C6H), 7.48 (*d*, $^3J_{HH}$ = 6.2 Hz, 1H, C7H), 7.98 (*s*, 1H, C4H). ♦ ^{13}C{^{1}H} NMR (126 MHz, $CDCl_3$, 20 °C): δ_C 21.2 and 23.5 (*para*-Me of Mes), 62.8 and 63.6 (C2 and C9), 68.0 (Cp), 71.8

(C1), 86.1 (C3), 89.7 (C8), 127.1 (C7), 128.1 (aromatic CH of Mes), 129.4 (C6), 138.2 (*para*-quaternary C of Mes), 140.7 (*ortho*-quaternary C of Mes), 142.0 (*b s*, C5 of Ind bound to B), 142.0 (*b s*, *ipso*-quaternary C of Mes), 145.3 (C4). ♦ $^{11}B\{^1H\}$ NMR (96 MHz, $CDCl_3$, 20 °C): δ_B 75. ♦ Elemental microanalysis: calc. for $C_{32}H_{33}BFe(C_6H_{14})_{0.4}$: C, 79.65%; H 7.50%. Found: C, 79.77%; H, 7.42%. ♦ MS (EI+), *m/z* (%): 484.2 (100%), accurate mass (calc. for M+, ^{56}Fe and ^{10}B isotopomer) 483.205356, (meas.) 483.20780, isotopic pattern correct for $C_{32}H_{33}BFe$. ♦ $E_{1/2}$= + 15 mV (Fe^{II}/Fe^{III}) *vs* Fc / Fc^+ couple with 0.1 M [$^nBu_4N$][PF_6] in thf.

3.3.4 Anion binding by indenyl receptors

*[K(18-crown-6)][**IIIe**·CN]*

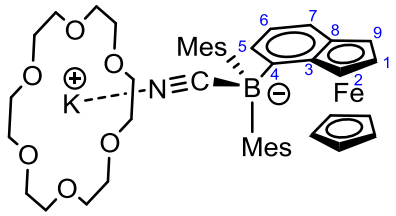

IIIe (300 mg, 0.62 mmol) was treated with both potassium cyanide (403 mg, 6.20 mmol) and 18-crown-6 (163 mg, 0.62 mmol) in acetone (30mL). The red solution was stirred for two hours, filtered and concentrated. Crystals suitable for X-ray crystallography were obtained from an acetone solution cooled to -25° C. Upon dissolution in $CDCl_3$, the cyanide adduct is in equilibrium with the free **IIIe**, rendering the assignment difficult, thus no NMR shifts can be accurately reported for this compound.

MS (ESI-), *m/z* (%): 510.2 (100%), accurate mass (calc. for M-, ^{56}Fe and ^{11}B isotopomer) 510.2067, (meas.) 510.2050, isotopic pattern correct for $[C_{33}H_{33}BNFe]^-$. ♦ Elemental microanalysis: calc. for $C_{45}H_{57}BFeKNO_6{\cdot}2H_2O$: C, 63.61%; H 7.24%. Found: C, 63.77%; H, 7.24%. ♦ Crystallographic data: $C_{45}H_{57}BFeKNO_6$, M_r = 813.71, triclinic, *P-1*, *a* = 11.80090(10) Å, *b* = 12.70250(10) Å, *c* = 14.5226(2) Å, α = 76.3891(5)°, β = 84.0128(5)°, γ = 82.2242(6)°, *V* = 2090.42(4) Å^3, *Z* = 2, *T* = 150 K, λ = 0.71073 Å. 65025 reflections collected, 9499

independent [R(int) = 0.021] used in all calculations, with 371 refined parameters, GOF on F^2 = 0.9115. R_1 = 0.0375, wR_2 = 0.0853 for observed unique reflections [I>2σ(I)] and R_1 = 0.0465, wR_2 = 0.0923 for all unique reflections. Max. and min. residual electron densities 0.39 and -0.41 e Å^{-3}.

*[^{n}Bu$_4$N][**IIIe**$^{\cdot}$CN]*

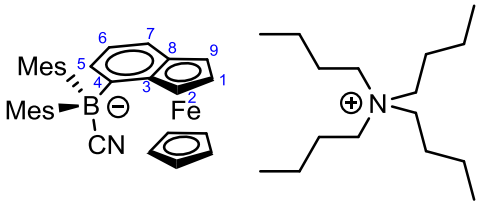

IIIe (25 mg, 0.05 mmol) and [^{n}Bu$_4$N][CN]$^{\cdot}$3H$_2$O (20 mg, 0.06 mmol) were dissolved in dry thf-d$_8$ and analysed in situ by multinuclear NMR spectroscopy.

^{1}H NMR (300 MHz, CD_2Cl_2, 20°C): δ_H 1.01 (*t*, $^3J_{HH}$ = 5.9 Hz, Me of [^{n}Bu$_4$N]), 1.49 (*sextet*, $^3J_{HH}$ = 6.0 Hz, CH_2 of [^{n}Bu$_4$N]), 1.57 (*quintet*, $^3J_{HH}$ = 6.0 Hz, CH_2 of [^{n}Bu$_4$N]), 1.65 (*s*, 6H, *ortho-Me* of Mes), 2.14 (*s*, 9H, *ortho* and *para-Me* of Mes), 2.25 (*s*, 3H, *para-Me* of Mes), 3.06 (*t*, $^3J_{HH}$ = 6.1 Hz, NCH_2 of [^{n}Bu$_4$N]), 3.88 (*s*, 5H, Cp), 3.91 (*t*, $^3J_{HH}$ = 3.1 Hz, 1H, C1H), 4.78 (*m*, 1H, C9H), 5.22 (*m*, 1H, C9H), 6.36 (*d*, $^3J_{HH}$ = 5.9 Hz, 1H, C5H), 6.46 (*s*, 2H, aromatic CH of Mes), 6.66 (*dd*, $^3J_{HH}$ = 6.0 Hz and 9.1 Hz, 1H, C6H), 6.68 (s, 2H, aromatic CH of Mes), 7.23 (*d*, $^3J_{HH}$ = 9.1 Hz, 1H, C7). ♦ ^{13}C{^{1}H} NMR (75 MHz, CD_2Cl_2, 20°C): δ_C 14.0 (ME of [^{n}Bu$_4$N]), 20.2 (CH_2 of [^{n}Bu$_4$N]), 21.0 and 21.1 (*para-Me* of Mes), 24.4 (CH_2 of [^{n}Bu$_4$N]), 24.7 and 25.67 (*ortho-Me* of Mes), 59.0 (CH_2 of [^{n}Bu$_4$N]), 59.9 (C2), 65.7 (C9), 68.5 (C1), 69.0 (Cp), 87.9 (C3), 97.6 (C8), 124.4 (C7), 124.8 (C6), 128.8 (aromatic CH of Mes), 128.9 (C5), 129.1 (aromatic CH of Mes), 132.0 and 132.4 (*para*-quaternary C of Mes), 142.9 and 143.2 (*ortho*-quaternary C of Mes), 145.2 (CN), 150.9 and 151.9 (*ipso*-quaternary C of Mes), 157.8 (b *s*, C4 bound to B). ♦ ^{11}B{^{1}H} NMR(96 MHz, CD_2Cl_2, 20° C) : δ_B -15.

*[^{n}Bu$_4$N][**IIIe**·F]*

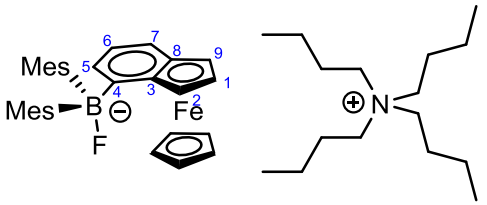

IIIe (25 mg, 0.05 mmol) and [^{n}Bu$_4$N]F·4H$_2$O (22 mg, 0.06 mmol) were dissolved in dry thf-d$_8$ and analysed in situ by multinuclear NMR spectroscopy. ^{1}H NMR (300 MHz, thf-d$_8$, 20°C): δ_H 0.99 (*b s*, Me of [^{n}Bu$_4$N]), 1.37 (*b s*, CH$_2$ of [^{n}Bu$_4$N]), 1.60 (*b s*, CH$_2$ of [^{n}Bu$_4$N]), 2.06 (*b s*, 3H, *para*-Me of Mes), 2.15 and 2.17 (*b s*, each 6H, *ortho*-Me of Mes), 2.55 (*b s*, 3H, *para*-Me of Mes), 3.12 (*b s*, NCH$_2$ of [^{n}Bu$_4$N]), 3.67 (*b s*, 6H, Cp and C1H), 4.54 (*dd*, $^{3}J_{HH}$ = 6.0 Hz and 3 Hz, 1H, C2H), 5.17 (*b s*, 1H, C9H), 6.29 (*b s*, 2H, aromatic CH of Mes), 6.44 (*b s*, 1H, C5H), 6.47 (*b s*, 2H, aromatic CH of Mes), 6.55 (*b t*, $^{3}J_{HH}$ = 6.3 Hz, 1H, C6H), 6.99 (*d*, $^{3}J_{HH}$ = 8.9 Hz, 1H, C7H). ♦ ^{13}C{^{1}H} NMR (75 MHz, thf-d$_8$, 20°C): δ_C 14.2 (Me of [^{n}Bu$_4$N]), 20.6 (CH$_2$ of [^{n}Bu$_4$N]), 21.4 (*para*-Me of Mes), 24.6 (CH$_2$ of [^{n}Bu$_4$N]), 25.0 (*ortho-Me* of Mes), 59.1 (CH$_2$ of [^{n}Bu$_4$N]), 59.6 (C2), 66.4 (C9), 68.5 (C1), 69.1 (Cp), 88.5 (C3), 98.1 (C8), 123.3 (C7), 125.4 (C6), 126.9 (C5),127.0 (*para*-quaternary C of Mes), 128.8 (aromatic CH of Mes), 130.7 (*para*-quaternary C of Mes), 142.5 and 143.1 (*ortho*-quaternary C of Mes), 156.3 (*b s*, *ipso*-quaternary C of Mes), 165.3 (*b s*, C4 of Ind bound to B). ♦ ^{11}B{^{1}H} NMR (96 MHz, thf-d$_8$, 20°C): δ_B 6. ♦ ^{19}F NMR (282 MHz, thf-d$_8$, 20°C): δ_F -179.5. ♦ MS (ESI-), *m/z* (%): 503.2 (100%), accurate mass (calc. for M-, ^{56}Fe and ^{11}B isotopomer) 503.2020, (meas.) 503.2030, isotopic pattern correct for [C$_{32}$H$_{33}$BFFe]$^{-}$.

*[Cs(18-crown-6][**IVe**·F]*

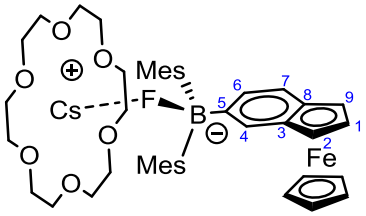

IVe (300 mg, 0.62 mmol) is treated with both caesium fluoride (942 mg, 6.20 mmol) and 18-crown-6 (163 mg, 0.62 mmol) in acetonitrile (30mL). The resulting red solution is left to react for two hours, filtered and concentrated. Crystals suitable for X-ray crystallography were obtained from cold acetonitrile. In CD_2Cl_2 or thf-d_8, a mixture of the free sensor and the adduct were observed in 8 to 10 ratio. Only the adduct's shift is reported here.

^{1}H NMR (300 MHz, CD_2Cl_2, -80 °C): δ_H 1.93 (*b s*, 3H, *para-Me* of Mes), 1.98 (*b s*, 3H, *para-Me* of Mes), 2.10, 2.13, 2.14, 2.16 (s, each 3H, *ortho-Me* of Mes), 3.56 (*b s*, 24H, 18-crown-6), 3.74 (s, 5H, Cp), 3.79 (*s*, 1H, C1H), 4.45 (*s*, 1H, C2H), 4.66 (*s*, 1H, C9H), 6.53 and 6.62 (*s*, each 2H,aromatic CH of Mes), 6.69 (*s*, 1H, C4H), 7.05 (*d*, $^3J_{HH}$ = 6.1 Hz, 1H, C7H), 7.42 (*d*, $^3J_{HH}$ = 6.1 Hz, 1H, C6H). ♦ ^{11}B{^{1}H} NMR (96 MHz, CD_2Cl_2, -80 °C): δ_B 5. ♦ ^{19}F NMR (282 MHz, CD_2Cl_2, **-80 °C**): δ_F -169.1. ♦ MS (ESI-), *m/z* (%): 503.2 (100%), exact mass (calc. for M-, ^{56}Fe and ^{11}B isotopomer) 503.2020, (meas.) 503.2011, isotopic pattern correct for $[C_{32}H_{33}BFFe]^-$. ♦ Crystallographic data: $C_{48}H_{63}BCsFFeN_2O_6$, M_r = 982.60, Triclinic, *P-1*, *a* = 10.70690(10) Å, *b* = 14.1228(2) Å, *c* = 17.6276(3) Å, α = 98.9703(6)°, β = 105.8289(7)°, γ = 105.9933(6)°, *V* = 2386.97(6) Å^3, *Z* = 2, *T* = 150 K, λ = 0.71073 Å. 105726 reflections collected, 10840 independent [R(int) = 0.039] used in all calculations, with 541 refined parameters, GOF on F^2 = 0.9522. R_1 = 0.0432, wR_2 = 0.0889 for observed unique reflections [I>2σ(I)] and R_1 = 0.0724, wR_2 = 0.1167 for all unique reflections. Max. and min. residual electron densities 1.71 and -1.69 e Å^{-3}.

*[^{n}Bu$_4$N][**IVe**·F]*

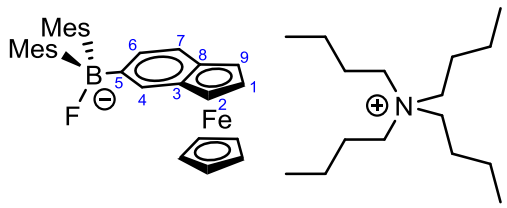

IVe (25 mg, 0.05 mmol) and [^{n}Bu$_4$N]F·4H$_2$O (21 mg, 0.06 mmol) were dissolved in dry bromobenzene-d$_5$ or thf-d$_8$ and analysed in situ by multinuclear NMR spectroscopy.

^{1}H NMR (500 MHz, bromobenzene-d$_5$, 100 °C): δ_H 1.10 (*b s*, Me of [^{n}Bu$_4$N]), 1.54 (*b s*, CH$_2$ of [^{n}Bu$_4$N]), 1.76 (*b s*, CH$_2$ of [^{n}Bu$_4$N]), 2.39 (*b s*,6H, *para-Me* of Mes), 2.52 (*b s*,12H, ortho-Me of Mes), 3.45 (*b s*, NCH$_2$ of [^{n}Bu$_4$N]), 3.96 (*b s*, 1H, CH of five membered ring of ind), 4.00 (*b s*, 5H, Cp), 4.76 (*b s*, 1H, CH of five member ring of ind), 4.88 (*b s*, 1H, CH of five member ring of ind), 6.85 (*b s*, 4H, aromatic CH of Mes), 7.41 (*bd*, $^3J_{HH}$ = 6.0 Hz, C6H or C7H), 7.76 (*m*, 2H, C7H or C6H and C4H). ♦ ^{13}C{^{1}H} NMR (126 MHz, thf-d$_8$, 25 °C): δ_C 13.3 (Me of [^{n}Bu$_4$N]), 19.6 (CH$_2$ of [^{n}Bu$_4$N]), 23.9 (CH$_2$ of [^{n}Bu$_4$N]), 20.4 (*para*-Me of Mes), 24.9 and 25.1 (*ortho*-Me of Mes), 57.9 (CH$_2$ of [^{n}Bu$_4$N]), 59.6 (C9), 59.9 (C2), 67.0 (C1), 67.2 (Cp), 87.2 (C3), 90.5 (C8), 122.4 (C7), 127.7 (aromatic CH of Mes), 128.5 (C4), 129.9 (*para*-quaternary C of Mes), 134.3 (C6), 141.4 (*ortho*-quaternary C of Mes), 155.8 (*ipso*-quaternary C of Mes) and 158.8 (C5 of ind bound to B). ♦ ^{11}B{^{1}H} NMR (160 MHz, bromobenzene-d$_5$, 100 °C): δ_B 6. ♦ ^{19}F NMR (282 MHz, thf-d$_8$, 25 °C): δ_F -172.2.

*[^{n}Bu$_4$N][**IVe**·CN]*

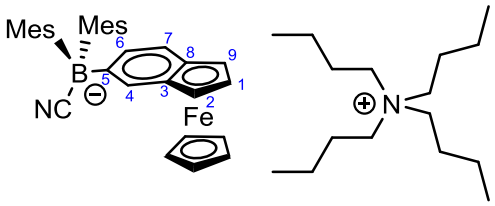

IVe (25 mg, 0.05 mmol) and [^{n}Bu$_4$N][CN]·3H$_2$O (19 mg, 0.06 mmol) were dissolved in dry bromobenzene-d$_5$ or thf-d$_8$ and analysed in situ by multinuclear NMR spectroscopy.

^{1}H NMR (500 MHz, bromobenzene-d$_5$, 100 °C): δ_H 1.05 (*t*, $^3J_{HH}$ = 6.0 Hz, Me of [^{n}Bu$_4$N]), 1.40 (*sextet*, $^3J_{HH}$ = 6.0 Hz, CH$_2$ of [^{n}Bu$_4$N]), 1.57 (*b s*,CH$_2$ of [^{n}Bu$_4$N]), 2.37 and 2.40 (*b s*, each 3H, *para-Me* of Mes), 2.50 and 2.55 (*b s*, each 6H, *ortho-Me* of Mes), 3.15 (b t, $^3J_{HH}$ = 6.1 Hz, NCH$_2$ of [^{n}Bu$_4$N]), 3.96 (*s*, 1H, five membered ring of ind), 4.04 (*s*, 5H, Cp), 4.59 and 4.95 (s, each 1H,

five membered ring of ind), 6.84 and 6.95 (*s*, each 2H, aromatic CH of Mes), 7.47 (*s*, 1H, C4H), 7.50 and 8.24 (*d*, $^{3}J_{HH}$ = 2.9 Hz, each 1H, C6H and C7H). ♦ ^{1}H NMR (500 MHz, thf-d_8, 25 °C): δ_H 0.98 (*t*, $^{3}J_{HH}$ = 7.1 Hz, Me of [^{n}Bu$_4$N]), 1.38 (*sextet*, $^{3}J_{HH}$ = 7.2 Hz, CH_2 of [^{n}Bu$_4$N]), 1.66 (*quintet*, $^{3}J_{HH}$ = 7.3 Hz, CH_2 of [^{n}Bu$_4$N]), 1.94, 1.98, 2.03 and 2.05 (*b s*, each 3H, *ortho-Me* of Mes), 2.14 and 2.17 (*b s*, each 3H, *para-Me* of Mes), 3.29 (*t*, $^{3}J_{HH}$ = 8.9 Hz, NCH_2 of [^{n}Bu$_4$N]), 3.71 (*b s*, 5H, Cp), 3.74, 4.48 and 4.64 (*b s*, each 1H, CH of five membered ring of ind), 6.47 and 6.52 (*b s*, each 2H, aromatic CH of Mes), 6.88 (*s*, 1H, C4H), 7.16 (*d*, $^{3}J_{HH}$ = 9.0 Hz, 1H, C7H), 7.72 (*d*, $^{3}J_{HH}$ = 9.1 Hz, 1H, C6H). ♦ ^{13}C{^{1}H} NMR (126 MHz, bromobenzene-d_5, 100 °C): δ_C 13.2 (Me of [^{n}Bu$_4$N]), 19.7 (CH_2 of [^{n}Bu$_4$N]), 20.3 (*para*-Me of Mes), 23.9 (CH_2 of [^{n}Bu$_4$N]), 25.3, 25.3, 25.6 and 25.7 (*ortho*-Me of Mes), 58.1 (CH_2 of [^{n}Bu$_4$N]), 59.8, 60.1 and 67.0 (C1, C2 and C9), 67.2 (Cp), 87.0 (C3), 90.1 (C8), 122.8 (C7), 128.3 and 128.4 (aromatic CH of Mes), 130.5 (C4), 130.6 (*para*-quaternary C of Mes), 136.1 (C6), 141.3, 141.8, 141.8 and 141.9 (*ortho*-quaternary C of Mes) 144.9 (CN), 151.4 (*ipso*-quaternary C of Mes), 153.2 (C5 of Ind bound to B). ♦ ^{11}B{^{1}H} NMR (160 MHz, bromobenzene-d_5, 100 °C): δ_B -13.

3.4. Results and discussion

3.4.1 Syntheses of the phenylferrocene based systems

The target sensors were synthesised *via* lithiation and subsequent electrophile capture from the respective bromophenyl ferrocenes (**I**). In the case of precursor **I**, the bromophenyl moiety can be introduced by nucleophilic aromatic substitution of the corresponding diazonium salt by ferrocene. Lithiation of the resulting bromide by treatment with a slight excess of *n*-butyllithium followed by quenching with a fluoro(dimesityl)borane leads to the desired products **II** with yields ranging from 35 to 73%.

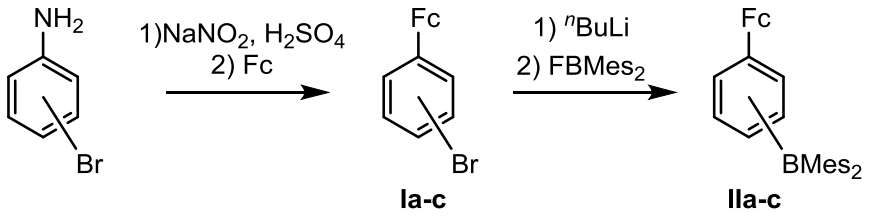

Figure 3.6: Reaction pathway of compounds **IIa-c**.

All three compounds are air and moisture stable; literature precedent implies that the steric shielding provided around the boron atom by the two *ortho*-methyl groups of the mesityl substituents prevents any reaction with water.[11] Lewis acids **IIa-c** were thus characterized fully by standard spectroscopic and analytical methods. The low-field ^{11}B NMR shifts at δ_B 78, 80 and 82 ppm for **IIa**, **IIb** and **IIc** respectively; are consistent with the presence of three-coordinate triarylboranes. The effects of the electron withdrawing borane can also be observed in the redox potential for the Fe(II)/Fe(III) couple, with an anodic shift being observed (-160 mV, -95 mV and +14 mV *vs* ferrocene / ferrocenium couple for **IIa-c**)[12,13]; thus the systems presented here appear to be slightly more electron rich than $FcBMes_2$ (*c.f.* +181 mV in acetonitrile *vs* ferrocene / ferrocenium couple).[4]

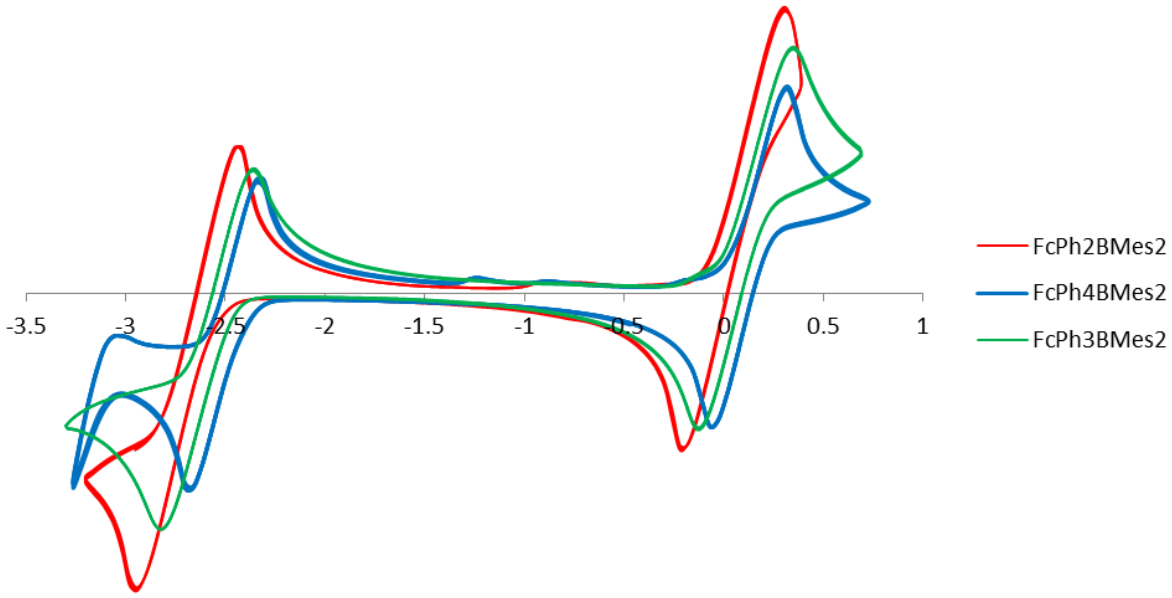

Figure 3.7: Cyclic voltammogram of **IIa-c** (0.1 M $[NH_4][PF_6]$ in thf, rate: 0.1 $V.s^{-1}$) referenced with respect to the Fc/Fc^+ couple.

In the solid state, the molecular structures of **IIa-c** (Figure 3.8 - Figure 3.10) exhibit common characteristics, notably a propeller geometry around the boron centre to accommodate the large steric profile of the aryl substituents, and a boron centre with a trigonal planar geometry ($\Sigma_{CBC} \sim 360°$). The angles between the least squares planes of the phenyl moiety and the mesityl groups are 66.9° and 70.1° for the least hindered **IIc** to the more congested **IIa** due to the close proximity of the ferrocene (**IIa**, *P*(Mes)-*P*(Ph)= 63.2° and 89.3°). The B—C bond distances are virtually identical ranging from 1.569(2) Å to 1.583(3) Å and similar to those reported in the literature ($FcBMes_2$, $B—C_{Mes}$: 1.581(7) and 1.597(7) Å).[4] In **IIa** (Figure 3.8), the close proximity of the ferrocenyl unit and the $—BMes_2$ substituent is presumably responsible for the phenyl group being aligned at a 44.2° angle to the cyclopentadienyl ligand. With the borane installed at either the *meta* or *para* position less steric buttressing is apparent and the corresponding angles are 12.5° and 27.2°, respectively (Figure 3.9 and Figure 3.10). It can therefore be expected that the orbital overlap between the two π-systems should decrease following the series **IIb**, **IIc**, **IIa**.

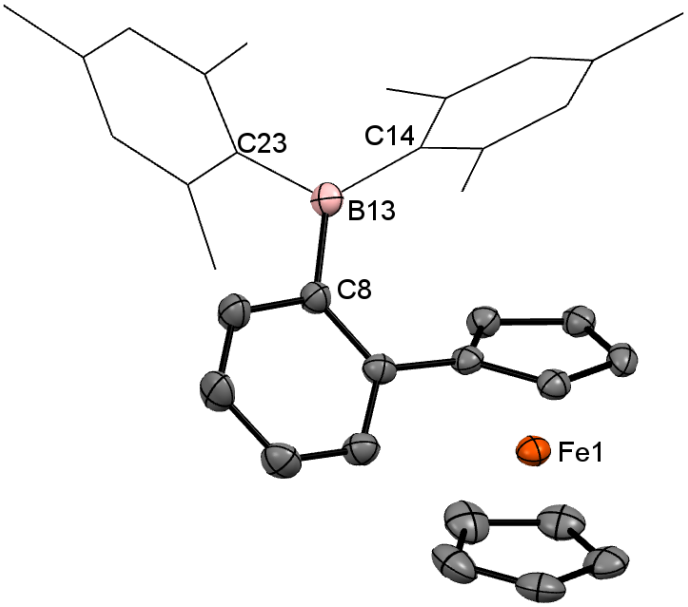

Figure 3.8: Molecular structure of **IIa**. Thermal ellipsoids set at the 50% probability level, mesityl groups shown in wireframe format and hydrogen atoms omitted for clarity (light pink: boron; black: carbon; orange: iron). Selected bond lengths [Å] and angles [°]: B13−C14 1.583(4), B13−C23 1.577(4), C8−B13 1.583(3), C8−B13−C14 123.8(2), C8−B13−C23 115.8(2), C14−B13−C23 120.3(2), *P*(Cp)—*P*(Ph) 44.2(calc.), *P*(Mes)—*P*(Ph) 63.2(calc.) and 89.3(calc.).

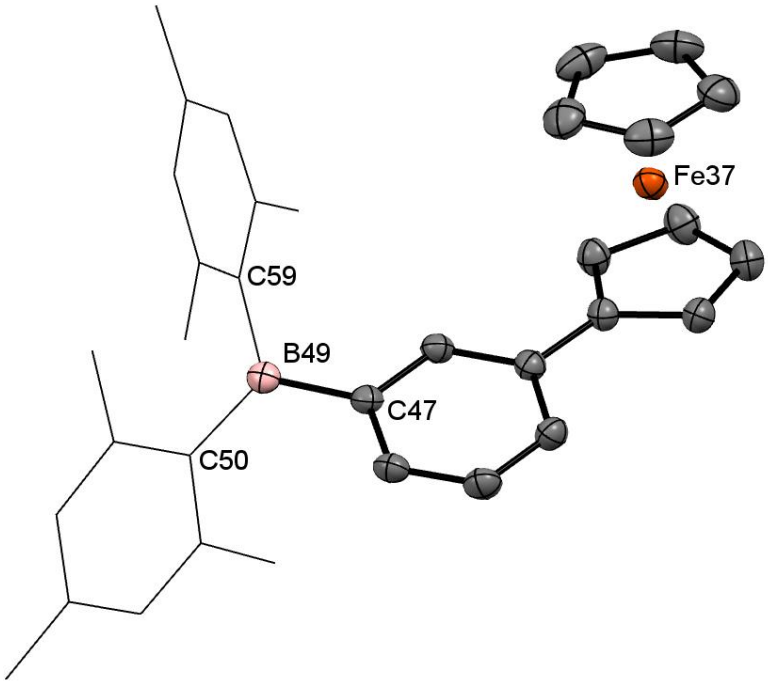

Figure 3.9: Molecular structure of **IIb**. Thermal ellipsoids set at the 50% probability level; mesityl groups shown in wireframe format and hydrogen atoms omitted for clarity (light pink: boron; black: carbon; orange: iron). Selected bond lengths [Å] and angles [°]: C47−B49 1.569(3), B49−C50 1.584(3), B49−C59 1.577(3), C47−B49−C50 118.5(2), C47−B49−C59 118.2(2), C50−B49−C59 123.3(2), *P*(Cp)—*P*(Ph) 12.5(calc.), *P*(Mes)—*P*(Ph) 75.7(calc.) and 65.1(calc.).

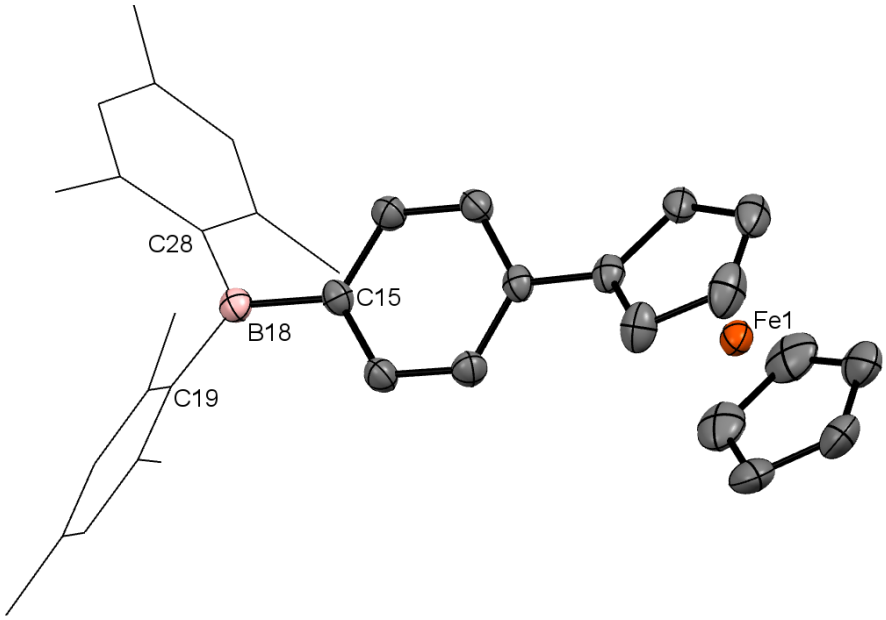

Figure 3.10: Molecular structure of **IIc**. Thermal ellipsoids set at the 50% probability level; mesityl groups shown in wireframe format and hydrogen atoms omitted for clarity (light pink: boron; black: carbon; orange: iron). Selected bond lengths [Å] and angles [°]: C19—B18 1.581(2), C15—B18 1.569(2), C28—B18 1.581(2), C28—B18—C19 123.91(13), C28—B18—C15 119.25(13), C19—B18—C15 116.81(12), *P*(Cp)—*P*(Ph) 27.2(calc.), *P*(Mes)—*P*(Ph) 66.9(calc.) and 70.1(calc.).

Distances/Angles	93	IIa	IIb	IIc
B—C_{aryl}	1.546(7) 1.581(7) 1.597(7)	1.583(4) 1.577(4) 1.583(3)	1.569(3) 1.584(3) 1.577(3)	1.581(2) 1.569(2) 1.581(2)
$\sum_{CBC}$	359.8	359.9	360.0	359.9
P(Ar)—*P*(Mes)	53.6 62.6	63.2 89.3	65.1 75.7	66.9 70.1
P(Cp)—*P*(Ph)	n/a	44.2	12.5	27.2
LUMO	-2.37 eV 34% B	-2.39 eV 41% B	-2.49 eV 42% B	-2.50 eV 34% B
HOMO	-4.27 eV 80% Fe	-3.98 eV 79% Fe	-4.11 eV 81% Fe	-4.22 eV 78% Fe

Table 3.2: Important bond lengths (Å), angles (°) and data compilation of LUMO and HOMO.

DFT calculations were also carried out on receptors **IIa-c**, and on $FcBMes_2$ (**93**) as a point of comparison (Figure 3.11). In each case the experimentally observed geometry was reproduced well by computational methods, and molecular orbital energies/compositions were used to assess the Lewis acidity of the receptor. The LUMO of all three phenylferrocene based systems is centred for the most part on the boron atom (*e.g.* 42% in **IIb**) and found at a similar energy in each case (-2.39 eV, -2.49 eV and -2.50 eV for **IIa**, **IIb** and **IIc**). The extension of the aromaticity could explain the slight decrease in energy levels for the LUMO of **IIa-c** with respect to $FcBMes_2$, with -2.50 eV for **IIc** against -2.37 eV for $FcBMes_2$. It should be noted that all four receptorss have significant contributions to the HOMO and HOMO-1 carried by the metal centre, with a contribution up to 81% of the *d*-orbitals in the case of HOMO(**IIb**).

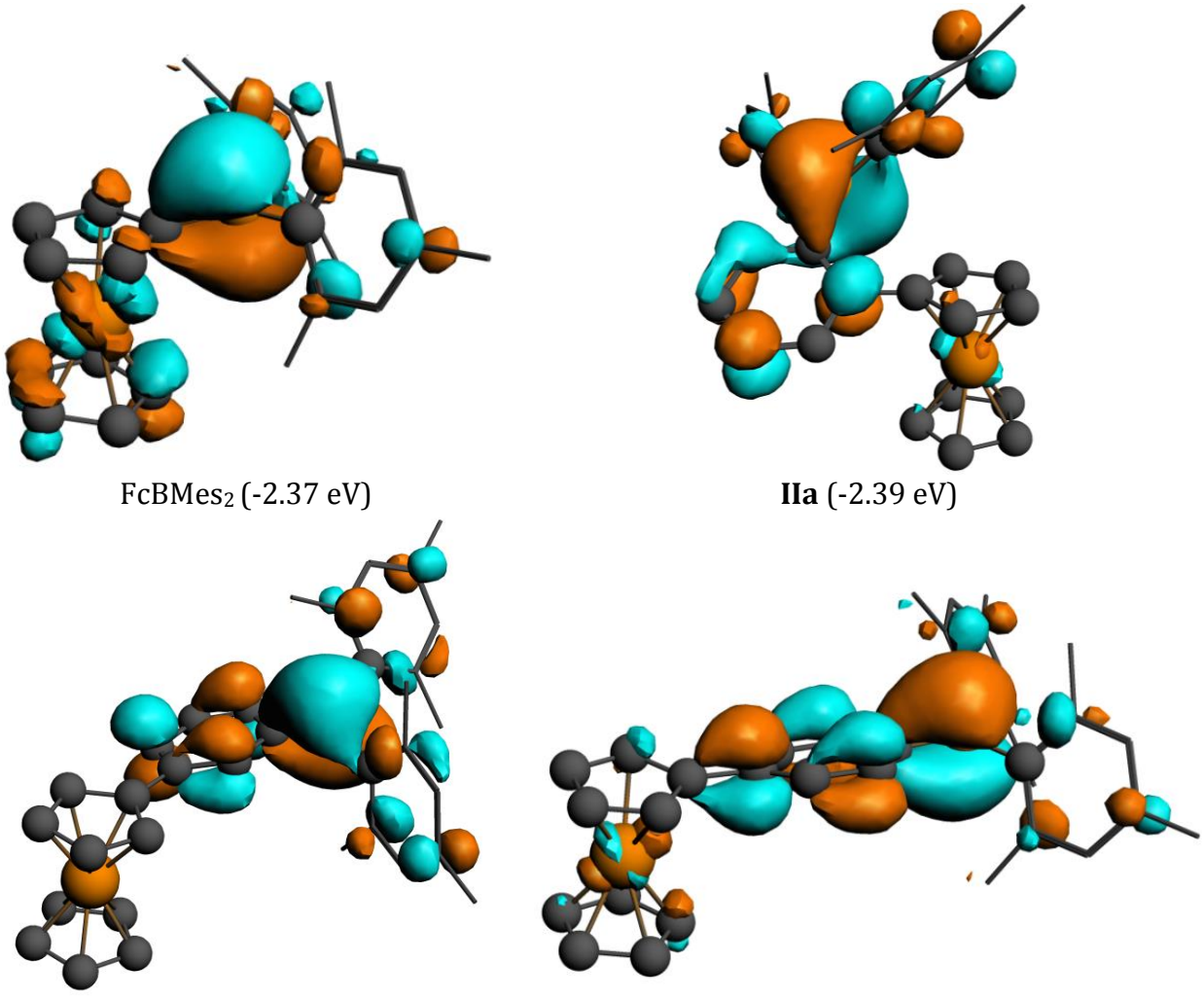

$FcBMes_2$ (-2.37 eV) **IIa** (-2.39 eV)

IIb (-2.49 eV) **IIc** (-2.50 eV)

Figure 3.11: Contour plot of the LUMO and energy level of $FcBMes_2$ (**93**) and **IIa-c** (density isovalues = 0.03).

3.4.2 Anion binding of the phenylferrocene systems

The propensity of the phenylferrocene derived receptors to bind either fluoride or cyanide in non-aqueous media has been examined by means of a range of spectroscopic methods. The exposure of **IIa-c** to a source of fluoride such as $[^{n}Bu_4N]F{\cdot}4H_2O$ or KF with 18-crown-6, in dry tetrahydrofuran or chloroform leads to the binding of fluoride in a 1:1 fashion. The fixation of the anion is accompanied by a large upfield shift in the ^{11}B NMR spectrum (from $\delta_B \sim 77$ to ~ 7 ppm); in addition the presence of a single peak in respective ^{19}F NMR spectra (δ_F *ca.* -170 ppm) is consistent with the formation of a fluoroborate ion. Furthermore, the resulting negatively charged fluoride adducts are detectable *via* negative ion ESI-MS as a peak envelope matching the expected $[\mathbf{II}{\cdot}F]^-$ isotopic profile (and with the correct accurate mass). Under the same anhydrous conditions, receptors **IIa-c** can also bind the cyanide ion. As with fluoride, upon treatment with $[^{n}Bu_4N][CN]{\cdot}3H_2O$, the ^{11}B NMR spectrum exhibits a sharp upfield-shifted resonance (at δ_B *ca.* -13 ppm); a broad peak at about δ_C 150 ppm in the ^{13}C NMR spectrum corresponds to the cyanide carbon bound to the quadrupolar boron nucleus.

To appraise the relative binding affinities for fluoride and cyanide, the addition of cyanide to $[\mathbf{II}{\cdot}F]^-$ was examined. The fluoride ion is rapidly displaced by cyanide, as observed by characteristic ^{11}B and ^{19}F NMR shifts. The reverse competition experiment was also carried out, although addition of excess fluoride to $[\mathbf{II}{\cdot}CN]^-$ yields no change in either ^{11}B or ^{19}F NMR spectra for any of the three receptors (Figure 3.12). These experiments imply that cyanide binding is the more thermodynamically favourable process.

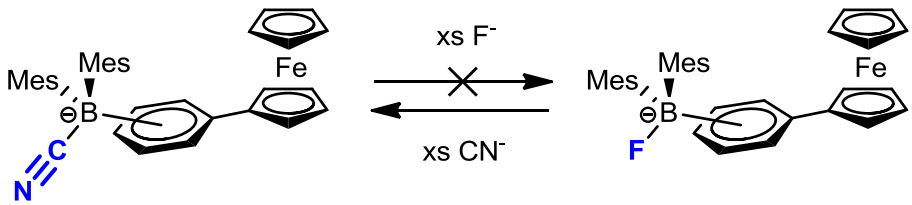

Figure 3.12: Competition experiments of **IIa-c** with fluoride and cyanide.

The binding constants of **IIa-c** for cyanide and fluoride ion can be assessed explicitly by monitoring the incremental addition of an aliquot of either anion using UV-vis spectroscopy (Figure 3.13 to Figure 3.15). The binding constants were fitted to a 1:1 binding isotherm in each case, and the results listed in Table 3.3. The binding constants fall within the typical range for triarylboranes, although the extended π-conjugation highlighted in the solid state and the lower LUMO in the DFT calculations, are consistent with an increase of the binding constants for **IIb** and **IIc** when compared to $FcBMes_2$. For instance, the binding of cyanide is increased by a factor of 34 from $FcBMes_2$ to **IIc**, and the corresponding fluoride affinity is 26 times higher. The effect is minor with receptor **IIa**, since the pyramidalization process that comes with fluoride binding is impeded by the large steric hindrance of the boron centre.

Entry	K(F), M^{-1}	K(CN), M^{-1}
$FcBMes_2$ (**93**)	$7.8(1.2) \times 10^4$	$8.3(2.0) \times 10^4$
IIa	$6.05(0.4) \times 10^5$	$3.98(0.4) \times 10^5$
IIb	$2.69(0.5) \times 10^6$	$7.01(0.4) \times 10^5$
IIc	$2.06(0.4) \times 10^6$	$2.80(0.4) \times 10^6$

Table 3.3: Binding constants of **IIa-c** in thf and $FcBMes_2$ in DCM.[4]

The absence of isosbestic points in all spectra is not the result of a simple dilution since any excess addition of either fluoride or cyanide leads to no change in the absorbance profile (*c.f.* insets of Figure 3.13 to Figure 3.15). Instead it should be interpreted as evidence of the large contribution of the boron centre to the low energy absorption. Moreover the superimposed spectra in Figure 3.16 highlight the similar behaviour for all three quenched sensors in the visible spectrum, with an absorbance maximum centred at about 445 nm. Interestingly the λ_{max} for ferrocene is at 440 nm, thus the main absorbance of the quenched Lewis acids could be attributable to the weak *d-d* electron transitions of the ferrocene unit.[14]

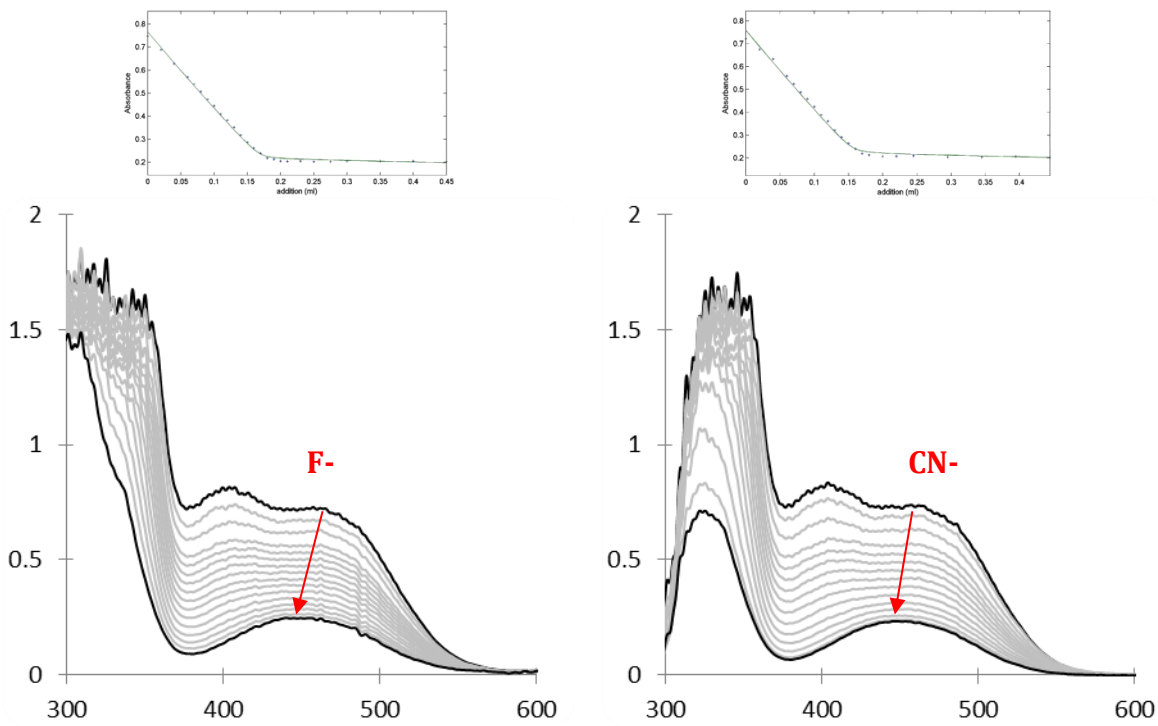

Figure 3.13: Left: Changes in the UV-vis absorption spectra of a solution of **IIa** (3 mL, 9.72 × 10^{-4} M in THF) upon the addition of $[^{n}Bu_4N]F{\cdot}4H_2O$ (1.90 × 10^{-2} M in thf). Right: Changes in the UV-vis absorption spectra of a solution of **IIa** (3 mL, 9.76 × 10^{-4} M in thf) upon the addition of $[^{n}Bu_4N][CN]{\cdot}3H_2O$ (2.12 × 10^{-2} M in thf). Inset: fitting curves log*K*(F)= 5.782 ± 0.033 (*σr*= 0.0074, *ssq*= 0.111); log*K*(CN)= 5.600 ± 0.052 (*σr*= 0.052, *ssq*= 0.361).

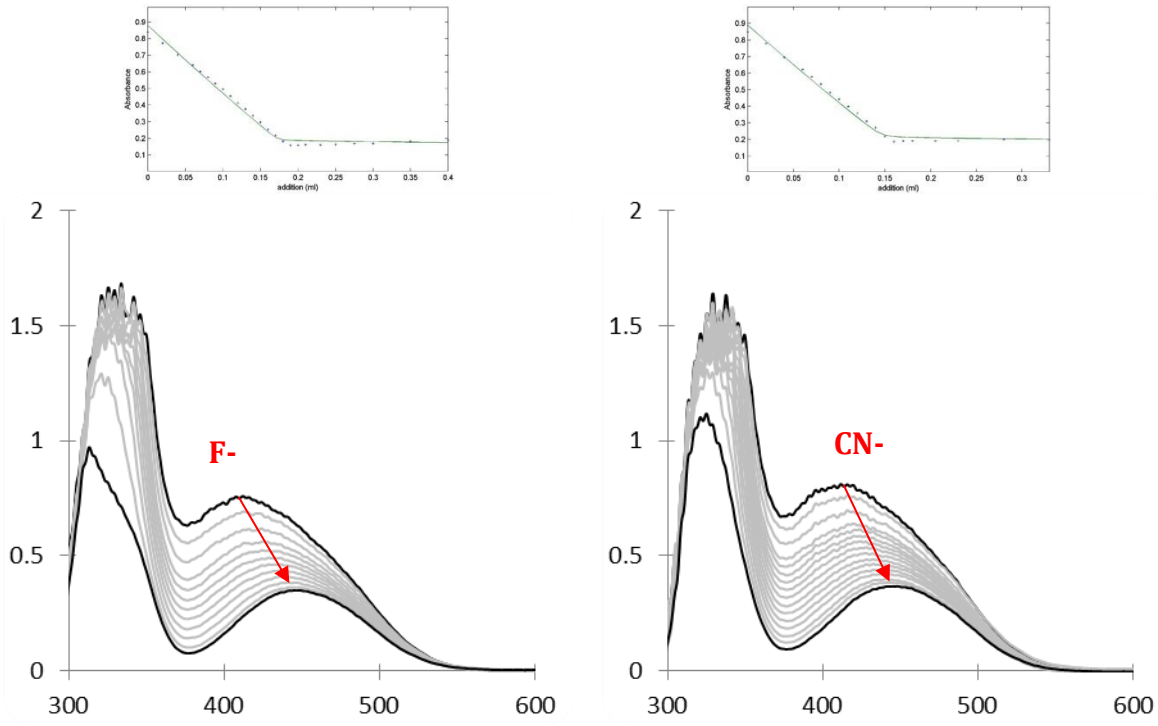

Figure 3.14: Left: Changes in the UV-vis absorption spectra of a solution of **IIb** (3 mL, 1.39 × 10^{-4} M in THF) upon the addition of $[^{n}Bu_4N]F{\cdot}4H_2O$ (2.39 × 10^{-2} M in thf). Right: Changes in the UV-vis absorption spectra of a solution of **IIb** (3 mL, 1.34 × 10^{-4} M in thf) upon the addition of $[^{n}Bu_4N][CN]{\cdot}3H_2O$ (3.14 × 10^{-2} M in thf). Inset: fitting curves log*K*(F)= 6.429 ± 0.138 (*σr*= 0.0131, *ssq*= 0.327); log*K*(CN)= 5.846 ± 0.076 (*σr*= 0.0138, *ssq*= 0.288).

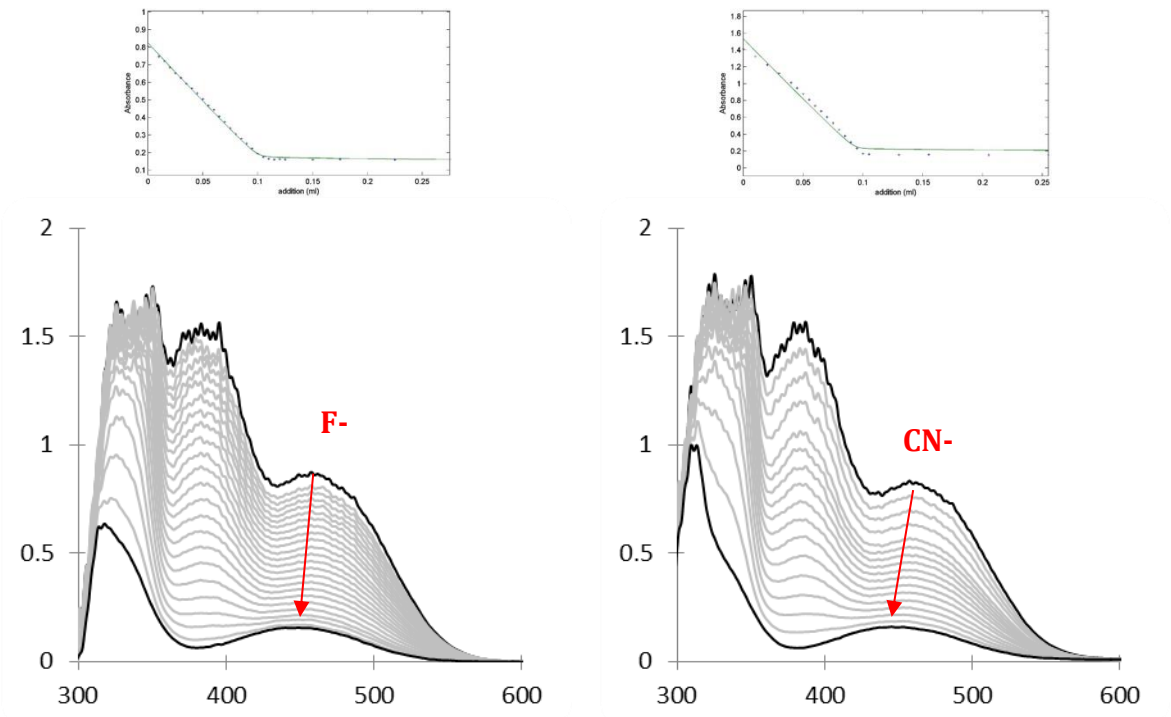

Figure 3.15: Left: Changes in the UV-vis absorption spectra of a solution of **IIc** (3 mL, 3.61 × 10^{-4} M in THF) upon the addition of [^{n}Bu$_4$N]F·4H$_2$O (1.23 × 10^{-2} M in thf). Right: Changes in the UV-vis absorption spectra of a solution of **IIc** (3 mL, 3.61 × 10^{-4} M in thf) upon the addition of [^{n}Bu$_4$N][CN]·3H$_2$O (1.20 × 10^{-2} M in thf). Inset: fitting curves log*K*(F)= 6.3138 ± 0.038 (*σr*= 0.0089, *ssq*= 0.134); log*K*(CN)= 6.447 ± 0.136 (*σr*= 0.0586, *ssq*= 5.05).

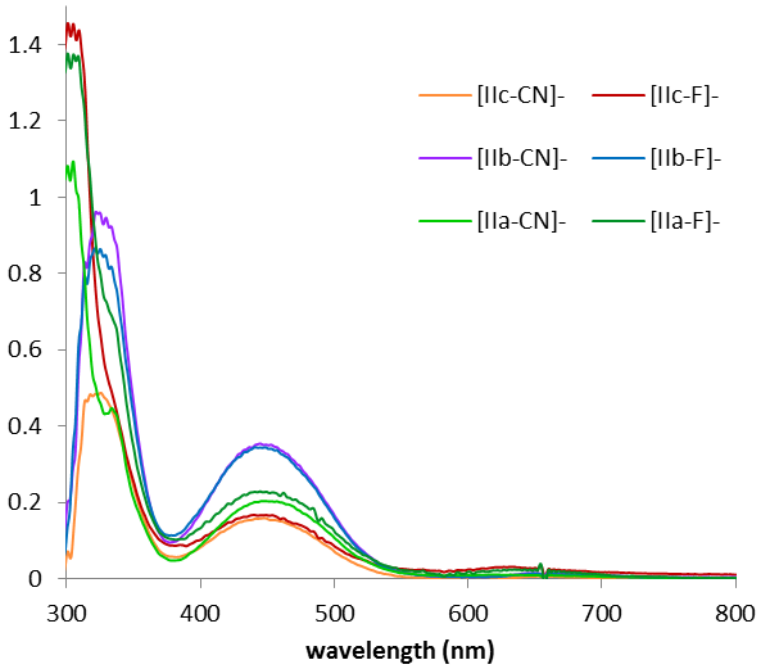

Entry	λ_{max} (nm)
[**IIc**·CN]$^-$	448
[**IIc**·F]$^-$	440
[**IIb**·CN]$^-$	445
[**IIb**·F]$^-$	441
[**IIa**·CN]$^-$	446
[**IIa**·F]$^-$	445
Ferrocene	440

Figure 3.16: (*left*) UV-vis absorption spectrum of **IIa-c** in presence of an excess of fluoride or cyanide ion. (*right*) table of the maximum absorption in the visible spectrum of the sensor's adduct and ferrocene for reference.

A main objective of this project was to develop a series of receptors offering a distinct change of colour upon anion binding. Unfortunately the response observed here is only detectable by UV-vis spectroscopy. Furthermore in the presence of a small amount of water (*e.g.* thf/water 95:5 vol.) rendered the binding null for either cyanide or fluoride ion (with the exception of **IIc** which binds cyanide in water, albeit with very slow kinetics of uptake).

The mode of binding of fluoride and cyanide by **IIa-c** was also investigated by X-ray crystallography. Thus, the structures of [^{n}Bu$_4$N][**IIa**·F], [^{n}Bu$_4$N][**IIc**·F], [K(18-crown-6)][**IIb**·CN] and [K(18-crown-6)][**IIc**·CN] reveal consistently similar geometric and bond distance patterns (Figure 3.17 to Figure 3.20). For instance, the B—F bonds are similar for **IIa** and **IIb** (1.471(3) and 1.479(5) Å respectively) and similar observations can be made for the cyanide adducts **IIb** and **IIc** (B—CN: 1.666(5) and 1.641(3) Å). All adduct structures confirm the formation of a tetrahedral boron centre (Σ_{CBC} = 339.0°, 337.9°, 339.9° and 341.1° for [**IIa**·F]$^-$, [**IIc**·F]$^-$, [**IIb**·CN]$^-$ and [**IIc**·CN]$^-$ respectively). In addition, a general elongation of the phenyl B—C$_{ipso}$ can also be observed, with a maximum of +5.5% from **IIa** to [**IIa**·F]$^-$ (1.569(3) Å to 1.656(3) Å). Secondary supramolecular interactions can be identified in the solid state structures originating from the residual Lewis basicity at the nitrogen atom of the bonded cyanide ion. This manifests itself as a short contact between the cyanide and the potassium counter-ion (*e.g.* K39—N15 2.762 Å, K2—N12 2.785 Å for [**IIb**·CN]$^-$ and [**IIc**·CN]$^-$) which falls within the sum of the relevant Van der Waals' radii ($\sum_{VdW}$(K—N) = 4.30 Å).[15]

Bonds/Angles	FcB(CN)Mes$_2$	[^{n}Bu$_4$N][**IIa**·F]	[^{n}Bu$_4$N][**IIc**·F]	K[**IIb**·CN]	K[**IIc**·CN]
B—C$_{aryl}$	1.672(4)	1.656(3)	1.656(3)	1.641(3)	1.665(5)
	1.661(4)	1.674(3)	1.674(3)	1.674(3)	1.643(5)
	1.639(4)	1.661(3)	1.661(3)	1.651(3)	1.666(5)
B—X (X= F, CN)	1.621(3)	1.471(3)	1.479(5)	1.631(3)	1.631(5)
$\sum_{CBC}$	337.21	339.02	337.9	339.88	341.1
P(Cp)—*P*(Ph)	n/a	30.80	15.5	37.5	15.8

Table 3.4: Important bond lengths (Å) and angles (°).

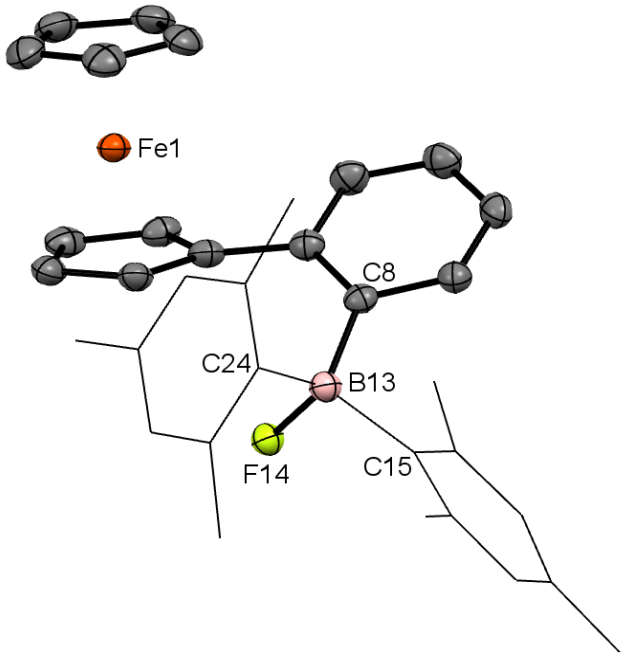

Figure 3.17: Molecular structure of [^{n}Bu$_4$N][**IIa**$^{\cdot}$F]. Thermal ellipsoids set at the 50% probability level; mesityl groups shown in wireframe format and hydrogen atoms omitted for clarity (light pink: boron; black: carbon; orange: iron, yellow: fluoride). Selected bond lengths [Å] and angles [°]: C8—B13 1.656(3), C15—B13 1.674(3), C24—B13 1.661(3), B13—F14 1.471(3), C15—B13—C24 110.13(17), C15—B13—C8 110.63(18), C24—B13—C8 118.26(18), (Cp)—(Ph) 30.80(calc.).

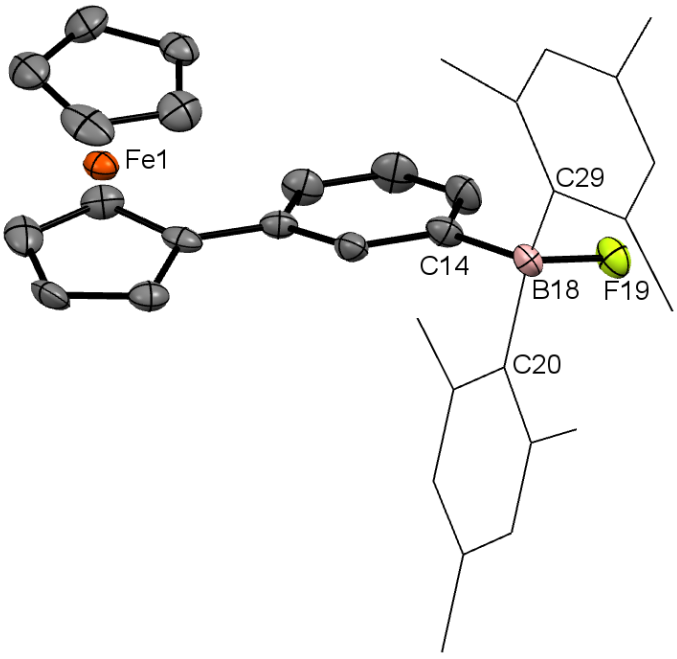

Figure 3.18: Molecular structure of [^{n}Bu$_4$N][**IIb**$^{\cdot}$F]. Thermal ellipsoids set at the 50% probability level; mesityl groups shown in wireframe format, and hydrogen atoms and the tetrabutylammonium counter cation omitted for clarity (light pink: boron; black: carbon; orange: iron, yellow: fluoride). Selected bond lengths [Å] and angles [°]: B55—F56 1.479(5), B55—C57 1.650(6), B55—C66 1.666(6), C14—B18 1.631(7), C14—B18—C20 104.8(3), C14—B18—C29 119.2(4), C20—B18—C29 113.9(4), *P*(Cp)—*P*(Ph) 15.5(calc.).

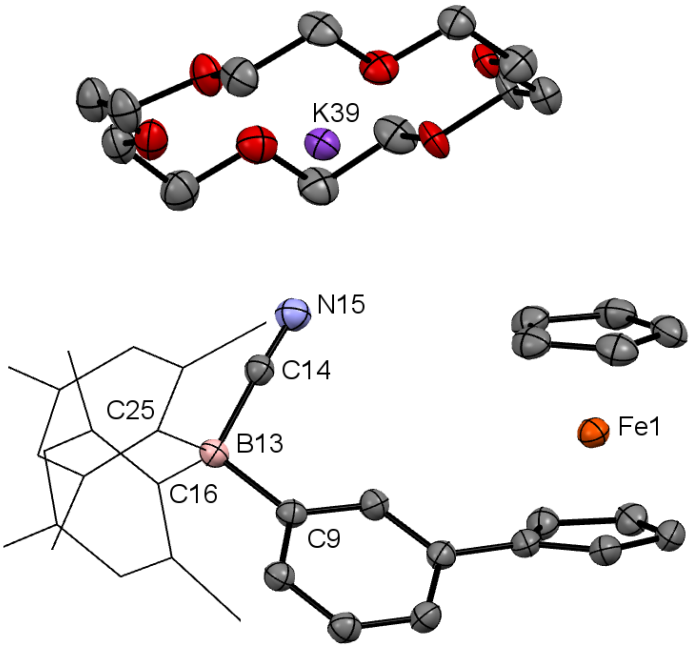

Figure 3.19: Molecular structure of [K(18-crown-6)][**IIb**·CN]. Thermal ellipsoids set at the 50% probability level; mesityl groups shown in wireframe format and hydrogen atoms omitted for clarity (light pink: boron; black: carbon; orange: iron; blue: nitrogen; purple: potassium; red: oxygen). Selected bond lengths [Å] and angles [°]: B13−C9 1.641(3), B13−C14 1.631(3), B13−C16 1.674(3), B13−C25 1.651(3), K39−N15 2.762(calc.), C14−N15 1.152(3), C9−B13−C16 118.70(19), C9−B13−C25 106.48(18), C16−B13−C25 114.70(19), B13−C14−N15 175.1(2), *P*(Cp)−*P*(Ph) 37.5(calc.).

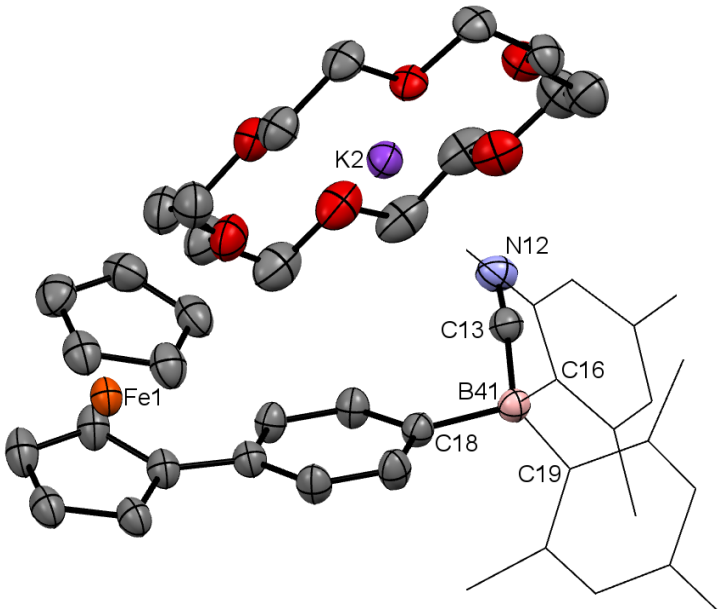

Figure 3.20: Molecular structure of [K(18-crown-6)][**IIc**·CN]. Thermal ellipsoids set at the 50% probability level; mesityl groups shown in wireframe; hydrogen atoms and chloroform solvent molecules are omitted for clarity (light pink: boron; black: carbon; orange: iron, blue: nitrogen; purple: potassium). Selected bond lengths [Å] and angles [°]: B41−C13 1.631(5), B41−C16 1.665(5), B41−C18 1.643(5), B41−C19 1.666(5), C13−N12 1.153(4) , K2−N12 2.785(calc.), C16−B41−C18 107.7(3), C16−B41−C19 115.0(3), C18−B41−C19 118.4(3), B41−C13−N12 172.9(3), K39−N24−C23 144.55(calc.), *P*(Cp)−*P*(Ph) 15.8(calc.).

The molecular structure of the [**IIa**·F]$^-$ anion is consistent with the presence of significant steric hindrance, with a relatively short distance between the centroid of the substituted cyclopentadienyl ligand and the bound fluoride (3.67 Å, Figure 3.17) implying comparatively close contact between the *ortho* aligned ferrocenyl and borate entities. The structural rearrangement upon the fixation of fluoride or cyanide by the boron centre could therefore be at the origin of a lower binding constants measured for **IIa** (*c.f.* Table 3.3).

Finally, the effects of fluoride and cyanide binding on **IIa-c** were probed by cyclic voltammetry measurements (Figure 3.21); unfortunately the anion-binding induced electrochemical shifts are not high. For instance, **IIb** undergoes a shift of -179 mV on binding and -283 mV for **IIc** in thf (*c.f.* $\Delta(E^0)$= -560 mV for $FcBMes_2$ in dichloromethane).

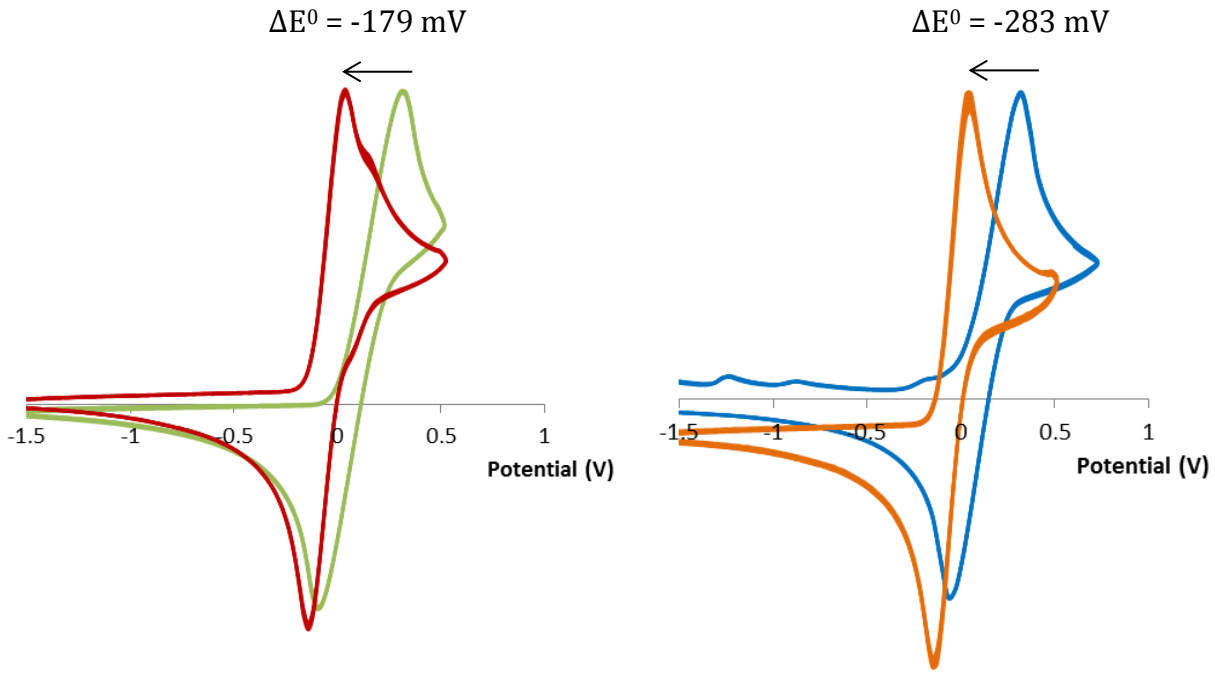

Figure 3.21: Cyclic voltammograms of (*left*) **IIb** and [**IIb**·CN]$^-$ and (*right*) **IIc** and [**IIc**·CN]$^-$ (0.1 M $[NH_4][PF_6]$ in thf, rate: 0.1 V s^{-1}) referenced with respect to the Fc/Fc+ couple.

Thus, in conclusion it seems that series **II** compounds are not good candidates as colorimetric anionic receptors in that they possess; (*i*) little or no binding activity in presence of water, (*ii*) small effects on either the colour or the electrochemical response upon binding. A potential solution to those two problems would be to enhance the communication pathway

between the reporter and binding site, while increasing the Lewis acidity by strengthening the π-conjugation of the free receptor. Thus an iron cyclopentadienyl-indenyl scaffold would seem to be more suitable for the tasks at hand.

3.4.3 Syntheses of the indenyl based systems

For the synthesis of the indenyl receptors **IIIe** and **IVe** (Figure 3.22) several routes were considered, but the path highlighted in Figure 3.23 is the only one that allows the final compounds to be isolated with workable yields and with ease of scale-up.

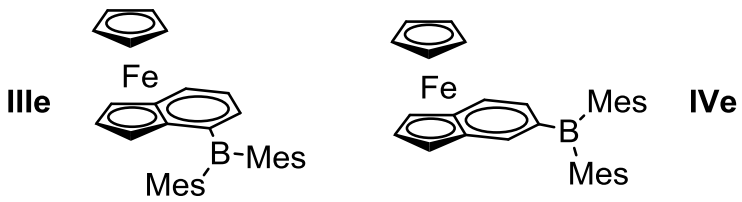

Figure 3.22: Indenyl based receptors **IIIe** and **IVe**.

The synthesis of **IVe** is possible by starting from commercially available 3-(3-bromophenyl) propionic acid; only the first step differs from the synthesis of **IIIe**, with chlorosulfonic acid being employed instead of thionyl chloride/aluminium chloride for the cyclisation step. Once the indenone is formed, it undergoes sequential reduction/dehydration steps before being introduced to [FeCp(naphthalene)][PF_6], a source of $[FeCp]^+$ in which the naphthalene ligand is easily displaced by the stronger donor indenyl ligand. The last step consists of the substitution of bromine by the dimesitylboryl function *via* a lithiation/$FBMes_2$ quench protocol.

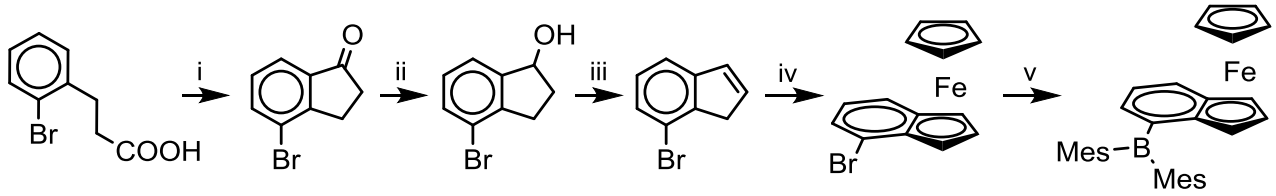

Figure 3.23: Synthesis of **IIIe**, key reagents and conditions: (*i*) reflux in $SOCl_2$ neat / $AlCl_3$, (*ii*) $NaBH_4$ (*iii*) *p*-TsOH in toluene 120° C, (*iv*) KH (1.05 equiv.) / [CpFe(η^6-$C_{10}H_8$)][PF_6] (1.05 equiv.) (*v*) ^{n}BuLi (1.05 equiv.), -78 ^{o}C / $FBMes_2$ (1.05 equiv.).

The products **IIIe** and **IVe** were fully characterized by multinuclear spectroscopy and while no unusual shifts were observed in the ^{11}B NMR spectrum (δ_B 77 and 75 ppm for **IIIe** and **IVe**), the ^{1}H NMR of **IIIe** features noticeable peak broadening not observed for **IVe**. Variable temperature ^{1}H NMR measurements were carried out at temperatures as low as -50° C to probe for fluxional processes (Figure 3.24). At -40° C in deuterated chloroform the signals for the mesityl units are "frozen out", the broad signal at δ_H 2.13 ppm splits into four sharp signals (δ_H 1.48, 1.97, 2.25 and 2.40 ppm) one for each *ortho*-methyl group. Concurrently, in the aromatic region four sharp signals (δ_H 6.65, 6.76, 6.88 and 6.91 ppm) integrating to one proton each emerge from the broad singlet (δ_H 6.84 ppm) observed at 20° C. The signals in question are attributed to the *ortho*-methyl groups and *meta*-CH protons of the mesityl substituents; the source of the broadening at room temperature is thought to be restriction of free rotation of the mesityl groups due to close interactions between the adjacent proton of the cyclopentadienyl ligand and the mesityl *ortho* methyl substituents.

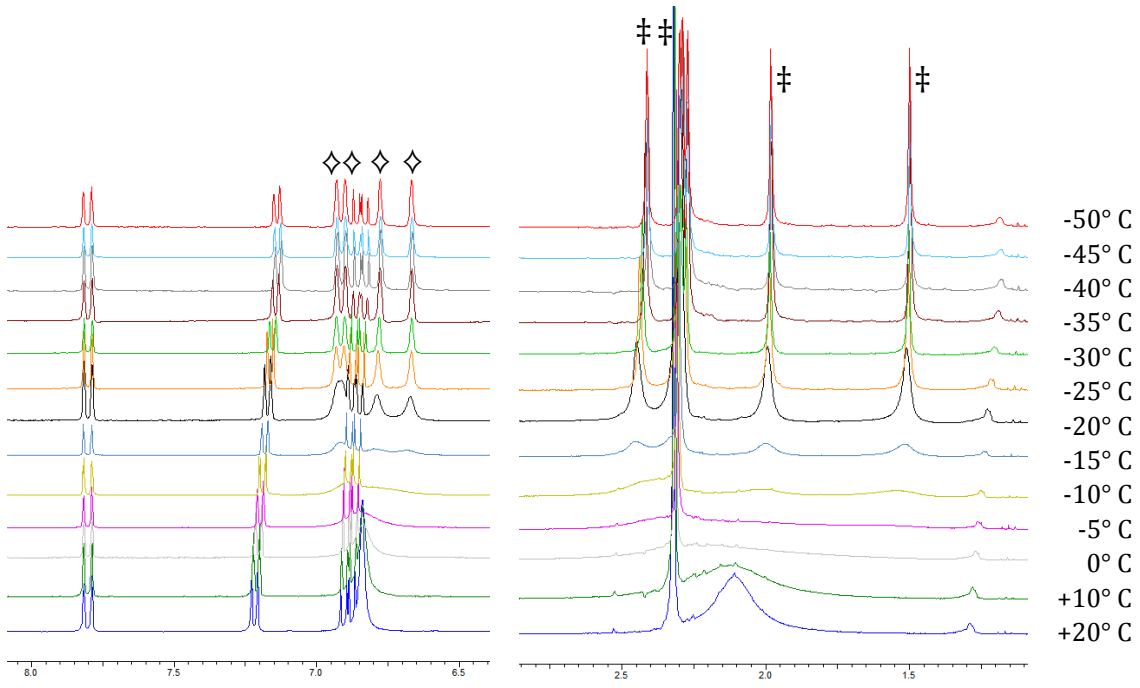

Figure 3.24: Alkyl and aromatic regions of the ^{1}H NMR of **IIIe** in chloroform as a function of temperature (^{1}H signals for the *meta*-CH (♢) and the *ortho*-methyls (‡) of the mesityl substituents).

The congestion at the boron centre is also noticeable in the molecular structure of **IIIe** (Figure 3.26). Thus the angle between the least squares planes of the cyclopentadienyl ligand and the indenyl moiety in the bromo-indenyl starting material (**IIId**) is only 1.10° (Figure 3.25); whereas the dimesitylborane compound **IIIe** exhibits an angle of 7.30° consistent with a significant increase in steric crowding.

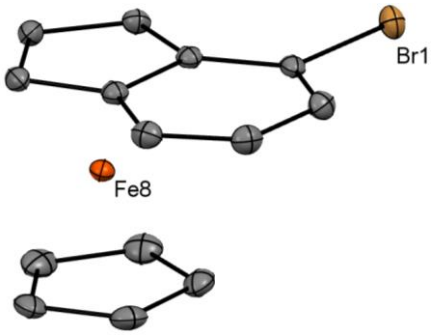

Figure 3.25: Molecular structure of **IIId**. Thermal ellipsoids set at the 50% probability level and hydrogen atoms omitted for clarity (auburn: bromine; black: carbon; orange: iron).

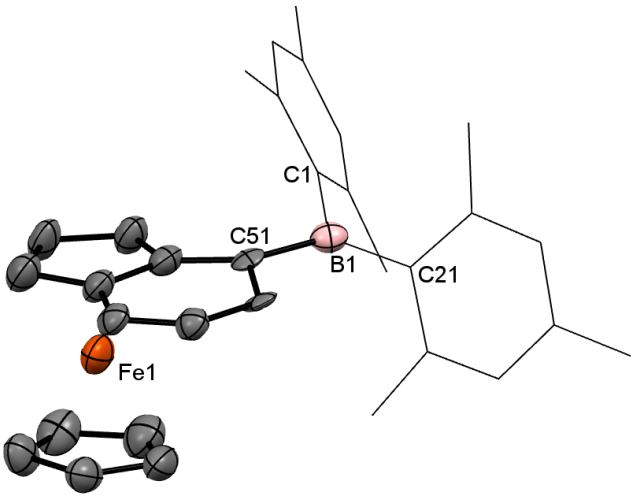

Figure 3.26: Molecular structure of **IIIe**. Thermal ellipsoids set at the 50% probability level; mesityl groups shown in wireframe format and hydrogen atoms omitted for clarity (light pink: boron; black: carbon; orange: iron). Selected bond lengths [Å] and angles [°]:B1—C1 1.613(4), B1—C21 1.510(6), B1—C51 1.585(5), C1—B1—C21 124.8(7), C1—B1—C51 114.6(5), C21—B1—C51 120.0(6), *P*(Mes)—*P*(ind) 67.5 and 65.9.

The other dimensions of receptor **IIIe** are statistically similar to the receptors **IIa-c**; from the propeller like geometry (66.0° and 66.3° between the least squares planes of the phenyl moiety and mesityl groups) to the trigonal planar boron ($\sum_{CBC}$ = 359.4°) and the B—C bond distances (B—C_{Mes} : 1.613(4) and 1.510(6), B—$C_{indenyl}$: 1.585(5)).

Additionally, the redox potentials of the iron centres in **IIIe** and **IVe** can be assessed by cyclic voltammetry measurements. These systems exhibit reversible waves centred at +16 mV and +15 mV respectively, when referenced against the ferrocene/ferrocenium couple (Figure 3.27). The more electron rich indenyl ligand is at the origin of the cathodic shift when compared to the receptors **IIa-c** (*c.f.* +628 mV for **IIc**).

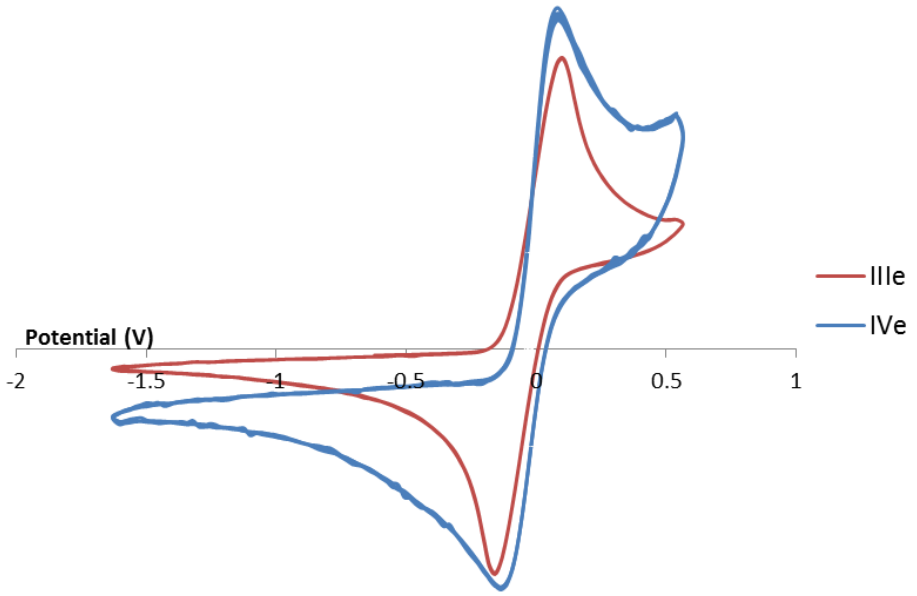

Figure 3.27: Cyclic voltammograms of receptors **IIIe** and **IVe** (0.1 M $[NH_4][PF_6]$ in thf, rate: 0.1 V s^{-1}) referenced with respect to the ferrocene/ferrocenium couple.

3.4.4 Anion binding by indenyl receptors

As with the phenylferrocene systems, the addition of either cyanide or fluoride leads to the quenching of the Lewis acidic boron centre as per the observed ^{11}B NMR shifts to *ca.* δ_B -15 and 6 ppm respectively. The fluoride adducts exhibit a single peak in the respective ^{19}F NMR spectra at δ_F -169.1 and -179.5 ppm for [**IIIe**·F]$^-$ and [**IVe**·F]$^-$, consistent with the formation of a fluoroborate anion.[11] Mass spectroscopy further confirms the formation of all four adducts and accurate masses consistent with the target compounds. Several attempts to measure the redox potentials of the anion adducts met with little success; unfortunately the fluoro or cyanoborate products both exhibit irreversible behaviour for the oxidation of the iron centre. A possible reason for this is ring slippage, *i.e.* a change of the indenyl hapticity

from η^5 to η^6 induced by oxidation at the iron centre and the extra electron density introduced by the formation of the borate (Figure 3.28).

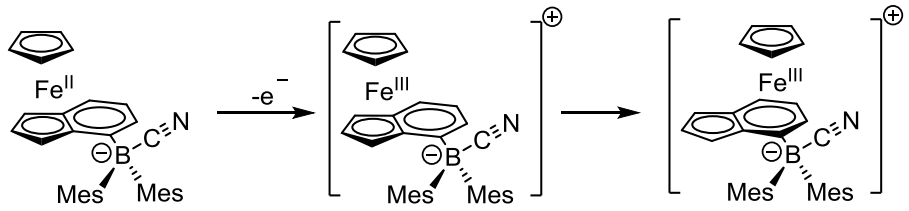

Figure 3.28: Proposed mechanism for the irreversible oxidation of [**IIIe**·CN]$^-$.

The binding events for **IIIe** and **IVe** are readily discernible by the naked eye. For instance while the free sensors **IIIe** is dark green, the cyanide or fluoride adducts are of a vivid red colour (Figure 3.29). The fluoride and cyanide affinities were measured using UV-vis titrations (Figure 3.30 and Figure 3.31), and the results are summarised in Table 3.5 along with the results from section 3.4.2. The binding of cyanide by **IIIe** is four times stronger than fluoride in dry solvents, for **IIIe** (K = 2.28(0.5) × 10^6 M^{-1} and 10.19(3.8) × 10^6 M^{-1} for fluoride and cyanide respectively). The affinity for fluoride does not seem to benefit as much from the extended π-aromaticity, unlike the cyanide affinity which increased by 25 fold compared to receptor **IIa**.

Entry	K(F), M^{-1}	K(CN), M^{-1}
IIa	0.605(0.4) × 10^6	0.398(0.4) × 10^6
IIb	2.69(0.5) × 10^6	0.701(0.4) × 10^6
IIc	2.06(0.4) × 10^6	2.80(0.4) × 10^6
IIIe	2.28(0.5) × 10^6	10.19(3.8) × 10^6
IVe	1.91(0.1) × 10^6	9.31(0.8) × 10^6

Table 3.5: Fluoride and cyanide binding constants of **IIa-c**, **IIIe** and **IVe** in dry thf.

Figure 3.29: (*left*) sensor **IIIe** in thf (*right*) **IIIe** in the presence of $[^{n}Bu_4N]F{\cdot}4H_2O$ or $[^{n}Bu_4N][CN]{\cdot}3H_2O$ in dry thf.

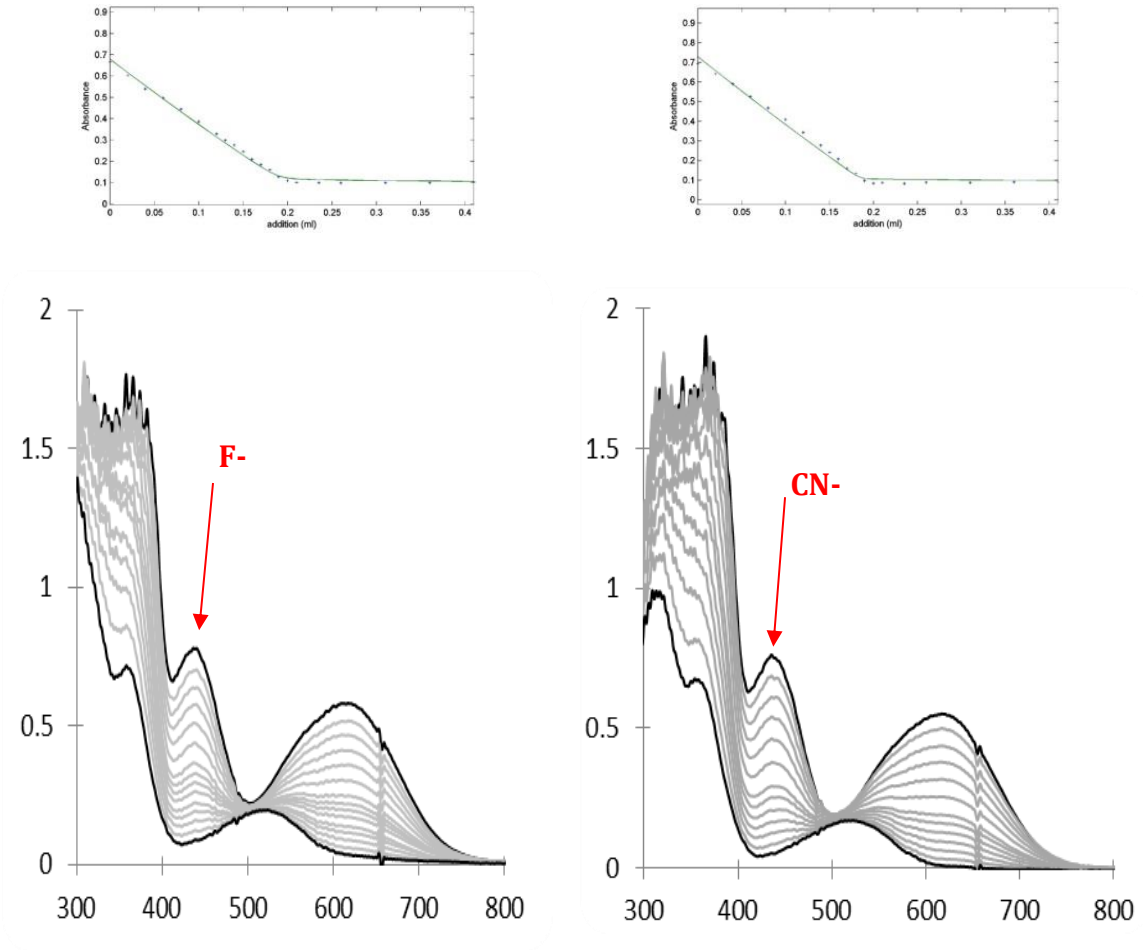

Figure 3.30: Left: Changes in the UV-vis absorption spectra of a solution of **IIIe** (3 mL, 6.37 × 10^{-4} M in THF) upon the addition of $[^{n}Bu_4N]F{\cdot}4H_2O$ (1.0 × 10^{-2} M in thf). Right: Changes in the UV-vis absorption spectra of a solution of **IIIe** (3 mL, 6.29 × 10^{-4} M in thf) upon the addition of $[^{n}Bu_4N][CN]{\cdot}3H_2O$ (1.07 × 10^{-2} M in thf). Inset: fitting curves. log*K*(F)= 6.358 ± 0.102 (*σr*= 0.0152, *ssq*= 0.291); log*K*(CN)= 7.008 ± 0.205 (*σr*= 0.0122, *ssq*= 0.196).

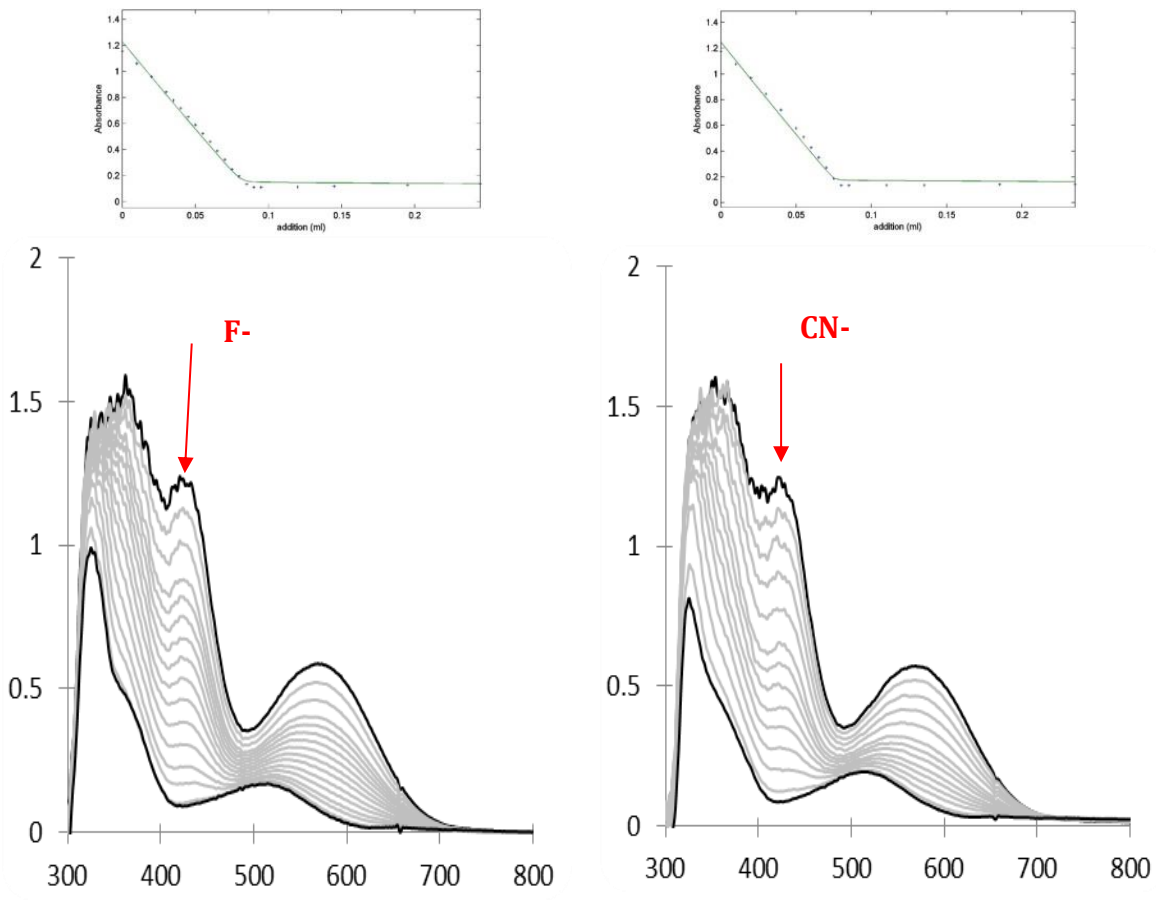

Figure 3.31: Left: Changes in the UV-vis absorption spectra of a solution of **IVe** (3 mL, 6.27 × 10^{-4} M in THF) upon the addition of $[^{n}Bu_4N]F{\cdot}4H_2O$ (2.30 × 10^{-2} M in thf). Right: Changes in the UV-vis absorption spectra of a solution of **IVe** (3 mL, 6.10 × 10^{-4} M in thf) upon the addition of $[^{n}Bu_4N][CN]{\cdot}3H_2O$ (2.04 × 10^{-2} M in thf). Inset: fitting curves log*K*(F)= 6.282 ± 0.0280 (*σr*= 0.00355, *ssq*= 0.0199); log*K*(CN)= 6.969 ± 0.392 (*σr*= 0.0427, *ssq*= 1.46).

Additionally, DFT calculations were carried out on the free sensor **IIIe** and the cyanide adduct [**IIIe**·(CN)]$^{-}$ (Figure 3.32). As expected the LUMO and LUMO+1 in the free sensor are distributed over a large π-system centred on the boron atom with a contribution of up to 25% from boron *p*-orbitals in the LUMO. The HOMO and HOMO-1 are mainly composed of *d*-orbitals from the iron atom (>75%). Receptor **IIIe** exhibits a greater aromaticity across the entire molecule compared to the phenylferrocene series. Thus the LUMO of **IIIe** appears to be lower in energy (*i.e.* more Lewis acidic) than **IIc** for instance by at least 14.5 kJ.mol^{-1}. This observation is in line with the stronger binding constants measured for the indenyl systems (Table 3.5). The representation of the LUMO of [**IIIe**·(CN)]$^{-}$ illustrates the electronic

consequences of the population of the empty *p*-orbital of the boron by a Lewis base. The resulting aromatic system is limited to the (cyclopentadienyl)(indenyl)-iron moiety, with little or no conjugation with the mesityl substituents (Figure 3.32). The low energy of the UV-vis spectra of such a system is usually dominated by the electronic transition of the filled molecular orbitals into the LUMO, thus an increase of the HOMO-LUMO gap by 48 kJ mol^{-1} is consistent with the changes observed in the visible region of the spectrum.

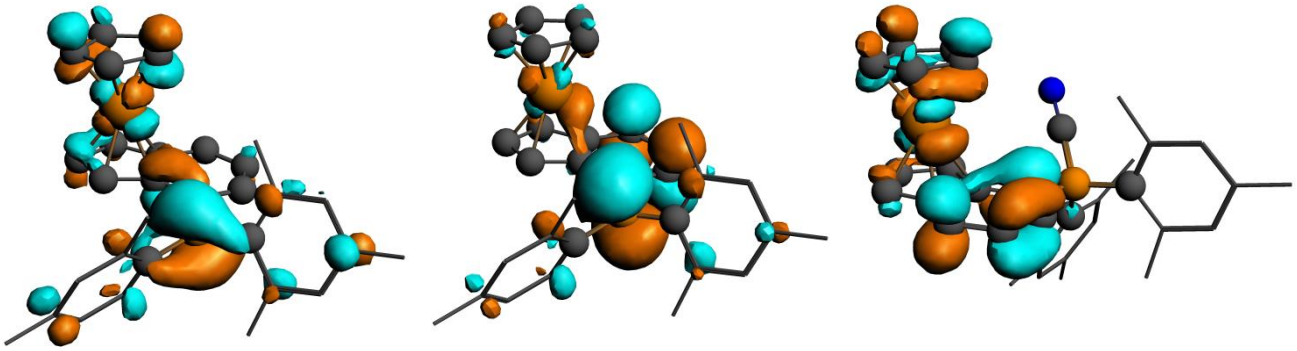

IIIe
LUMO+1 (-1.75 eV)

IIIe
LUMO (-2.65 eV)

[**IIIe**·(CN)]$^-$
LUMO (0.74 eV)

Figure 3.32: Contour plot of the frontier orbitals of **IIIe** and [**IIIe**·(CN)]$^-$ (density isovalues = 0.03).

The structures of [K(18-crown-6)][**IIIe**·CN] and [Cs(18-crown-6)][**IVe**·F] (Figure 3.34 and Figure 3.33) further corroborate the mode of anion binding. Most of the dimensions are unremarkable, from the conventional elongation of the B—C bonds (*i.e.* 1.613(4), 1.510(6), 1.585(5) Å for **IIIe**; 1.649(2), 1.661(2), 1.676(2) Å for [**IIIe**·CN]$^-$), to the pyramidalization of the boron centre ($\sum_{CBC}$ = 359.5° and 342.9° for [**IIIe**·CN]$^-$and [**IVe**·F]$^-$). The B—F and B—CN bond lengths also fall within the usual ranges (B11—C12: 1.633(2) Å and B12—F13: 1.496(5) Å). As with [K(18-crown-6)][**IIc**·CN] and [K(18-crown-6)][**IIb**·CN] additional supramolecular interactions are in evidence, *e.g.* the close contact between the linear boron-cyanide unit of **IIIe** with its potassium counterion (N13—K37: 2.808(2) Å). The situation is different in the case of the larger caesium counter-ion, which sits 1.49 Å away from the 18-crown-6 ligand, with an average Cs—O distance of 3.17 Å (*c.f.* $\sum_{VdW}$(Cs—O)= 4.95 Å);[15] auxiliary stabilizations

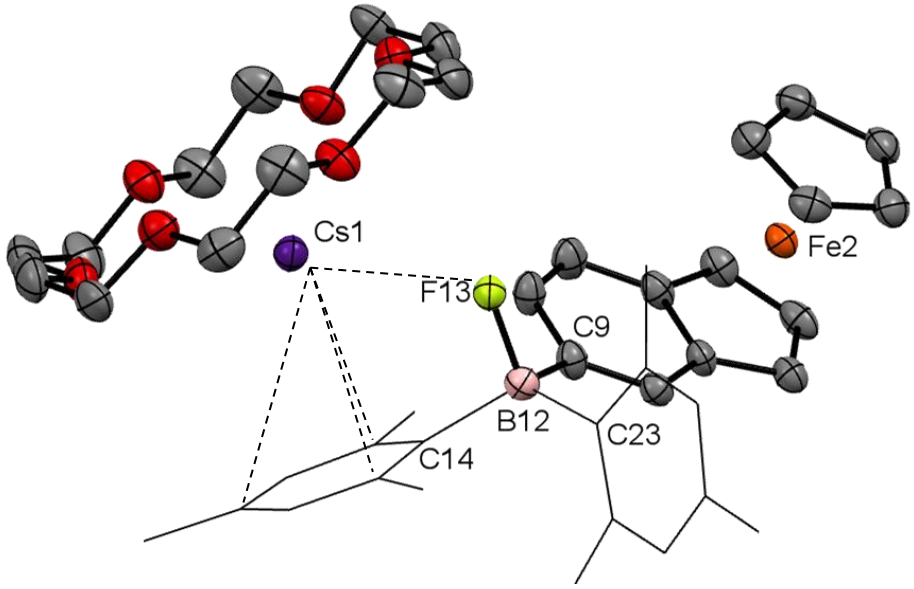

Figure 3.33: Molecular structure of [Cs(18-crown-6)][**IVe**·F]. Thermal ellipsoids set at the 50% probability level; mesityl groups shown in wireframe format, and hydrogen atoms and acetonitrile solvate molecules omitted for clarity (yellow: fluoride; light pink: boron; black: carbon; orange: iron; purple: caesium; red: oxygen). Selected bond lengths [Å] and angles [°]: B12—F13 1.496(5), B12—C9 1.629(6), B12—C14 1.670(6), B12—C23 1.655(6), Cs1—{Centroid of Mes(C14)} 3.357(calc.), Cs1—F13 3.034(calc.), C9—B12—C14 120.3(3), C9—B12—C23 110.3(3), C14—B12—C23 112.3(3).

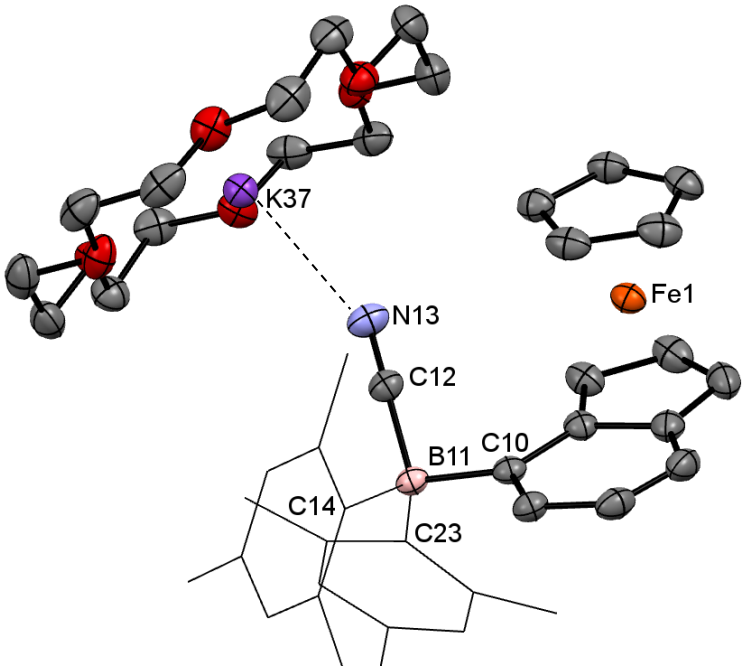

Figure 3.34: Molecular structure of [K(18-crown-6)][**IIIe**·CN]. Thermal ellipsoids set at the 50% probability level; mesityl groups shown in wireframe format and hydrogen atoms omitted for clarity (blue: nitrogen; light pink: boron; black: carbon; orange: iron; red: oxygen; purple: potassium). Selected bond lengths [Å] and angles [°]: B11—C10 1.649(2), B11—C14 1.661(2), B11—C23 1.676(2), B11—C12 1.633(2), N13—K37 2.808(2), C12—N13 1.153(2), C23—B11—C14 115.84(12), C14—B11—C10 107.11(12), C23—B11—C10 116.59(12), B11—C12—N13 176.47(19), K39—N24—C23 144.48(calc.).

are apparently provided by the bound fluoride (Cs—F: 3.034 Å, $\sum_{VdW}$(Cs—F)= 4.90 Å)[15] and the electron rich mesityl ring (Cs1—{Centroid of Mes}: 3.357 Å). Finally the fixation of cyanide by **IIIe** somewhat eases the steric hindrance, thus reducing the angle between the least squares planes of the cyclopentadienyl ligand and the indenyl moiety from 7.30° to 3.99°.

Further spectroscopic studies were performed on the receptor **IIIe**. Thus the pH window where the sensor maintains its integrity was determined. The results shown in Figure 3.35 were obtained by UV-vis monitoring of the effect of the pH of a thf solution of **IIIe** in a thf/water as a 50:50 volume ratio. The interpretation of the results shows that **IIIe** can be used in a wide pH range from *ca.* 4 to 12 (Figure 3.35).

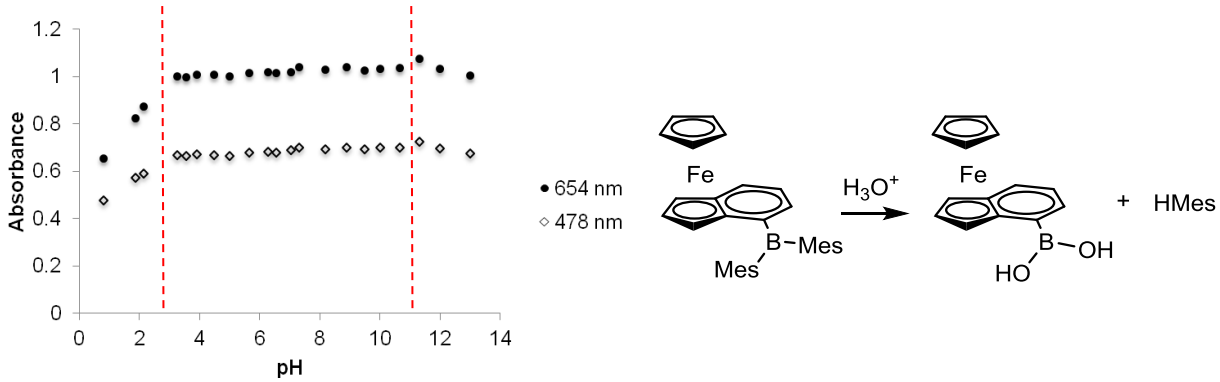

Figure 3.35: (*left*) Absorbance of **IIIe** at two different wavelengths (λ = 654 nm and 478 nm) as a function of the pH. (*right*) proposed decomposition pathway in acidic conditions.

The change in the UV-vis band intensity observed for **IIIe** at a pH under 4 can be attributed to the formation of the parent boric acid along with mesitylene as seen by ^{1}H and ^{11}B NMR spectroscopy; while there is lack of affinity for the hydroxide anion even at high concentration (Figure 3.35). So far receptor **IIIe** does not discriminate between cyanide and fluoride, even though the binding constant for cyanide ion is marginally greater, as confirmed by NMR competition experiments. Thus, the fluoride ion can be displaced from the [**IIIe**·**F**]$^-$ by excess CN^-, but the reverse is not true. The selectivity for cyanide can be dramatically

enhanced by exploiting the very strong solvent dependence of the relative basicities of F^- and CN^- (*c.f.* HF: pK_a 3 in H_2O, 15 in DMSO; HCN: pK_a 9 in H_2O, 13 in DMSO).[16] Since receptor **IIIe** is not moisture sensitive and relatively robust to oxidation (*i.e.* stable for several of hours in non-degassed thf), a systematic study was undertaken of the response of receptor **IIIe** to a range of anions in a 50:50 mixture of thf/water (Figure 3.36). The change of colour from green to pink/red occurs only in the presence of potassium cyanide. In this solvent system, excess of potassium fluoride (>34 equiv.) does not lead to the formation of the fluoroborate probably due to a combination of a high hydration enthalpy of fluoride ($\Delta H^{\theta}_{hydration}(F^-)$= -504 kJ.mol^{-1}) and the fact that it is an intrinsically weaker base than CN^- in water.**Error! Bookmark not defined.**

Figure 3.36: Exposure of receptor **IIIe** in thf (2.89 mmol.L^{-1}) to various potassium or sodium anions salts in water in a 50:50 mixtures (0.1 mol L^{-1}).

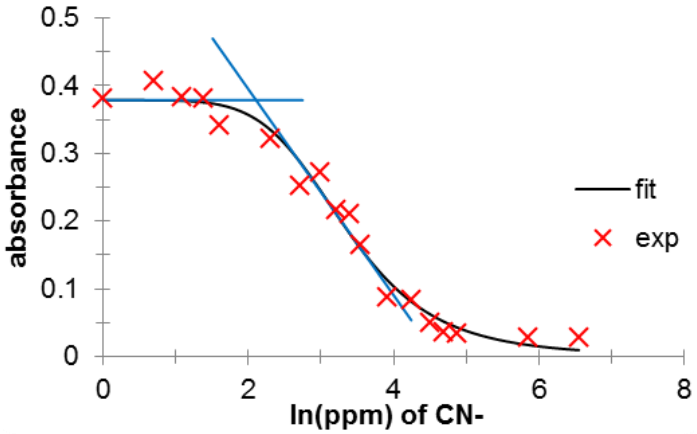

Estimation of the detection limit (*DL*):

$\ln(DL) = a \Leftrightarrow -0.152a + 0.6987 = 0.37836$
$\Leftrightarrow a = 2.1075$

Then $DL = e^a \Leftrightarrow DL = 8.22$ ppm

Figure 3.37: Evolution of the absorbance of **IIIe** (1.15 x 10^{-4} M in THF) at λ_{max}= 340.6 nm upon addition of KCN in water (thf/H_2O in 50:50 vol.). The black curve is fitted using an arbitrary expression purely as a guide to the eye using OriginPro 8.5.1 software. Blue tangents: *absorbance*= 0.37836 and ln(DL) = -0.152*x* + 0.6987

While the colorimetric detection of cyanide is limited to relatively high concentration, UV-vis monitoring can lower down the detection limit (Figure 3.37). The addition of aqueous cyanide of increasing concentrations to a stock solution of **IIIe** in thf (1.15×10^{-4} M) was monitored *via* the intensity of the absorption band centred at λ = 340.6 nm (Figure 3.37). A simple arithmetical estimate thereby gives a cyanide detection lower limit of *ca.* 10 ppm for **IIIe**.

3.5. Conclusions

Synthetic routes to novel ferrocenyl boranes have shown promising results for cyanide and fluoride binding. The phenyl systems were proven to be stable to air and moisture although they possess similar binding activity to systems previously reported, such as ferrocenyl boranes. The photochemical and electrochemical responses to anion binding are too weak to have real applications.

The second series of sensors synthesised with an indenyl framework are available in two simple steps from organic precursors (in ca. 50% yield). They displayed higher binding constant for both cyanide and fluoride compared to the phenylferrocene systems. Receptor **IIIe** also binds cyanide in protic media with an accompanying green to red/pink colour change. Extremely high selectivity over fluoride and hydroxide and a detection limit of *ca*. 10 ppm represent a highly desirable combination among borane derived cyanide receptors.

An advance from the systems described in this chapter would be the introduction of a second binding site in close proximity to the first boryl function. From the results outlined in

section 3.4.4, the indenyl scaffold would be used as the backbone for such systems since it offers the best photochemical response upon fixation of the targeted analytes.

3.6. References

(1) J. Havir, *Collect. Czech. Chem. Commun.* **1961**, 26, 1775.

(2) C. Bresner, S. Aldridge, I. A. Fallis, C. Jones and L.-L. Ooi, *Angew. Chem. Int. Ed.* **2005**, 44, 3606.

(3) A. Broomsgrove, D. A. Addy, C. Bresner, I. A. Fallis, A. L. Thompson and S. Aldridge, *Chem. Eur. J.* **2008**, 14, 7525.

(4) A. E. J. Broomsgrove, D. A. Addy, A. Di Paolo, I. R. Morgan, C. Bresner, V. Chislett, I. A. Fallis, A. L. Thompson, D. Vidovic and S. Aldridge, *Inorg. Chem.* **2010**, 49, 157.

(5) C. Bresner, C. J. E. Haynes, D. A. Addy, A. E. J. Broomsgrove, P. Fitzpatrick, D. Vidovic, A. L. Thompson, I. A. Fallis and S. Aldridge, *New J. Chem.* **2010**, 34, 1652.

(6) I. R. Morgan, A. E. J. Broomsgrove, P. Fitzpatrick, D. Vidovic, A. L. Thompson, I. A. Fallis, and S. Aldridge, *Organometallics* **2010**, 29, 4762.

(7) (*a*) J. D. Hoefelmeyer and F. P. Gabbaï, *Organometallics* **2002**, 21, 982. (*b*) C. L. Dorsey, Pawel Jewula, T. W. Hudnall, J. D. Hoefelmeyer, T. J. Taylor, N. R. Honesty, C.-W. Chiu, M. Schulte and F. P. Gabbaï, *Dalton Trans.* **2008**, 4442.

(8) (*a*) T. W. Hudnall and F. P Gabbaï, *J. Am. Chem. Soc.* **2007**, 129, 11978. (*b*) Y. Kim, H. Zhao and F. P. Gabbaï, *Angew. Chem. Int. Ed.* **2009**, 48, 4957. (*c*) T. W. Hudnall, Y.-M. Kim, M. W. P. Bebbington, D. Bourissou and F. P. Gabbaï, *J. Am. Chem. Soc.* **2008**, 130, 10890.

(9) (*a*) V. Clifford Williams, W. E. Piers, W. Clegg, M. R. J. Elsegood, S. Collins and T. B. Marder, *J. Am. Chem. Soc.* **1999,** *121,* 3244. (*b*) V. C. Williams, G. J. Irvine, W. E. Piers, Z. Li, S. Collins, W. Clegg, M. R. J. Elsegood and T. B. Marder, *Organometallics* **2000,** *19,* 1619. (*c*) S. P. Lewis, N. J. Taylor, W. E. Piers and S. Collins, *J. Am. Chem. Soc.* **2003**, 125,

14686. (*d*) P. A. Chase, L. D. Henderson, W. E. Piers, M. Parvez, W. Clegg and M. R. J. Elsegood, *Organometallics* **2006,** *25,* 349.

(10) O. N. Kadkin, E. Ho Kim, Y. Joon Rha, S. Yeon Kim, J. Tae and M.-G. Choi, *Chem. Eur. J.* **2009**, 15, 10343.

(11) C. R. Wade, A. E. J. Broomsgrove, S. Aldridge and F P Gabbaï, *Chem. Rev.* **2010**, 110, 3958.

(12) A. J. Bard, E. Garcia, S. Kukharenko and V. V Strelets, *Inorg. Chem.* **1993**, 32, 3528.

(13) J. Ruiz Aranzaes, M.-C. Daniel and D. Astruc, *Can. J. Chem.* **2006**, 84: 288.

(14) A. V. Soudackov and K. Jug, *Int. J. Quant. Chem.* **1997**, 62, 403.

(15) M. Mantina, A. C. Chamberlin, R. Valero, C. J. Cramer and D. G. Truhlar, *J. Phys. Chem. A* **2009**, 113, 5806.

(16) See for example: http://evans.rc.fas.harvard.edu/pdf/evans_pKa_table.pdf

CHAPTER 4: Bidentate indenyl receptors

4.1. Introduction

A range of examples have been reported in the literature exploiting the chelate effect to enhance the binding affinity of a receptor towards the fluoride anion. These include, for instance the work conducted by Jurkschat[1] and Tamao[2] on 1,2-disubstituted benzene systems, and the 1,8-disubstituted naphthalene receptors (**68**) developed by Winterman *et al.*[3] In the latter case, the chelate effect is highlighted by the competition experiment shown in Figure 4.1; complete abstraction of fluoride from [**67**·F]$^-$ by the bidentate receptor **68** provides strong evidence for cooperative action by both boron centres.

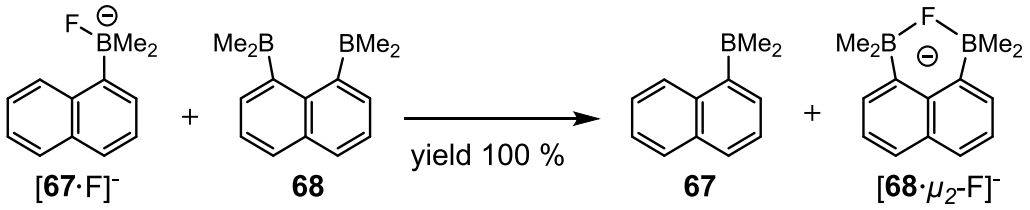

Figure 4.1: Competition reaction between the monodentate receptor **67** and the bidentate receptor **68**.3

Despite this, only a handful of *bis-boranes* able to chelate fluoride have been reported in the literature. These include wholly organic receptors such as the 1,8-naphthalene systems (**69** - **72**$^+$)[4] developed by Gabbaï, and Piers' highly electron deficient 1,2-diborylated benzenes (**106**),[5] together with organometallic systems such as the cobaltocenium bis-boryl (**74**) reported by Herberich and co-workers (Figure 4.2).[6]

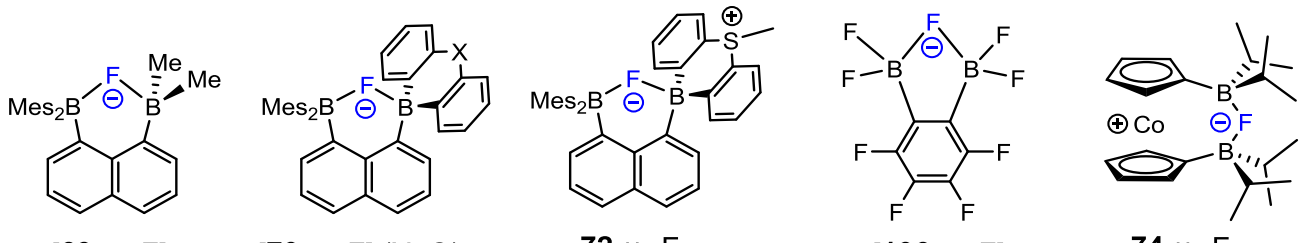

Figure 4.2: Chelating bis-boryl systems capable of fluoride recognition.

For receptors such as **106** and **74**$^+$ fluoride chelation is evident in the molecular structure determined crystallographically, with equivalent B—F bonds being found in each case (*e.g.* 1.487(4) Å for **106**·μ_2-F). By contrast, the differences in Lewis acidity between the two boron centres in **69** to **72**$^+$ is reflected in disparate contacts to the bridging fluoride. Evidence in solution for chelated fluoride can be provided by NMR spectroscopy, with a coupling constant between the fluoride and the *ortho*-methyl group of the mesityl ligand in [**71**·μ_2-F]$^-$ (J_{HF}= 4.4 and 6.0 Hz).

Receptor **107**, developed by Yamamoto and co-workers, represents a hybrid between Ito's bis-silane (**28**)[7] and the corresponding benzene bis-borane (Figure 4.3).[8] In the adduct [**107**·μ_2-F]$^-$ the fluoride ion is tightly bound to the boron centre (B—F 1.508(2) Å) to form a fluoroborate, with a secondary interaction to silicon (Si—F 2.2655(14) Å, *c.f.* Si—F 1.898(4) and 2.065(4) Å in [**28**·μ_2-F]$^-$) yielding a pseudo-pentacoordinate geometry. The relatively weak connection between the fluoride and silicon is evident in solution: the Si—F coupling constant is much smaller than that observed in the corresponding bis-silane compound (J_{SiF}= 17 and 135 Hz for [**107**·μ_2-F]$^-$ and [**28**·μ_2-F]$^-$ respectively). The assistance of the silane function at the *ortho* position for the fixation of the fluoride anion is however chemically significant, as demonstrated by a competition experiment in which receptor **107** quantitatively abstracted fluoride from PhB(F)Mes$_2$.

Figure 4.3: Chelation of the fluoride anion by the receptors **28** and **107**.

A related approach which can be envisioned is that developed by Gabbaï *et al.*, the so-called "onium strategy" (Figure 4.4). A series of Lewis acids with a proximal cationic group

has been developed, involving combinations of receptor sites including silyl sulfonium ({Si;S$^+$}[9]), borane phosphonium ({B;P$^+$}[10]) and borane ammonium ({B;N$^+$}[11]). In these systems the inductive effect of the ancillary substituent enhances the Lewis acidity at boron, while Coulombic attraction assists the anion binding. Moreover, once the anion is bound to the borane function an additional donor-acceptor interaction to the cationic $-PR_3^+$, $-NR_3^+$ or $-SR_2^+$ function stabilizes the zwitterionic complex (Figure 4.4).

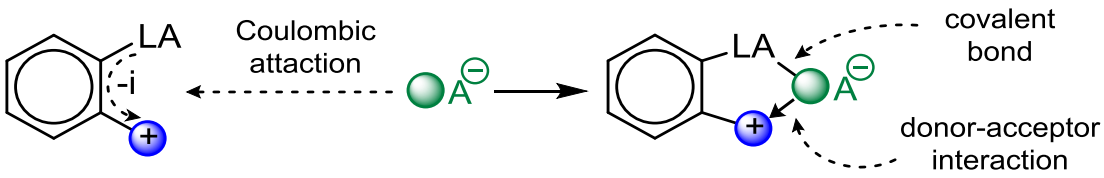

Figure 4.4: "Onium strategy", with LA: Si or B and ⊕ $-PR_3^+$, $-NR_3^+$ or $-SR_2^+$.

The difference in the fluoride affinities of ***p*-108$^+$** and ***o*-108$^+$** is a good demonstration of the advantage provided by the "onium strategy" (Figure 4.5). DFT calculations reveal that the LUMO energies of the two receptors are virtually identical (-2.57 and -2.56 eV for ***p*-108$^+$** and ***o*-108$^+$**), thus the Lewis acidities of the boron centres are similar. Yet the binding constants for fluoride in methanol are drastically different: K_a(***o*-108$^+$**) exceeds K_a(***p*-108$^+$**) by at least four orders of magnitudes (10^6 M^{-1} vs 400(50) M^{-1}).[10b] A competition experiment highlighted in Figure 4.5 further demonstrates the superiority of ***o*-108$^+$**. The interaction of the fluoride anion with both the boron and phosphonium centres is perceptible by NMR, with a ^{11}B signal at δ_B 5.7 ppm, a ^{31}P peak at δ_P 28.3 ppm ($^1J_{P\text{-}F}$= 24.3 Hz), and a broad signal in the ^{19}F NMR spectrum at δ_F -158 ppm for ***o*-108**$\cdot\mu_2$-F. Furthermore, structural studies also support the idea of chelation in the solid state with B—F and P—F contacts well within the sum of the respective Van der Waals' radii (B—F 1.482(3) Å, P—F 2.666(2) Å). The donor-acceptor interaction from the lone pair of the fluoride into the σ^* of the P—C_{Ph} bond (*i.e.* *lp*(F)→σ^*(P—C)) is further confirmed by natural bond order (NBO) analysis performed at the optimized geometry.

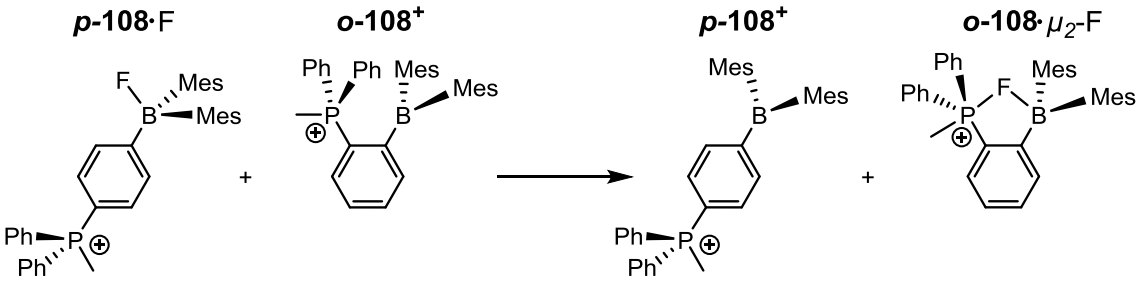

Figure 4.5: Competition experiment between ***p*-108**$^+$ and ***o*-108**$^+$.

Finally, the ammonium derivatized receptor **109**$^+$ demonstrates peculiar selectivity depending on the position of the cationic centre (Figure 4.6).[11b] Gabbaï *et al.* studied the binding properties in a H_2O/DMSO mixture (60:40 vol.); receptor ***p*-109**$^+$ exhibits a high affinity for cyanide as the Coulombic effects are not sufficient enough to overcome the hydration enthalpy of fluoride. The receptor ***o*-109**$^+$ exhibits complementary behaviour, the boron centre is only quenched in the presence of fluoride. The authors attributed the selectivity of each isomer to a delicate balance between steric hindrance and Lewis acidity. The LUMO of receptor ***o*-109**$^+$ lies at a lower energy (-2.12 eV) than ***p*-109**$^+$ (-2.02 eV); thus the latter would not be strong enough to abstract fluoride in an aqueous media whereas the binding of cyanide by ***o*-109**$^+$ is reported to be hampered on steric grounds.

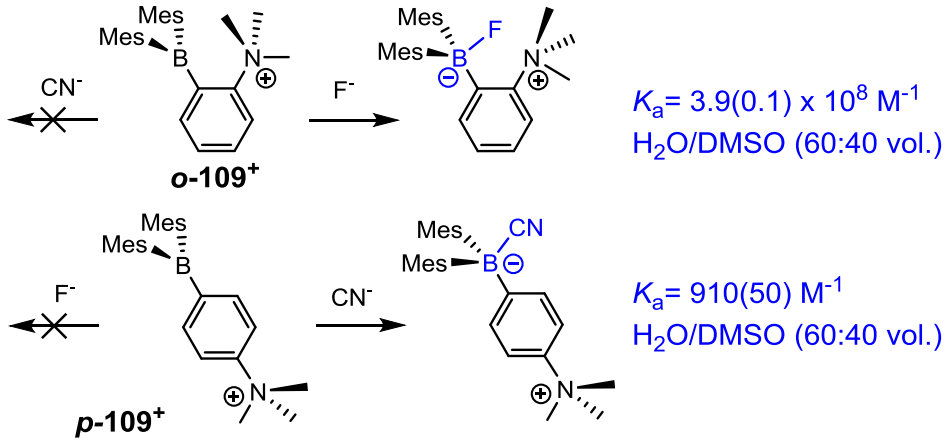

Figure 4.6: Reactivity of ***o*-109**$^+$ and ***p*-109**$^+$ towards cyanide and fluoride ions in a H_2O/DMSO mixture (60:40 vol.).

4.2. Aims

The word chelate is derived from the greek *khêlê*, meaning tweezers. The systems described in Chapter 3 represent only half of a pair of "molecular pliers"; hence the aim for this chapter at the outset was to introduce a second Lewis acidic centre for the selective binding of the fluoride anion.

On the basis of the precedent offered by cobaltocene system **74**, a series of *bis*(borane-indenyl) complexes were developed for iron and cobalt. The premise was to investigate the effect of the oxidation state and size of the metal on anion binding. The receptors shown in Figure 4.8 could be synthesised readily from 7-bromoindene and $CoBr_2$ and $FeCl_2$ respectively; the borane function can subsequently be introduced using $FBMes_2$, and the oxidation of cobalt(II) then effected by using a mild oxidant (*i.e.* $FcPF_6$). However, while preliminary results for receptors **110** and **111**$^+$ (achieved by Ms. Gaya Sri Navaneetha a project student under my supervision) demonstrated anion binding competence (Figure 4.7), this line of research was abandoned since these receptors were found to be very prone to decomposition (*i.e.* oxidation of the iron centre).

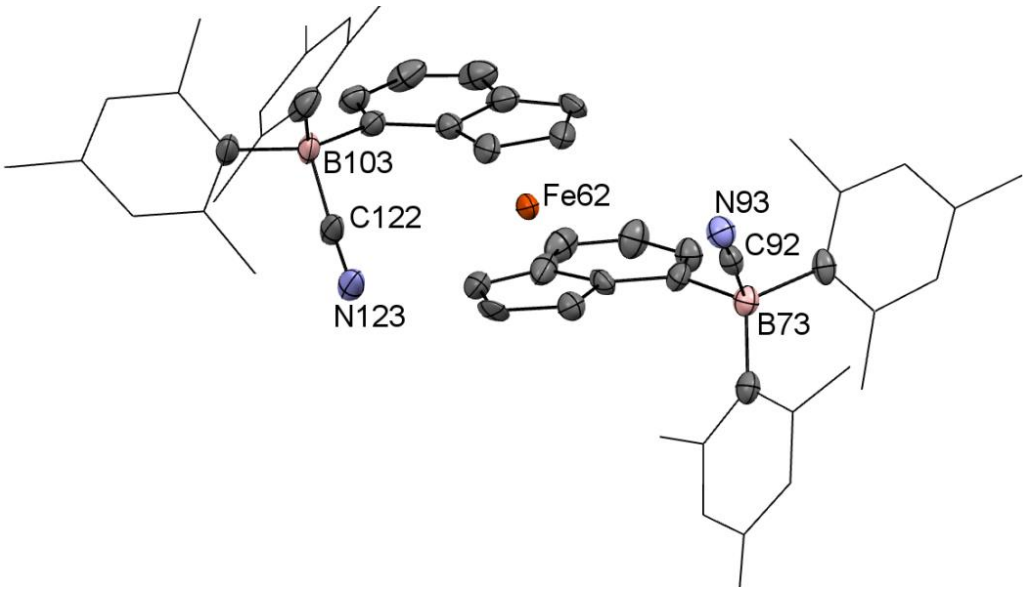

Figure 4.7: Molecular structure of [**110**$^{\cdot}$$(CN)_2]^{2-}$. Thermal ellipsoids set at the 50% probability level; mesityl groups shown in wireframe; hydrogen atoms and the tetrabutylammonium molecule are omitted for clarity (black: carbon; orange: iron; light pink: boron; blue: nitrogen).

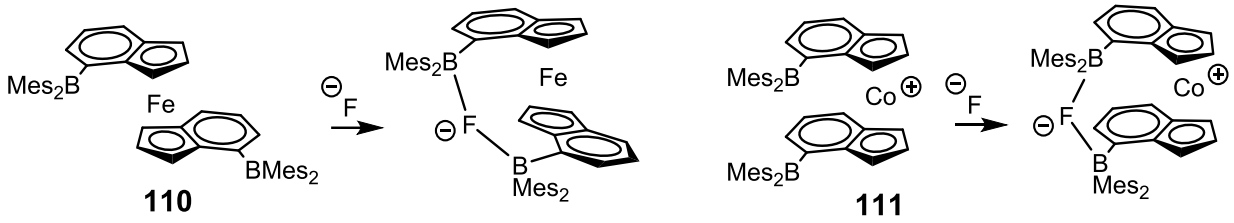

Figure 4.8: Proposed mode of fluoride chelation by the *bis*(borane-indenyl) systems **110** and **111**$^{+}$.

Thus the focus was redirected onto the (cyclopentadienyl)iron indenyl scaffold, with receptors **Ve** and **VIe** being targeted (Figure 4.9). It was hoped that the binding event at the boron centres in each case should lead to a marked change in the electronic conjugation, and hence to the possibility for electrochemical or UV-vis determination of anion uptake.

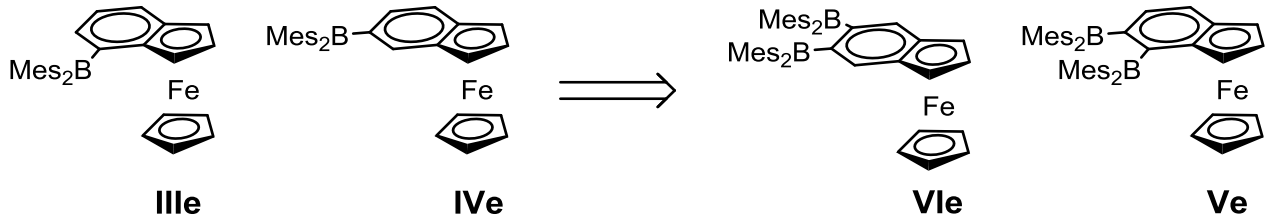

Figure 4.9: Schematic representation of the targeted receptor for chelation of the fluoride.

4.3. Experimental

4.3.1 Syntheses of the receptors

Note: to avoid confusion, the nomenclature for each series of compound is retained from the original dihalogeno-indanone precursor.

*6,7-dibromoindanone (**VIIIa**)*

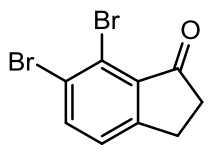

3-(2,3-dibromophenyl) propionic acid (22.14 g, 72.00 mmol) was refluxed in an excess of thionyl chloride (40 ml) for 1 h. The excess thionyl chloride was then removed in vacuo, yielding a brown oil. Aluminium chloride (14.40 g, 108.03 mmol) was then added to the oil in dichloromethane (300 ml), and the mixture stirred for a further 2 h at room temperature, before quenching with ice cold water. The aqueous layer was acidified with HCl (2 M) then extracted with dichloromethane. The combined organic fractions were washed with HCl (2 M) then water, and dried over $MgSO_4$. The dichloromethane was then removed under reduced pressure to yield a brown solid. The undesired isomeric product 5,6-dibromoindanone was precipitated from dichloromethane by addition of diethyl ether, and the more soluble 6,7-dibromoindanone then isolated from the ether fraction after removal of the solvent. **VIIIa**: yield: 6.40 g, 31%.

^{1}H NMR (400 MHz, $CDCl_3$, 25 °C): δ_H 2.76 (*t*, $^3J_{HH}$ =6.1 Hz, 2H, CH_2), 3.03 (*t*, $^3J_{HH}$ = 6.1 Hz, 2H, CH_2), 7.29 (*d*, $^3J_{HH}$ = 8.0 Hz, 1H, H aromatic), 7.76 (*d*, $^3J_{HH}$ = 8.0 Hz, 1H, H aromatic). ♦ $^{13}C\{^1H\}$ NMR (120 MHz, $CDCl_3$, 25 °C): δ_C 24.4, 37.2, 122.0, 126.2, 126.7, 136.4, 138.6, 156.6, 202.6 (CO).

*6,7-dibromo-4-methyl-indanone (**IXa**)*

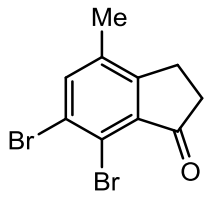

Following a method related to the work of Langhauser *et al.* for **IIIa**,[12] (chapter 2, section 2.3.2): 3-(4,5-dibromo-2-methylphenyl) propionic acid (32.05 g, 99.53 mmol) was treated with thionyl chloride (40 ml) for 1 h, then with aluminium chloride (19.90 g, 149.30 mmol). Yield: 24.20 g, 80%.

^{1}H NMR (400 MHz, $CDCl_3$, 25 °C): δ_H 2.29 (*s*, 3H, Me), 2.76(*t*, $^3J_{HH}$ = 6.0 Hz, 2H, CH_2), 2.90 (*t*, $^3J_{HH}$ = 6.0 Hz, 2H, CH_2), 7.62 (*s*, 1H, H aromatic). ♦ $^{13}C\{^1H\}$ NMR (120 MHz, $CDCl_3$, 25 °C): δ_C 17.3, 23.3, 36.8, 118.67, 125.9, 135.8, 136.3, 138.8, 155.7, 202.9 (CO). ♦ MS (EI+), *m/z* (%): 303.9 (100%), 301.9 (51%), 305.9 (48%), accurate mass (calc. for M^+) 303.8922, (meas.) 303.8952, isotopic pattern correct for $C_{10}H_8Br_2O$.

*5,6-dibromoindanol (**VIIb**)*

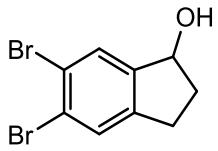

Following a method related to the work of Gibson *et al.* for **IIIb**,[13] 5,6-dibromoindanone (8.80 g, 30.35 mmol) was treated with sodium borohydride (2.87 g; 75.88 mmol). The product was isolated as pale yellow solid. Yield: 8.34 g, 94%.

^{1}H NMR (400 MHz, $CDCl_3$, 25 °C): δ_H 1.87 (*m*, 1H, CH_2), 2.44 (*m*, 1H, CH_2), 2.71 (*m*, 1H, CH_2), 2.85 (*b s,* 1H, OH), 2.92 (*ddd*, $^3J_{HH}$ = 4.3 Hz, $^3J_{HH}$ = 8.5 Hz, $^2J_{HH}$ = 16.3 Hz, 1H, CH_2), 5.09 (*t*, $^3J_{HH}$ = 6.4 Hz, 1H, CH(OH)), 7.45 (*s*, 1H, H aromatic), 7.55 (*s*, 1H, H aromatic). ♦ $^{13}C\{^1H\}$ NMR (120 MHz, $CDCl_3$, 25 °C): δ_C 29.3, 36.2, 75.5, 122.5, 124.3, 129.4, 130.0, 144.3, 146.2. ♦ MS (EI+), *m/z* (%): 291.9 (100%), 289.9 (51%), 293.9 (48%), accurate mass (calc. for M^+) 291.8922, (meas.) 291.8887, isotopic pattern correct for $C_9H_8Br_2O$. ♦ Crystallographic data: $C_9H_8Br_2O$, M_r = 291.97, triclinic, *P-1*, *a* = 9.1092(2) Å, *b* = 9.2039(2) Å, *c* = 12.6228(3) Å, α = 87.902(2)°, β = 80.555(2)°, γ = 63.185(3)°, *V* = 930.85(4) Å^3, *Z* = 4, *T* = 150 K, λ = 1.54180 Å. 17164 reflections collected, 3831 independent [R(int) = 0.0396] used in all calculations, with 217 refined parameters, GOF on F^2 = 1.0552. R_1 = 0.0395, wR_2 = 0.1050 for observed unique reflections [I>2σ(I)] and R_1 = 0.0396, wR_2 = 0.1050 for all unique reflections. Max. and min. residual electron densities 1.43 and -1.21 e Å^{-3}.

*6,7-dibromoindanol (**VIIIb**)*

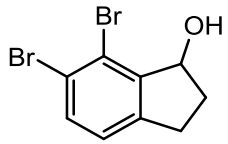

Following a method related to the work of Gibson *et al.* for **IIIb**,[13] 6,7-dibromoindanone (13.34 g, 46.00 mmol) was treated with sodium borohydride (4.35 g; 115 mmol). The product was isolated as pale yellow solid. Yield: 13.40 g, 99%.

^{1}H NMR (400 MHz, $CDCl_3$, 25 °C): δ_H 2.09 (*m*, 1H, CH_2), 2.36 (*m*, 1H, CH_2), 2.84 (*ddd*, $^3J_{HH}$ = 3.1 Hz, $^3J_{HH}$ = 8.9 Hz, $^2J_{HH}$ = 16.4 Hz, 1H, CH_2), 3.16 (*dt*, $^3J_{HH}$ = 8.2 Hz, $^2J_{HH}$ = 16.4 Hz, 1H, CH_2), 3.24 (*b s,* 1H, OH), 5.23 (*d*, $^3J_{HH}$ = 4.3 Hz, 1H, CH(OH)), 7.05 (*d*, $^3J_{HH}$ = 8.0 Hz, 1H, CH aromatic), 7.47 (*d*, $^3J_{HH}$ = 8.0 Hz, 1H, CH aromatic). ♦ ^{13}C{^{1}H} NMR (120 MHz, $CDCl_3$, 25 °C): δ_C 30.8, 33.8, 77.5, 122.2, 122.2, 125.2, 133.6, 144.9, 146.4. ♦ MS (EI+), *m/z* (%): 291.9 (100%), 289.9 (51%), 293.9 (49%), accurate mass (calc. for M^+) 291.8922, (meas.) 291.8957, isotopic pattern correct for $C_9H_8Br_2O$.

*6,7-dibromo-4-methyl-indanol (**IXb**)*

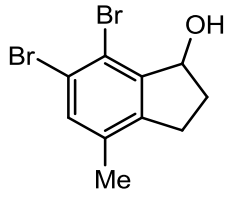

Following a method related to the work of Gibson *et al.* for **IIIb**:[13] 6,7-dibromo-4-methyl-indanone (24.61 g, 80.96 mmol) was treated with sodium borohydride (7.66 g; 202 mmol). The product was isolated as pale yellow solid. Yield: 23.81 g, 96%.

^{1}H NMR (400 MHz, $CDCl_3$, 25 °C): δ_H 2.19 (*s*, 3H, Me), 2.15 (*m*, 1H, CH_2), 2.39 (*m*, 1H, CH_2), 2.49 (*b s,* 1H, OH), 2.77 (*ddd*, $^3J_{HH}$ = 3.0 Hz, $^3J_{HH}$ = 9.0 Hz, $^2J_{HH}$ = 16.5 Hz, 1H, CH_2), 3.05 (*m*, 1H, CH_2), 5.31 (*dd*, $^3J_{HH}$ = 2.1 Hz, $^3J_{HH}$ = 7.0 Hz, 1H, C*H*(OH)), 7.35 (*s*, 1H, CH aromatic). ♦ ^{13}C{^{1}H} NMR (120 MHz, $CDCl_3$, 25 °C): δ_C 18.4, 29.7, 33.0, 77.9, 118.8, 122.5, 134.2, 135.3, 143.9, 145.8. ♦ MS

(EI$^+$), m/z (%): 305.9 (100%), 303.9 (51%), 307.9 (49%), accurate mass (calc. for M$^+$) 305.9078 (meas.) 305.9093, isotopic pattern correct for $C_{10}H_{10}Br_2O$.

*5,6-dibromoindene (**VIIc**)*

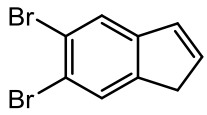

Following a method related to the work of Gibson *et al.* for **IIIc**,[13] 5,6-dibromoindanol (8.34 g, 28.56 mmol) and *p*-TsOH (cat.) in toluene (200 mL) were heated overnight at 110 °C. The product was isolated as a white solid. Yield: 7.06 g, 90%.

^{1}H NMR (400 MHz, $CDCl_3$, 25 °C): δ_H 3.35 (*s*, 2H, CH_2), 6.59 (*d*, $^3J_{HH}$ = 5.5 Hz, 1H, CH alkene), 6.78 (*d*, $^3J_{HH}$ = 5.5 Hz, 1H, CH alkene), 7.64 (*s*, 1H, H aromatic), 7.70 (*s*, 1H, H aromatic). ♦ ^{13}C{^{1}H} NMR (120 MHz, $CDCl_3$, 25 °C): δ_C 38.8, 120.4, 122.3, 125.6, 128.7, 130.8, 136.24, 144.3, 145.8. ♦ Elemental microanalysis: calc. for $C_9H_6Br_2$: C, 39.46%; H, 2.21%. Found: C, 39.92%; H, 2.20%. ♦ MS (EI+), m/z (%): 273.9 (100%), 271.9 (51%), 275.9 (49%), accurate mass (calc. for M$^+$) 273.8816, (meas.) 273.8831, isotopic pattern correct for $C_9H_6Br_2$.

*4,5-dibromoindene (**VIIIc**)*

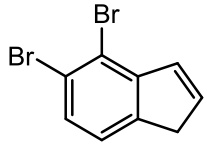

Following a method related to the work of Gibson *et al.* for **IIIc**,[13] 6,7-dibromoindanol (4.05 g, 3.45 mmol) and *p*-TsOH (cat.) in toluene (250 mL) were heated to 125° C overnight. The product was isolated as a white solid. Yield: 3.00 g, 79%.

^{1}H NMR (400 MHz, $CDCl_3$, 25 °C): δ_H 3.28 (s, 2H, CH_2), 6.47 (*d*, $^3J_{HH}$ = 5.50 Hz, 1H, CH alkene), 6.79 (*d*, $^3J_{HH}$ = 5.5 Hz, 1H, CH alkene), 7.04 (*dd*, $^3J_{HH}$ = 7.9 Hz, $^4J_{HH}$ = 3.2 Hz, 1H, CH aromatic), 7.25 (*d*, $^3J_{HH}$ = 7.9 Hz, 1H, CH aromatic). ♦ ^{13}C{^{1}H} NMR (120 MHz, $CDCl_3$, 25 °C): δ_C 40.4, 117.5,

122.6, 123.6, 129.5, 132.7, 136.7, 143.6, 147.3. ♦ Elemental microanalysis: calc. for $C_9H_6Br_2$: C, 39.46%; H, 2.21%. Found: C, 39.77%; H, 2.37%. ♦ MS (EI+), *m*/*z* (%): 273.9 (100%), 271.9 (51%), 275.9 (49%), accurate mass (calc. for M^+) 273.8816, (meas.) 273.8865, isotopic pattern correct for $C_9H_6Br_2$.

*6,7-dibromo-4-methyl-indene (**IXc**)*

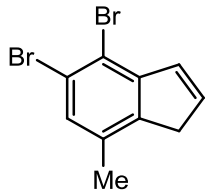

Following a method related to the work of Gibson *et al.* for **IIIc**,[13] 6,7-dibromo-4-methyl-indanol (23.81 g, 73.99 mmol) and *p*-TsOH (cat.) in toluene (600 mL) were heated overnight at 110 °C. The product was isolated as a white solid. Yield: 19.27 g, 92%.

^{1}H NMR (400 MHz, $CDCl_3$, 25 °C): δ_H 2.29 (*s*, 3H, Me), 3.35 (*s*, 2H, CH_2), 3.64 (*d*, $^3J_{HH}$ = 5.8 Hz, 1H, CH alkene), 6.96 (*d*, $^3J_{HH}$ = 5.8 Hz, 1H, CH alkene), 7.28 (*s*, 1H, H aromatic). ♦ ^{13}C{^{1}H} NMR (120 MHz, $CDCl_3$, 25 °C): δ_C 18.2 (Me), 36.5, 114.8, 122.6, 130.7, 133.1, 133.4, 136.2, 142.6, 146.6. ♦ MS (EI+), *m*/*z* (%): 287.9 (100%), 285.9 (51%), 289.9 (49%), accurate mass (calc. for M^+) 287.8972 (meas.) 287.9018, isotopic pattern correct for $C_{10}H_8Br_2$.

*(6,7-Dichloroindenyl)cyclopentadienyliron(II) (**Vd**)*

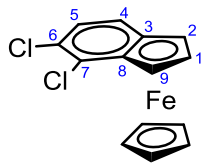

A solution of 6,7-dichloroindene (5.00 g, 27.02 mmol) in dry thf (250 mL) was added to solid potassium hydride (973 mg, 40.53 mmol), and the reaction mixture stirred for 1 h. The resulting brown solution was transferred onto [FeCp(naph)][PF_6] (10.56 g, 27.02 mmol), and

the mixture stirred overnight. Volatiles were then removed in vacuo yielding a purple residue which was extracted with hexane, and the solvent removed under reduced pressure. The resulting crude product was purified by air free chromatography (silica column eluted with hexane) yielding a purple solid. Crystals suitable for X-ray crystallography were obtained from a cold solution of hexane (-25° C) Yield: 4.56 g, 55%.

^{1}H NMR (300 MHz, $CDCl_3$, 25 °C): δ_H 3.91 (s, 5H, Cp), 4.17 (*t*, $^{3}J_{HH}$ = 2.3 Hz, 1H, C1H), 4.96 (s, 1H, C2H), 5.13 (*s*, 1H, C9H), 6.92 (*d*, $^{3}J_{HH}$ = 9.2 Hz, 1H, C5H), 7.48 (*d*, $^{3}J_{HH}$ = 9.2 Hz, 1H, C4H). ♦ $^{13}C\{^{1}H\}$ NMR (126 MHz, $CDCl_3$, 25 °C): δ_C 62.1 (C9), 63.4 (C2), 68.7 (Cp), 71.5 (C1), 86.8 (C3), 88.0 (C8), 124.5 (C6), 125.4 (C5), 129.4 (C4), 131.1 (C7). ♦ Elemental microanalysis: calc. for $C_{14}H_{10}Cl_2Fe$: C, 55.13%; H, 3.30%. Found: C, 54.95%; H, 3.39%. ♦ MS (EI$^+$), *m/z* (%): 303.9 (100%), 305.9 (60%), accurate mass (calc. for M^+, ^{54}Fe isotopomer) 301.9578, (meas.) 301.9546, isotopic pattern correct for $C_{14}H_{10}Cl_2Fe$. ♦ Crystallographic data: $C_{14}H_{10}Cl_2Fe$, M_r = 304.99, monoclinic, $P2_1/c$, a = 10.3015(2) Å, b = 19.1263(3) Å, c = 24.3549(5) Å, β = 91.5229(7)°, V = 4796.94(15) Å^3, Z = 16, T = 150 K, λ = 0.71073 Å. 19968 reflections collected, 10728 independent [R(int) = 0.0998] used in all calculations, with 759 refined parameters, GOF on F^2 = 0.9579. R_1 = 0.0717, wR_2 = 0.1377 for observed unique reflections [I>2σ(I)] and R_1 = 0.0998, wR_2 = 0.1506 for all unique reflections. Max. and min. residual electron densities 1.06 and -0.90 e Å^{-3}.

*(5,6-Dichloroindenyl)cyclopentadienyliron(II) (**VId**)*

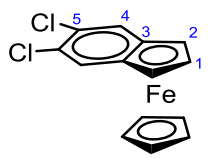

Following the same procedure as for **Vd**: a solution of 5,6-dichloroindene (5.00 g, 27.02 mmol) in dry thf (250 mL) was added to potassium hydride (973 mg, 40.53 mmol), then transfered onto [FeCp(naph)][PF_6] (10.56 g, 27.02 mmol) and stirred overnight. The product

was isolated as a purple solid, crystals suitable for X-ray crystallography were obtained from a cold hexane solution (-25° C). Yield: 2.90 g, 35%.

^{1}H NMR (300 MHz, $CDCl_3$, 25 °C): δ_H 3.91 (*s*, 5H, Cp), 4.11 (*t*, $^{3}J_{HH}$ = 2.3 Hz, 1H, C1H), 4.93 (*d*, $^{3}J_{HH}$ = 2.3 Hz, 2H, C2H), 7.93 (*s*, 2H, C4H). ♦ $^{13}C\{^{1}H\}$ NMR (126 MHz, $CDCl_3$, 25 °C): δ_C 61.9 (C2), 68.5 (Cp), 71.8 (C1), 87.5 (C3), 117.5 (C5), 133.5 (C4). ♦ Elemental microanalysis: calc. for $C_{14}H_{10}Cl_2Fe$: C, 55.13%; H, 3.30%. Found: C, 55.01%; H, 3.56%. ♦ MS (EI^+), *m*/*z* (%): 303.9 (100%), 305.9 (70%), isotopic pattern correct for $C_{14}H_{10}Cl_2Fe$. ♦ Crystallographic data: $C_{14}H_{10}Cl_2Fe$, M_r = 304.99, monoclinic, $P2_1/c$, a = 9.67740(10) Å, b = 7.71550(10) Å, c = 16.3108(2) Å, β = 105.6442(7)°, V = 1172.75(2) Å^3, Z = 4, T = 150 K, λ = 0.71073 Å. 32518 reflections collected, 2661 independent [R(int) = 0.0407] used in all calculations, with 154 refined parameters, GOF on F^2 = 0.9046. R_1 = 0.0318, wR_2 = 0.0691 for observed unique reflections [I>2σ(I)] and R_1 = 0.0407, wR_2 = 0.0777 for all unique reflections. Max. and min. residual electron densities 0.47 and -0.47e Å^{-3}.

*(5,6-dibromoindenyl)cyclopentadienyliron(II) (**VIId**)*

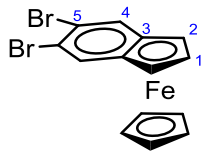

Following the same procedure as for **Vd**: a solution of 5,6-dibromoindene (7.06 g, 25.77 mmol) in dry thf (250 mL) was added to potassium hydride (1.55 g, 38.66 mmol) then transfered onto $[FeCp(naph)][PF_6]$ (10.66 g, 27.06 mmol), and the reaction mixture stirred overnight. The product was isolated as a purple solid, crystals suitable for X-ray crystallography were obtained from a cold hexane solution (-25° C). Yield: 6.24 g, 62%.

^{1}H NMR (400 MHz, $CDCl_3$, 25 °C): δ_H 3.91 (*s*, 5H, Cp), 4.11 (*t*, $^{3}J_{HH}$ = 2.3 Hz, 1H, C1H), 4.93 (*d*, $^{3}J_{HH}$ = 2.3 Hz, 2H, C2H), 7.93 (*s*, 2H, C4H). ♦ $^{13}C\{^{1}H\}$ NMR (120 MHz, $CDCl_3$, 25 °C): δ_C 62.0 (C2), 68.5 (Cp), 71.9 (C1), 87.5 (C3), 117.5 (C5), 133.6 (C4). ♦ Elemental microanalysis: calc. for

$C_{14}H_{10}Br_2Fe$: C, 41.69%; H, 2.56%. Found: C, 41.71%; H, 2.30%. ♦ MS (EI+), *m/z* (%): 393.8 (100%), 391.8 (55%), 395.8 (45%), accurate mass (calc. M^+, ^{54}Fe isotopomer) 389.85447, (meas.) 389.3990, isotopic pattern correct for $C_{14}H_{10}Br_2Fe$. ♦ Crystallographic data: $C_{14}H_{10}Br_2Fe$, M_r = 393.89, triclinic, *P-1*, *a* = 9.7245(7) Å, *b* = 9.9197(6) Å, *c* = 14.1774(8) Å, α = 107.226(5)°, β = 100.672(5)°, γ = 104.655(6)°, *V* = 1212.67(15) Å^3, *Z* = 4, *T* = 150 K, λ = 1.54180 Å. 11204 reflections collected, 5002 independent [R(int) = 0.0556] used in all calculations, with 307 refined parameters, GOF on F^2 = 0.9621. R_1 = 0.0468, wR_2 = 0.1180 for observed unique reflections [I>2σ(I)] and R_1 = 0.0556, wR_2 = 0.1273 for all unique reflections. Max. and min. residual electron densities 1.65 and -1.02 e Å^{-3}.

*(6,7-dibromoindenyl)cyclopentadienyliron(II) (**VIIId**)*

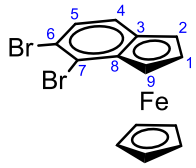

Following the same procedure as for **Vd**: a solution of 6,7-dibromoindene (3.00 g, 10.93 mmol) in dry thf (250 mL) was added to potassium hydride (658 mg, 16.39 mmol), then onto [FeCp(naph)][PF_6] (4.52 g, 11.48 mmol). The product was isolated as a purple solid, crystals suitable for X-ray crystallography were obtained from a cold hexane solution (-25° C). Yield: 1.59 g, 37%.

^{1}H NMR (400 MHz, $CDCl_3$, 25 °C): δ_H 3.91 (*s*, 5H, Cp), 4.14 (*s*, 1H, C1H), 4.99 (*s*, 1H, C2H), 5.10 (*s*, 1H, C9H), 7.02 (*d*, $^3J_{HH}$ = 9.0 Hz, 1H, C5H), 7.45 (*d*, $^3J_{HH}$ = 9.0 Hz, 1H, C4H). ♦ $^{13}C\{^1H\}$ NMR (120 MHz, $CDCl_3$, 25 °C): δ_C 63.8 (C9), 64.4 (C2), 68.7 (Cp), 71.5 (C1), 86.7 (C3), 90.2 (C8), 117.3 (C6), 125.1 (C4), 127.7 (C5), 130.1 (C7). ♦ Elemental microanalysis: calc. for $C_{14}H_{10}Br_2Fe$: C, 42.69%; H, 2.56%. Found: C, 42.70%; H, 2.55%. ♦ MS (EI+), *m/z* (%): 393.8 (100%), 391.8 (55%), 395.8 (45%), accurate mass (calc. for M^+, ^{54}Fe isotopomer) 389.85536,

(meas.) 389.854560, isotopic pattern correct for $C_{14}H_{10}Br_2Fe$. ♦ Crystallographic data: $C_{14}H_{10}Br_2Fe$, M_r = 393.89, monoclinic, *P 2₁/c*, *a* = 14.0382(2) Å, *b* = 12.4233(2) Å, *c* = 16.0159(3) Å, β = 115.666(2)°, *V* = 2517.59(8) Å^3, *Z* = 8, *T* = 150 K, λ = 1.54180 Å. 27126 reflections collected, 5207 independent [R(int) = 0.0631] used in all calculations, with 499 refined parameters, GOF on F^2 = 0.9969. R_1 = 0.0589, wR_2 = 0.1439 for observed unique reflections [$I>2\sigma(I)$] and R_1 = 0.0631, wR_2 = 0.1473 for all unique reflections. Max. and min. residual electron densities 2.55 and -1.66e Å^{-3}.

*(6,7-dibromo-4-methyl-indenyl)cyclopentadienyliron(II) (**IXd**)*

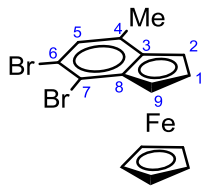

Following the same procedure as for **Vd**: A solution of 6,7-dibromo-4-methyl indene (19.27 g, 66.91 mmol) in thf (250 mL) was added to potassium hydride (5.37 g, 133.82 mmol), then transfered onto [FeCp(naph)][PF_6] (29.00 g, 73.60 mmol). The product was isolated as a purple solid, crystals suitable for X-ray crystallography were obtained from a cold hexane solution (-25° C). Yield: 13.10 g, 48%.

^{1}H NMR (400 MHz, $CDCl_3$, 25 °C): δ_H 2.44 (*s*, 3H, Me), 3.89 (*s*, 5H, Cp), 4.14 (*s*, 1H, C1H), 4.92 (*s*, 1H, C2H), 5.09 (*s*, 1H, C9H), 6.86 (*s*, 1H, C5H). ♦ ^{13}C{^{1}H} NMR (120 MHz, $CDCl_3$, 25 °C): δ_C 18.8 (Me), 62.2 (C2), 64.9 (C9), 68.6 (Cp), 71.1 (C1), 87.4 (C3), 90.0 (C8), 117.6 (C7), 121.3 (C6), 125.6 (C5), 140.3 (C4). ♦ Elemental microanalysis: calc. for $C_{15}H_{12}Br_2Fe$: C, 44.17%; H, 2.97%. Found: C, 43.79%; H, 2.88%. ♦ MS (EI+), *m/z* (%): 407.9 (100%), accurate mass (calc. for M^+, ^{54}Fe isotopomer) 407.8636, (meas.) 407.8653, isotopic pattern correct for $C_{15}H_{12}Br_2Fe$. ♦ Crystallographic data: $C_{15}H_{12}Br_2Fe$, M_r = 407.92, monoclinic, *P 2₁/n*, *a* = 9.1392(4) Å, *b* = 16.4041(5) Å, *c* = 9.6864(4) Å, β = 114.097(5)°, *V* = 1325.64(10) Å^3, *Z* = 4, *T* = 150 K, λ =

0.71073 Å. 8789 reflections collected, 4391 independent [R(int) = 0.037] used in all calculations, with 163 refined parameters, GOF on F^2 = 0.9939. R_1 = 0.0413, wR_2 = 0.0824 for observed unique reflections [I>2σ(I)] and R_1 = 0.0610, wR_2 = 0.0916 for all unique reflections. Max. and min. residual electron densities 1.37 and -1.38 e $Å^{-3}$.

*(5-dimesitylboryl-6-bromo-indenyl)cyclopentadienyliron(II) (**VIIh**)*

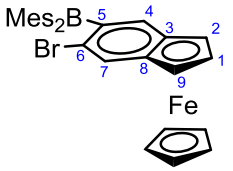

To a solution of **VIId** (500 mg, 1.27 mmol) in a mixture of thf and Et_2O (1:1 vol.) at -120° C was added a solution of ^{n}BuLi at -78° C (1.6 M in hexane, 0.83 mL, 1.33 mmol). The reaction mixture was stirred for a further 30 min at -120° C, then a solution of $FBMes_2$ (710 mg, 2.65 mmol) in a mixture of thf and Et_2O (1:1 vol.) cooled to -78° C added to the red solution. The reaction mixture was then stirred for 2 h at -120° C and warmed to room temperature overnight. Volatiles were removed under reduced pressure, the crude solid extracted with hexane and the resulting solid purified by an air-free chromatography column eluted with hexane. Crystals suitable for X-ray crystallography were obtained from a cold hexane solution (-25° C). Yield: 137 mg, 19%.

^{1}H NMR (400 MHz, $CDCl_3$, 25 °C): δ_H 2.04 (*b s,* 12H, *ortho*-Me of Mes), 2.31 (*s*, 6H, *para*-Me of Mes), 3.95 (*s*, 5H, Cp), 4.19 (*s*, 1H, C2H), 4.98 (*s*, 1H, C9H), 6.79 (*b s,* 4H, *meta-C*H of Mes), 7.62 (*s*, 1H, C7H), 7.76 (*s*, 1H, C4H). ♦ ^{13}C{^{1}H} NMR (101 MHz, $CDCl_3$, 25 °C): δ_C 21.5 (*para*-Me of Mes), 23.3 (*ortho*-Me of Mes), 68.1 (Cp), 62.5 (C9), 63.6 (C2), 71.9 (C1), 84.8 (C3), 90.2 (C8), 128.2 (*meta*-CH of Mes), 130.8 (C4), 138.9 and 141.0 (quaternary C of Mes), 142.3 (C7), 140.8 (quaternary C of Mes), 143.3 (*b s*, C10), 146.5 (*b s*, C6). ♦ ^{11}B{^{1}H} NMR (128 MHz, $CDCl_3$, 25 °C): δ_B 72. ♦ Crystallographic data: $C_{32}H_{32}BBrFe$, M_r = 563.17, triclinic, *P-1*, *a* = 7.2912(3) Å,

b = 12.2121(5) Å, c = 15.1883(7) Å, α = 79.543(3)°, β = 89.951(4)°, γ = 81.154(3)°, V = 1313.59(10) Å^3, Z = 2, T = 150 K, λ = 1.54180 Å. 11670 reflections collected, 5363 independent [R(int) = 0.0371] used in all calculations, with 362 refined parameters, GOF on F^2 = 0.9831. R_1 = 0.0334, wR_2 = 0.0770 for observed unique reflections [I>2σ(I)] and R_1 = 0.0371, wR_2 = 0.0795 for all unique reflections. Max. and min. residual electron densities 0.40 and -0.61 eÅ^{-3}.

*(5-diphenylphosphino-6-bromo-indenyl)cyclopentadienyliron(II) (**VIIe**)*

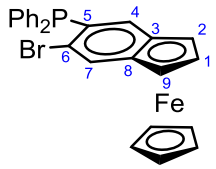

To a solution of **VIId** (2.41 g, 6.12 mmol) in a mixture of thf and Et_2O (1:1 vol.) at -120° C was added a solution of ^{n}BuLi at -78° C (1.6 M in hexane, 4.0 mL, 6.43 mmol). The reaction mixture was stirred for 30 min at -120° C, then a solution of PPh_2Cl (5.65 mL, 30.59 mmol) in a mixture of thf and Et_2O (1:1 vol.) at -78° C was added to the red solution. The reaction mixture was stirred for a further 2 h at -120° C and warmed to room temperature overnight. Volatiles were removed under reduced pressure, and the crude solid washed with hexane three times then extracted with dichloromethane. The solution was concentrated and crystals suitable for X-ray crystallography were obtained from a cold 2:1 mixture of dichloromethane/thf (-25° C). Yield: 2.55 g, 83 %.

^{1}H NMR (300 MHz, $CDCl_3$, 25 °C): δ_H 1.85 and 3.70 (thf) 3.91 (s, 5H, Cp), 4.10 (*t*, $^3J_{HH}$ = 2.1 Hz, 1H, C1H), 4.79 (*d*, $^3J_{HH}$ = 2.1 Hz, 1H, C2H), 4.96 (*d*, $^3J_{HH}$ = 2.1 Hz, 1H, C9H), 7.07 (*s*, 1H, C4H), 7.39 (*m*, 10H, PPh_2), 7.86 (s, 1H, C7H). ♦ ^{13}C{^{1}H} NMR (126 MHz, $CDCl_3$, 25 °C): δ_C 61.8 (C2), 63.9 (C9), 68.8 (Cp), 71.5 (C1), 85.6 (C3), 92.4 (C8), 128.5 (CH of Ph), 129.1 (C4), 133.3 (CH of Ph), 133.4 (quaternary C of Ph), 134.1 (C7), 134.2 (CH of Ph), 134.4 (C5), 128.7 (C6). ♦ ^{31}P{^{1}H} NMR (202 MHz, $CDCl_3$, 25° C): δ_P -4.1 (PPh$_2$). ♦ Elemental microanalysis: calc. for

$C_{26}H_{20}BrFeP{\cdot}(thf)_{0.25}$ C, 62.56%; H, 4.04%. Found: C, 61.78%; H, 4.11%. ♦ MS (EI^+), *m*/*z* (%): 498.0 (40%) and 500.0 (38%), accurate mass (calc. for M^+, ^{54}Fe isotopomer) 496.0013, (meas.) 495.9883, isotopic pattern correct for $C_{26}H_{20}BrFeP$. ♦ Crystallographic data: $C_{26}H_{20}BrFeP$, M_r = 499.17, triclinic, *P-1*, *a* = 9.2752(3) Å, *b* = 10.7752(6) Å, *c* = 10.8467(4) Å, α = 89.156(4)°, β = 84.520(3)°, γ = 76.998(4)°, *V* = 1051.40(8) $Å^3$, *Z* = 2, *T* = 150 K, λ = 1.54180 Å. 9431 reflections collected, 4347 independent [R(int) = 0.0266] used in all calculations, with 262 refined parameters, GOF on F^2 = 0.9999. R_1 = 0.0257, wR_2 = 0.0657 for observed unique reflections [I>2σ(I)] and R_1 = 0.0266, wR_2 = 0.0666 for all unique reflections. Max. and min. residual electron densities 0.65 and -0.40 e $Å^{-3}$.

*(7-diphenylphosphino-6-bromo-indenyl)cyclopentadienyliron(II) (**VIIIe**)*

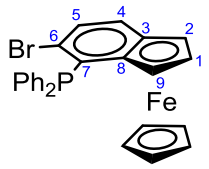

To a solution of **VIIId** (242 mg, 0.614 mmol) in a mixture of thf and Et_2O (1:1 vol.) at -120° C was added a cold solution of ^{n}BuLi at -78° C (1.6 M in hexane, 0.41 mL, 0.65 mmol). The reaction mixture was stirred for 30 min at -120° C, then a solution of PPh_2Cl (1.14 mL, 6.14 mmol) in a mixture of thf and Et_2O (1:1 vol.) at -78° C added to the red solution. The reaction mixture was stirred for a further 2 h at -120° C and warmed to room temperature overnight. The solvents were removed under reduced pressure, and the crude solid washed with hexane three times then extracted with dichloromethane. The solution was concentrated and crystals suitable for X-ray crystallography were obtained from the cold solution (-25° C). Yield: 174 mg, 57 %.

^{1}H NMR (500 MHz, $CDCl_3$, 25 °C): δ_H 3.82 (*s*, 5H, Cp), 4.10 (*s*, 1H, C1H), 4.79 (*s*, 1H, C2H), 4.95 (s, 1H, C9H), 7.05 (*t*, $^3J_{HH}$ = 7.0 Hz, 1H, C4H), 7.13 (*t*, $^3J_{HH}$ = 7.0 Hz, 1H, C5H), 7.36 (*m*, 10H, PPh).

♦ $^{13}C\{^1H\}$ NMR (126 MHz, $CDCl_3$, 25 °C): δ_C 61.9 (C2), 62.5 (C9), 68.3 (Cp), 71.5 (C1), 85.8 (C3), 89.1 (C8), 115.4 (C7), 124.1 (C6), 129.0 and 130.1 (CH of Ph), 131.9 (C4 or C5), 134.2 (CH of Ph), 136.8 (quaternary C of Ph), 138.3 (C4 or C5). ♦ $^{31}P\{^1H\}$ NMR (202 MHz, $CDCl_3$, 25 °C): δ_P -4.2. ♦ Crystallographic data: $C_{26}H_{20}BrFeP$, M_r = 499.17, triclinic, *P-1*, *a* = 9.6706(4) Å, *b* = 9.7052(4) Å, *c* = 11.2273(3) Å, α = 90.005(3)°, β = 82.855(3)°, γ = 75.548(4)°, *V* = 1011.94(7) Å^3, *Z* = 2, *T* = 150 K, λ = 1.54180 Å. 20190 reflections collected, 4207 independent [R(int) = 0.0257] used in all calculations, with 262 refined parameters, GOF on F^2 = 1.0077. R_1 = 0.0255, wR_2 = 0.0692 for observed unique reflections [I>2σ(I)] and R_1 = 0.0257, wR_2 = 0.0693 for all unique reflections. Max. and min. residual electron densities 0.46 and -0.62 e Å^{-3}.

(4-methyl-6-bromo-7-diphenylphosphino-indenyl)cyclopentadienyliron(II) ***(IXe)***

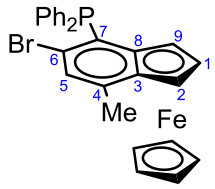

To a solution of **XId** (1.00 g, 2.45 mmol) in a mixture of thf and Et_2O (1:1 vol.) at -120° C was added a solution of ^{n}BuLi at -78° C (1.6 M in hexane, 1.61 mL, 2.57 mmol). The reaction mixture was stirred for 30 min at -120° C, then a solution of PPh_2Cl (1.36 mL, 7.35 mmol) in a mixture of thf and Et_2O (1:1 vol.) at -78° C added to the red solution. The reaction mixture was stirred for a further 2 h at -120° C and warmed to room temperature overnight. The solvents were removed under reduced pressure, and the crude solid washed with cold hexane three times then extracted with dichloromethane. The solution was concentrated and crystals suitable for X-ray crystallography were obtained from the cold solution (-25° C). Yield: 460 mg, 37 %.

^1H NMR (400 MHz, $CDCl_3$, 25 °C): δ_H 2.50 (*d*, $^4J_{HH}$ = 0.9 Hz, 3H, Me), 3.59 (*s*, 5H, Cp), 3.89 (*t*, $^3J_{HH}$ = 2.6 Hz, 1H, C1H), 4.10 (*dd*, $^3J_{HH}$ = 2.6 Hz, 1H, C2H), 4.80 (*dd*, $^3J_{HH}$ = 2.6 Hz, 1H, C9H), 5.30

(CH_2Cl_2), 6.95 (*dd*, $^3J_{HP}$ =3.2 Hz, 1H, C5H), 7.27 (*m*, 3H, CH of Ph), 7.48 (*m*, 5H, CH of Ph), 7.78 (*td*, $^3J_{HH}$ = 7.5 Hz, 2H, *para*-CH of Ph). ♦ $^{13}C\{^1H\}$ NMR (100.6 MHz, $CDCl_3$, 25 °C): δ_C 19.2 (Me), 60.0 (C9), 64.7 (C2), 68.7 (Cp), 71.1 (C1), 86.2 (C3), 92.4 (C8), 126.9 (C5), 128.4 and 128.6 (CH of Ph), 128.9 (*meta*-CH of Ph), 130.3 (C6), 133.1 (CH of Ph), 134.1 (*para*-CH Ph), 136.9 (CH of Ph), 144.6 (C4). ♦ $^{31}P\{^1H\}$ NMR (162 MHz, $CDCl_3$, 25 °C): δ_P -0.2. ♦ Elemental microanalysis: calc. for $C_{27}H_{22}BrFeP\cdot(CH_2Cl_2)_{0.2}$: C, 61.62%; H, 4.26%. Found: C, 61.78%; H, 4.66%. ♦ MS (EI+), *m/z* (%): 512.0 (100%), 514.0 (95%), accurate mass (calc. for M^+, ^{56}Fe isotopomer) 511.9994, (^{79}Br isotopomer) and 513.9976 (^{81}Br isotopomer), (meas.) 511.9986 and 513.9961, isotopic pattern correct for $C_{27}H_{22}BrFeP$. ♦ Crystallographic data: $C_{27}H_{22}BrFeP$, M_r = 513.20, triclinic, *P-1*, *a* = 9.6042(3) Å, *b* = 10.5337(5) Å, *c* = 11.2465(4) Å, α = 92.027(3)°, β = 95.965(3)°, γ = 107.132(3)°, *V* = 1078.80(7) Å^3, *Z* = 2, *T* = 150 K, λ = 1.54180 Å. 12199 reflections collected, 4507 independent [R(int) = 0.026] used in all calculations, with 272 refined parameters, GOF on F^2 = 1.0156. R_1 = 0.0310, wR_2 = 0.0842 for observed unique reflections [$I>2\sigma(I)$] and R_1 = 0.0312, wR_2 = 0.0844 for all unique reflections. Max. and min. residual electron densities 1.10 and -0.56 e Å^{-3}.

(5-diphenylphosphino-6-dimesitylboryl-indenyl)cyclopentadienyliron(II) ***(VIIf)***

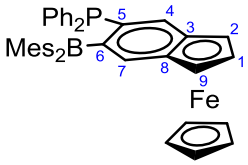

To a solution of **VIIe** (2.00 g, 4.00 mmol) in Et_2O was slowly added a solution of ^{t}BuLi (1.9 M in hexane, 4.75 mL, 9.06 mmol). The reaction mixture was stirred for 2 h at room temperature, cooled to -40° C, then a solution of $FBMes_2$ (1.29 g, 4.80 mmol) in Et_2O was added to the red solution. After stirring at room temperature overnight volatiles were removed under reduced pressure, the crude solid washed with hexane three times then extracted with

dichloromethane. Crystals suitable for X-ray crystallography were collected after the solution was concentrated and layered with hexane. Yield: 1.36 g, 51 %.

^{1}H NMR (400 MHz, $CDCl_3$, 25 °C): δ_H 0.85 and 1.20 (hexane), 1.89, 1.92, 2.00, 2.10, 2.29 and 2.38 (*b s*, each 3H, Me of Mes), 3.79 (*b s,* 3H, Cp), 3.90 (*b s,* 2H, Cp), 4.09 (*t*, $^{3}J_{HH}$ = 2.5 Hz, 1H, C1H), 4.82 (*d*, $^{3}J_{HH}$ = 1.5 Hz, 2H, C2H and C9H), 5.76 and 6.53 (*b s,* each 1H, *meta*-CH of Mes), 6.74 (*b s,* 2H, *meta*-CH of Mes), 6.86, 6.98, 7.06 and 7.17 (*b s*, 10H total, *Ph*), 7.36 (*d*, $^{3}J_{HH}$ = 5.0 Hz, 1H, C4H), 7.55 (*b s,* 1H, C7H). ♦ ^{1}H NMR (500 MHz, bromobenzene-d_5, 100 °C): δ_H 2.37 (*b s,* 18H, Me of Mes), 4.10 (s, 5H Cp), 4.23 (*s*, 1H, C1H), 4.93 and 4.94 (*s*, 1H each, C2H and C9H), 5.31 (dichloromethane), 6.84 (*b s,* 4H, *meta*-CH of Mes), 7.19 and 7.26 (*b s,* each 1H, *para*-CH Ph), 7.31 and 7.33 (*d*, $^{3}J_{HH}$ = 6.7 Hz, each 2H, *ortho*-CH Ph), 7.39 and 7.48 (*b s,* each 2H, *meta*-CH of Ph), 7.87 (*d*, $^{3}J_{HP}$ = 4.7 Hz, 1H, C4H), 7.99 (*s*, 1H, C7H). ♦ ^{13}C{^{1}H} NMR (126 MHz, $CDCl_3$, 25 °C): δ_C 20.0, 20.2, 21.3, 22.0, 22.2 and 23.6 (Me of Mes), 62.2 and 62.5 (C2 and C9), 66.6 (Cp), 70.5 (C1), 85.7 (C8), 86.5 (C3), 126.2 and 126.4 (*para*-CH of Ph), 126.6 (*meta*-CH of two Mes), 126.7 (*metha*-CH of Ph), 126.8 and 126.9 (*meta*-CH of Mes), 127.0 (*metha*-C of Ph), 131.5, 131.7, 132.1 and 132.3 (*ortho*-CH of Ph), 132.98 and 133.54 (*ipso*-quaternary C of Ph), 136.1 (C6), 136.2 (C7), 137.5 (*para*-quaternary C of two Mes), 138.5 (C4), 139.1, 139.6, 139.8 and 140.8 (*ortho*-C of Mes), 143.0 (b *s*, *ipso*-C of two Mes), 151.7 (*d*, $^{1}J_{CP}$ = 45.8 Hz, C5). ♦ ^{13}C NMR (126 MHz, bromobenzene-d_5, 100 °C): 21.2 (*para*-Me of Mes), 23.6 (*ortho*-Me of Mes), 63.2 (C2), 63.6 (C9), 67.8 (Cp), 71.8 (C1), 87.0 (C3), 88.1 (C8), 127.6 and 127.9 (Ph), 128.4 (*meta*-CH of Mes), 133.3 and 133.4 (resp. J_{CP} = 8.0 Hz and J_{CP} = 7.3 Hz, CH of Ph), 135.4 (C6), 138.1 (C7), 138.2 (C4), 138.5 (*para*-quaternary C of Mes), 139.3 and 140.8 (*ortho*-quaternary C of Mes), 144.1 (*ipso*-quaternary C of Mes), 152.9 (C5). ♦ ^{31}P{^{1}H} NMR (202 MHz, bromobenzene-d_5, 25 °C): δ_P -6.5 and -9.5. ♦ ^{31}P{^{1}H} NMR (202 MHz, bromobenzene-d_5, 100 °C): δ_P -7.7. ♦ ^{31}P{^{1}H} NMR (202 MHz, bromobenzene-d_5, 25 °C): δ_P -9.5 and -6.5. ♦ ^{11}B{^{1}H} NMR (128 MHz, $CDCl_3$, 25 °C): δ_B 74 (*b s*). ♦ MS (EI+), *m/z* (%): 653.2 (10%, M^+-CH_3), accurate

mass (calc. for M^+, ^{56}Fe and ^{11}B isotopomer) 668.2475, (meas.) 668.2480, isotopic pattern correct for $C_{44}H_{42}BFeP$. ♦ Elemental microanalysis: calc. for $C_{44}H_{42}BFeP\cdot(CH_2Cl_2)$ (Hexane): C, 72.96%; H, 6.96%. Found: C, 73.06%; H, 6.56%. ♦ $E_{1/2}$= +166 mV (Fe^{II}/Fe^{III}) *vs* ferrocene/ferrocenium couple with 0.1 M [$^nBu_4N$][PF_6] in thf. ♦ UV-vis (thf): λ_{max} = 421 (ε = 2530 mol^{-1} L^{-1} cm^{-1}), 511 nm (ε = 1110 mol^{-1} L^{-1} cm^{-1}). ♦ Crystallographic data: $C_{44}H_{42}BFeP$, M_r = 668.45, triclinic, *P-1*, *a* = 11.4666(5) Å, *b* = 11.4707(6) Å, *c* = 13.8882(6) Å, α = 74.346(4)°, β = 77.185(4)°, γ = 86.432(4)°, *V* = 1715.14(14) $Å^3$, *Z* = 2, *T* = 150 K, λ = 1.54180 Å. 16124 reflections collected, 7086 independent [R(int) = 0.0380] used in all calculations, with 424 refined parameters, GOF on F^2 = 0.9858. R_1 = 0.0334, wR_2 = 0.0809 for observed unique reflections [I>2σ(I)] and R_1 = 0.0380, wR_2 = 0.0837 for all unique reflections. Max. and min. residual electron densities 0.41 and -0.46e $Å^{-3}$.

*(4-methyl-6-dimesitylboryl-7-diphenylphosphino-indenyl)cyclopentadienyliron(II) (**IXf**)*

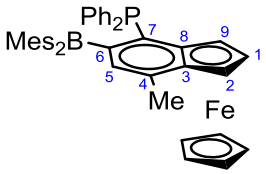

To a solution of **IXe** (2.00 g, 3.90 mmol) in thf at -78° C was slowly added a solution of ^{n}BuLi (1.9 M in hexane, 4.90 ml, 7.79 mmol). The reaction mixture was stirred for 1 h at -78° C, then a solution of $FBMes_2$ (2.09 g, 7.79 mmol) in thf added to the red solution and the mixture warmed to room temperature overnight. Volatiles were removed under reduced pressure, and the crude solid washed with hexane three times then extracted with dichloromethane. Crystals suitable for X-ray crystallography were collected after the solution was concentrated and layered with hexane. Yield: 836 mg, 31 %.

^{1}H NMR (400 MHz, $CDCl_3$, 25 °C): δ_H 0.85 and 1.25 (hexane), 1.99 and 2.16 (*b s,* each 6H, *ortho*-Me of Mes), 2.20 and 2.34 (*s*, each 3H, *para*-Me of Mes), 2.46 (*s*, 3H, Me), 3.52 (*s*, 5H, Cp), 4.00

(*t*, $^{3}J_{HH}$ = 2.3 Hz, 1H, C1H), 4.45 (*d*, $^{3}J_{HH}$ = 1.5 Hz, 1H, C2H), 4.89 (*d*, $^{3}J_{HH}$ = 1.5 Hz, 1H, C9H), 5.29 (dichloromethane), 6.64 (*b s*, 2H, *meta*-CH of Mes), 6.71 (s, 1H, C5H), 6.81 (s, 2H, *meta*-CH of Mes), 6.94 - 7.31 (*m*, 10H, Ph). ♦ $^{13}C\{^{1}H\}$ NMR (100.6 MHz, $CDCl_3$, 25 °C): δ_C 19.8 (Me), 21.2 and 21.4 (*para*-Me of Mes), 23.7 (*b s, ortho*-Me of Mes), 59.6 (C9), 65.1 (C2), 67.9 (Cp), 70.9 (C1), 88.6 (C3), 124.6 (C5), 127.1 and 127.6 (*meta*-CH of Ph), 127.9 and 128.0 (*para*-CH of Ph), 128.1 (C4), 128.2 (*b s*, *meta*-CH of Mes), 132.7 (*d*, J_{PC} = 19.2 Hz, *ortho*-C Ph), 133.9 (*d*, J_{PC} = 17.1 Hz, *ortho*-CH Ph), 134.4 and 136.0 (*ipso*-quaternary C Ph), 138.9 (*para*-quaternary C of Mes), 140.9 (*b s, meta*-CH of Mes), 141.1 (C7), 147.0 (b s, C6), 159.5 (*ipso*-quaternary C of Mes). ♦ $^{11}B\{^{1}H\}$ NMR (128 MHz, $CDCl_3$, 25 °C): δ_B 76 (*bs*). ♦ $^{31}P\{^{1}H\}$ NMR (162 MHz, $CDCl_3$, 25 °C): δ_P -5.8 (*bs*). ♦ MS (EI+), *m/z* (%): 667.2 ($[M\text{-}CH_3]^+$), isotopic pattern correct for $C_{44}H_{41}BFeP$. ♦ Elemental microanalysis: calc. for $C_{45}H_{44}BFeP\cdot(CH_2Cl_2)_{2.75}$(hexane): C, 64.42 %; H, 6.39 %. Found: C, 64.69 %; H, 6.26 %. ♦ $E_{1/2}$= +43 mV (Fe^{II}/Fe^{III}) *vs* ferrocene/ferrocenium couple with 0.1 M [$^{n}Bu_4N$][PF_6] in thf. ♦ UV-vis (thf): λ_{max} = 351 (ε = 5560 mol^{-1} L^{-1} cm^{-1}) and 531 nm (ε = 1340 mol^{-1} L^{-1} cm^{-1}). ♦ Crystallographic data: $C_{45}H_{44}BFeP$, M_r = 682.48, triclinic, $P2_1/c$, *a* = 20.2118(2) Å, *b* = 8.13040(10) Å, *c* = 22.8385(2) Å, α = 90°, β = 108.4989(11)°, γ = 90°, *V* = 3559.13(7) $Å^3$, *Z* = 4, *T* = 150 K, λ = 1.54180 Å. 20753 reflections collected, 7344 independent [R(int) = 0.042] used in all calculations, with 433 refined parameters, GOF on F^2 = 0.9877. R_1 = 0.0435, wR_2 = 0.1119 for observed unique reflections [I>2σ(I)] and R_1 = 0.0483, wR_2 = 0.1166 for all unique reflections. Max. and min. residual electron densities 0.63 and -0.45 e $Å^{-3}$.

*(5-Methyldiphenylphosphonium-6-dimesitylboryl-indenyl)cyclopentadienyliron(II) iodide ([**VIIg**]I)*

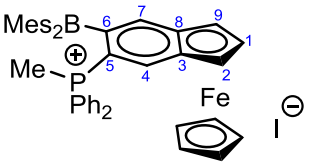

To a dichloromethane solution of **VIIf** (500 mg, 0.75 mmol) was added excess MeI (1.0 mL, 16.0 mmol), and the reaction mixture stirred at room temperature overnight. Volatiles were removed under reduced pressure and single crystals suitable for X-ray crystallography were obtained from a thf/heptane mixture. Yield: 595 mg, 98 %.

^{1}H NMR (major isomer 81%, 400 MHz, dmso-d_6, 25 °C): δ_H 1.67, 1.92, 1.97, 2.13, 2.29 and 2.45 (*s*, each 3H, Me of Mes), 2.72 (*d*, $^{2}J_{PH}$ = 13.4 Hz, 3H, PMe), 4.07 (*s*, 5H, Cp), 4.62 (s, 1H, C1H), 5.31 (*s*, 1H, C2H), 5.39 (*s*, 1H, C9H), 6.66, 6.78 and 7.04 (*s*, each 1H, H aromatic of Mes), 7.45 - 7.84 (*m*, 12H, PPh_2), 8.03 (*s*, 1H, H aromatic of Mes), 8.05 (*s*, 1H, C4H), 8.10 (*s*, 1H, C7H). ♦ ^{1}H NMR (minor isomer 19%, 400 MHz, dmso-d_6, 25 °C): δ_H 1.77, 1.81, 2.05, 2.17, 2.19 and 2.25 (s, each 3H, Me of Mes), 2.58 (d, $^{2}J_{PH}$ = 13.9 Hz, 3H, PMe), 4.66 (s, 1H, C1H), 5.29 (s, 1H, C2H), 5.37 (s, 1H, C9H), 6.70 and 6.89 (s, each 1H, *meta*-CH of Mes), 7.36 - 7.84 (m, 10H, PPh_2), 8.00 and 8.08 (s, each 1H, *meta*-CH of Mes), 8.05 (s, 1H, C4H), 8.10 (s, 1H, C7H). ♦ ^{13}C{^{1}H} NMR (major isomer 81%, 125 MHz, dmso-d_6, 25 °C): δ_C 6.9 (PMe), 19.3, 19.5, 21.5, 21.6, 24.0 and 20.9 (each Me of Mes), 65.3 (C9), 65.5 (C2), 67.2 (Cp), 74.4 (C1), 81.9 (C8), 84.4 (C3), 111.6 (J_{PC} = 88.0 Hz, C5), 116.1 (J_{PC} = 87.0 Hz, *ipso*-quaternary C of PPh_2), 123.4 (*d*, J_{PC} = 90.0 Hz, *ipso*-quaternary C of PPh_2), 126.3, 126.9, 127.5 and 127.9 (*meta*-CH of Mes), 128.0 and 128.5 (*d*, J_{PC} = 12 Hz, *ortho*-C of Ph), 128.0 and 128.6 (C of Mes), 129.8 (*d*, J_{PC} = 9.0 Hz, *meta*-C of Ph), 131.6 (*d*, J_{PC} = 9 Hz, *meta*-CH of Ph), 132.13 (*para*-CH of Ph), 132.9 (*para*-CH of Ph), 139.26, 139.9, 140.9 and 141.8 (quaternary C of Mes), 143.3 (*d*, J_{PC} = 13.5 Hz, C4), 147.8 (*d*, J_{PC} = 12.0 Hz, C7). *Note: the majority of the signals attributed to the minor isomer were too weak to be distinguished.* ♦ ^{31}P{^{1}H} NMR (major isomer 81%, 162 MHz, dmso-d_6, 25 °C): δ_P 23.4. ♦ ^{31}P{^{1}H} NMR (minor isomer 19%, 162 MHz, dmso-d_6, 25 °C): δ_P 24.4. ♦ ^{11}B{^{1}H} NMR (128 MHz, d_6-dmso, 25 °C): δ_B 72. ♦ Elemental microanalysis: calc. for $C_{45}H_{45}FeBPI\cdot(heptane)_{0.1}$: C, 66.15 %; H, 5.56 %. Found: C, 65.91 %; H, 5.95 %. ♦ MS (EI+), *m*/*z* (%): 683.3 (100%), accurate mass (calc. for M^+, ^{54}Fe and ^{10}B isotopomer) 683.2704 (meas.) 683.2700, isotopic pattern correct

for $[C_{45}H_{45}BFeP]^+$. ♦ UV-vis (thf): λ_{max} =325 (ε = 26600 mol^{-1} L^{-1} cm^{-1}), 445 nm (ε = 6380 mol^{-1} L^{-1} cm^{-1}). ♦ Crystallographic data: $C_{46}H_{47}BCl_2FeIP$, M_r = 895.32, monoclinic, *P* $2_1/n$, *a* = 11.18020(10) Å, *b* = 33.6816(2) Å, *c* = 12.03180(10) Å, β = 100.2961(8)°, *V* = 4457.82(6) $Å^3$, *Z* = 4, *T* = 150 K, λ = 1.54180 Å. 9225 reflections collected, 9225 independent [R(int) = 0.0515] used in all calculations, with 535 refined parameters, GOF on F^2 = 0.9982. R_1 = 0.0489, wR_2 = 0.1219 for observed unique reflections [I>2σ(I)] and R_1 = 0.0515, wR_2 = 0.1238 for all unique reflections. Max. and min. residual electron densities 1.96 and -1.50e $Å^{-3}$.

*(5-Methyldiphenylphosphonium-6-dimesitylboryl-indenyl)cyclopentadienyliron(II) trifluoromethylsulfonate ([**VIIg**][CF_3SO_3])*

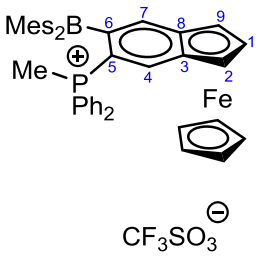

To a dichloromethane solution of **VIIf** (350 mg, 0.512 mmol) was added excess CF_3SO_3Me (0.60 mL, 5.12 mmol), and the reaction mixture stirred at room temperature for 4 h. Volatiles were removed under reduced pressure and single crystals suitable for X-ray crystallography were obtained from a thf / heptane mixture. Yield: 417 mg, 98 %. ^{1}H NMR identical to parent compound [**VIIg**]I. $^{11}B\{^1H\}$ NMR (128 MHz, $CDCl_3$, 25 °C): δ_B 73. ♦ $^{31}P\{^1H\}$ NMR (162 MHz, $CDCl_3$, 25 °C): δ_P 22.6 and 23.3. ♦ ^{19}F NMR (376 MHz, $CDCl_3$, 25 °C): δ_F -78.1. ♦ $E_{1/2}$= + 575 mV (Fe^{II}/Fe^{III}) and – 1978 mV ($B^{\cdot-}$/B) *vs* ferrocene/ferrocenium couple with 0.1 M [^{n}Bu_4N][PF_6] in acetonitrile.

*(4-Methyldiphenylphosphonium-5-dimesitylboryl-7-methyl-indenyl)cyclopentadienyliron(II) trifluoromethylsulfonate ([**IXg**][CF_3SO_3])*

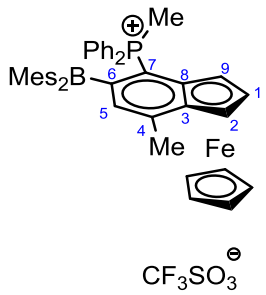

To a chloroform solution of **IXf** (500 mg, 0.732 mmol) was added an excess of CF_3SO_3Me (0.83 mL, 7.33 mmol), and the reaction mixture stirred at room temperature overnight. Volatiles were removed under reduced pressure, and single crystals suitable for X-ray crystallography were obtained from a dichloromethane/heptane mixture. Yield: 620 mg, 97 %.

Note: #1 and #2 used to discriminate the distinctive phenyl units of the —P(Me)Ph₂ moiety.

^{1}H NMR (400 MHz, $CDCl_3$, 25 °C): δ_H 1.78 (*b s,* 3H, *para*-Me of Mes), 1.95 (*b s,* 6H, *ortho*-Me of Mes), 2.19 (*b s,* 6H, *ortho*-Me of Mes), 2.32 (*s*, 3H, *para*-Me of Mes), 2.56 (*s*, 6H, PMe and Me of C4), 3.78 (*s*, 5H, Cp), 4.23 (*s*, 1H, C9H), 4.30 (*t*, $^3J_{HH}$ = 2.6 Hz, 1H, C1H), 5.15 (*s*, 1H, C2H), 5.30 (dichloromethane), 6.26 ($CDCl_3$), 6.75, 6.77, 6.80 and 6.82 (*b s,* each 1H, *meta*-CH of Mes), 6.88 (*d*, $^3J_{PH}$ = 3.3 Hz, 1H, C5H), 7.18 (*dd*, $^3J_{HH}$ = 13.1 Hz, $^4J_{HH}$ = 7.4 Hz, 2H, *ortho*-CH of Ph#1), 7.44 (*td*, $^3J_{HH}$ = 8.1 Hz, $^4J_{HP}$ = 3.7 Hz, 2H, *meta*-CH of Ph#1), 7.65 (*td*, $^3J_{HH}$ = 7.4 Hz, $^5J_{HP}$ = 1.3 Hz, 1H, *para*-CH of Ph#1), 7.76 (*td*, $^3J_{HH}$ = 7.4 Hz, $^4J_{HP}$ = 3.6 Hz, 2H, *meta*-CH of Ph#2), 7.85 (*m*, 3H, *para* and *ortho*-CH of Ph#2). ♦ ^{1}H NMR (500 MHz, CD_2Cl_2, -80 °C, major isomer 55%): δ_H 1.83, 1.95 and 1.99 (*s*, each 3H, *ortho*-Me of Mes), 2.27 (*s*, 3H, *para*-Me of Mes), 2.42 (*s*, 3H, *ortho*-Me of Mes), 2.53 (*d*, $^2J_{PH}$ = 10.9 Hz, 3H, PMe), 2.55 (*s*, 3H, Me of C4), 3.76 (*s*, 5H, Cp), 4.01 (*s*, 1H, C9H), 4.23 (*s*, 1H, C1H), 5.17 (*s*, 1H, C2H), 5.28 (dichloromethane), 6.26 ($CDCl_3$), 6.68, 6.76 and 6.82 (*s*, 4H, *meta*-CH of Mes), 6.96 (*s*, 1H, C5H), 7.02 (*dd*, $^3J_{PH}$ = 12.9 Hz, $^3J_{HH}$ = 7.3 Hz, 2H, *ortho*-CH of Ph), 7.38 (*t*, $^3J_{HH}$ = 7.5 Hz, 2H, *meta*-CH of Ph), 7.58 (*dd*, $^3J_{PH}$ = 13.4 Hz, $^3J_{HH}$ = 7.3 Hz, 2H, *ortho*-CH of Ph), 7.72 (*t*, $^3J_{HH}$ = 7.5 Hz, 2H, *meta*-CH of Ph), 7.79 (*m*, 1H, *para*-CH of Ph), 7.88 (*t*, $^3J_{HH}$ = 7.3 Hz, 1H, *para*-CH of Ph). ♦ ^{1}H NMR (500 MHz, CD_2Cl_2, **-80° C**, minor isomer 45%): δ_H 1.89, 1.90 and 2.05 (*s*, each 3H, *ortho*-Me of Mes), 2.27 (*s*, 3H, *para*-Me of Mes), 2.28 (*d*, $^2J_{PH}$ =

11.0 Hz, 3H, PMe), 2.31 (*s*, 3H, *ortho*-Me of Mes), 2.50 (*s*, 3H, Me of C4), 3.71 (*s*, 5H, Cp), 4.18 (*s*, 1H, C9H), 4.29 (*s*, 1H, C1H), 5.15 (s, 1H, C2H), 5.28 (dichloromethane), 6.26 ($CDCl_3$), 6.60 (*s*, 1H, *meta*-CH of Mes), 6.82 (*s*, 1H, C5H), 6.86 (*s*, 1H, *meta*-CH of Mes), 7.13 (*dd*, $^3J_{PH}$ = 12.6 Hz, $^3J_{HH}$ = 8.0 Hz, 2H, *ortho*-CH of Ph), 7.49 (*t*, $^3J_{HH}$ = 7.5 Hz, 2H, *meta*-CH of Ph), 7.69 (*t*, $^3J_{HH}$ = 7.5 Hz, 2H, *meta*-CH of Ph), 7.77 (*m*, 1H, *para*-CH of Ph), 7.82 (*dd*, $^3J_{PH}$ = 13.9 Hz, $^3J_{HH}$ = 7.8 Hz, 2H, *ortho*-CH of Ph), 7.90 (*t*, $^3J_{HH}$ = 7.3 Hz, 1H, *para*-CH of Ph). ♦ $^{13}C\{^1H\}$ NMR (126 MHz, $CDCl_3$, 25 °C): δ_C 15.0 (J_{CP} = 57.0 Hz, PMe), 20.4 (Me), 21.1, 21.3, 23.9 and 24.2 (Me of Mes), 61.0 (C2), 64.5 (C9), 68.4 (Cp), 74.2 (C1), 87.9 (C3), 92.4 (C8), 114.2 (*d*, J_{CP} = 90.0 Hz, C7), 119.2 (CF_3SO_3), 119.6 (*d*, J_{CP} = 50.0 Hz, *ipso*-quaternary C of Ph), 126.0 (C5), 129.4 (*ortho*-quaternary C of Mes), 130.0 and 130.1 (*meta*-CH of Mes), 130.2 (*meta*-CH of Ph), 130.3 (*meta*-CH of Mes), 130.4 (*meta*-CH of Ph), 132.2 (*b s, ortho*-CH of Ph), 132.6 (*d*, J_{CP} = 11.0 Hz, *ortho*-CH of Ph), 134.2 and 134.5 (*d*, J_{CP} = 2.8 Hz, *para*-CH of Ph), 141.3 and 142.4 (each *para*-quaternary C of Mes), 150.2 (C4), 160.2 (*b s, ipso*-quaternary C of Mes), C6 bound to the boron atom not found. ♦ $^{11}B\{^1H\}$ NMR (128 MHz, $CDCl_3$, 25 °C): δ_B 75. ♦ $^{31}P\{^1H\}$ NMR (162 MHz, $CDCl_3$, 25 °C): δ_P 17.5. ♦ ^{19}F NMR (376 MHz, $CDCl_3$, 25 °C): δ_F -77.8. ♦ MS (ESI+), *m/z* (%): 697.3 (100%), 698.3 (48%), accurate mass (calc. for M^+, ^{11}B and ^{56}Fe isotopomer) 697.2861, (meas.) 697.2876, isotopic pattern correct for $[C_{47}H_{50}BFeP]^+$. ♦ Elemental microanalysis: calc. for $C_{48}H_{50}BF_3FeO_3PS\cdot(CHCl_3)_4(CH_2Cl_2)_{0.5}$: C, 45.64 %; H, 4.01 %. Found: C, 45.32 %; H, 3.84 %. ♦ $E_{1/2}$= -1302 mV ($B^{\cdot-}$/B) *vs* ferrocene/ferrocenium couple with 0.1 M [^{n}Bu$_4$N][PF_6] in thf, + 576 mV (Fe^{II}/Fe^{III}) and– 1179 mV ($B^{\cdot-}$/B) *vs* ferrocene/ferrocenium couple with 0.1 M [^{n}Bu$_4$N][PF_6] in acetonitrile. ♦ UV-vis (thf): λ_{max} = 340 (ε = 24250 mol^{-1} L^{-1} cm^{-1}) and 596 (ε = 1070 mol^{-1} L^{-1} cm^{-1}) nm.

4.3.2 Anion binding by indenyl systems

*[^{n}Bu$_4$N][**VIIf**CN]*

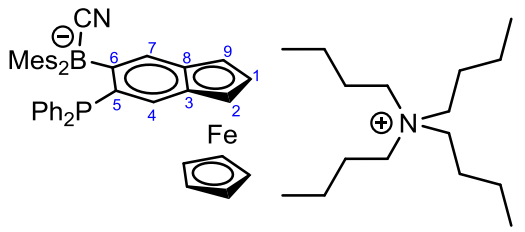

A thf solution of **VIIf** (250 mg, 0.374 mmol) was stirred with [^{n}Bu$_4$N][CN]·4H$_2$O (110 mg, 0.411 mmol) for 24 h at room temperature. Volatiles were removed from the resulting red solution in vacuo and the residue extracted with diethyl ether. After removal of the solvent in vacuo, crystals suitable for X-ray crystallography were obtained from a heptane/chloroform mixture. Yield: 140 mg, 40 %.

^{1}H NMR (500 MHz, CDCl$_3$, 25 °C): δ_H 0.94 (*t*, $^3J_{HH}$ = 7.2 Hz, 12H, CH$_3$ of [^{n}Bu$_4$N]), 1.30 (*b sextet*, $^3J_{HH}$ = 7.1 Hz, 8H, CH$_2$ of [^{n}Bu$_4$N]), 1.45 (*collapsed quintet*, 8H, CH$_2$ of [^{n}Bu$_4$N]), 2.09 (*b s*, 12H, *ortho*-Me of Mes), 2.21 and 2.26 (*b s*, each 3H, *para*-Me of Mes), 2.94 (*collapsed t*, 8H, NCH$_2$), 3.79 (*s*, 5H, Cp), 3.87 (*s*, 1H, C1H), 3.96 (*b s*, 2H, C2H and C9H), 6.57 and 6.63 (*b s*, each 2H, *meta*-CH of Mes), 6.93 and 6.99 (*b s,* each 1H, *para*-CH of Ph), 7.23 (*b s,* 1H, C7), 7.16 and 7.24 (*b s,* each 4H, *ortho*-CH of Ph), 7.26 (CHCl$_3$), 7.37 and 7.47 (*b s,* each 4H, *meta*-CH of Ph), 7.62 (*b s,* 1H, C4). ♦ ^{13}C{^{1}H} NMR (126 MHz, CDCl$_3$, 25 °C): δ_C 13.8 (CH$_3$ of [^{n}Bu$_4$N]), 19.7 (CH$_2$ of [^{n}Bu$_4$N]), 20.8 (*para*-Me of Mes), 23.9 (CH$_2$ of [^{n}Bu$_4$N]), 26.6 (*ortho*-Me of Mes), 58.4 (NCH$_2$ of [^{n}Bu$_4$N]), 60.3 and 61.0 (C2 and C9), 67.0 (Cp), 68.7 (C1), 86.2 (C8), 90.7 (b s, C3), 126.4 (*d*, J_{CP} = 31.0 Hz, *ortho*-CH of Ph), 128.5 (*meta*-CH of Mes), 131.6 (C7), 132.6 (*b d,* J_{CP} = 18.0 Hz, *para*-CH of Ph), 133.9 and 134.1 (*d*, J_{CP} = 20.0 Hz, *meta*-CH of Ph), 138.6 (*d*, J_{CP} = 31.0 Hz, *ipso*-quaternary C of Ph), 139.3 (C4), 140.2 (*para*-quaternary C of Mes), 143.2 (*ortho*-quaternary C of Mes), 144.0 (*d*, J_{CP} = 25.5 Hz, C5), 146.2 (CN bound to B), 151.3 (C6), 151.7 (*ipso*-quaternary

C of Mes). ♦ $^{11}B\{^1H\}$ NMR (160 MHz, $CDCl_3$, 25 °C): δ_B -13. ♦ $^{31}P\{^1H\}$ NMR (162 MHz, $CDCl_3$, 25 °C): δ_P -9.9 and -9.8. ♦ MS (ESI-), *m/z* (%): 694.3 (100%), accurate mass (calc. for M-, ^{11}B and ^{56}Fe isotopomer) 694.2500, (meas.) 694.3254, isotopic pattern correct for $[C_{45}H_{42}BFeNP]^-$. ♦ Elemental microanalysis: calc. for $C_{61}H_{78}BFeN_2P\cdot(CHCl_3)_{0.25}$: C, 76.10 %; H, 8.16 %. Found: C, 76.05 %; H, 7.99 %. ♦ UV-vis (thf): λ_{max} = 511 nm (ε = 1650 mol^{-1} L^{-1} cm^{-1}). ♦ Crystallographic data: $C_{61}H_{78}BFeN_2P$, M_r = 936.93, triclinic, *P-1*, *a* = 11.2105(3) Å, *b* = 11.4654(4) Å, *c* = 22.1928(7) Å, α = 95.295(3)°, β = 98.013(2)°, γ = 110.098(3)°, *V* = 2622.34(15) $Å^3$, *Z* = 2, *T* = 150 K, λ = 1.54180 Å. 27662 reflections collected, 10811 independent [R(int) = 0.032] used in all calculations, with 651 refined parameters, GOF on F^2 = 0.9811. R_1 = 0.0433, wR_2 = 0.1108 for observed unique reflections [I>2σ(I)] and R_1 = 0.0468, wR_2 = 0.1139 for all unique reflections. Max. and min. residual electron densities 0.88 and -0.56 e $Å^{-3}$.

*[^{n}Bu$_4$N][**IXf**CN]*

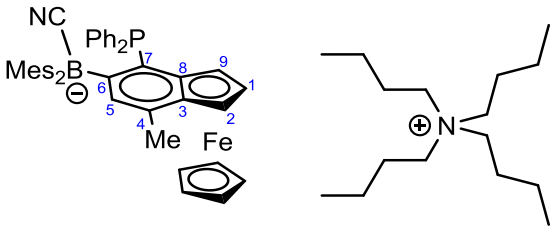

A thf solution of **IXf** (250 mg, 0.366 mmol) was stirred with $[^nBu_4N][CN]\cdot 4H_2O$ (108 mg, 0.403 mmol) for 24 h at room temperature. Volatiles were removed from the resulting red solution in vacuo and the residue extracted with diethyl ether. After removal of the solvent in vacuo, crystals suitable for X-ray crystallography were obtained from a heptane/dichloromethane mixture. Yield: 97 mg, 28 %.

^1H NMR (500 MHz, $CDCl_3$, 25 °C): δ_H 0.94 (*t*, $^3J_{HH}$ = 7.2 Hz, 12H, CH_3 of $[^nBu_4N]$), 1.27 (*b sextet*, $^3J_{HH}$ = 7.09 Hz, 8H, CH_2 of $[^nBu_4N]$), 1.44 (*collapsed quintet*, 8H, CH_2 of $[^nBu_4N]$), 1.98 (*s*, 3H, Me bound to C4), 2.08 (*s*, 6H, *ortho*-Me of Mes), 2.14 (*s*, 6H, *para*-Me of Mes), 2.28 (*s*, 6H, *ortho*-Me

of Mes), 2.94 (*t*, $^{3}J_{HH}$ = 7.85 Hz, 8H, NCH_2 of [$^{n}Bu_4N$]), 3.42 (*s*, 5H, Cp), 3.68 (*s*, 1H, C1H), 4.27 (*s*, 1H, C2H), 4.62 (*s*, 1H, C9H), 5.34 (dichloromethane), 6.36 and 6.69 (*s*, each 2H, *meta*-CH of Mes), 6.91 (*s*, 1H, C5H), 7.00 and 7.05 (*d*, $^{3}J_{HH}$ = 5.75 Hz, each 2H, *ortho*-CH of Ph), 7.21 and 7.31 (*t*, $^{3}J_{HH}$ = 7.25 Hz, each 2H, *meta*-CH of Ph), 7.91 (*t*, $^{3}J_{HH}$ = 6.10 Hz, 2H, *para*-CH of Ph). ♦ $^{13}C\{^{1}H\}$ NMR (126 MHz, $CDCl_3$, 25 °C): δ_C 13.6 (CH_3 of [$^{n}Bu_4N$]), 19.5 (CH_2 of [$^{n}Bu_4N$]), 20.7 and 20.8 (*ortho*-Me of Mes), 23.9 (CH_2 of [$^{n}Bu_4N$]), 26.2 (*para*-Me of Mes), 26.4 (Me bound to C4), 7.5 (C9), 58.2 (NCH_2 of [$^{n}Bu_4N$]), 65.1 (C2), 67.6 (C1), 67.8 (Cp), 86.1 (C3), 95.1 (*d*, J_{CP} = 5.4 Hz, C8), 125.8 (*d*, J_{CP} = 27.0 Hz, quaternary C of Ph), 126.6 (*d*, J_{CP} = 4.5 Hz, *para*-CH of Ph), 127.3 (*d*, J_{CP} = 4.20 Hz, *para*-CH of Ph), 128.4 (C4), 128.5 (*meta*-CH of Mes), 131.1 (*para*-quaternary C of Mes), 133.4 (*d*, J_{CP} = 18.30 Hz, *ortho*-CH of Ph), 133.2 (*d*, J_{CP} = 18.20 Hz, *ortho*-CH of Ph), 134.2 (*d*, J_{CP} = 16.7 Hz, *meta*-CH of Ph), 135.5 (C5), 138.1 (*d*, J_{CP} = 16.90 Hz, *meta*-CH of Ph), 142.1 (*d*, J_{CP} = 25.28 Hz, C7), 142.9 and 143.3 (*ortho*-quaternary C of Mes), 147.4 (*b s,* CN bound to the B), 152.1 (*b s, ipso*-quaternary C of Mes), 169.8 (*b s,* C6). ♦ $^{11}B\{^{1}H\}$ NMR (128 MHz, $CDCl_3$, 25 °C): δ_B -13. ♦ $^{31}P\{^{1}H\}$ NMR (162 MHz, $CDCl_3$, 25 °C): δ_P -12.3. ♦ MS (ESI-), *m/z* (%): 708.3 (100%), accurate mass (calc. for M^-, ^{11}B and ^{56}Fe isotopomer) 708.2657, (meas.) 708.3428, isotopic pattern correct for $[C_{46}H_{44}BFeNP]^-$. ♦ Elemental microanalysis: calc. for $C_{62}H_{80}BFeN_2P\cdot(CH_2Cl_2)_{0.4}$: C, 76.09 %; H, 8.27 %. Found: C, 75.75 %; H, 8.66 %. ♦ UV-vis (thf): λ_{max} = 531 nm (ε = 1060 mol^{-1} L^{-1} cm^{-1}). ♦ Crystallographic data: $C_{62}H_{80}BFeN_2P$, M_r = 950.96, monoclinic, *P2₁*, *a* = 11.36940(10) Å, *b* = 19.00260(10) Å, *c* = 12.16980(10) Å, β = 90.0233(6)°, *V* = 2629.26(3) $Å^3$, *Z* = 2, *T* = 150 K, λ = 1.54180 Å. 26989 reflections collected, 10492 independent [R(int) = 0.027] used in all calculations, with 604 refined parameters, GOF on F^2 = 1.0009. R_1 = 0.0787, wR_2 = 0.1880 for observed unique reflections [I>2σ(I)] and R_1 = 0.0799, wR_2 = 0.1891 for all unique reflections. Max. and min. residual electron densities 0.39 and -0.28 e $Å^{-3}$.

VIIg*·μ_2-*F

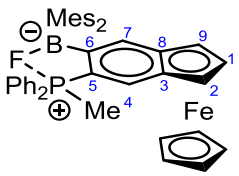

A thf solution of [**VIIg**]I (250 mg, 0.374 mmol) was stirred with [^{n}Bu$_4$N]F·3H$_2$O (113 mg, 0.411 mmol) for 6 h at room temperature. Volatiles were removed from the resulting red solution in vacuo and the residue extracted with diethyl ether. After removal of the solvent in vacuo, crystals suitable for X-ray crystallography were obtained from a heptane/chloroform mixture. Yield: 47 mg, 18 %.

^{1}H NMR (400 MHz, $CDCl_3$, 25 °C): δ_H 0.84, 1.25 and 1.29 (heptane), 2.02 (*b s,* 3H, *ortho*-Me of Mes), 2.08 (*b s,* $^2J_{HP}$ = 10.9 Hz, 3H, PMe), 2.32 and 2.35 (*b s,* each 3H, *para*-Me of Mes), 2.48, 2.50 and 2.57 (*b s,* each 3H, *ortho*-Me of Mes), 3.74 and 3.77 (*s*, 5H, Cp), 3.88 (*s*, 1H, C1H), 4.48 (*s*, 1H, C2H), 4.67 (*s*,1H, C9H), 6.81, 6.89, 6.97 and 7.08 (*b s,* each 1H, *meta*-CH of Mes), 6.93-7.13 (*m*, 8H, *ortho* and *meta*-CH of Ph), 7.26 ($CHCl_3$), 7.41 (*s*, 2H, *para*-CH of Ph), 7.67 (*d*, $^3J_{HP}$ = 17.0 Hz, 1H, C4H), 8.19 (*s*, 1H, H of C7). ♦ ^{13}C{^{1}H} NMR (126 MHz, $CDCl_3$, 25 °C): δ_C 13.8 (*dd*, J_{CP} = 62.7 Hz, J_{CF} = 13.6 Hz, PMe), 21.3 (*para*-Me of Mes), 24.8, 25.5 and 25.8 (*ortho*-Me of Mes), 27.4 (*para*-Me of Mes), 29.1 (*b s, ortho*-Me of Mes), 62.4 (C2), 63.2 (C9), 67.8 (C1), 68.2 and 72.3 (Cp), 84.2 (J_{CP} = 19.5 Hz, C3), 91.9 (C8), 125.1 (*d*, J_{CP} = 93.2 Hz, *ipso*-quaternary C of Ph), 128.9, 129.0, 129.29 and 129.3 (*meta*-CH of Mes), 130.1 (*d*, J_{CP} = 85.4 Hz, quaternary-C of C5), 131.8 (*b s, meta*-CH of Ph), 132.2 (*para*-CH of Ph), 132.4 (*b s, para*-quaternary C of Mes), 133.1 (*d*, J_{CP} = 33.3 Hz, *ortho*-CH of Ph), 135.6 (C7), 140.4, 140.8, 142.1 and 144.3 (*ortho*-quaternary C of Mes), 144.6 (*d*, J_{CF} = 16.9 Hz, C4), 154.0 (*b s,* C6), 159.5 (*b s, ispo*-quaternary-C of Mes). ♦ ^{11}B{^{1}H} NMR (160 MHz, $CDCl_3$, 25 °C): δ_B 7. ♦ ^{31}P{^{1}H} NMR (202 MHz, $CDCl_3$, 25 °C): δ_P 29.2 (*d*, J_{FP} = 26.0 Hz, major product 70%), 28.9 (*d*, J_{FP} = 26.0 Hz, minor product 30%). ♦ ^{19}F NMR (376 MHz, $CDCl_3$, 25 °C): δ_F -149.0 (*b s,* minor product 38 %) and -148.6 (*b s,* major product

62 %). ♦ Elemental microanalysis: calc. for $C_{45}H_{45}FeBPF\cdot(heptane)_2(CHCl_3)_2$: C, 64.06%; H, 7.14%. Found: C, 63.88%; H, 7.46%. ♦ UV-vis (thf): λ_{max} = 496 nm (ε = 2660 mol^{-1} L^{-1} cm^{-1}). ♦ Crystallographic data: $C_{45}H_{45}BFFeP$, M_r = 702.48, monoclinic, *P2₁/c*, *a* = 11.43420(10) Å, *b* = 14.3860(2) Å, *c* = 22.2354(2) Å, β = 94.4213(9)°, *V* = 3646.67(7) $Å^3$, *Z* = 4, *T* = 150 K, λ = 1.54180 Å. 7519 reflections collected, 7489 independent [R(int) = 0.029] used in all calculations, with 442 refined parameters, GOF on F^2 = 0.9823. R_1 = 0.0502, wR_2 = 0.1352 for observed unique reflections [$I>2\sigma(I)$] and R_1 = 0.0586, wR_2 = 0.1412 for all unique reflections. Max. and min. residual electron densities 1.51 and -0.87 e $Å^{-3}$.

***IXg**·μ₂-F*

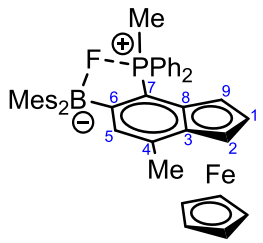

A thf solution of [**IXg**][CF_3SO_3] (250 mg, 0.374 mmol) was stirred with [^{n}Bu_4N]F·$3H_2O$ (113 mg, 0.411 mmol) for 6 h at room temperature. Volatiles were removed from the resulting red solution in vacuo and the residue extracted with diethyl ether. The volatiles were removed in vacuo and the by-product [^{n}Bu_4N][CF_3SO_3] can be filtered off from a dichloromethane and diethyl ether mixture at low temperature (-25° C). Crystals of **IXg**·F suitable for X-ray crystallography were then obtained from a heptane/thf mixture. Yield: 47 mg, 18 %.

Note: #1 and #2 used to discriminate the distinctive phenyl units of the —P(Me)Ph₂ moiety.

^{1}H NMR (400 MHz, $CDCl_3$, 25 °C): δ_H 1.67 (*b s,* 3H, *ortho*-Me of Mes), 1.90 (*b s,* 9H, *ortho*-Me of Mes), 2.16 (*s*, 6H, *para*-Me of Mes), 2.18 (*d*, $^2J_{PH}$ = 14.6 Hz, 3H, PMe), 2.41 (*s*, 3H, Me of C4), 3.77 (*s*, 5H, Cp), 3.82 (*s*, 2H, C1H and C9H), 4.82 (*s*, 1H, C2H), 6.49, 6.57 and 6.62 (each *s*, 4H, *meta*-CH of Mes), 7.12 (*s*, 1H, CH of C5H), 7.15 (*b s,* 2H, *ortho*-CH of Ph#1), 7.36 (*t*, $^3J_{HH}$ = 6.5 Hz, 2H,

meta-CH of Ph#1), 7.52 (*t*, $^3J_{HH}$ = 6.8 Hz, 1H, *para*-CH of Ph#1), 7.72 (*t*, $^3J_{HH}$ = 7.7 Hz, 1H, *para*-CH of Ph#2), 7.76 (*t*, $^3J_{HH}$ = 7.2 Hz, 2H, *meta*-CH of Ph#2), 7.81 (*d*, $^3J_{HH}$ = 7.2 Hz, 2H, *ortho*-CH of Ph#2). ♦ $^{13}C\{^1H\}$ NMR (126 MHz, $CDCl_3$, 25 °C): δ_C 18.5 (*dd*, J_{PC} = 64.4 Hz, J_{FC} = 19.2 Hz, PMe), 20.0 (*d*, J_{PC} = 1.8 Hz, Me of C4), 20.9 (*s*, *para*-Me of Mes), 24.2 and 24.9 (*b s, ortho*-Me of Mes), 59.7 (C2), 63.9 (C1), 68.9 (Cp), 69.5 (*b s,* C9), 86.3 (*d*, J_{PC} = 8.5 Hz, C3), 94.3 (*d*, J_{PC} = 18.8 Hz, C8), 108.5 (*d*, J_{PC} = 97.2 Hz, C7), 116.8 (*d*, J_{PC} = 101.5 Hz, *ipso*-quaternary C of Ph), 128.6, 128.7, 129.1 and 129.3 (*meta*-CH of Mes), 129.5 (*d*, J_{PC} = 11.2 Hz, *meta*-CH of Ph#1), 129.6 (*d*, J_{PC} = 12.5 Hz, *meta*-CH of Ph#2), 132.0 (*d*, J_{PC} = 9.2 Hz, *ortho*-CH of Ph#2), 132.5 (*d*, J_{PC} = 8.0 Hz, C5), 132.6 and 132.7 (*d*, J_{PC} = 7.6 Hz, *para*-CH of Ph), 133.0 and 133.2 (*para*-quaternary C of Mes), 133.3 (*d*, J_{PC} = 11.5 Hz, *ortho*-CH of Ph#1), 140.8 and 142.9 (*b s, ortho*-quaternary C of Mes), 143.7 (C4), 153.1 (*b s, ipso*-quaternary C of Mes), 183.8 (*b s,* C6). ♦ $^{11}B\{^1H\}$ NMR (128 MHz, $CDCl_3$, 25 °C): δ_B 6. ♦ $^{31}P\{^1H\}$ NMR (162 MHz, $CDCl_3$, 25 °C): δ_P 21.3 (J_{PF} = 22.9 Hz). ♦ ^{19}F NMR (376 MHz, $CDCl_3$, 25 °C): δ_F -145.1 (*b s*). ♦ $E_{1/2}$= -13 mV (Fe^{II}/Fe^{III}) *vs* ferrocene/ferrocenium couple with 0.1 M [$^nBu_4N$][PF_6] in acetonitrile. ♦ UV-vis (thf): λ_{max} = 531 nm (ε = 1185 mol^{-1} L^{-1} cm^{-1}). ♦ Crystallographic data: $C_{46}H_{47}BFFeP$, M_r = 716.51, monoclinic, *P2₁/n*, *a* = 17.1968(2) Å, *b* = 12.00440(10) Å, *c* = 18.0916(2) Å, β = 101.5347(12)°, *V* = 3659.35(7) $Å^3$, *Z* = 4, *T* = 150 K, λ = 1.54180 Å. 21019 reflections collected, 7549 independent [R(int) = 0.067] used in all calculations, with 497 refined parameters, GOF on F^2 = 0.9907. R_1 = 0.0550, wR_2 = 0.1422 for observed unique reflections [I>2σ(I)] and R_1 = 0.0599, wR_2 = 0.1496 for all unique reflections. Max. and min. residual electron densities 0.85 and -0.89 e $Å^{-3}$.

***VIIg**·CN*

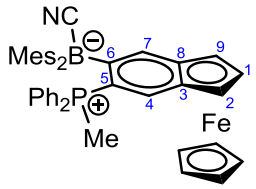

A thf solution of [**VIIg**]I (250 mg, 0.374 mmol) was stirred with [^{n}Bu$_4$N][CN]·4H$_2$O (110 mg, 0.411 mmol) for 12 h at room temperature. Volatiles were removed from the resulting red solution in vacuo and the residue extracted with diethyl ether. After removal of the solvent in vacuo, crystals suitable for X-ray crystallography were obtained from a heptane/thf mixture. Yield: 55 mg, 21 %.

^{1}H NMR (major isomer 63 %, 500 MHz, $CDCl_3$, 25 °C): δ_H 2.12 and 2.26 (*b s,* each 3H, *ortho*-Me of Mes), 2.32 (*b s,* 6H, *para*-Me of Mes), 2.34 (*b s,* 3H, PMe), 2.60 and 2.83 (*b s,* each 3H, *ortho*-Me of Mes), 3.74 (*s*, 1H, C1H), 3.88 (s, 5H, Cp), 4.39 (*s*, 1H, C9H), 4.53 (*s*, 1H, C2H), 6.78, 6.81, 6.84 and 6.90 (*s*, each 1H, *meta*-CH of Mes), 7.02 (*m*, 4H, *ortho*-CH of Ph), 7.22 (*b s*, 4H, *meta*-CH of Ph), 7.52 (*dt*, 2H, $^{3}J_{HH}$ = 10.6 Hz, $^{5}J_{HP}$ = 5.0 Hz, 2H, *para*-CH of Ph), 7.74 (*d*, $^{3}J_{HP}$ = 20.0 Hz, 1H, C4H), 8.34 (*d*, $^{4}J_{HP}$ = 4.8 Hz, 1H, C7H). ♦ ^{1}H NMR (minor isomer 37 %, 500 MHz, $CDCl_3$, 25 °C): δ_H 2.30 (*bs*, 6H, *ortho*-Me of Mes), 2.33 (*s*, 3H, PMe), 2.36 (*bs*, 6H, *para*-Me of Mes), 2.40 and 2.65 (*b s,* each 3H, *ortho*-Me of Mes), 3.77 (*s*, 1H, C1), 3.79 (*s*, 5H, Cp), 4.45 (*s*, 2H, C2H and C9H), 6.86 (*s*, 2H, *meta*-CH of Mes), 6.92 and 6.94 (*s*, each 1H, *meta*-CH of Mes), 7.02 (*m*, 4H, *ortho*-CH of Ph), 7.22 (*b s,* 4H, *meta*-CH of Ph), 7.35 (*dt*, 2H, $^{3}J_{HH}$ = 12.7 Hz, $^{5}J_{HP}$ = 7.5 Hz, 2H, *para*-CH of Ph), 7.74 (d, $^{3}J_{HP}$ = 20.8 Hz, 1H, C4H), 8.22 (*d*, $^{4}J_{HP}$ = 4.6 Hz, 1H, C7). ♦ ^{13}C{^{1}H} NMR (major isomer 63 %, 126 MHz, $CDCl_3$, 25 °C): δ_C 14.1 (*d*, J_{CP} = 55.3 Hz, PMe), 21.1 (*para*-Me of Mes), 25.8, 26.0, 26.9 and 27.6 (*ortho*-Me of Mes), 62.4 (C9), 63.7 (C2), 68.1 (Cp), 72.8 (C1), 83.4 (*d*, J_{CP} = 18.2 Hz, C8), 91.8 (*d*, J_{CP} = 27.6 Hz, C3), 119.7 (*d*, J_{CP} = 83.1 Hz, C5), 124.0 (*d*, J_{CP} = 87.3 Hz, *ipso*-quaternary C of Ph), 129.3 (*d*, J_{CP} = 12.8 Hz, *ortho*-CH of Ph), 129.6, 129.7, 130.0 and 130.1 (*meta*-CH of Mes), 132.3 (*d*, J_{CP} = 9.1 Hz, *meta*-CH of Ph), 133.5 (*para*-CH of Ph), 133.7 (*para*-quaternary C of Mes), 139.4 (*d*, J_{CP} = 16.7 Hz, C7), 142.2, 142.7, 143.7 and 144.9 (*ortho*-quaternary C of Mes), 146.6 (*d*, J_{CP} = 15.3 Hz, C4), 149.1 (*b s, ipso*-quaternary C of Mes), 151.8 (*b s,* CN bound to B), 153.3 (*b s,* C6). ♦ ^{13}C{^{1}H} NMR (minor isomer 27 %, 126 MHz, $CDCl_3$, 25 °C): δ_C 14.2 (*d*, J_{CP} = 55.4 Hz, PMe), 21.2 (*para*-Me of Mes), 25.6, 26.2, 26.5 and 29.3

(*ortho*-Me of Mes), 62.4 (C9), 63.3 (C2), 67.5 (Cp), 72.8 (C1), 83.4 (*d*, J_{CP} = 18.0 Hz, C8), 91.84 (*d*, J_{CP} = 27.6 Hz, C3), 119.4 (*d*, J_{CP} = 83.1 Hz, C5), 123.7 (*d*, J_{CP} = 88.2 Hz, *ipso*-quaternary C of Ph), 129.5 and 129.5 (*meta*-CH of Mes), 130.5 (*d*, J_{CP} = 13.8 Hz, *ortho*-CH of Ph), 130.7 and 130.7 (*meta*-CH of Mes), 132.1 (*d*, J_{CP} = 9.0 Hz, *meta*-CH of Ph), 133.3 (*para*-CH of Ph), 133.5 (*para*-quaternary C of Mes), 138.2 (*d*, J_{CP} = 16.6 Hz, C7), 141.9, 143.1, 143.2 and 144.9 (*ortho*-quaternary C of Mes), 146.1 (*d*, J_{CP} = 15.1 Hz, C4), 149.1 (*b s, ipso*-quaternary C of Mes), 151.8 (*b s,* CN bound to B), 153.3 (*b s,* C6). ♦ $^{11}B\{^1H\}$ NMR (160 MHz, $CDCl_3$, 25 °C): δ_B -13. ♦ $^{31}P\{^1H\}$ NMR (202 MHz, $CDCl_3$, 25 °C): δ_P 29.1 and 30.1. ♦ UV-vis (thf): λ_{max} = 491 nm (ε = 2941 mol^{-1} L^{-1} cm^{-1}). ♦ Crystallographic data: $C_{47}H_{47}BCl_2FeNP$, M_r = 794.43, triclinic, *P-1*, *a* = 11.1866(3) Å, *b* = 11.5719(2) Å, *c* = 18.3926(4) Å, α = 81.8709(18)°, β = 76.516(2)°, γ = 73.129(2)°, *V* = 2208.68(9) $Å^3$, *Z* = 2, *T* = 150 K, λ = 1.54180 Å. 9253 reflections collected, 9253 independent [R(int) = 0.0380] used in all calculations, with 488 refined parameters, GOF on F^2 = 0.9990. R_1 = 0.0400, wR_2 = 0.1070 for observed unique reflections [I>2σ(I)] and R_1 = 0.0417, wR_2 = 0.1085 for all unique reflections. Max. and min. residual electron densities 0.53 and -0.56 e $Å^{-3}$.

***IXg**·CN*

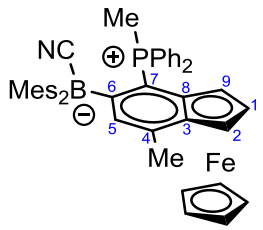

A thf solution of [**IXg**][CF_3SO_3] (250 mg, 0.732 mmol) was stirred with [^{n}Bu$_4$N]F·3H$_2$O (243 mg, 0.878 mmol) for 6 h at room temperature. Volatiles were removed from the resulting red solution in vacuo and the residue extracted with diethyl ether. After removal of the solvent in vacuo, crystals suitable for X-ray crystallography were obtained from a heptane/thf mixture. Yield: 154 mg, 29 %.

^{1}H NMR (500 MHz, $CDCl_3$, 25 °C): δ_H 1.71, 1.87, 1.93, 2.08, 2.09 and 2.17 (*b s,* each 3H, Me of Mes), 2.22 (*d*, $^{2}J_{HP}$ =11.2 Hz, 3H, PMe), 2.30 (*s*, 3H, Me of C4), 3.74 (b *s*, 1H, C1H), 3.77 (*s*, 5H, Cp), 3.92 (*s*, 1H, C9H), 4.72 (*s*, 1H, C2H), 6.62, 6.66, 6.70 and 6.73 (*b s,* each 1H, *meta*-CH of Mes), 7.20 (s, 1H, C5H), 7.23 (*b s,* 2H, *ortho*-CH of Ph), 7.36 (*b t*, 2H, *meta*-CH of Ph), 7.43 (*t*, $^{3}J_{HH}$ = 8.1 Hz, 1H, *para*-CH of Ph), 7.63 (*td*, $^{3}J_{HH}$ = 7.9 Hz, $^{3}J_{HH}$ = 1.8 Hz, 1H, *para*-CH of Ph) 7.78 (*m*, 4H, *ortho* and *meta*-CH of Ph). ♦ ^{13}C{^{1}H} NMR (126 MHz, $CDCl_3$, 25 °C): δ_C 18.6 (*d*, J_{PC} = 55.0 Hz, PMe), 19.7 (Me), 20.6, 20.8, 23.3, 25.1, 26.6, and 27.5 (Me of Mes), 58.5 (C2), 64.7 (C9), 68.5 (Cp), 69.4 (C1), 85.5 (C3), 95.7 (C8), 109.2 (C7), 119.3 and 121.8 (*ipso*-quaternary C of Ph), 126.9 and 128.3 (*meta*-CH of Mes), 128.5 (*meta*-CH of Ph), 129.2 (*meta*-CH of Mes), 129.4 (*ortho*-CH of Ph), 130.8 (*d*, J_{PC} = 9.5 Hz, *para*-CH of Ph), 132.2 (CH of Ph), 133.6 (*para*-CH of Ph), 135.2 (*d*, J_{PC} = 20.0 Hz, C5), 137.7 and 138.8 (*para*-quaternary C of Mes), 141.7 and 142.5 (*ortho*-quaternary C of Mes), 144.3 (C4), 145.9 and 150.0 (b s, *ipso*-quaternary C of Mes), 179.4 (C6), C of the cyanide bound to the boron atom was not found. ♦ ^{11}B{^{1}H} NMR (128 MHz, $CDCl_3$, 25 °C): δ_B -13. ♦ ^{31}P{^{1}H} NMR (162 MHz, $CDCl_3$, 25 °C): δ_P 21.5. ♦ Elemental microanalysis: calc. for $C_{47}H_{47}BFeNP\cdot$(thf): C, 76.99 %; H, 6.97 %. Found: C, 77.17 %; H, 6.94 %. ♦ UV-vis (thf): λ_{max} = 532 nm (ε = 1650 mol^{-1} L^{-1} cm^{-1}). ♦ Crystallographic data: $C_{47}H_{47}BFeNP$, M_r = 723.53, monoclinic, *C2/c, a* = 18.4347(2) Å, *b* = 12.65370(10) Å, *c* = 36.2152(3) Å, β = 97.0569(9)°, *V* = 8383.82(13) Å^3, *Z* = 8, *T* = 150 K, λ = 1.54180 Å. 8735 reflections collected, 8735 independent [R(int) = 0.053] used in all calculations, with 460 refined parameters, GOF on F^2 = 1.0162. R_1 = 0.0427, wR_2 = 0.1061 for observed unique reflections [I>2σ(I)] and R_1 = 0.0466, wR_2 = 0.1086 for all unique reflections. Max. and min. residual electron densities 0.39 and -0.60 e Å^{-3}.

4.4. Results and discussion

4.4.1 Syntheses from dichloro-indene precursors

Several synthetic routes were considered towards the 5,6 and 6,7 isomers of (dichloroindenyl)cyclopentadienyliron(II), but the one shown in Figure 4.10 was proven to be the most efficient. The reaction of methyl acrylate and the activated dichloro phenyl diazonium salt, followed by reduction and deprotection afforded the desired propionic acid precursors. Following the same onward pathway as outlined for the mono-functional indenyl systems described in chapter 3, compounds **Vd** and **VId** were then isolated as dark purple crystals and fully characterized, including structurally by single X-ray crystallography (Figure 4.11).

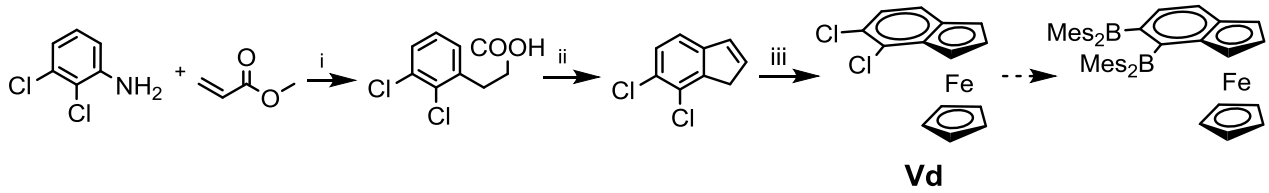

Vd

Figure 4.10: Synthesis of **Vd**: HBr, $NaNO_2$, CuBr, Zn, 10% *aq.* NaOH; (ii) $SOCl_2$ reflux, $AlCl_3$, then $NaBH_4$ and *p*-TsOH; (iii) KH and $[FeCp(\eta^6\text{-}C_{10}H_8)]PF_6$].

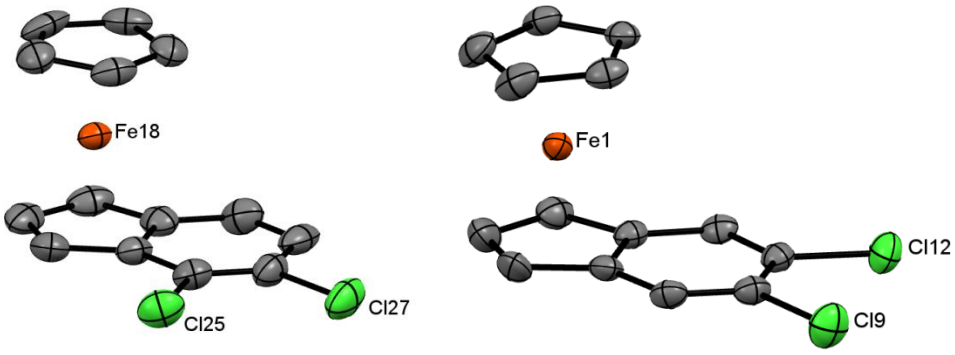

Figure 4.11: Molecular structures of **Vd** and **VId**. Thermal ellipsoids set at the 50% probability level and hydrogen atoms omitted for clarity (green: chloride; black: carbon; orange: iron).

From this point the intention was to introduce the desired dimesitylboryl functions either in a one-pot synthesis or by sequential lithiation/borane quench. Several protocols

were attempted at different temperatures and using either ^{n}BuLi and ^{t}BuLi, for the lithium-halogen exchange. However, these lithiation processes met with little success using either **Vd** and **VId**, and instead of isolating the bis-borane systems, a series of decomposition products was isolated (Figure 4.12 and Table 4.1).

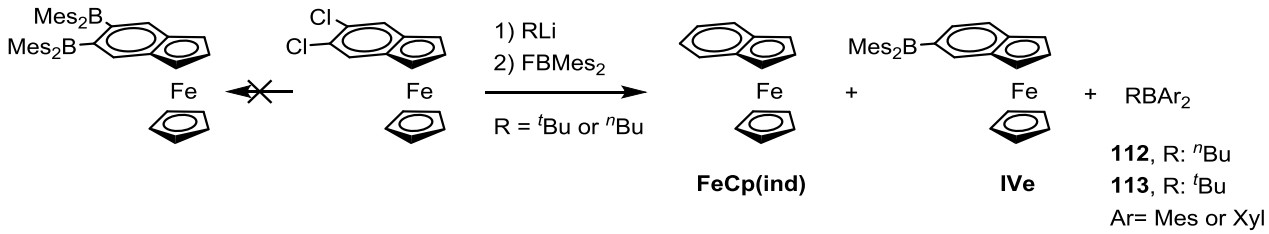

Figure 4.12: Examples of the reaction pathways evident from the attempted lithiation of **VId** (entries 1-7, Table 4.1).

Entry	RLi	Equiv. of RLi	Temperature of $FBMes_2$ addition	Identified products
1	^{n}BuLi	2.1	-78° C	**IVe**, FeCp(ind), **112**
2	^{n}BuLi	2.1	RT	FeCp(ind), **112**
3	^{n}BuLi	1.1	-78° C	**IVe**, FeCp(ind), $FBMes_2$
4	^{n}BuLi	1.1	-120° C	**IVe**, FeCp(ind), $FBMes_2$
5	^{t}BuLi	2.1	-78° C	**IVe**, FeCp(ind), $FBMes_2$, **113**
6	^{t}BuLi	4.2	-78° C	**IVe**, FeCp(ind), $FBMes_2$, **113**
7	^{t}BuLi	4.2	@RT	FeCp(ind), **113**

Table 4.1: Reaction conditions tested for lithium/halogen exchange with **VId** in ether or thf(5 equivalents of $FBMes_2$ used in each case).

Intriguingly, one of the reaction products, compound **112**, features an ^{11}B NMR shift of δ_B 85 ppm, and if exposed to a source of fluoride a sharp peak at δ_B 2 ppm was observed to grow in. **112** was subsequently crystallized as the fluoride adduct shown in Figure 4.13. The molecular structure of [K(18-crown-6)] [$Xyl_2B^{n}Bu{\cdot}F$] confirms that $Xyl_2B^{n}Bu$ is formed in the reaction mixture, presumably as a result of incomplete lithiation of **VId** by ^{n}BuLi prior to addition of the Xyl_2BF electrophile. The same reactivity was observed with ^{t}BuLi leading to **113** with a ^{11}B NMR shift at δ_B 89 ppm as reported in the literature.[14]

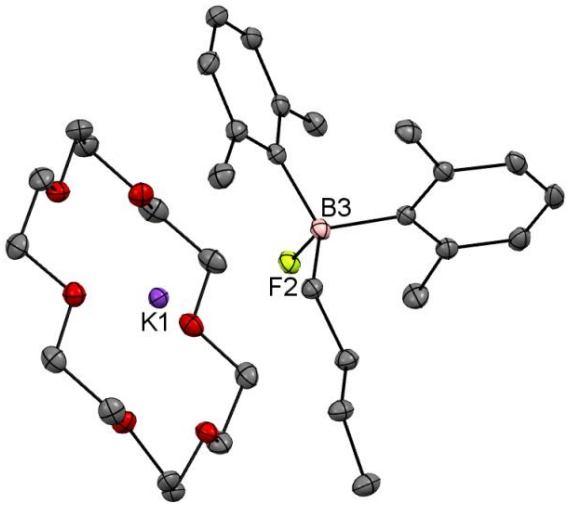

Figure 4.13: Molecular structure of [K(18-crown-6)][**112**·F)]. Thermal ellipsoids set at the 50% probability level and hydrogen atoms omitted for clarity (light pink: boron; black: carbon; yellow: fluoride; purple: potassium; red: oxygen).

For a plausible explanation for the formation of the mono-functional borane **IVe** and FeCp(ind), a parallel analogy can be drawn with the chemistry of *o*-dilithiobenzene. First reported in the pioneering work of Wittig, it was isolated as a deep-red solid from the reduction of the *ortho*-phenylene mercury trimer with lithium metal.[15] Several authors have attempted to isolate *o*-dilithiobenzene *via* the lithiation of the parent 1,2-*bis*-halogen-benzene, although the *β*-elimination of lithium halide leading to the formation of benzyne is usually a competitive reaction pathway.[16] For instance, Bettinger and Filthaus synthesised compound **114** using 1,2-dibromobenzene, ^{t}BuLi and TMSOTf (Figure 4.14).[17] The authors demonstrated that the formation of **114** is possible only because of two key factors: (*i*) the temperature is kept below -90° C to reduce the propensity of the 2-bromophenyllithium intermediate to undergo *β*-elimination and (*ii*) the fortuitously non-labile coexistence of TMSOTf and ^{t}BuLi. Under such conditions they established that the second bromine at the *ortho* position of the carbanion is kinetically inert to lithium halogen exchange, thus the formation of the dilithiobenzene is less favoured by this route.

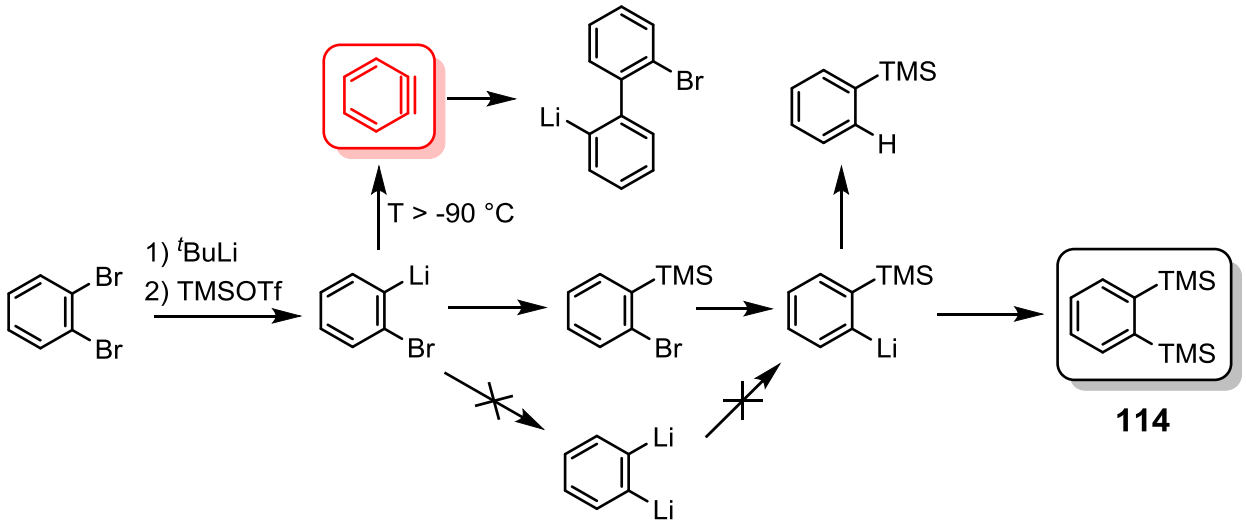

Figure 4.14: Proposed reaction pathway to synthesise **114**.[17]

On this basis it is conceivable that the formation of (indenyl)FeCp and possibly its mono-borylated counterpart is due to the formation of a highly reactive benzyne species, followed by decomposition (*e.g.* protonation from solvent or ^{t}BuCl). Even at low temperatures (*i.e.* -120° C) this intermediate is apparently not stable, presumably reflecting the high lattice enthalpy of LiCl; thus the use of a heavier halogen (*i.e.* bromine or iodine) might be synthetically preferable. Finally, in addition to behaving as a weak electrophile, $FBMes_2$ is also not stable in presence of an organolithium base (*cf.* the formation of $Xyl_2B^{n}Bu$), and thus the pathway for double lithium halogen exchange observed by Bettinger and Filthaus is not likely to be possible here (Figure 4.15).[17]

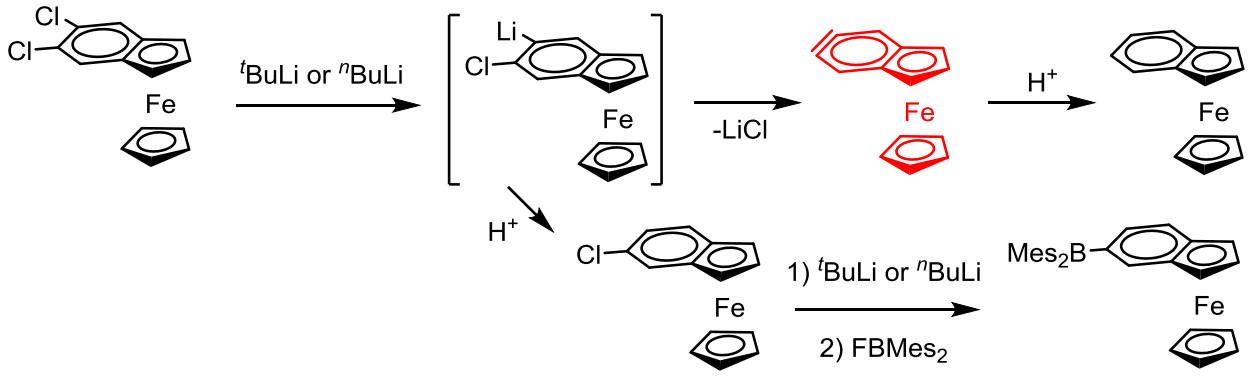

Figure 4.15: Proposed reaction pathways occuring on treatment of **VId** with ^{t}Buli or ^{n}BuLi.

4.4.2 Synthesis from dibromo-indene precursors

Since dichloroindenyl precursors were found to be unsuitable for lithium-halogen exchange, other borylation approaches were considered, and with this in mind, intermediates **Vd** and **VId** featuring pendant bromines (rather than chlorines) were isolated (Figure 4.16).

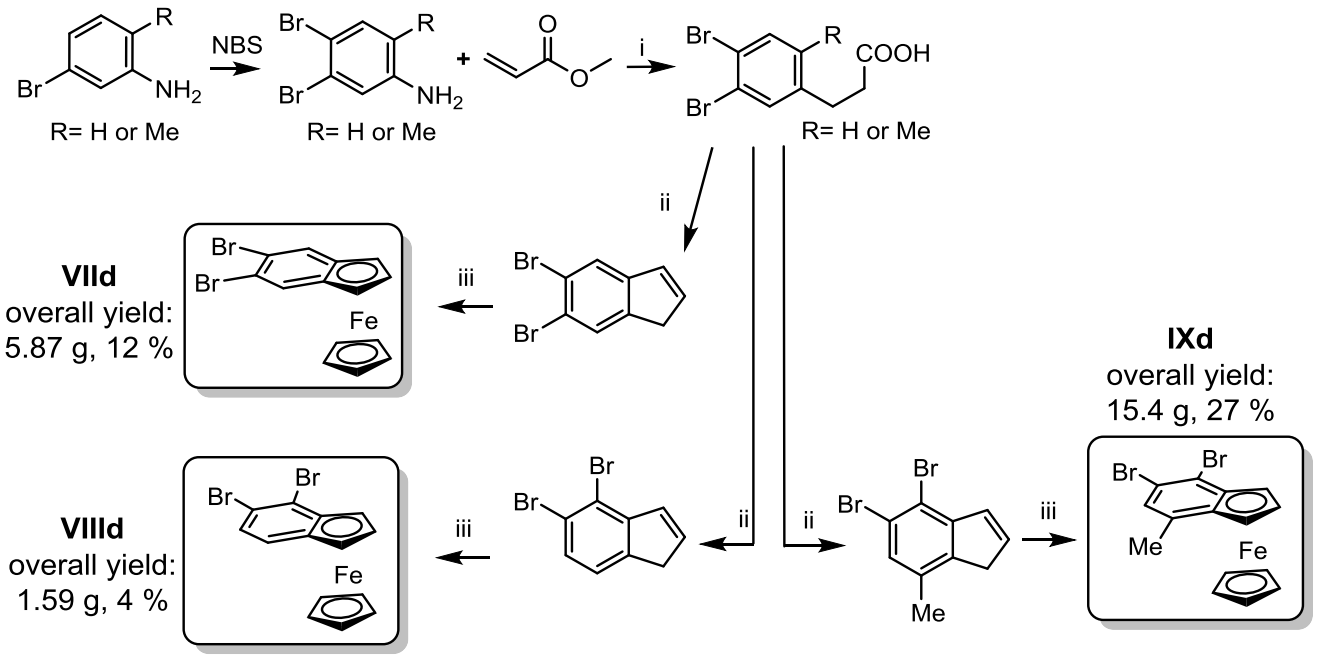

Figure 4.16: Syntheses of the dibromoindenyl series **VIId** – **IXd**: (*i*) HBr, $NaNO_2$, CuBr, Zn, 10% *aq.* NaOH; (*ii*) $SOCl_2$ reflux, $AlCl_3$, then $NaBH_4$ and *p*-TsOH; (*iii*) KH and $[FeCp(\eta^6\text{-}C_{10}H_8)]PF_6$].

The syntheses of **VIId**, **VIIId** and **IXd** are similar to those outlined in section 4.4.1, with an additional step being employed for the introduction of the second bromine onto the aniline core utilising N-bromosuccinimide (NBS). The only contention here was the lack of selectivity during the cyclisation process using aluminium chloride. While compound **VIIa** could be isolated as crystals from the mixture of isomers, this proved not to be the case for **VIIIa**. Thus the introduction of a blocking methyl substituent *ortho* to the propionic acid was investigated, resulting in an increased overall yield of compound **IXd** compared to **VIIId** (27% and 4% respectively). The three dibromo-indenyl precursors were isolated as dark purple crystalline materials and fully characterised spectroscopically (Figure 4.17).

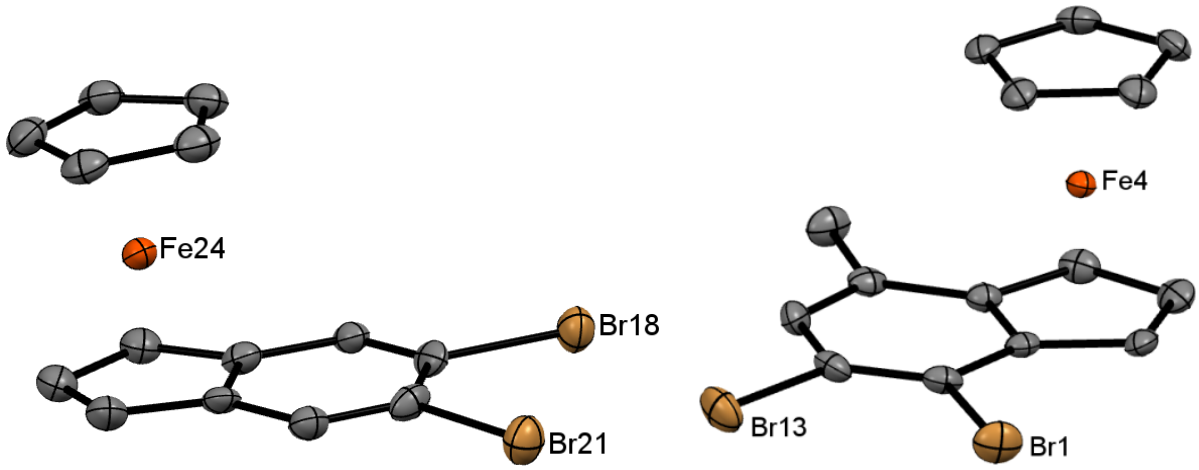

Figure 4.17: Molecular structures of **VIId** and **IXd**. Thermal ellipsoids set at the 50% probability level; hydrogen atoms are omitted for clarity (auburn: bromine; black: carbon; orange: iron).

Hypothesizing that the formation of an *o*-dilithioindenyl unit is improbable (*c.f.* Figure 4.14), introduction of the boryl functions was attempted in a stepwise fashion. The treatment of **VIId** with one equivalent of ^{n}BuLi at -120° C followed by addition of fluorodimesityl borane yields the desired (5-dimesitylboryl-6-bromo-indenyl)cyclopentadienyliron(II) (**VIIh**, Figure 4.18). The crude product can be purified by air-free column chromatography and is obtained as a red solid in low yield (19 %). Because $FBMes_2$ is a bulky and relatively weak electrophile a major portion of the bromo-lithium indenyl intermediate is not quenched when the temperature is raised, thus leading to the formation of the mono-bromoindenyl species by protonation of the lithium intermediate.

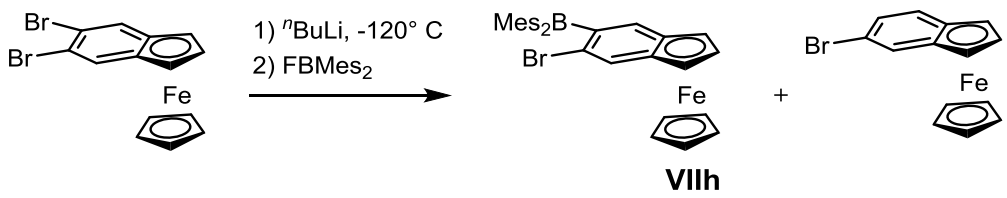

VIIh

Figure 4.18: Formation of the receptor **VIIh**.

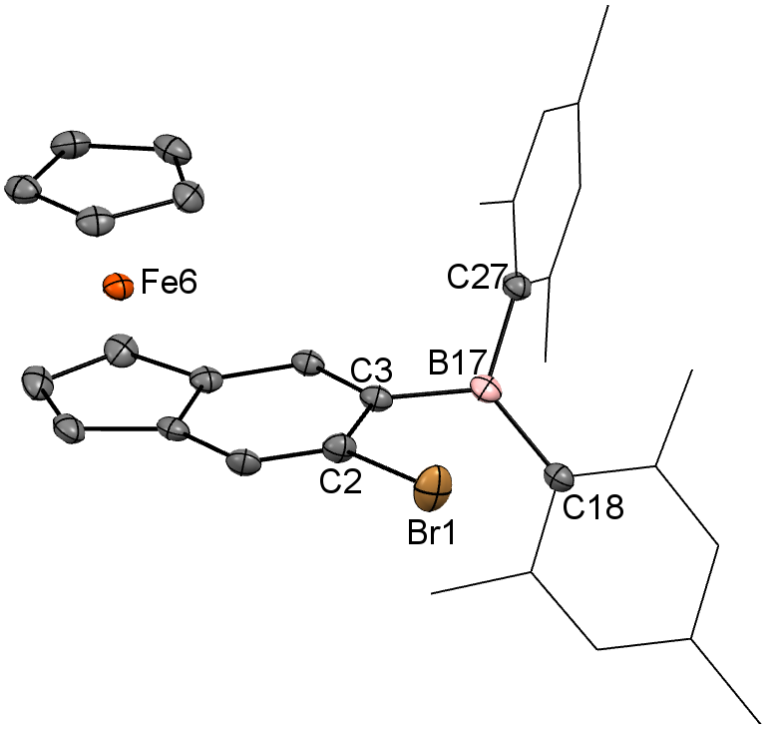

Figure 4.19: Molecular structure of (R_p)-**VIIh** (isolated as racemic mixtures). Thermal ellipsoids set at the 50% probability level; mesityl groups shown in wireframe format and hydrogen atoms omitted for clarity (auburn: bromine; black: carbon; orange: iron, light pink: boron). Selected bond lengths [Å] and angles [°]: B17—C18 1.571(3), B17—C27 1.581(3), B17—C3 1.566(3), C3—B17—C18 122.23(18), C3—B17—C27 115.81(18), C18—B17—C27 121.84(18), C2—C3—B17 126.73(19).

The formation of **VIIh** can be confirmed by ^{11}B NMR spectroscopy with a shift typical of a tris-arylborane being observed (δ_B = 77 ppm) and the presence of the mesityl signals also being confirmed in the ^{1}H NMR spectrum. In addition, the crystal structure of **VIIh** was obtained from a small red block and is depicted in Figure 4.19. A number of structural features imply that the steric hindrance around the boron centre is greater than that found in related compounds such as 1,2-Fc(BMes$_2$)Br and (7-dimesitylboryl-indenyl)cyclopentadienyl-iron(II) (**IIIe**). Firstly the mesityl rings in **VIIh** are almost perpendicular to the indenyl plane (**VIIh**, 88.7° and 87.4°; **IIIe**, 66.0° and 66.3°; 1,2-Fc(BMes$_2$)Br, 51.2° and 81.5°) and secondly the C2—C3—B17 angle of 126.7(2)° deviates from the ideal 120° to accommodate the large BMes$_2$ unit *ortho* to the bromine atom.

The implications of this degree of steric hindrance became increasingly apparent in the next synthetic step. A range of different bases and reaction conditions were tested for the incorporation of the second —$BMes_2$ unit, but unfortunately these endeavours were not successful. The high steric hindrance of the mesityl rings presumably prevents the formation of the desired bis-boranes, and also might explain the absence of *any* 1,2-bis($BMes_2$) benzene derivatives in the literature. Consequently the incorporation of an alternative proximal Lewis acid was targeted. Given that the ferrocenyl systems [1,2-Fc(PPh_2Me)($BMes_2$)]$^+$ (**115**) and [1,1'-Fc(PPh_2Me)($BMes_2$)]$^+$ (**116**), have both previously been synthesized in the Aldridge group, the incorporation of a comparable phosphonium moiety into the indenyl skeleton was investigated. This approach has the advantage that Ph_2PCl, for example, is known to be a much more labile electrophile towards aryllithium species than Mes_2BF.

The synthetic route highlighted in Figure 4.20 is comparable to those reported in the literature for compounds **115** and **116**.[18] The reactions of Ph_2PCl with the lithiates generated *in situ* from ^{n}BuLi and either **VIId** or **IXd** at -120° C, are shown to be efficient and practical routes to **VIIe** and **IXe** (in yields of 83% and 37 %, respectively, without the need for column chromatography). The isolation of **VIIe** and **IXe** (rather than their use *in situ*) renders the subsequent incorporation of the borane function easier, since lithiation is now not limited to very low temperature conditions. Moreover, the resulting crude products **VIIf** and **IXf** can be purified merely by washing/extraction procedures rather than necessitating chromatography. In the final step, [**VIIg**]$^+$ and [**IXg**]$^+$ can be synthesized *via* a simple methylation process; introduction of a large excess of methyl iodide or methyl trifluoromethansulfonate generates the final products [**VIIg**]I and [**IXg**][CF_3SO_3] in almost quantitative yields.

At each step intermediates were fully characterised by multinuclear NMR spectroscopy and X-ray crystallography. The formation of indenylphosphine intermediates **VIIe** and **IXe** is evident by the appearance of a signal in the respective ^{31}P NMR spectra at δ_P -4.14 and

-0.17 ppm (*c.f.* PPh_3, δ_P -6.0 ppm) and the molecular structure of both compounds can be confirmed crystallographically (Figure 4.21). Interestingly, **IXe** is formed selectively with the —PPh_2 group incorporated at the C7 position of the indenyl ring. This selectivity is implied by the results obtained from a single crystal, but can be extended to the bulk since the *in situ* ^1H NMR spectrum exhibits only one set of signals. In the case of **VIIe**, a racemic mixture of R_p and S_p is generated which crystallizes as such.

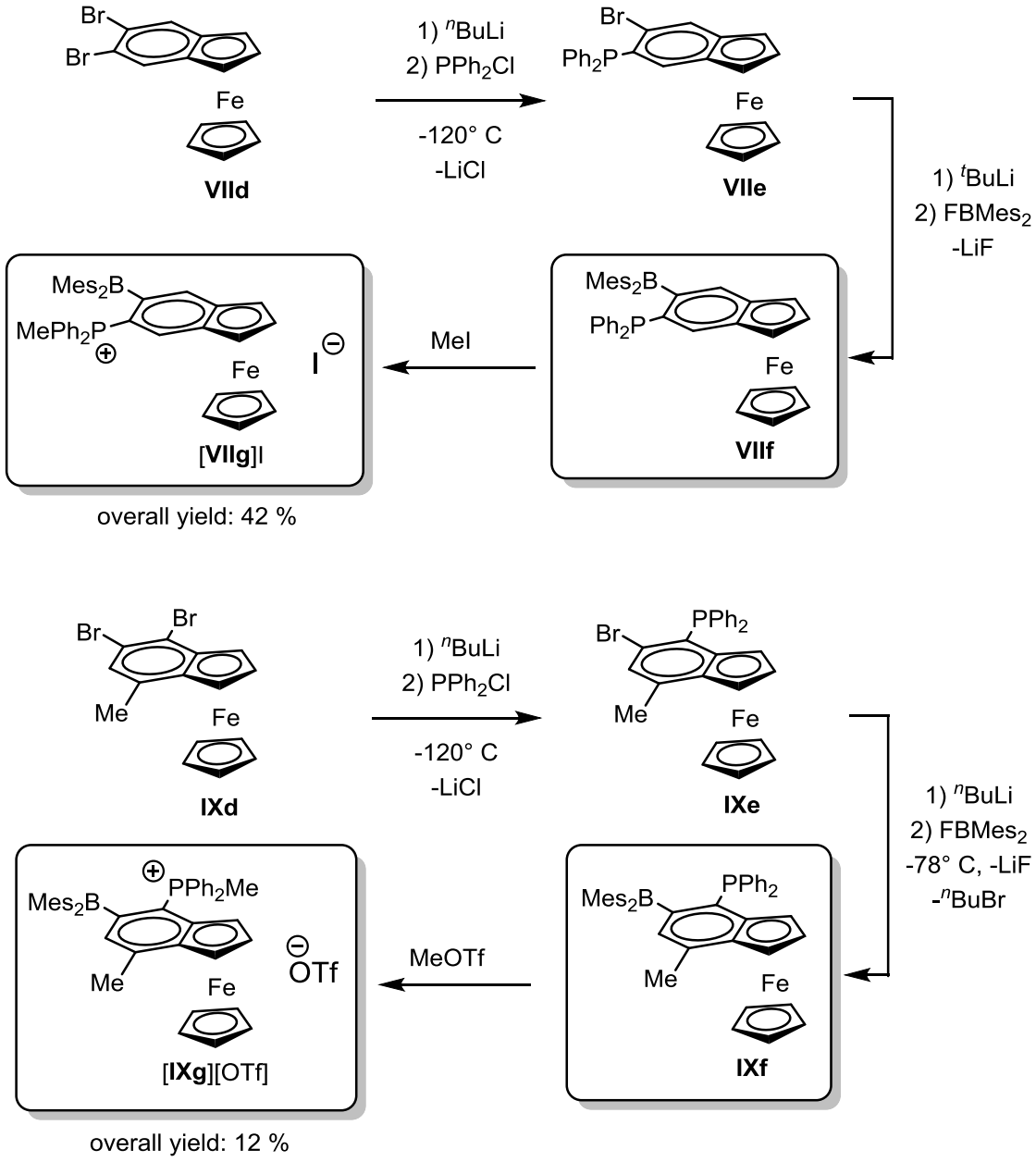

Figure 4.20: Synthetic routes to [**VIIg**]I and [**IXg**][CF_3SO_3].

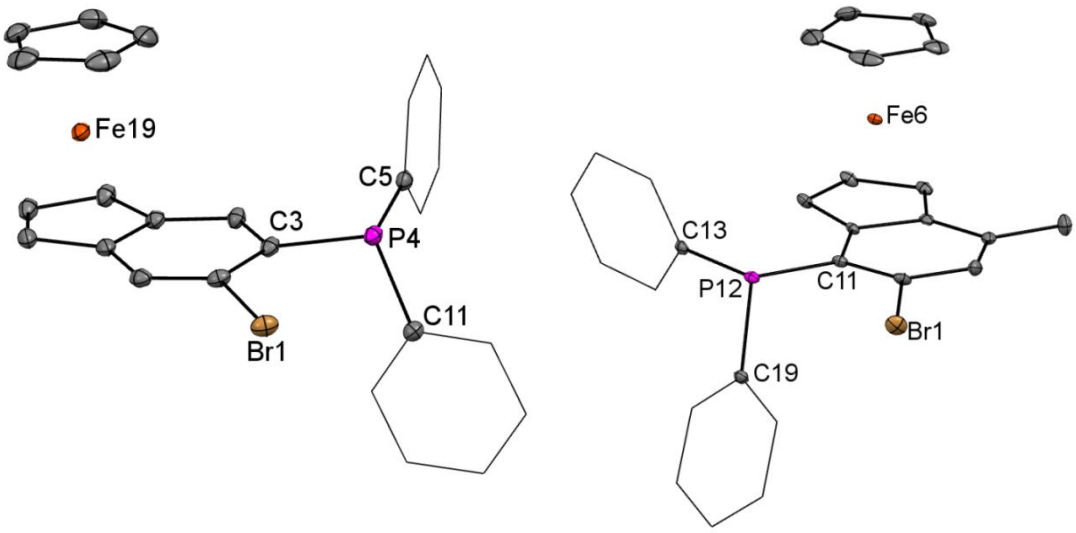

Figure 4.21: Molecular structure of (R_p)-**VIIe** and (S_p)-**IXe** (isolated as a racemic mixture). Thermal ellipsoids set at the 50% probability level; phenyl groups shown in wireframe; hydrogen atoms are omitted for clarity (auburn: bromine; black: carbon; orange: iron; purple: phosphine). Selected bond lengths [Å] and angles [°]:(*pR*)-**VIIe**; C3—P4 1.8386(18), C3—P4—C5 100.28(8), C3—P4—C11 103.28(8), C5—P4—C11 100.85(8). (*pS*)-**IXe**; C11—P12 1.8411(18), C11—P12—C13 105.87(8), C11—P12—C19 102.88(8), C13—P12—C19 100.54(8).

After lithiation/Mes_2BF quenching, the broad signals at δ_B 74 and 76 ppm in the respective ^{11}B NMR spectra are consistent with the presence of a triaryl borane, confirming the formation of **VIIf** and **IXf** respectively. The incorporation of the Lewis acidic boryl function in place of the bromine perturbs slightly the ^{31}P NMR signals, leading to a slight upfield shift (*c.f.* **IXe**, δ_P -0.17 and **IXf**, δ_P -5.81 ppm). Interestingly, in solution compound **VIIf** features two distinct peaks in the ^{31}P NMR spectrum at room temperature (δ_P -6.5 and -9.5 ppm), which coalesce at high temperatures (*ca.* +80° C) at δ_P -7.7 ppm (Figure 4.22).

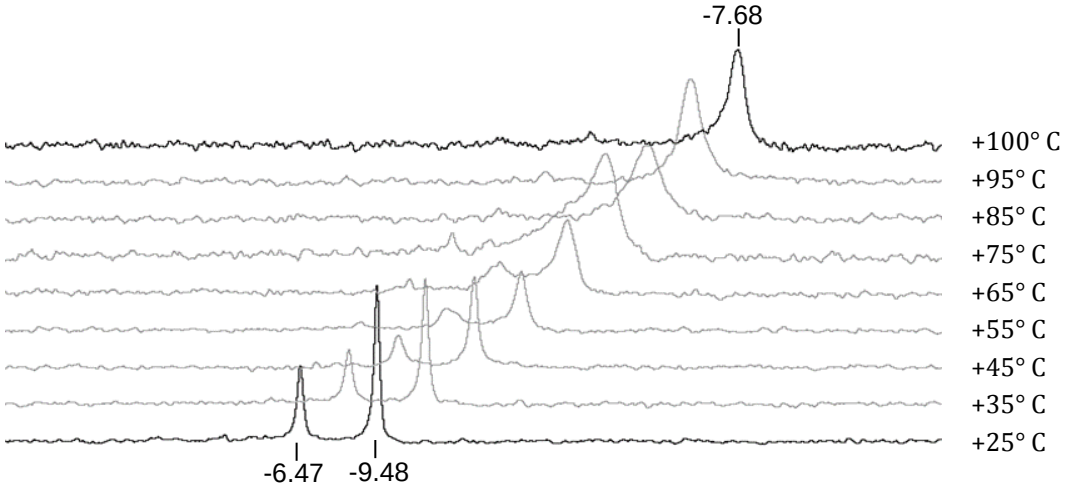

Figure 4.22: $^{31}P\{^1H\}$ NMR spectrum of **VIIf** in dmso-d_6 with increasing temperature from bottom to top, shifts are given in ppm.

The two bulky subunits, —PPh_2 and —$BMes_2$, would incur a significant energetic penalty by being located in the same plane, and a non-negligible torsion angle is thus introduced along the B—C—C—P chain. It is therefore proposed that there are two thermally interchangeable environments observable by ^{31}P NMR spectroscopy at room temperature. Morgan and co-worker observed a "windshield wiper" motion for the 1,2-dimesitylboryl-ferrocene system (**106**, *c.f.* chapter 3 section 3.1),[19] and a similar process could be envisaged for **VIIf** (Figure 4.23). **106** has a relatively low activation barrier ($\Delta G^{\ddagger}$ = 48 kJ mol^{-1}) and requires temperatures below -60° C to 'freeze out' the diastereomeric rotamers; **VIIf** on the other hand requires warming to >85° C to observe coalescence, presumably to overcome larger steric hindrance. For compound **IXf**, the single signal observed in the ^{31}P NMR spectrum could be attributed either to a higher or lower steric hindrance, *i.e.* either a locked structure or rapidly exchanging rotamers. The lack of temperature dependence would tend to imply the former, however, and this assertion appears to be corroborated by the results of the X-ray crystallographic study.

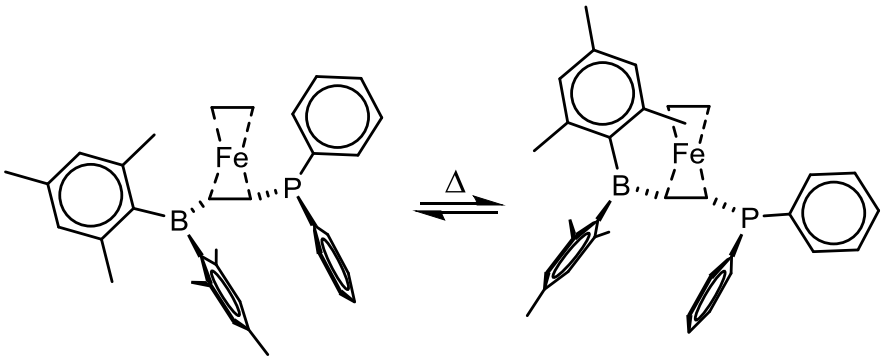

Figure 4.23: Thermal interconversion of the enantiomeric conformations of **VIIf** by synchronized motion of the —$BMes_2$ and —PPh_2 units.

The structural characterisation of both boryl phosphines **VIIf** and **IXf** further confirms the increase steric hindrance upon assimilation of the —$BMes_2$ unit (Figure 4.25 and Figure 4.26). For both systems, a propeller-like geometry is in evidence for the borane unit, although

the proximity of the FeCp moiety seems to interfere (Figure 4.24). In **VIIf**, several carbon atoms of either the mesityl or the phenyl ring lie less than 4 Å away from the cyclopentadienyl ring (C(*Ph*)—C(*Cp*) 3.781 Å and C(*Mes*) —C(*Cp*) 3.974 Å). The intramolecular contacts are even closer in the case of **IXf**: one phenyl unit comes as close as 3.583 Å from the cyclopentadienyl ligand and 4.027 Å for one of the mesityl units (Figure 4.24). Furthermore the mesityl rings in **IXf** lie almost perpendicular to the indenyl ligand (83.1° and 89.2°) and the angle between the least squares planes of the cyclopentadienyl and indenyl ligands deviates by *ca.* 5.6° from co-planarity (Figure 4.26). Moreover, the P—C—C—B torsion angles observed for **VIIf** and **IXf** are consistent with the differing observations made by ^{31}P NMR spectroscopy; the relatively high torsion angle in **VIIf** (22.5°) presumably underpins the factors giving rise to two signals in ^{31}P NMR spectrum, while in **IXf** the angle is too small (4.01°) to generate two distinguishable magnetic environments. As a result of the large steric hindrance in **IXf**, the —PPh_2 unit has to stay in the indenyl plane and hence there is only one conformation possible for **IXf**.

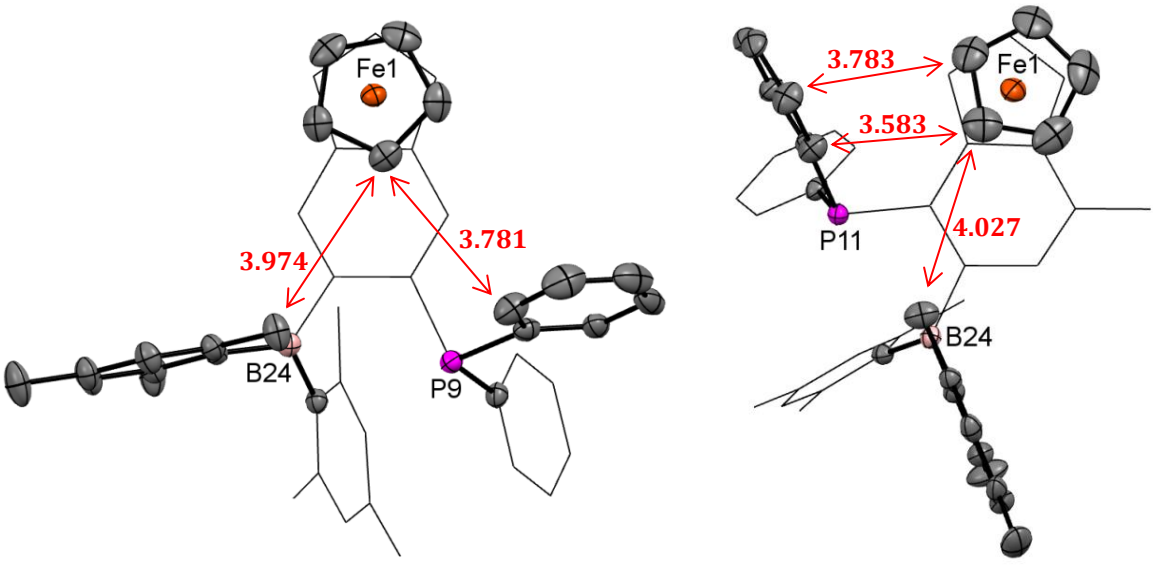

Figure 4.24: Close intramolecular interactions between the —PPh_2 or —$BMes_2$ units and the cyclopentadienyl rings observed for **VIIf** (left) and **IXf** (right) in the solid state (distances between carbons given in Å).

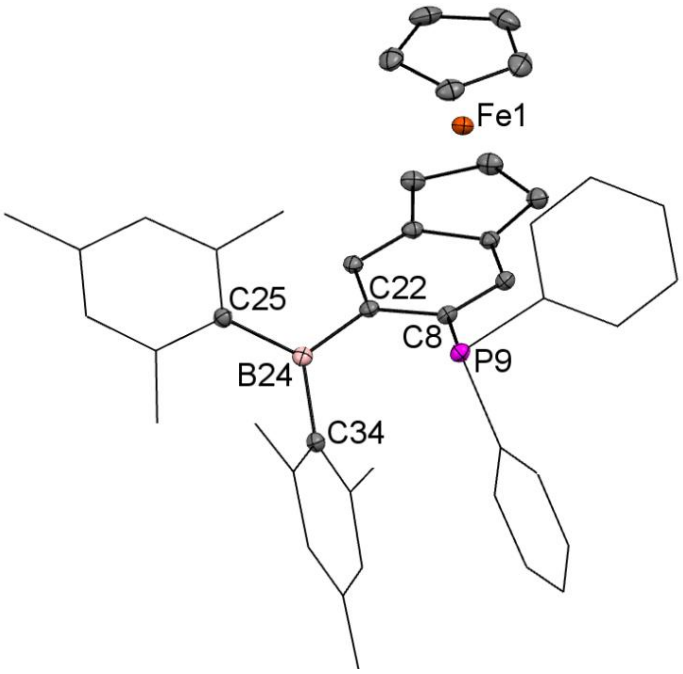

Figure 4.25: Molecular structure of (R_p)-**VIIf** (isolated as a racemic mixture). Thermal ellipsoids set at the 50% probability level; mesityl and phenyl groups shown in wireframe format and hydrogen atoms omitted for clarity (black: carbon; orange: iron; purple: phosphine; light pink: boron). Selected bond lengths [Å] and angles [°]: B24—C25 1.577(2), B24—C34 1.571(2), C22—B24 1.569(2), C22—B24—C25 118.79(13), C22—B24—C34 119.25(13), C25—B24—C34 121.91(13), C8—C22—B24 123.22(13), P9—C8—C22 116.08(11).

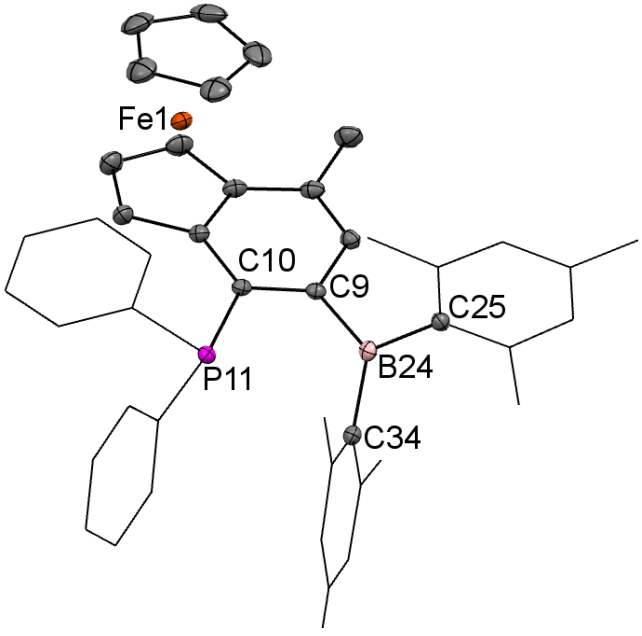

Figure 4.26: Molecular structure of (R_p)-**IXf** (isolated as a racemic mixture). Thermal ellipsoids set at the 50% probability level; mesityl and phenyl groups shown in wireframe; hydrogen atoms are omitted for clarity (light pink: boron; black: carbon; orange: iron; purple: phosphine). Selected bond lengths [Å] and angles [°]: C9—B24 1.584(3), B24—C25 1.575(3), B24—C34 1.578(3), C9—B24—C25 116.09(15), C9—B24—C34 121.27(15), C25—B24—C34 122.26(15), C10—C9—B24 124.21(15), C9—C10—P11 114.82(13).

The target cations **VIIg**$^+$ and **IXg**$^+$ were obtained *via* methylation of the phosphine function in each case, a reaction that can be monitored by multinuclear NMR spectroscopy. The ^{31}P signals in **VIIf** are shifted downfield to δ_P 23.4 and 24.4 ppm for **VIIg**$^+$, in good agreement with other examples of methylated phosphonium species (*e.g.* ***o*-108**$^+$: δ_P 23.9 ppm);[10b] on the other hand **IXg**$^+$ gives rise to only a single signal in the ^{31}P NMR spectrum at δ_P 17.5 ppm. The products **VIIg**$^+$ and **IXg**$^+$ are also discernible in positive ion ESI-MS as a peak envelope matching the expected isotopic profile and with the correct accurate mass.

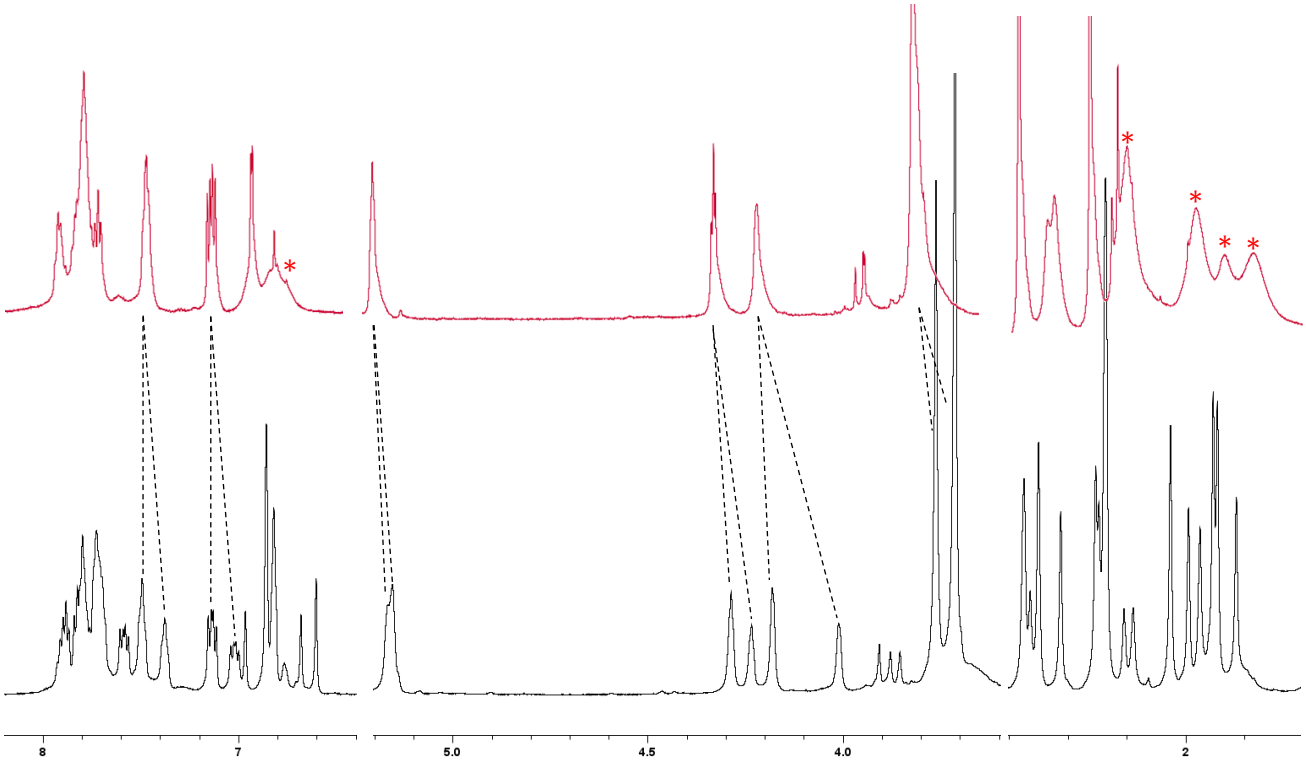

Figure 4.27: ^{1}H NMR spectra of [**IXg**][CF_3SO_3] in CD_2Cl_2 at room temperature (*red*) and at -80° C (*black*).

The ^{1}H NMR spectra of **VIIg**$^+$ recorded at room temperature, features two distinct sets of signals for two different conformers. On the other hand, **IXg**$^+$ displays broad ^{1}H NMR signals for the mesityl substituents at room temperature (both methyls and aromatic CHs marked with * in Figure 4.27). Surprisingly for temperatures below -70° C the associated fluxional process is slowed on the NMR timescale leading to the emergence of two sets of

signals for all the protons in **IXg**$^+$ (Figure 4.27). The largest upfield shifts are observed for the phenyl of —PPh_2 and the neighbouring CH of the five membered ring of the indenyl (dotted lines, Figure 4.27). The "windshield wiper" is a plausible explanation with some free rotation along the P—C and B—C bond (Figure 4.28); the swing of both phenyl and mesityl ligands will alter their magnetic interaction with the indenyl scaffold.

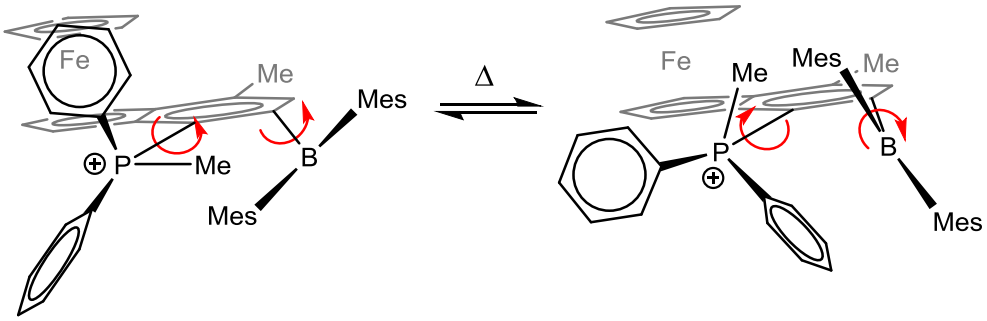

Figure 4.28: Thermal interconversion of the enantiomeric conformations of **VIIf** by synchronized motion of the —$BMes_2$ and —PPh_2 units.

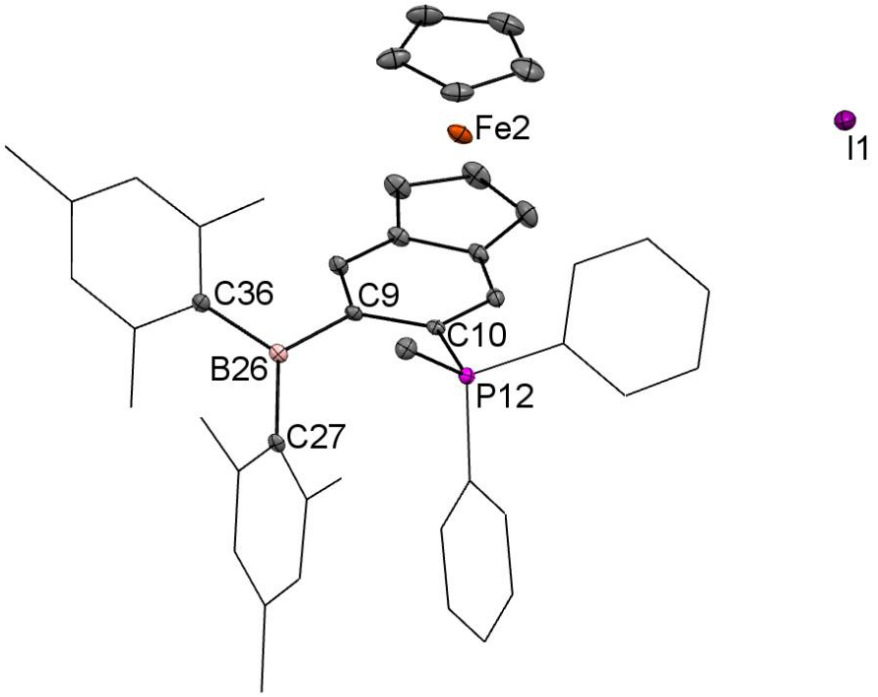

Figure 4.29: Molecular structure of [(R_p)-**VIIg**]I (isolated as a racemic mixture)**.** Thermal ellipsoids set at the 50% probability level; mesityl and phenyl groups shown in wireframe format and hydrogen atoms and dichloromethane solvent molecules omitted for clarity (light pink: boron; black: carbon; orange: iron; purple: phosphine, violet: iodide). Selected bond lengths [Å] and angles [°]: B26—C9 1.572(4), B26—C27 1.575(4), B26—C36 1.581(5), C9—B26—C27 121.9(3), C9—B26—C36 116.1(3), C27—B26—C36 121.2(3), C10—C9—B26 129.3(3), C9—C10—P12 123.1(2).

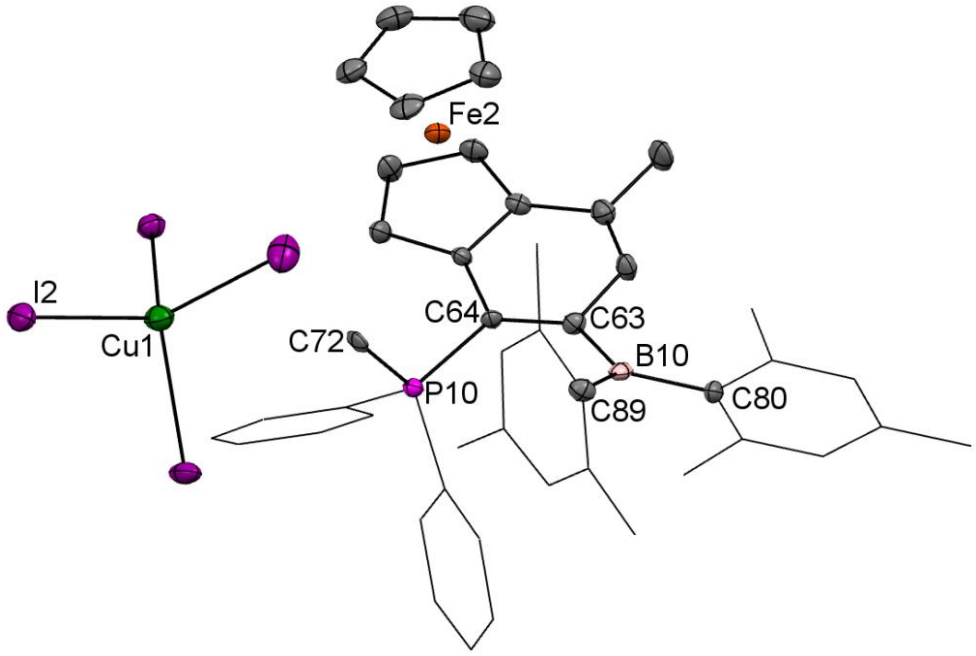

Figure 4.30: Molecular structure of [(S_p)-**IXg**]$_2$[CuI$_4$] (isolated as a racemic mixture). Thermal ellipsoids set at the 50% probability level; mesityl and phenyl groups shown in wireframe format and hydrogen atoms omitted for clarity (light pink: boron; black: carbon; orange: iron; magenta: phosphine; green: copper; purple: iodide). Selected bond lengths [Å] and angles [°]: B10—C63 1.599(14), B10—C80 1.587(15), B10—C89 1.550(15), C63—B10—C80 117.5(9), C63—B10—C89 123.1(9), C80—B10—C89 119.1(9), C64—C63—B10 131.0(9), C63—C64—P10 126.0(7). Note: copper is used as a stabiliser for the methyl iodide reagent.

Bond/angle	VIIf	VIIIg$^+$	IXf	IXg$^+$	115$^{+\,(*)}$	*o*-108$^+$
B—C$_{aryl}$	1.577(2)	1.575(4)	1.584(3)	1.599(14)	1.598	1.562(4)
	1.571(2)	1.581(5)	1.575(3)	1.587(15)	1.596	1.577(4)
	1.569(2)	1.572(4)	1.578(3)	1.550(15)	1.586	1.585(4)
$\sum_{CBC}$	359.9	359.2	359.6	359.7	359.8	359.7
B···P	3.205	3.483	3.063	3.431	3.865	3.494(3)
B—C—C—P	22.48	18.78	4.01	0.91	5.48	16.55
P—C—C	116.08(11)	123.1(2)	114.82(13)	126.0(7)	133.6	124.4(2)
B—C—C	123.22(13)	129.3(3)	124.21(15)	131.0(9)	135.6	130.1(3)
P(Cp)—*P*(ind)	1.64	1.70	5.60	9.97	-	-

Table 4.2: Selected bond lengths (Å), angles (°). $^{(*)}$ *the parameters given in the table are extrapolated from the optimised structure.*

The transformation of **VIIf** and **IXf** to the respective phosphonium products also leads to manifest changes in the solid state structures (Figure 4.25 to Figure 4.30). The introduction of the methyl group transforms the geometry at the phosphorus centre from trigonal pyramidal to tetrahedral. There is a consequent increase in the intermolecular B···P distance (by 0.278 and 0.368 Å, for **VII** and **IX** respectively; Table 4.2) and the C—C—P and C—C—B angles are wider in both cases, presumably in order to accommodate the increased steric bulk. The boron centres maintain trigonal planar geometries, with the sum of the C—B—C angles close to 360° ($\sum_{CBC}$ = 359.2° and 359.7° for **VIIg**$^+$ and **IXg**$^+$ respectively). In the case of **IXg**$^+$, the close interaction of the —P(Me)Ph_2^+ unit and one of the $BMes_2$ mesityl substituents with the cyclopentadienyl ring (*e.g.* {Me of Mes}—{CH of Cp} = 3.53 Å ; {C of Ph}—{CH of Cp} = 2.99 Å) imposes an increase of 4.4° between the least squares planes of the Cp and the indenyl moiety (Table 4.2). Furthermore a parallel can be perceived between the ^{31}P NMR result and the B—C—C—P torsion angle observed in **VIIg**$^+$, the large torsion angle of 19.29° is consistent with the two ^{31}P shifts observed in solution at room temperature.

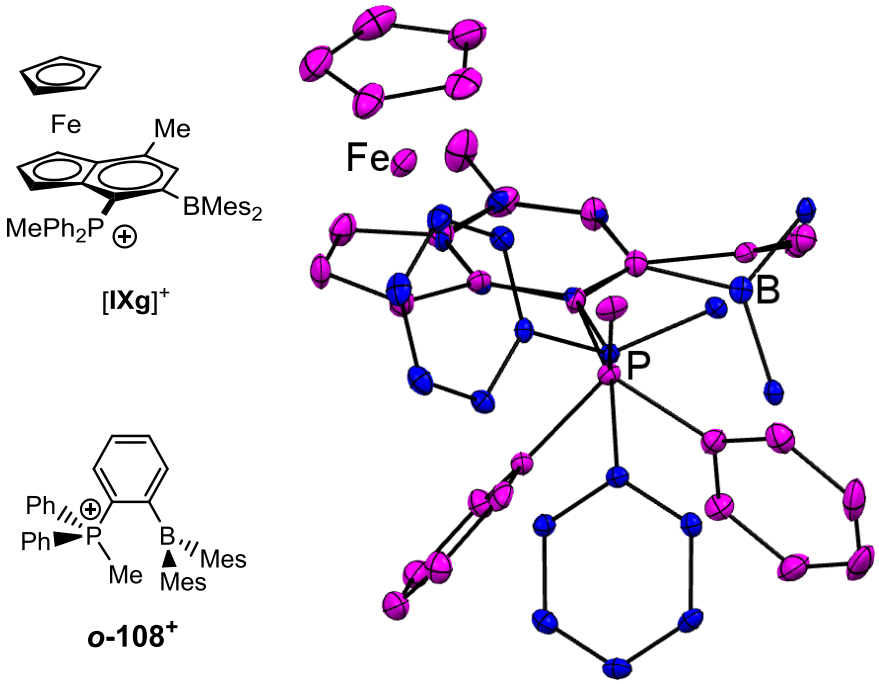

Figure 4.31: (*left*) Schematic representation of **IXg**$^+$ and ***o*-108**$^+$ (*right*) Molecular structure of **IXg**$^+$ (magenta) and ***o*-108**$^+$ (blue) overlaid. Thermal ellipsoids set at the 50% probability level; mesityl units and hydrogen atoms are omitted for clarity

The B···P distances are similar between **VIIg$^+$**, **IXg$^+$** and ***o*-108$^+$** (*ca.* 3.4 Å), while for the optimised structure of **115$^+$** with the ferrocene backbone the B···P distance is slightly longer (**115$^+$**, 3.865 Å). From the structure overlay of ***o*-108$^+$** with the receptor **IXg$^+$** (Figure 4.31) it is obvious that the conformation in **IXg$^+$** is dictated by steric hindrance. The phenyl groups on the phosphorus are pushed away from the FeCp moiety in **IXg$^+$**; but in ***o*-108$^+$** the phenyl groups are on both sides of the supporting benzene ring — *i.e.* the -PPh_2Me unit rotated by 75° with respect to **IXg$^+$**.

DFT calculations were carried out on the receptors **VIIf**, **VIIg$^+$**, **IXf** and **IXg$^+$** in order to probe issues of electronic structure/Lewis acidity; moreover, in order to put these results in perspective analogous calculations at the same level of theory were performed on $[Fc(BMes_2)(PPh_2Me)]^+$ (**115$^+$**) and ***o*-108$^+$** (Table 4.2 and Figure 4.32). Firstly, the HOMO-1 and HOMO are dominated by the *d*-orbitals of the iron atom (at least 78% contribution). The formation of the phosphonium cations *via* the methylation of the phosphine function in **VIIf** and **IXf** not unexpectedly leads to major alterations of the molecular orbital distribution. The LUMO and LUMO+1 on the other hand fall in energy by 3.0 eV for **IX** and 2.7 eV for **VII** on alkylation (Table 4.3); in the parent neutral systems the Lewis acid character is centred on the boron atom, but a large contribution is attributed to the phosphorus atom in both **VIIg$^+$** and **IXg$^+$**. For instance in the **IX** receptor series, the Lewis acidic boron atom of **IXf** has the highest contribution in both the LUMO and LUMO+1 (23% in both); in the case of **IXg$^+$**, however, the boron atom is still dominant in the LUMO while the (formally cationic) phosphorus centre is the main contributor to the LUMO+1 (12%, Table 4.3). The stabilization of the LUMO is as expected on the basis of other examples reported previously in the literature, indeed the frontier orbitals in receptor **115$^+$** (LUMO, -5.18 eV; LUMO+1, -4.86 eV) and ***o*-108$^+$** (LUMO, -5.42 eV; LUMO+1, -4.94 eV) exhibit similar energy levels (Table 4.3).

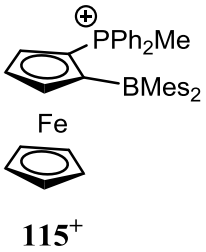

115^{+}

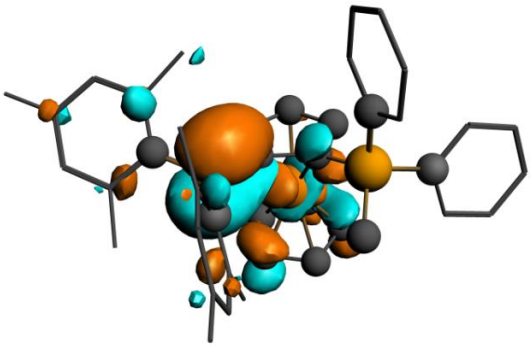

115^{+}
LUMO (-5.18 eV)
33% on Fe, 27% on B

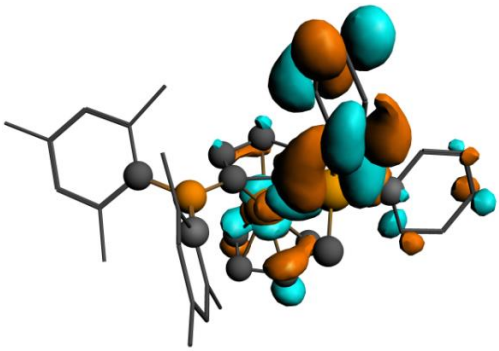

115^{+}
LUMO+1 (-4.86 eV)
8% on P

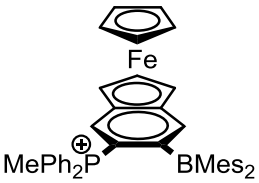

VIIg^{+}

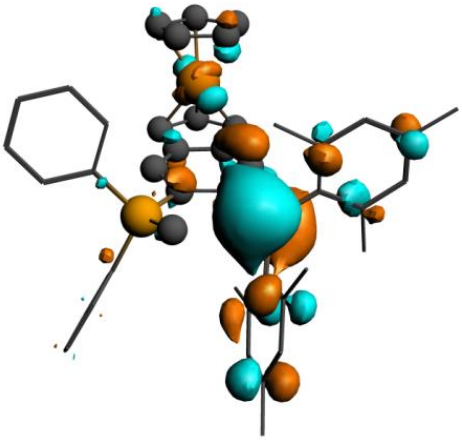

VIIg^{+}
LUMO +1 (-4.84 eV)
36% on B

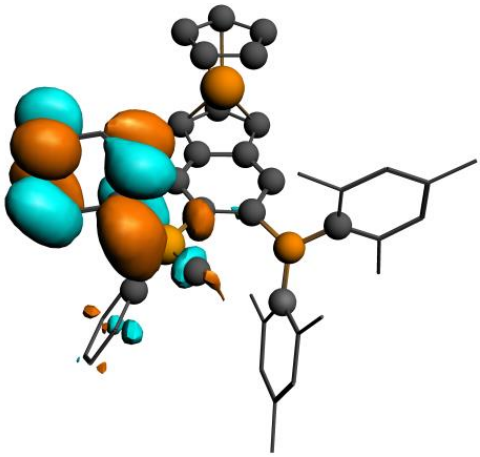

VIIg^{+}
LUMO +2 (-4.71 eV)
13% on P

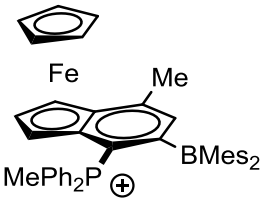

IXg^{+}

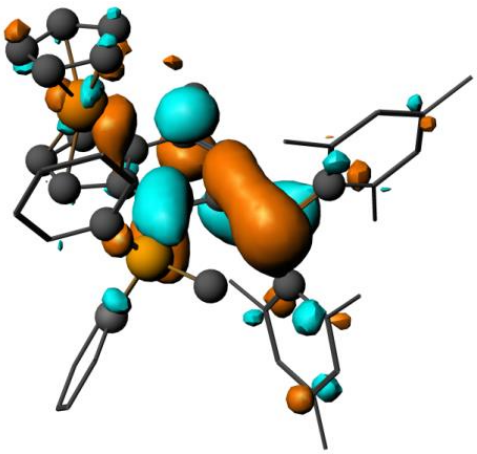

IXg^{+}
LUMO (-5.37 eV)
19% on B

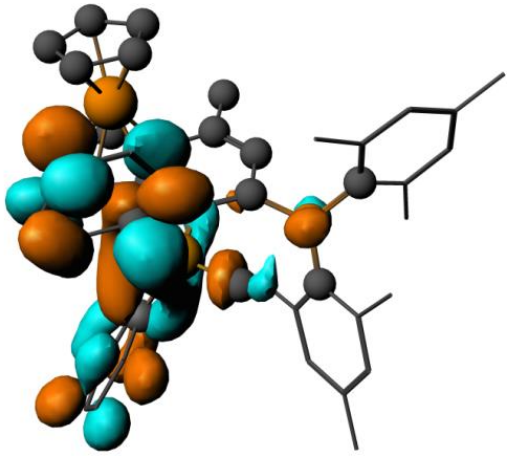

IXg^{+}
LUMO +1 (-4.72 eV)
4% on B, 12% on P

Figure 4.32: NBO contour plot for receptor **115**$^{+}$, **VIIg**$^{+}$ and **IXg**$^{+}$ (density isovalues = 0.03).

Level	VIIf	VIIg$^+$	IXf	IXg$^+$	115$^+$	*o*-108$^+$
HOMO-1	-4.23 eV *78% Fe*	-6.78 eV *80% Fe*	-3.69 eV *79% Fe*	-6.64 eV *79% Fe*	-7.30 eV *76% Fe*	-7.93 eV
HOMO	-3.98 eV *25% Fe* *12% B*	-6.58 eV *75% Fe*	-3.46 eV *78% Fe*	-6.42 eV *78% Fe*	-7.22 eV *77% Fe*	-7.81 eV
LUMO	-2.40 eV *12% B* *28% Fe*	-5.13 eV *5% P* *23% Fe*	-2.27 eV *23% B* *14% Fe*	-5.37 eV *19% on B*	-5.18 eV *27% B* *33% Fe*	-5.42 eV *28% B* *4% P*
LUMO+1	-2.13 eV *31% B* *12% Fe*	-4.84 eV *36% B*	-1.64 eV *23% B* *20% Fe*	-4.72 eV *4% B* *12% P*	-4.86 eV *8% P* *26% Fe*	-4.94 eV *3% B* *12% P*
LUMO+2	-1.60 eV *2% B* *35% Fe*	-4.71 eV *13% P*	-1.35 eV *50% Fe*	-4.60 eV *6% P*	-4.79 eV *3% P* *17% Fe*	-4.84 eV *13% P*

Table 4.3: Selected energy levels for receptor **VIIf**, **VIIg$^+$**, **IXf**, **IXg$^+$**, **115$^+$** and ***o*-108$^+$**.

Cyclic voltammetry measurements were also carried out on these receptor systems. The measurements for **VIIf** and **IXf** were carried out in thf and gave values of +166 mV and +43 mV respectively for the iron-centred oxidation event (*vs* ferrocene/ferrocenium couple, Figure 4.33). In addition, an irreversible reduction wave centred at -2683 mV is assigned the $B^{\bullet-}$/B redox couple for **VIIf**. Moreover the CV measurements for **VIIg$^+$** and **IXg$^+$** were first conducted in thf; the iron redox potential was beyond the oxidation potential of the solvent however it was possible to observe the reduction of the boron centre in **IXg$^+$** (-1279 mV). In acetonitrile both **VIIg$^+$** and **IXg$^+$** display non-reversible waves for both Fe^{II}/Fe^{III} and $B^{\bullet-}$/B events (Figure 4.34), yet an estimated potential can be extrapolated from the data (Table 4.4). It should be noted that trifluoromethylsulfonate salts were preferred over the parent iodide salts in the cases of the cationic metal systems, for the simple reason that it eliminates the redox wave associated with the I^-/I_2 redox process.

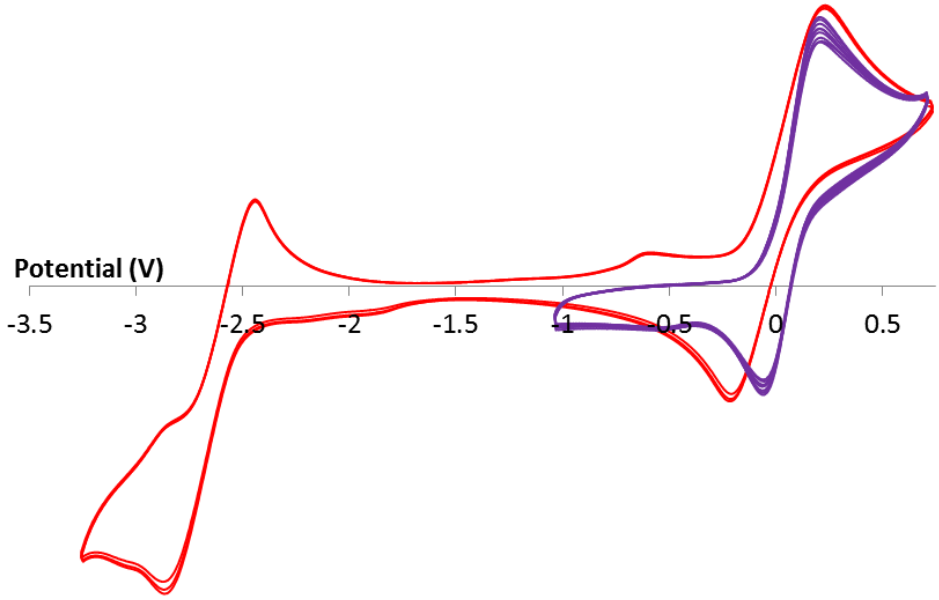

Figure 4.33: Cyclic voltammograms of receptor **VIIf** (red) and **IXf** (purple) *vs* the ferrocene/ferrocenium couple with 0.1 M [^{n}Bu$_4$N][PF$_6$] in thf (scan rate 0.1 V s^{-1}).

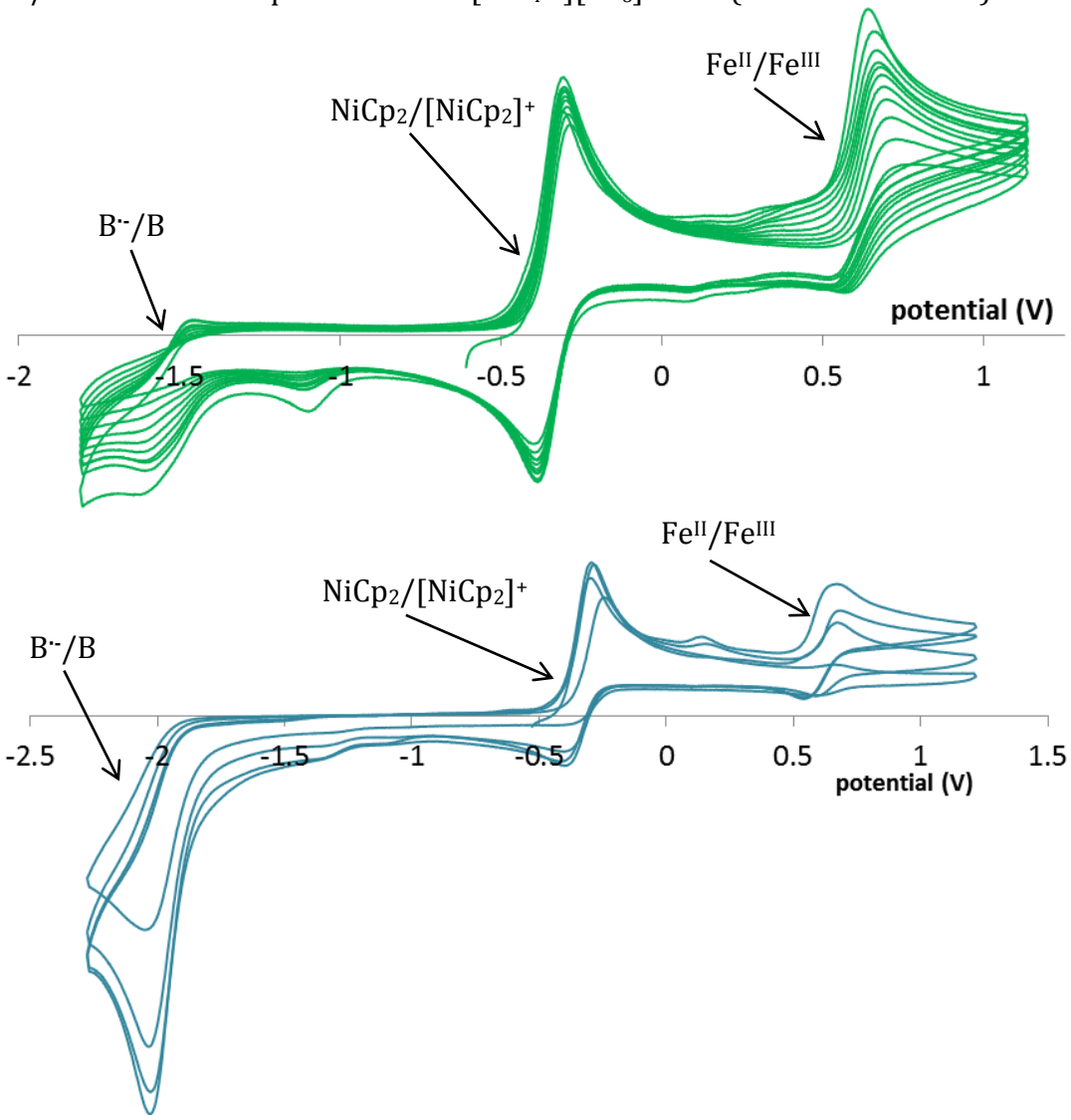

Figure 4.34: Cyclic voltammograms of (*top*) [**IXg**][CF$_3$SO$_3$] and (*bottom*) [**VIIg**][CF$_3$SO$_3$] *vs* the ferrocene/ferrocenium couple with 0.1 M [^{n}Bu$_4$N][PF$_6$] in acetonitrile (scan rate 0.1 V s^{-1}).

Receptor	Fe^{II}/Fe^{III}	$B^{\bullet-}/B$
IIa	+75[a]	-2403[a]
IIb	+140[a]	-2315[a]
IIc	+249[a]	-2389[a]
IIIe	+16[a]	-2356
IVe	+15[a]	-
VIIf	+166[a]	-2683[a]
IXf	+43[a]	-
VIIg$^+$	+575[b]	*ca.* -1979[b]
IXg$^+$	+576[b]	*ca.* -1479[b] and -1279[a]

Table 4.4: Redox potential for Fe^{II}/Fe^{III} and $B^{\bullet-}/B$, results are given in mV with respect to the couple ferrocene/ferrocenium couple, with 0.1 M [^{n}Bu$_4$N][PF$_6$] (*a*) in thf or (*b*) in acetonitrile.

Examination of the redox potentials of all four receptors gives an insight into their Lewis acidity (Table 4.4). For instance, the Fe^{II}/Fe^{III} redox potentials of receptors **VIIf** and **IXf** — respectively +166 and +43 mV — are in the same range as the potentials measured for **IIa-c** (Table 4.4). The cathodic shift for the reduction of the boron atom compared to **IIIe** is presumably the result of the introduction of the electron rich diphenylphosphine unit. The introduction of the cationic phosphonium unit is responsible for the substantial anodic shifts of at least +350 and +500 mV for **VIIg$^+$** and **IXg$^+$** respectively. The $B^{\bullet-}/B$ redox couple is found around -2.3 V for the simple receptor **II** series and **IIIe**, whereas it lies at -2.0 V and -1.5 V for **VIIg$^+$** and **IXg$^+$**, respectively. This large anodic shift is in line with the energies calculated for the frontier orbitals; for the **II** series and **IIIe** the energy of the LUMO lies between -2.39 and -2.65 eV, while the LUMO+1, centred on boron for **VIIg$^+$**, is found at at -4.84 eV.

4.4.3 Anion binding

The binding capabilities of the **VII** and **IX** receptor series can be monitored by multinuclear spectroscopy *i.e.* ^{11}B and ^{31}P, and ^{19}F NMR when appropriate. The phosphine-

borane receptors **VIIf** and **IXf** were exposed to cyanide or fluoride in dry thf or chloroform, but only on addition of cyanide was a binding event detected. For both isomers, the ^{11}B NMR spectrum exhibits a new resonance at δ_B *ca.* -12 ppm characteristic of a dimesitylborane-cyanide adduct. Addition of a large excess of fluoride in dry chloroform (4 equivalents of $[^nBu_4N]F{\cdot}4H_2O$ or $[S(NMe_2)_3][Me_3SiF_2]$), however, does not seem to quaternize the Lewis acidic boron centre, and an ^{11}B NMR spectrum displaying a broad signal at δ_B *ca.* 77 ppm is observed, together with free fluoride in the ^{19}F NMR spectrum (δ_F -157.5 ppm). The absence of a peak for the fluoride adduct detected by negative ion ESI-MS further suggests that fluoride is neither bound by **VIIf** nor **IXf** even in dry aprotic solvents. By contrast, the corresponding spectra obtained in the presence of cyanide display the molecular ion peak and expected isotopic distributions for both [**VIIf**·CN]$^-$ and [**IXf**·CN]$^-$. This selectivity can be explained by the lower Lewis basicity of fluoride *vs* cyanide in combination with the high steric loading provided by adjacent dimesitylborane and diphenylphosphine functions, that renders the formation of the fluoride adduct enthalpically disfavoured. The molecular structures of $[^nBu_4N]$[**VIIf**·CN] and $[^nBu_4N]$[**IXf**·CN] were determined by single X-ray crystallography (Figure 4.35 and Figure 4.36). The binding of cyanide is accompanied by pyramidalization of the boron centre ($\sum_{CBC}$ = 340.7° and 340.5° for [**VIIf**·CN]$^-$ and [**IXf**·CN]$^-$ respectively), elongation of the B—C bonds by at least 0.09 Å and widening of the intramolecular B···P separation (Table 4.6). The B—CN bond length in each case falls within the range of previously reported cyanide adduct structures (1.631(5) Å, [**IIc**·CN]$^-$; 1.633(2) Å, [**IIIe**·CN]$^-$; 1.625(2) Å, [**VIIf**·CN]$^-$; 1.626(7) Å, [**IXf**·CN]$^-$). The long contacts between the phosphorus centre and the cyanide guest (3.102 Å for [**VIIf**·CN]$^-$ and 3.240 Å for [**IXf**·CN]$^-$) together with the marginal shifts in the respective ^{31}P NMR spectra suggests that there is effectively no interaction between the phosphorus atom and the bound cyanide.

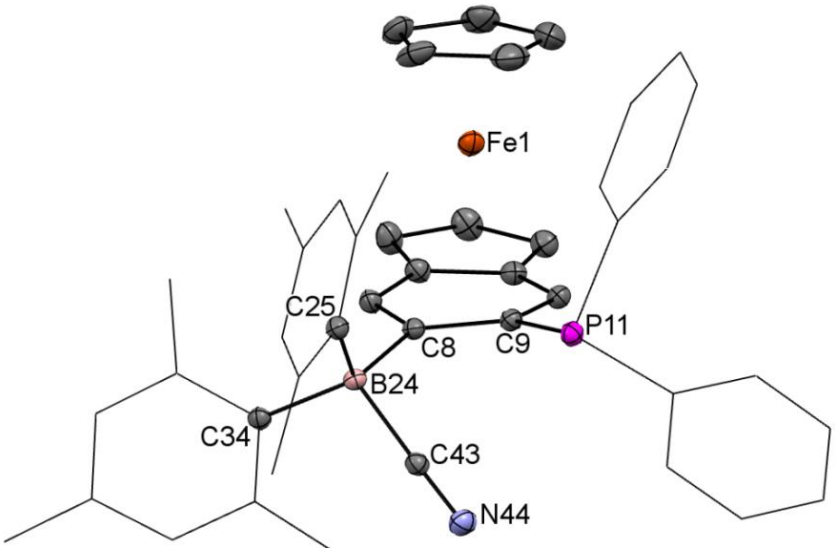

Figure 4.35: Molecular structure of [^{n}Bu$_4$N][(S_p)-**VIIf**·CN] (isolated as a racemic mixture). Thermal ellipsoids set at the 50% probability level; mesityl and phenyl groups shown in wireframe format and hydrogen atoms and tetrabutylammonium counter-ion omitted for clarity (black: carbon; orange: iron; purple: phosphine; light pink: boron; blue: nitrogen). Selected bond lengths [Å] and angles [°]: B24−C8 1.661(2), B24−C25 1.663(2), B24−C34 1.667(2), B24−C43 1.625(2), C8−B24−C25 119.62(13), C8−B24−C34 110.01(13), C25−B24−C34 111.04(13), C9−C8−B24 124.17(14), C8−C9−P11 119.15(12), B24−C43−N44 178.57(17).

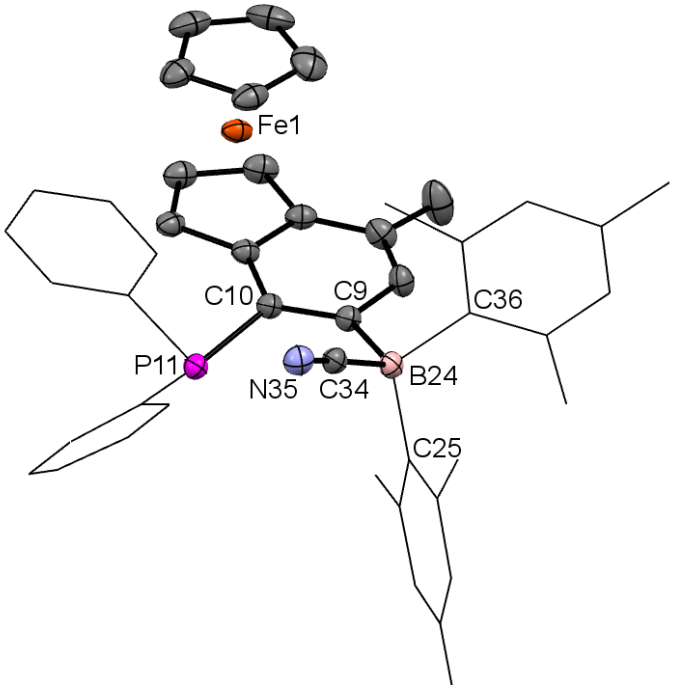

Figure 4.36: Molecular structure of [^{n}Bu$_4$N][(R_p)-**IXf**·CN] (isolated as a racemic mixture). Thermal ellipsoids set at the 50% probability level; mesityl and phenyl groups shown in wireframe format and hydrogen atoms and tetrabutylammonium counter-ion omitted for clarity (light pink: boron; black: carbon; orange: iron; purple: phosphine, blue: nitrogen). Selected bond lengths [Å] and angles [°]: B24−C9 1.677(6), B24−C25 1.669(7), B24−C36 1.678(7), B24−C34 1.626(7), C9−B24−C25 120.9(4), C9−B24−C36 106.5(3), C25−B24−C36 113.1(3), B24−C34−N35 174.9(4), C9−C10−P11 121.6(3), C10−C9−B24 128.9(4).

Bond/angle	VIIf	[VIIf·CN]⁻	IXf	[IXf·CN]⁻
B—C_{aryl}	1.577(2)	1.661(2)	1.584(3)	1.677(6)
	1.571(2)	1.663(2)	1.575(3)	1.669(7)
	1.569(2)	1.667(2)	1.578(3)	1.678(7)
$\sum_{CBC}$	359.95	340.7	359.62	340.5
B—X (X= F or CN)	-	1.625(2)	-	1.626(7)
B···P	3.205	3.349	3.063	3.455
B—C—C—P	22.48	19.29	4.01	21.03
P—C—C	116.08(11)	119.15(12)	114.82(13)	121.6(3)
B—C—C	123.22(13)	124.17(14)	124.21(15)	128.9(4)
P(Cp)—*P*(indenyl)	1.64	4.78	5.60	2.93

Table 4.5: Selected bond lengths (Å), angles (°) for **VIIf**, [**VIIf**·CN]⁻, **IXf** and [**IXf**·CN]⁻.

Binding studies were also conducted on the cationic receptors **VIIg**⁺ and **IXg**⁺ which reveal contrasting behaviour to the parent systems **VIIf** and **IXf**. Addition of cyanide, in the form of [^{n}Bu$_4$N][CN]·3H$_2$O, immediately brings about a rapid change of colour from green to red for both receptors; ^{11}B NMR spectroscopy confirms the formation of a cyanide adduct with a shift to δ_B -13 ppm observed for both **VIIg**·CN and **IXg**·CN. In contrast to the behaviour of charge neutral **VIIf** and **IXf**, however, the treatment of receptors **VIIg**⁺ and **IXg**⁺ with one equivalent of fluoride using either [S(NMe$_2$)$_3$][Me$_3$SiF$_2$] or [^{n}Bu$_4$N]F·4H$_2$O yields the fluoride adduct, with the accompanying colour change being similar to that observed with cyanide. Upfield shifts to *ca*. δ_B 7ppm are consistent with the formation of the respective fluoroborates, and additional new broad signals in the corresponding ^{19}F NMR spectra are also observed (at δ_F -149.0 and -145.1 ppm for **VIIg**·F and **IXg**·F respectively). Evidence for the chelation of the fluoride ion in solution involving both borane and phosphonium Lewis acids is provided by ^{31}P NMR spectroscopy. In both cases, a downfield shift from δ_P *ca.* 24 ppm to 29 ppm is accompanied by the appearance of a doublet coupling between the phosphorus and fluorine nuclei of 26.0 Hz for **VIIg**· μ_2-F and 22.9 Hz for **IXg**·μ_2-F (*cf.* ***o*-108**·μ_2-F, $^1J_{PF}$ = 24.3 Hz).[10b]

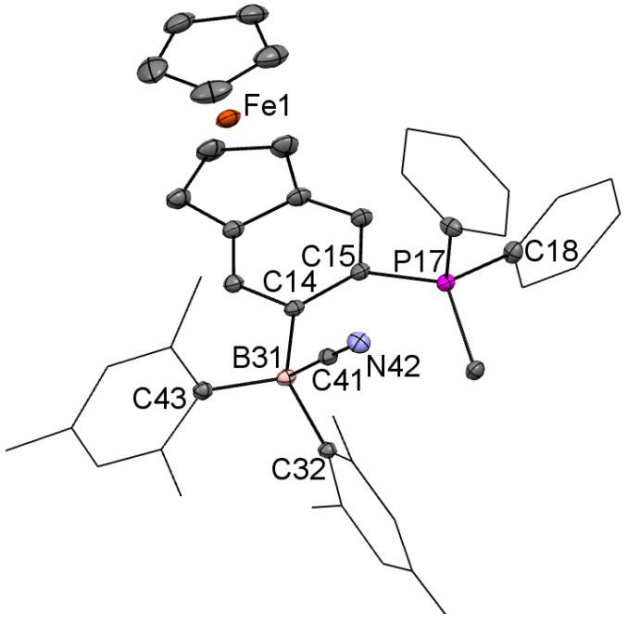

Figure 4.37: Molecular structure of (S_p)-**VIIg**·CN (isolated as a racemic mixture). Thermal ellipsoids set at the 50% probability level; mesityl and phenyl groups shown in wireframe format and hydrogen atoms and dichloromethane solvate molecules omitted for clarity (light pink: boron; black: carbon; orange: iron; purple: phosphine, blue: nitrogen). Selected bond lengths [Å] and angles [°]: B31—C32 1.663(2), B31—C41 1.624(2), B31—C43 1.663(2), B31—C14 1.656(2), C41—N42 1.149(2), C14—B31—C32 114.79(12), C14—B31—C43 112.23(12), C32—B31—C43 114.16(12), B31—C41—N42 178.82(16), C14—C15—P17 126.53(12), C15—C14—B31 127.14(13).

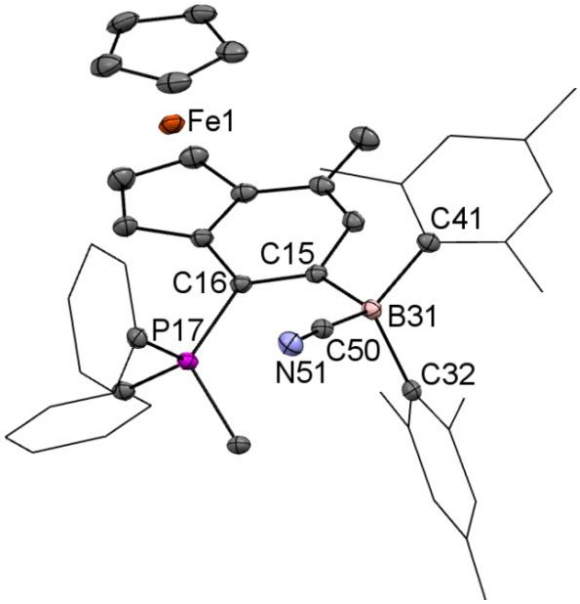

Figure 4.38: Molecular structure of (S_p)-**IXg**·CN (isolated as a racemic mixture). Thermal ellipsoids set at the 50% probability level; mesityl and phenyl groups shown in wireframe format and hydrogen atoms and dichloromethane solvate molecules omitted for clarity (light pink: boron; black: carbon; orange: iron; purple: phosphine, blue: nitrogen). Selected bond lengths [Å] and angles [°]: B31—C15 1.663(3), B31—C32 1.666(3), B31—C41 1.673(3), B31—C50 1.626(3), C50—N51 1.150(2), C15—B31—C32 116.91(15), C15—B31—C41 108.04(14), C32—B31—C41 115.37(15), B31—C50—N51 176.59(19), C16—C15—B31 129.91(15), C15—C16—P17 124.89(13).

Single crystals suitable for X-ray crystallography were obtained for **VIIg**·CN (Figure 4.37), **IXg**·CN (Figure 4.38), **VIIg**·F (Figure 4.39) and **IXg**·F (Figure 4.40); selected bond lengths and angles are included in Table 4.6. Examination of the structures of the various adducts in the solid state reveals a number of noteworthy features. Each features a tetra-coordinate boron centre featuring either a bound cyanide or fluoride ion ($\sum_{CBC}$ = 341.3°, **VIIg**·CN; 341.2°, **VIIg**·F ; 340.3°, **IXg**·CN ; 340.1°, **IXg**·F). The B—F (1.477 Å) or B—CN (1.625 Å) bond length are similar to those observed previously (1.471(3) Å, [**IIb**·F]$^-$; 1.631(3) Å, [**IIb**·CN]$^-$). Moreover in both receptors, the binding of cyanide increases the intramolecular B···P distance — from 3.483 to 3.559 Å in **VIIg**·CN and from 3.431 to 3.529 Å in **IXg**·CN. By contrast, fixation of fluoride leads to a corresponding *decrease* in this separation — to 3.335 and 3.295 Å for **VIIg**·F and **IXg**·F, respectively.

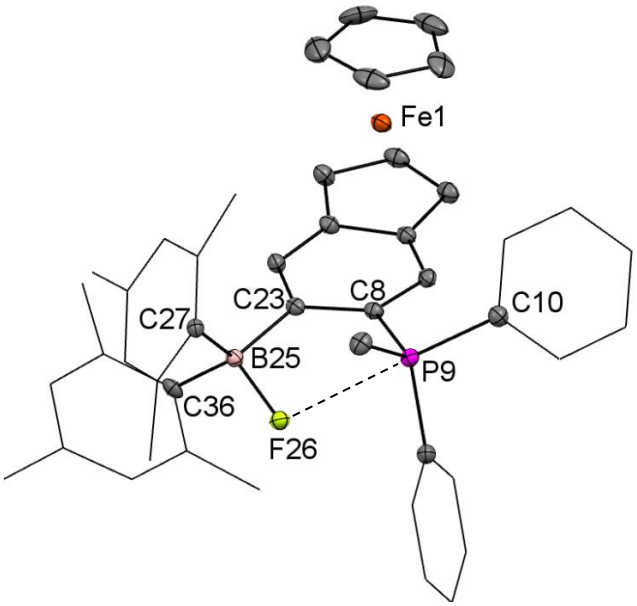

Figure 4.39: Molecular structure of (S_p)-**VIIg**·F (isolated as a racemic mixture). Thermal ellipsoids set at the 50% probability level; mesityl and phenyl groups shown in wireframe format and hydrogen atoms omitted for clarity (light pink: boron; black: carbon; orange: iron; purple: phosphine, yellow: fluoride). Selected bond lengths [Å] and angles [°]: B25—F26 1.478(3), B25—C27 1.657(3), B25—C36 1.663(4), B25—C23 1.649(3), C23—B25—C27 119.96(19), C23—B25—C36 109.15(18), C27—B25—C36 112.04(19), C8—C23—B25 121.6(2), P9—C8—C23 123.43(17), B25—P9 3.335(calc.), F26—P9 2.676(calc.), P9—C8—C23—B25 11.96(calc.), F26—P9—C10 179.0(calc.), *P*(Cp)—*P*(indenyl) 7.38.

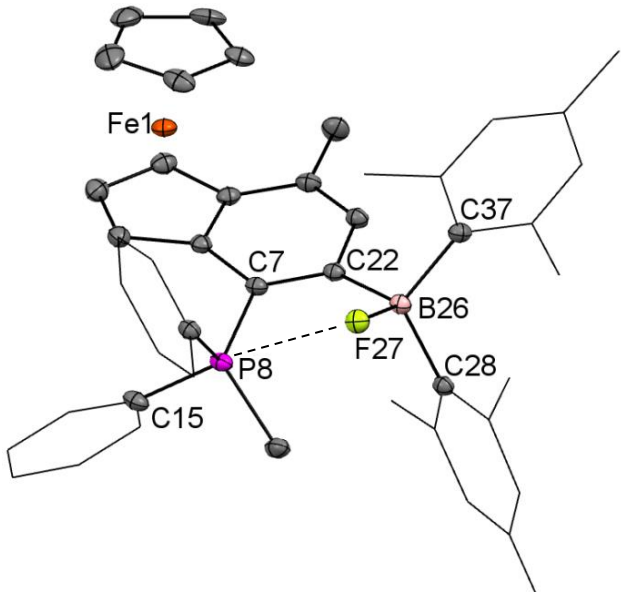

Figure 4.40: Molecular structure of (R_p)-**IXg**$^{\cdot}$F (isolated as a racemic mixture). Thermal ellipsoids set at the 50% probability level; mesityl and phenyl groups shown in wireframe; hydrogen atoms are omitted for clarity (light pink: boron; black: carbon; orange: iron; purple: phosphine, yellow: fluoride). Selected bond lengths [Å] and angles [°]: B26—C22 1.644(3), B26—C28 1.652(3), B26—C37 1.654(3), B26—F27 1.477(2), P8—F27 2.694(calc.), C7—C22—B26 124.18(18), C22—C7—P8 121.77(16), C22—B26—C28 118.67(17), C22—B26—C37 107.33(17), C28—B26—C37 114.09(17), F27—P8—C15 172.3(calc.), P8—C7—C22—B26 16.6(calc.), B26—P8 3.295(calc.), *P*(Cp)—*P*(indenyl) 9.48.

Bond/angle	**VIIIg**$^{+}$	**VIIg**$^{\cdot}$CN	**VIIg**$^{\cdot}$F	**IXg**$^{+}$	**IXg**$^{\cdot}$CN	**IXg**$^{\cdot}$F
B—C_{aryl}	1.575(4)	1.663(2)	1.657(3)	1.599(14)	1.663(3)	1.644(3)
	1.581(5)	1.656(2)	1.663(4)	1.587(15)	1.666(3)	1.652(3)
	1.572(4)	1.663(2)	1.649(3)	1.550(15)	1.673(3)	1.654(3)
$\sum_{CBC}$	359.2	341.29	341.15	359.7	340.32	340.09
B—X (X= F or CN)	-	1.624(2)	1.478(3)	-	1.626(3)	1.477(2)
B···P	3.483	3.559	3.335	3.431	3.529	3.295
B—C—C—P	18.78	12.26	11.96	0.91	19.54	16.6
P—C—C	123.1(2)	126.53(12)	123.43(17)	126.0(7)	124.89(13)	121.77(16)
B—C—C	129.3(3)	127.14(13)	121.6(2)	131.0(9)	129.91(15)	124.18(17)
P(Cp)—*P*(indenyl)	1.70	6.79	7.38	9.97	7.73	9.48

Table 4.6: Selected bond lengths (Å), angles (°) for **VIIIg**$^{+}$, **VIIg**$^{\cdot}$CN, **VIIg**$^{\cdot}$F, **IXg**$^{+}$, **IXg**$^{\cdot}$CN and **IXg**$^{\cdot}$F.

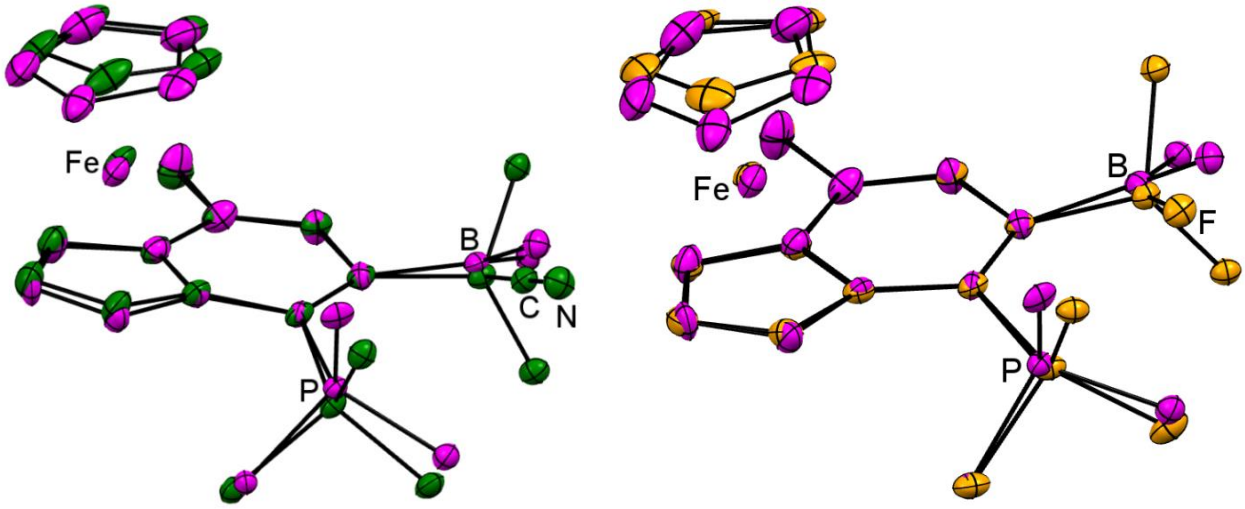

Figure 4.41: Overlaid molecular structures of **IXg**$^+$ (*magenta*) and **IXg**$^{\cdot}$CN (*green*) or **IXg**$^{\cdot}$F (*orange*). Thermal ellipsoids set at the 50% probability level; mesityl, phenyl units and hydrogen atoms are omitted for clarity

In the case of **VIIg**$^+$, fixation of the analyte leads to significant rearrangements of the pendant aryl rings to accommodate the increased degree of steric hindrance; this is most obviously apparent in the orientation of cyclopentadienyl ring, as manifested by the widening of the angle between the least squares planes of the cyclopentadienyl and indenyl units (Table 4.6). On the other hand, binding of either fluoride or cyanide by **IXg**$^+$ seems to release some of the steric strain between the -$BMes_2$ mesityl ring and the cyclopentadienyl ligand. Overlaid diagrams of the structures of **IXg**$^+$ and **IXg**$^{\cdot}$CN or **IXg**$^{\cdot}$F (Figure 4.41) illustrate the 0.482 and 0.449 Å shift of the Cp centroid between the free receptor **IXg**$^+$ and its fluoride and cyanide adducts, respectively.

The two fluoride adduct crystal structures show P···F distances of 2.6756(15) and 2.6936(15) Å both of which fall within the sum of the relevant Van der Waals' radii ($\sum_{VdW}$(P—F) = 3.27 Å),[20] and are similar to the P···F contact observed in ***o*-108**$^{\cdot}$F (2.666(2) Å).[10] That these contacts are structurally significant would be consistent with the observed contraction in the B···P distance in each case, and with the $^1J_{PF}$ coupling observed in the

respective ^{31}P NMR spectra. Gabbaï and co-workers report similar observations for the fluoride adduct ***o*-108**·F,[10] along with a relatively flat F—P—C_{phenyl} angle (176.4(1)°)) and an elongation of the P—Ph bond.[10] Similar geometric features can also be discerned here, *e.g.* F—P—C_{phenyl} = 179.0°, **VIIg**·F; 172.3°, **IXg**·F. Gabbaï attributed these spectroscopic/structural observations to the presence of a *lp*(F)→σ^*(C—Ph) interaction,[10] and a similar scenario can be postulated for **VIIg**·F and **IXg**·F (Figure 4.42). Thus, AIM (atoms in molecules) calculations reveal a bond path between P9 and F26 with an electron density ρ(r) of 2.13 × 10^{-2} e $Bohr^{-3}$ at the bond critical point, similar to the value reported for ***o*-108**·F (2.05 × 10^{-2} e $bohr^{-3}$).[10]

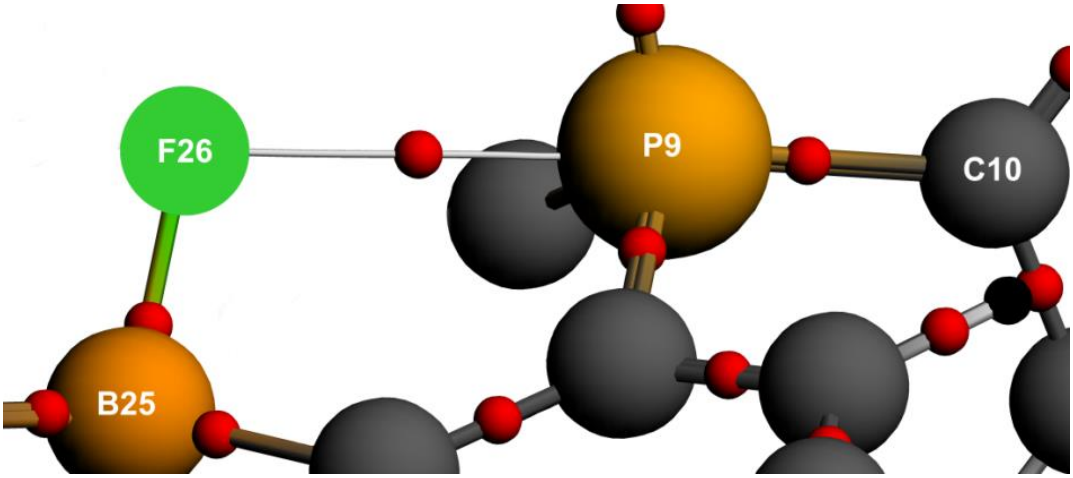

Figure 4.42: Atoms in molecules analysis of the BFP interaction in **VIIg**·F, with the relevant bond paths (*white connections*) and critical points (*red spheres*).

An assessment of the binding strength of all four receptors can be achieved by UV-Vis spectroscopy titration experiments. The neutral systems **VIIf** and **IXf** have already been shown to have no affinity for fluoride on the basis of multinuclear NMR and mass spectroscopy, while cyanide addition leads to a change of colour from a burgundy to light red (Figure 4.44, (a)). The addition of one equivalent of cyanide to **VIIf** and **IXf** leads to quenching of the bands centred at λ = 325 and 343 nm respectively (Figure 4.44, (c)), however the binding process appears to be relatively slow. Thus, on addition of one equivalent of cyanide

VIIf [^{n}Bu$_4$N][**VIIf**·CN] **IXf** [^{n}Bu$_4$N][**IXf**·CN]

Figure 4.43: Colour changes for **VIIf** (9.89 × 10^{-5} M) and **IXf** (9.72 × 10^{-5} M) with excess [^{n}Bu$_4$N][CN] in thf.

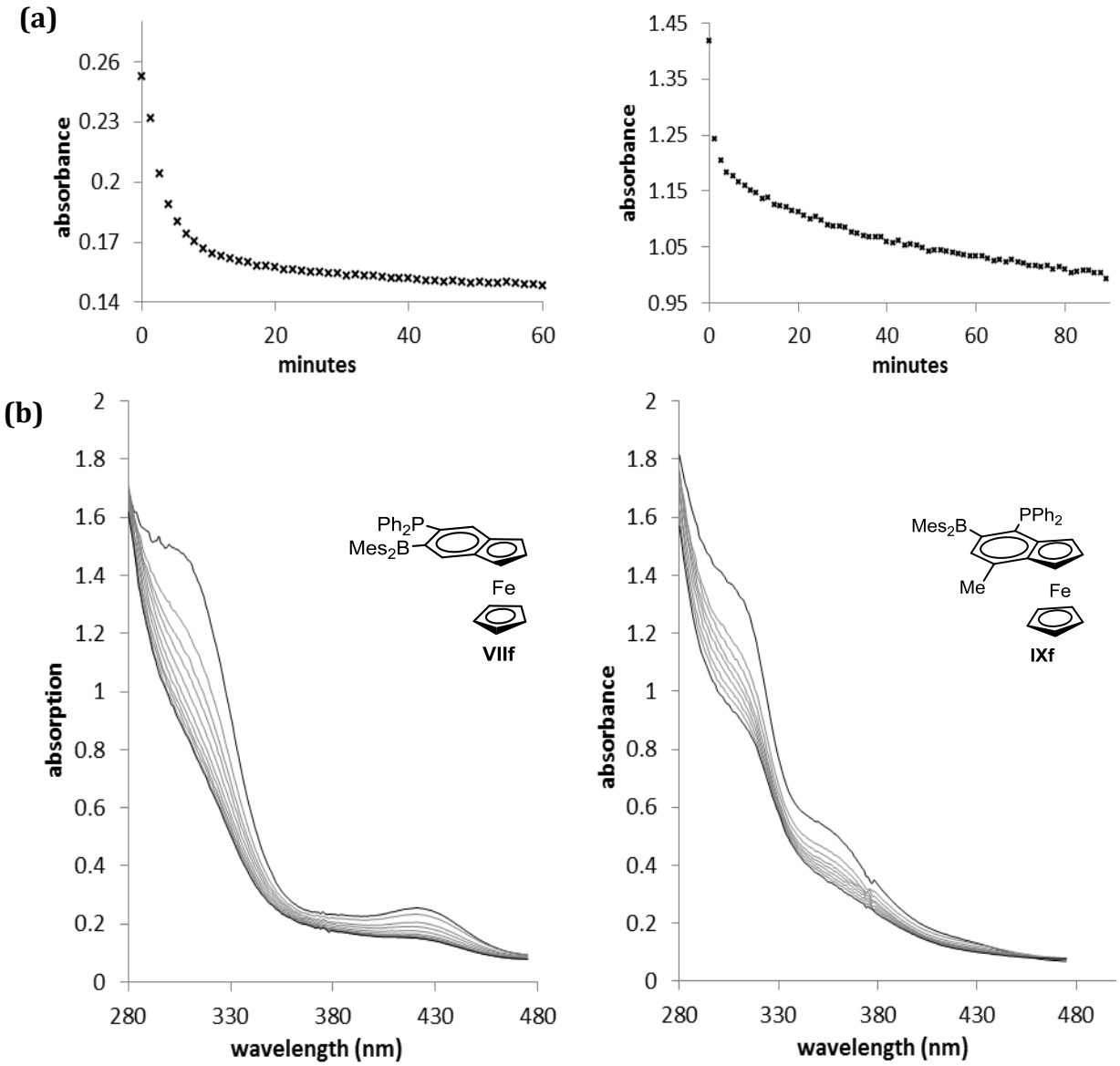

Figure 4.44: (b) Time dependency of the absorption of **VIIf** and **IXf** at λ = 423 and 300 nm respectively, after addition of one equivalent of cyanide. (c) Absorption spectrum for receptor **VIIf** taken at t= 0, 80 and 160 sec, 4, 7, 12, 20, 32, 40, 52 and 60 min after addition of one equivalent of cyanide. Absorption spectrum for receptor **IXf** taken at t= 0, 80 and 160 sec, 7, 12, 24, 40, 60 and 90 min after addition of one equivalent of cyanide.

to either **VIIf** and **IXf** in dry thf equilibrium is still not reached even after 1 h (Figure 4.44, (c)), rendering the determination of the binding constants extremely challenging.

The slow kinetics of binding could be attributed to the increased steric loading provided by the diphenylphosphine unit when compared to the monodentate **IIIe** and **IVe**. This result is similar to the slow uptake of fluoride observed within the cavity of the 1,2-bis(boryl)ferrocene **106**. Morgan *et al.* impugned the slow kinetics on steric shrouding of the binding site and the consequently high barrier to anion fixation.[19] On the other hand, the cationic boryl/phosphonium receptors are able to bind either cyanide or fluoride with very rapid uptake kinetics. Thus, receptors [**VIIg**]I and [**IXg**][CF_3SO_3] were subjected to sequential addition of aliquots of cyanide or fluoride (Figure 4.45 to Figure 4.48) in the form of thf solutions of [^{n}Bu$_4$N][CN]·3H$_2$O or [^{n}Bu$_4$N]F·4H$_2$O, respectively, and the resulting data fitted to a 1:1 binding isotherm. The derived binding affinities are summarized in Table 4.7, along with the corresponding results for related monodentate systems.

Receptor	*K*(F)	*K*(CN)
IIa	6.05(0.44) × 10^5	3.98(0.45) × 10^5
IIb	2.69(0.73) × 10^6	7.01(0.11) × 10^5
IIc	2.06(0.17) × 10^6	2.80(0.75) × 10^6
IIIe	2.28(0.48) × 10^6	1.02(0.38) × 10^7
IVe	1.91(0.12) × 10^6	9.31(0.55) × 10^6
[**VIIg**]I	6.92(0.41) × 10^7	1.92(0.50) × 10^7
[**IXg**][CF_3SO_3]	1.22(0.55) × 10^8	6.44(0.62) × 10^6

Table 4.7: Anion binding constants determined by UV-Vis titration in thf.

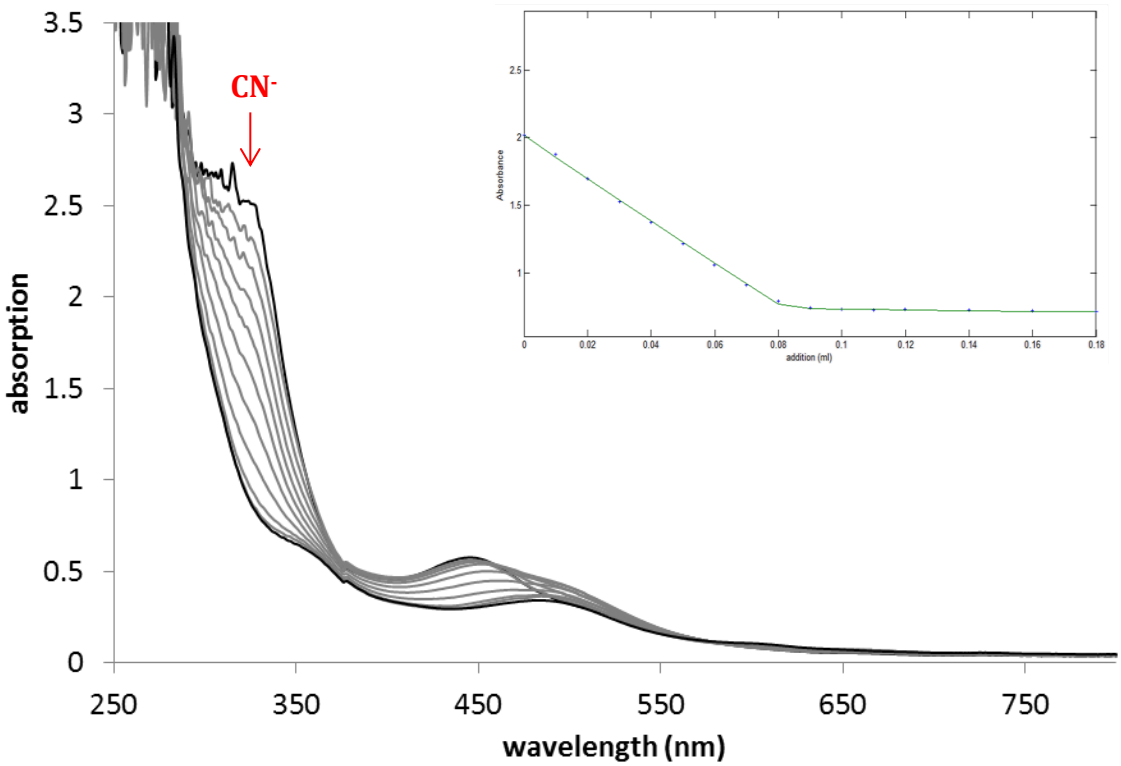

Figure 4.45: Changes in the UV-vis absorption spectra of a solution of [**VIIg**]I (3.0 mL, 1.02 × 10^{-4} M in thf) upon the addition of [^{n}Bu$_4$N][CN]·3H$_2$O (3.73 × 10^{-3} M in thf). Inset: fitting curves at 328 nm, log*K*(F)= 7.283 ± 0.131 (*σr*= 0.0189, *ssq*= 0.113).

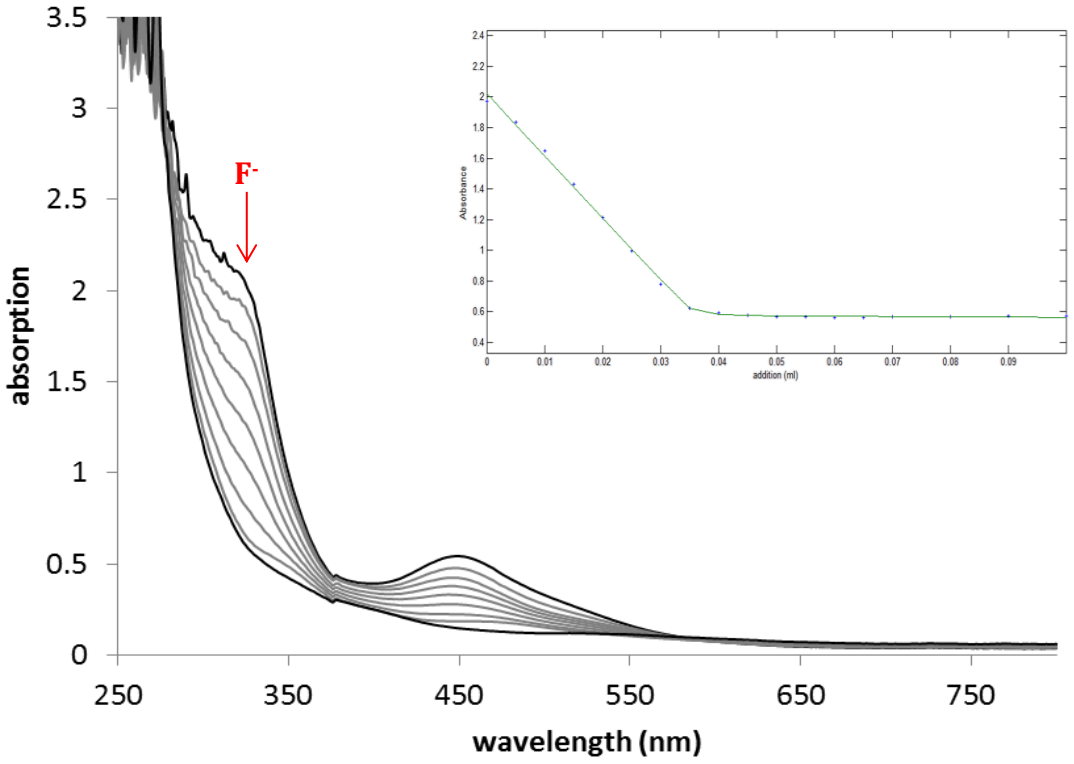

Figure 4.46: Changes in the UV-vis absorption spectra of a solution of [**VIIg**]I (3.0 mL, 9.40 × 10^{-5} M in thf) upon the addition of [^{n}Bu$_4$N]F·4H$_2$O (7.90 × 10^{-3} M in thf). Inset: curve ftting centred at 337 nm, log*K*(CN)= 7.840 ± 0.384 (*σr*= 0.0228, *ssq*= 0.156).

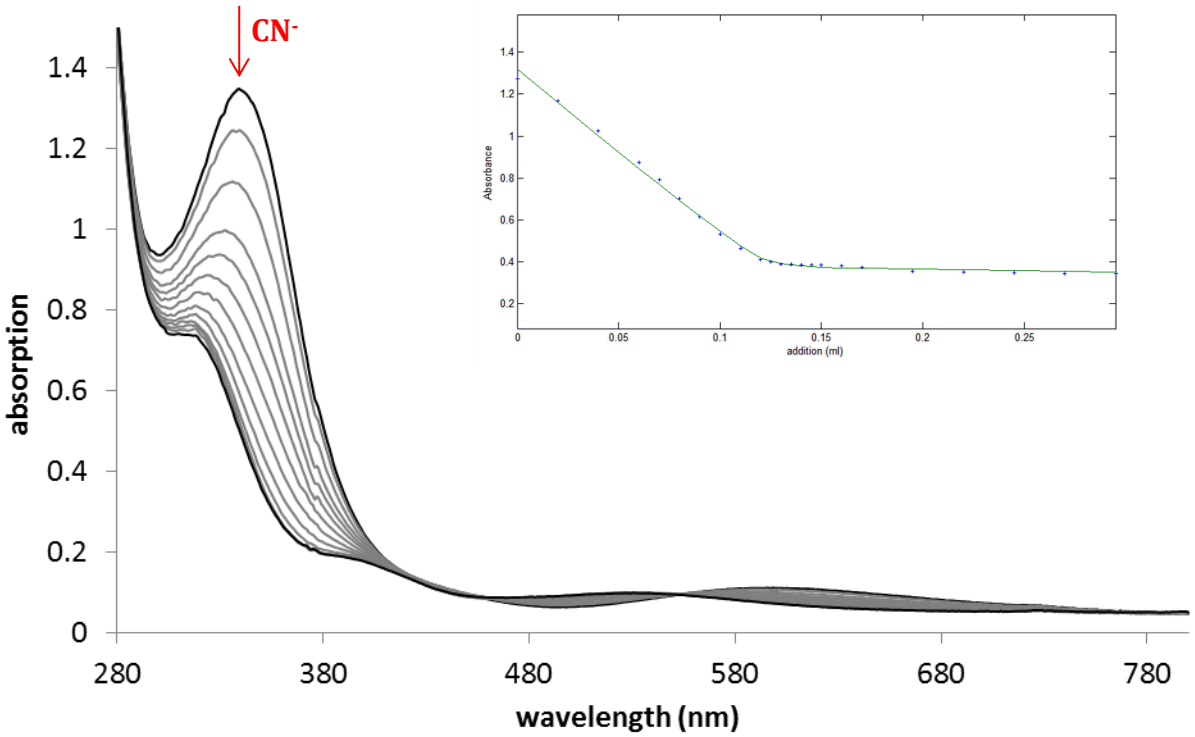

Figure 4.47: Changes in the UV-vis absorption spectra of a solution of [**IXg**][CF_3SO_3] (3 mL, 7.26×10^{-5} M in thf) upon the addition of [^{n}Bu$_4$N][CN]·3H_2O (1.78×10^{-3} M in thf). Inset: curve fitting centred at 351 nm log*K*(CN)= 6.809 ± 0.044 (*σr*= 0.0154, *ssq*= 0.367).

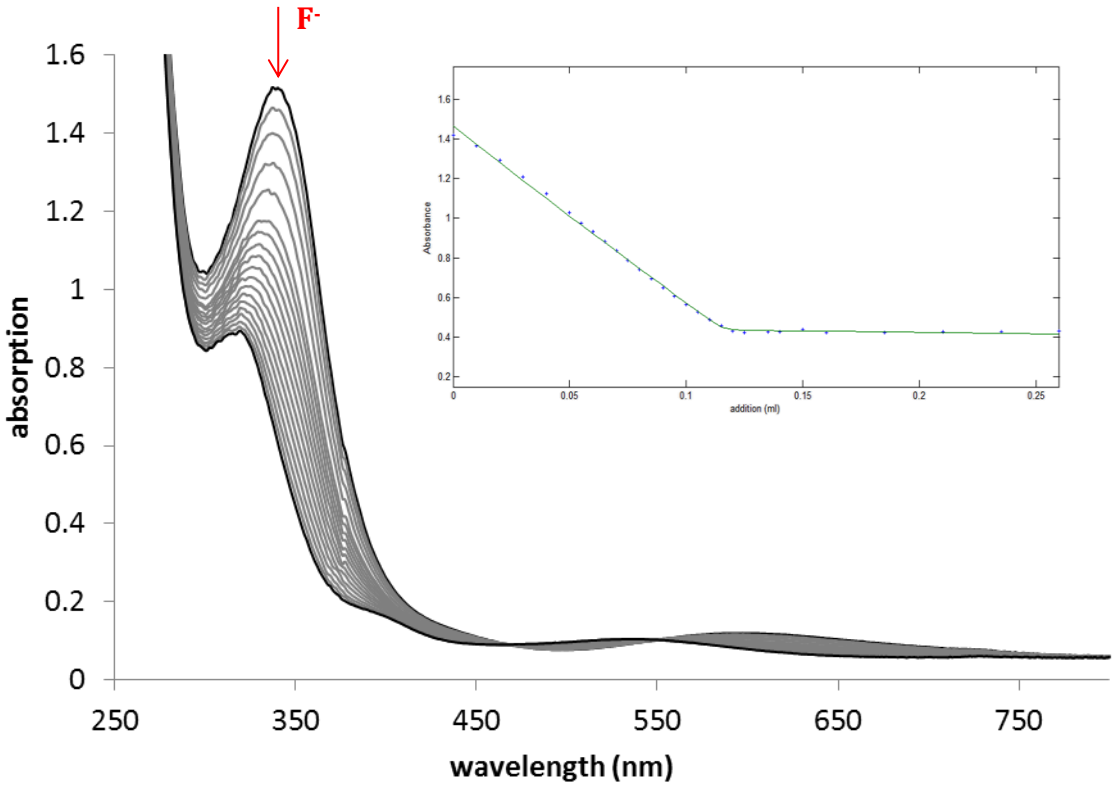

Figure 4.48: Changes in the UV-vis absorption spectra of a solution of [**IXg**][CF_3SO_3] (3.0 mL, 9.28×10^{-5} M in thf) upon the addition of [^{n}Bu$_4$N]F·4H_2O (2.40×10^{-3} M in thf). Inset: curve fitting centred at 351 nm, log*K*(F)= 8.085 ± 0.262 (*σr*= 0.0124, *ssq*= 0.172).

A general overview of all the binding constants for all of the receptors **IIa** to [**IXg**]$^+$ shows a clear increase of the association constant, from **II** to **IIIe** and **IVe** presumably as a result of the extension of the conjugated π-system. The incorporation of a cationic function, as in **VIIg**$^+$ and **IXg**$^+$ further enhances binding constants, by up to two orders of magnitude for the fluoride affinity (**IIIe**, logK_a(F) = 6.358(0.102); **IXg**$^+$, logK_a(F) = 8.085(0.262)). Moreover, the greater fluoride affinity observed for **IXg**$^+$ compared to **VIIg**$^+$ can be rationalised by a higher Lewis acidity in the case of **IXg**$^+$, based on the results from cyclic voltammetry and the LUMO energies derived from DFT. Furthermore, the chelation of fluoride by the boryl and cationic phosphonium functions in **IXg**$^+$ leads to a higher binding affinity for fluoride (logK_a(F) = 8.085 (0.262)) with respect to cyanide (logK_a(CN) = 6.809 (0.044)) (Table 4.7).

In general the binding constants of receptors [**VIIg**]I and [**IXg**][CF_3SO_3] are superior to [1,2-Fc($BMes_2$)(PPh_2Me)]$^+$ (**115**$^+$) and [1,1'-Fc($BMes_2$)(PPh_2Me)]$^+$ (**116**$^+$) (Figure 4.49). The change from a five- to a six-membered backbone ring clearly gives rise to a better pre-organized receptor geometry.

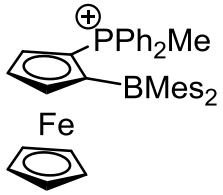

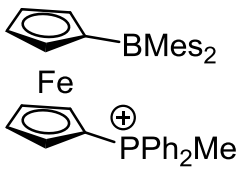

115$^+$
K(CN) = 1.0(0.4) x 10^6 M^{-1}
K(F) = 8.2(4.0) x 10^6 M^{-1}

116$^+$
K(CN) = 1.1(0.1) x 10^6 M^{-1}
K(F) =4.2(1.5) x 10^6 M^{-1}

Figure 4.49: Receptor **115**$^+$ and **116**$^+$ and their respective cyanide/fluoride binding constants in thf.[18]

From a detection perspective, the fixation of either cyanide or fluoride by the cationic receptors **VIIg**$^+$ and **IXg**$^+$ yields very noticeable colour changes; for instance 'free' **IXg**$^+$ is green (λ_{max} = 596 nm) whereas both the fluoride and cyanide adducts are purple (λ_{max} = 531

nm, Figure 4.50). **VIIg**$^+$ also undergoes a colour change upon fixation of these analytes, although the change is not so marked (Figure 4.51). Thus, the free receptor is a dark brown (λ_{max} = 445 nm) whilst the adducts are red (λ_{max} ~ 493 nm).

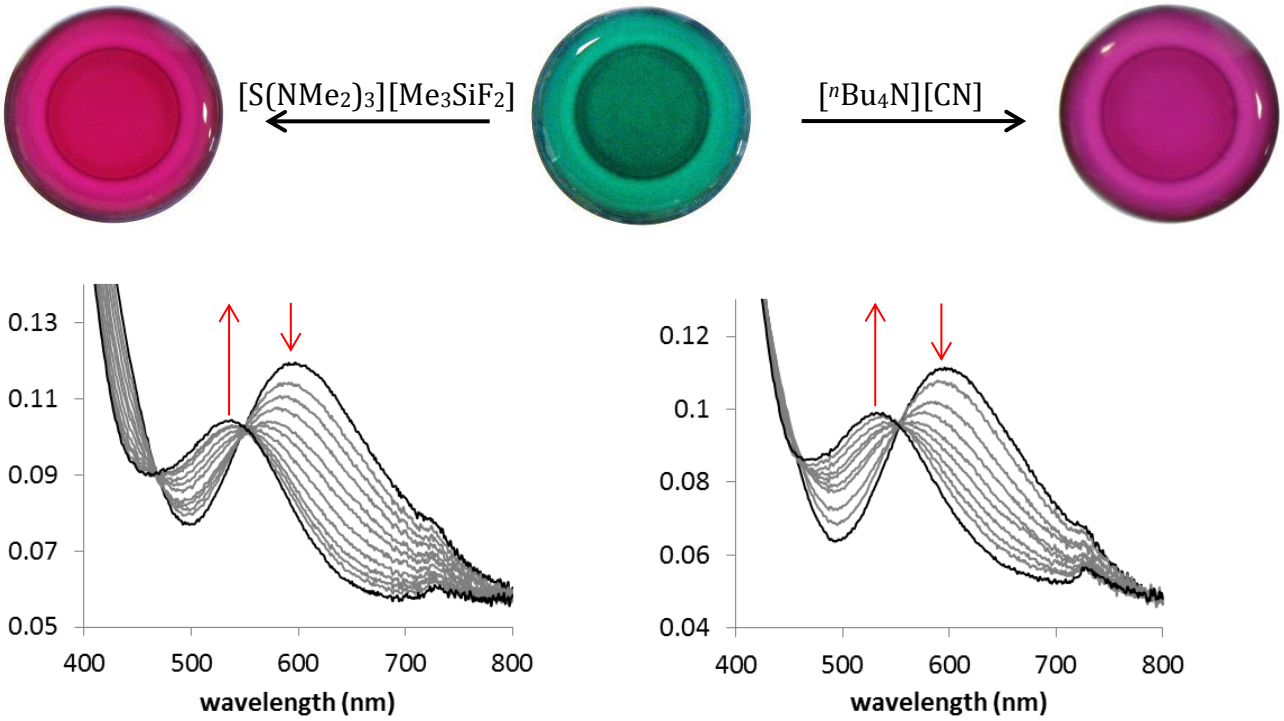

Figure 4.50: (*bottom*) Detail of [**IXg**][CF_3SO_3] spectrum upon addition of [^{n}Bu$_4$N][CN] or [S(NMe$_2$)$_3$][Me$_3$SiF$_2$], (*top*) colour change from [**IXg**][CF_3SO_3] to **IXg**·X (X = F or CN).

Figure 4.51: Colour change from the dark brown free receptor [**VIIXg**]I to the red adduct **VIIg**·X (X = F or CN).

Competition experiments for cyanide and fluoride were performed in deuterated chloroform for both **VIIg**$^+$ and **IXg**$^+$. In all cases, however, an excess of free cyanide or fluoride did not lead to the displacement of the previously bound cyanide or fluoride ion. This lack of

exchange is presumably kinetic in origin and can be accounted for by the high activation barriers, which in turn reflect the significant anion binding affinities of **VIIg**$^+$ and **IXg**$^+$ for both cyanide and fluoride. Treatment of either cationic species with a one-to-one mixture of fluoride and cyanide anions leads to the formation of *ca.* 45% of the cyanoborate and *ca.* 55% of the fluoroborate for both receptors. Here too, it is not possible to state definitively whether this is reflective of binding thermodynamics or kinetics, given the lack of reversible F^-/CN^- exchange.

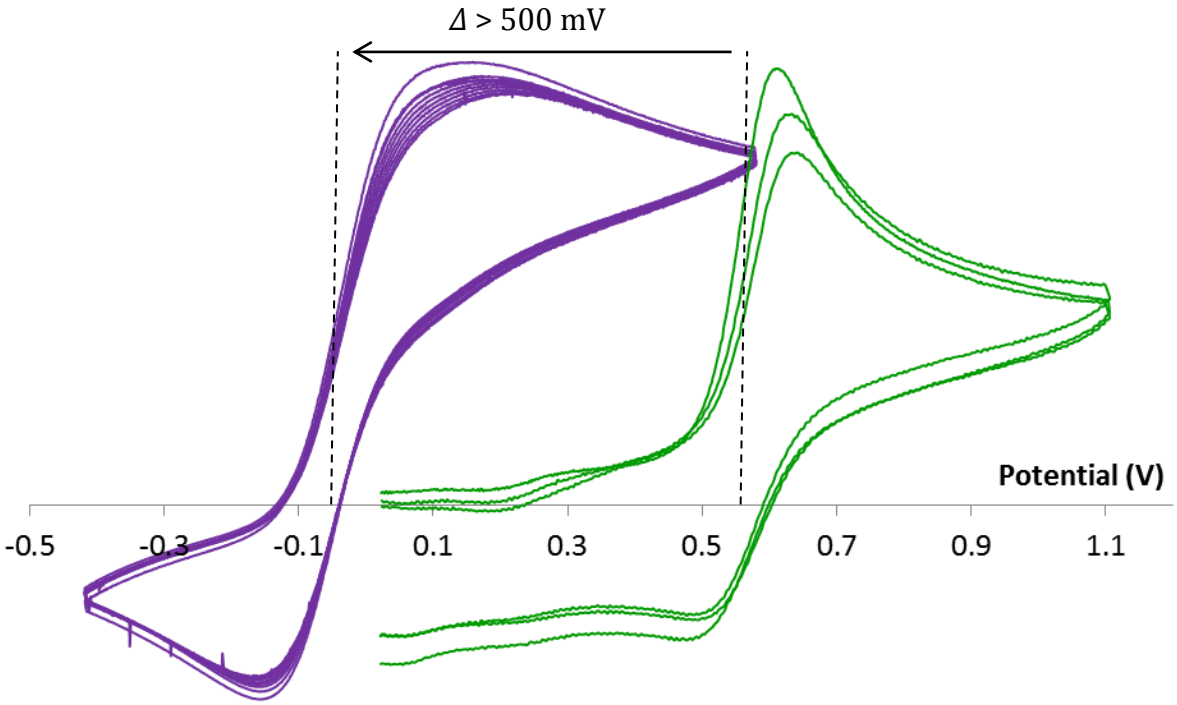

Figure 4.52: Cyclic voltammograms of [**IXg**][CF_3SO_3] (*green*) and **IXg**·F (*blue*) *vs* ferrocene / ferrocenium couple with 0.1 M [^{n}Bu$_4$N][PF_6] in acetonitrile (scan rate 0.1 V s^{-1}).

The complexation of the fluoride or cyanide ion by **IXg**$^+$ can also be monitored *via* the electrochemical potential of the iron centre. The large cathodic shift of at least -500 mV observed between the **IXg**$^+$ and **IXg**·F (Figure 4.52) is reflective of the incorporation of the electron rich fluoride at the Lewis acidic boron centre. Even though the redox process is not reversible for **IXg**·CN (Figure 4.53) a clear cathodic shift has occurred with waves centred around +120 mV with respect to the ferrocene/ferrocenium couple internal reference.

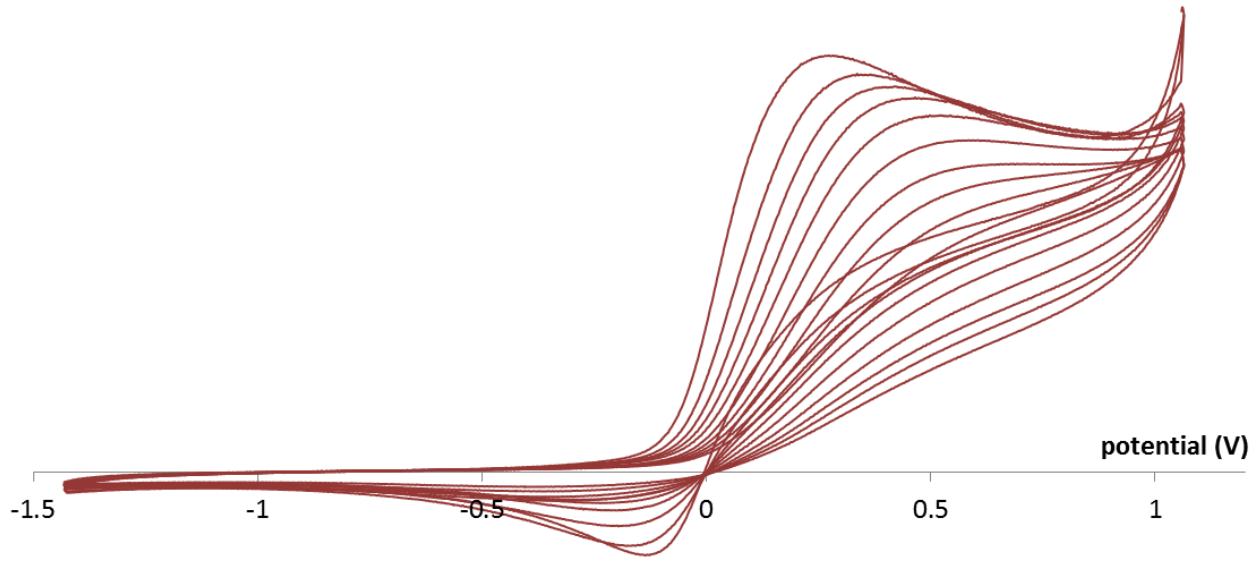

Figure 4.53: Cyclic voltammograms of **IXg**$^{\bullet}$CN *vs* ferrocene/ferrocenium couple with 0.1 M [^{n}Bu$_4$N][PF$_6$] in acetonitrile (scan rate 0.1 V s^{-1}).

In order to further the scope of the anion binding study, a series of tests in water and dimethylsulfoxide were performed. Although the control sample, as a 1:1 mixture of the receptor **IXg**$^{+}$ in thf and water, lead to a colour change. For instance, the ^{11}B NMR spectrum reveals a sharp peak at *ca.* δ_B -7 ppm upon addition of H_2O, consistent with the formation of a tetracoordinated boron. The same result was observed when dimethylsulfoxide was used as the solvent, probably due to trace amounts of water. The quenching of the boron centre by these two solvents could be attributed to a combination of a higher Lewis acidity of **IXg**$^{+}$ compared to the monodentate system from chapter 3 (**IIIe** and **IVe**).

4.5. Conclusions

The synthesis of bifunctional indenyl derived receptors has been attempted from both dichloro and dibromo precursors, with the latter proving to be the most amenable to contolled lithium/halogen exchange. Subsequent incorporation of a dimesitylboryl moiety,

however, renders these systems inert to further substitution of the remaining bromine atom. By contrast, phosphine borane receptors and their methylated phosphonium analogues can readily be synthesized through a synthetic approach which involves initial incorporation of a $-PPh_2$ unit.

A thorough spectroscopic study (X-ray crystallography and multinuclear NMR spectroscopy), was conducted on all four receptors (**VIIf**, **VIIg**$^+$, **IXf** and **IXg**$^+$), which highlighted the important steric loading around the phosphorus and boron centres. Cyclic voltammetry together with an examination of the frontier orbitals obtained by DFT calculations, further confirms the enhanced Lewis acidity of the phosphonium compounds over the phosphine borane precursor or the monodentate receptors of chapter 3.

Binding studies conducted with the phosphine borane receptors (**VIIf** and **IXf**) reveal a high selectivity for cyanide over fluoride. The lower basicity of the fluoride ion presumably does not compensate for the high energy penalty for the rearrangement of these sterically crowded systems on anion binding. The phosphonium derivatives do not apparently suffer from the same problem and were proven to fix both cyanide and fluoride, with a greater binding constant for the fluoride ion over cyanide. This selectivity can be attributed to a non-negligible interaction between the cationic phosphonium centre and fluoride (but not cyanide) as observed by ^{31}P and ^{19}F NMR spectroscopy, X-ray crystallography and DFT calculations (AIM).

4.6. References

(1) R. Altmann, K. Jurkschat, M. Schürmann, D. Dakternieks and A. Duthie, *Organometallics* **1998**, 17, 5858.

(2) K. Tamao, T. Hayashi and Y. Ito, *J Organomet. Chem.* **1996**, 506, 85.

(3) H. E. Katz, *J. Org. Chem.* **1985**, 50, 5027.

(4) (*a*) J. D. Hoefelmeyer and F. P. Gabbaï, *Organometallics* **2002**, 21, 982. (*b*) C. L. Dorsey, Pawel Jewula, T. W. Hudnall, J. D. Hoefelmeyer, T. J. Taylor, N. R. Honesty, C.-W. Chiu, M. Schulte and F. P. Gabbaï, *Dalton Trans.* **2008**, 4442. (*c*) M. Melaïmi, S. Solé, C.-W. Chiu, H. Wang and F. P. Gabbaï, *Inorg. Chem.* **2006**, 45, 8136. (*d*) S. Solé and F. P. Gabbaï, *Chem. Commun.* **2004**, 1284. (e) H. Zhao and F. P. Gabbaï, *Organometallics* **2012**, 31, 2327.

(5) (*a*) V. Clifford Williams, W. E. Piers, W. Clegg, M. R. J. Elsegood, S. Collins and T. B. Marder, *J. Am. Chem. Soc.* **1999,** *121,* 3244. (*b*) V. C. Williams, G. J. Irvine, W. E. Piers, Z. Li, S. Collins, W. Clegg, M. R. J. Elsegood and T. B. Marder, *Organometallics* **2000,** *19,* 1619. (*c*) S. P. Lewis, N. J. Taylor, W. E. Piers and S. Collins, *J. Am. Chem. Soc.* **2003**, 125, 14686. (*d*) P. A. Chase, L. D. Henderson, W. E. Piers, M. Parvez, W. Clegg and M. R. J. Elsegood, *Organometallics* **2006,** *25,* 349.

(6) (*a*) G. E. Herberich, A. Fischer and D. Wielbelhaus, *Organometallics* **1996**, 15, 3106. (*b*) G. E. Herberich, U. Englert, A. Fischer and D. Wiebelhaus, *Eur. J. Inorg. Chem.* **2004**, 4011.

(7) K. Tamao. T. Hayashi and Y. Ito, *J. Am. Chem. Soc.* **1990**, 112, 2424.

(8) A. Kawachi, A. Tani, J. Shimada and Y. Yamamoto, *J. Am. Chem. Soc.* **2008**, 130, 4222.

(9) Y. Kim, M. Kim and F. P. Gabbaï, *Org. Lett.* **2010**, 12, 600.

(10) (*a*) M. H. Lee, T. Agou, J. Kobayashi, T. Kawashima and F. P. Gabbaï, *Chem. Commun.* **2007**, 1133. (*b*) T. W. Hudnall, Y.-M. Kim, M. W. P. Beddington, D. Bourissou and F. P. Gabbaï, *J. Am. Chem. Soc.* **2008**, 130, 10890.

(11) (*a*) Y. Kim and F. P. Gabbaï, *J. Am. Chem. Soc.* **2009**, 131, 3363. (*b*) T. W. Hudnall and F. P. Gabbaï, *J. Am. Chem. Soc.* **2007**, 129, 11978.

(12) T. Sell, A Winter, M. Thorn, A. Dimeska, F. Langhauser, "New metallocene compounds, catalysts comprising them, process for producing an olefin polymer by use of the catalysts and olefin homo and copolymers", *WO2010/077230*, 8th July **2010**.

(13) D. R. Boyd, N. D. Sharma, N. I. Bowers, R. Boyle J. S. Harrison, K. Lee, T. D. H. Bugg, D. T. Gibson, *Org. Biomol. Chem.* **2003**, 1, 1298.

(14) A. Pelter, B. Singaram, L. Warren and J. W. Wilson, *Tetrahedron* **1993**, 49, 2965.

(15) (*a*) G. Wittig and F. Bickelhaupt, *Chem. Ber.* **1958**, 91, 883. (*b*) H. J. S. Winkler, and G. Wittig, *J. Org. Chem.* **1963**, 28, 1733.

(16) K. Durka, S. Lulinski, M. Dabrowski and J. Serwatowski, *Eur. J. Org. Chem.* **2014**, 4562.

(17) H. F. Bettinger and M. Filthaus, *J. Org. Chem.* **2007**, 72, 9750.

(18) M. J. Kelly, DPhil thesis: "*Hybrid Ferrocene-Based Systems*", October **2014**, Oxford University, Oxford, UK.

(19) I. R. Morgan, A. E. J. Broomsgrove, P. Fitzpatrick, D. Vidovic, A. L. Thompson, I. A. Fallis, and S. Aldridge, *Organometallics* **2010**, 29, 4762.

(20) M. Mantina, A. C. Chamberlin, R. Valero, C. J. Cramer and D. G. Truhlar, *J. Phys. Chem. A* **2009**, 113, 5806.

CHAPTER 5: Electron deficient boranes and activation of molecular oxygen

5.1. Introduction

Hydrogen peroxide, a simple multipurpose reagent, has had a rebirth in both industrial processes and academic research in recent years. Its industrial manufacture dates back to 1818, when L. J. Thenard treated barium peroxide with nitric acid to produce a low concentration of aqueous hydrogen peroxide.[1] Since then, commercial production has been optimised and rendered safer, following the ever-growing effort of "green chemistry". The array of applications of H_2O_2 is also expanding out of the traditional confines of the bleaching of wood pulp or the manufacture of pharmaceutical and fine chemicals. Thus, hydrogen peroxide is used in the manufacture of propellants (*e.g.* in the Soyuz launch vehicle)[2], mining (ore leaching), for recycling solar panels (*i.e.* recovery of indium, gallium, selenium *etc.*), food processing (*e.g.* preservation of natural proteins), electronics (cleaning agent) and in environmental applications (*e.g.* waste water treatment).[3]

5.1.1 Industrial production of hydrogen peroxide

The annual global production of H_2O_2 in 2012 was of the order of 4.2 million tonnes (*cf.* 0.705 million tonnes in 2008). This major growth of H_2O_2 production is driven by the introduction of new environmental regulations including the Elemental Chlorine Free (ECF) processes mandated by the Environment Protection Agency (EPA) in the United States.[4]

The autoxidation of anthrahydroquinone remains to date the main process for the manufacture of aqueous hydrogen peroxide on an industrial scale,[5] although between 1957 and 1980 Shell employed a process discovered by Harris in 1945, involving the autoxidation of propanol to form hydrogen peroxide and the associated ketone.[6]

5.1.2 Activation of oxygen by transition metals: Nature vs man-made

Whilst the industrial production of peroxides has flourished since the 1960s', aerobic organisms including, but not limited to, the human species have been producing peroxides for the past 1.5 billion years.[7] The eukaryotes managed to spread into a relatively dioxygen rich environment because of their capacity to use molecular oxygen for the oxidation of glucose, which provided a reliable source of energy (*i.e.* ATP formation). This is where the work of metalloenzymes comes into play, with one or more redox metal centres (e.g. Fe, Cu, Mn, Ni or Mo).[8] In the large array of metalloenzymes one can find the *photosystem II* protein[9] from thylakoids with an intermediate manganese-peroxide species; *hemerythrin*[10] from marine worms that reversibly binds dioxygen and *cytochrome c oxidase*, the last enzyme in the respiratory electron transport chain of mitochondria, which features a heme-peroxo-copper centre (Figure 5.1).[11]

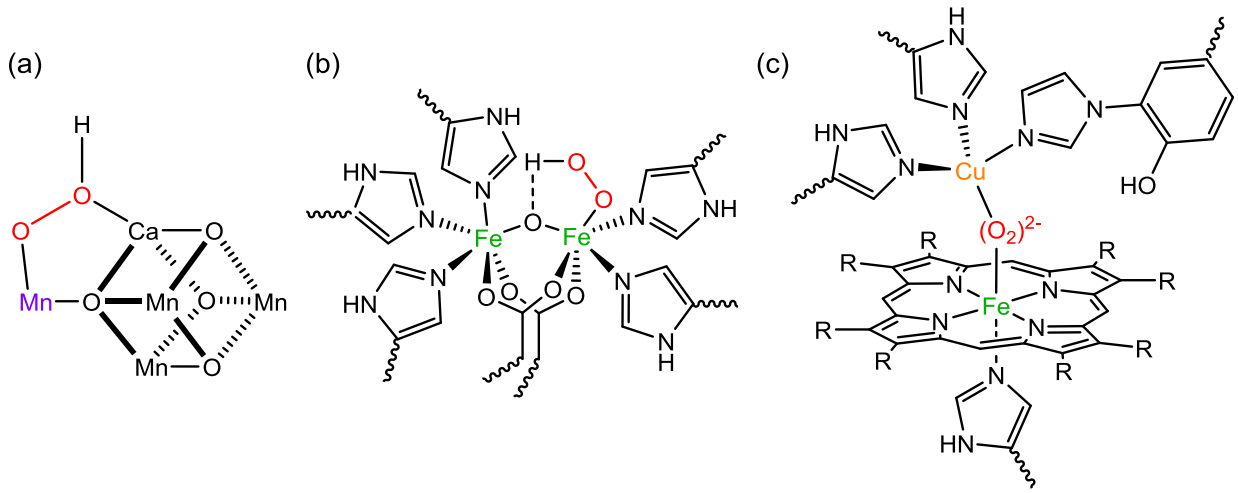

Figure 5.1: Examples of metalloenzymes for the activation of dioxygen into peroxide: (*a*) *Photosystem II*, (*b*) *hemerythrin* and (*c*) *Cytochrome c oxidase*.

A large amount of research has been conducted on organic reactions of singlet oxygen, and their mechanisms and pathways are well known.[12] At the same time exploration from an inorganic/organometallic perspective appears to be a path less travelled; nonetheless a range of metal centres has been exploited for the activation of dioxygen.[8] Thus, for example, Vaska's complex were among the first to be implicated in the oxidative addition of singlet oxygen.[13]

In certain systems the activation of molecular oxygen is not complete, leading to the formation of a superoxide, as for example seen in chromium(II) complex **117**$^{+}$ synthesized by Theopold and co-workers (Figure 5.2).[14] These authors exposed [**117**][BAr$^{f}_{4}$] to an excess of O_2 at -78° C which led to a rapid colour change from blue to red. The solid-state IR spectrum shows a $\nu(^{16}O—^{16}O)$ vibration at 1071 cm^{-1}, which is shifted to 1007 cm^{-1} upon treatment with $^{18}O_2$. The magnetic moment measured for [**117**$\cdot\eta^2$-O_2]BAr^{F} (μ_{eff}(295 K) = 2.8(1) μ_B) can then be accounted for by antiferromagnetic coupling between the Cr^{III} ion (d^3, S = 3/2) and the coordinated superoxide (S = 1/2). The crystal structure of [**117**$\cdot\eta^2$-O_2] [BAr$^{f}_{4}$] confirms the presence of a Cr^{III}-superoxo adduct featuring "side-on" binding and a O1—O2 distance of 1.327(5) Å which fall within the expected superoxo range.[14]

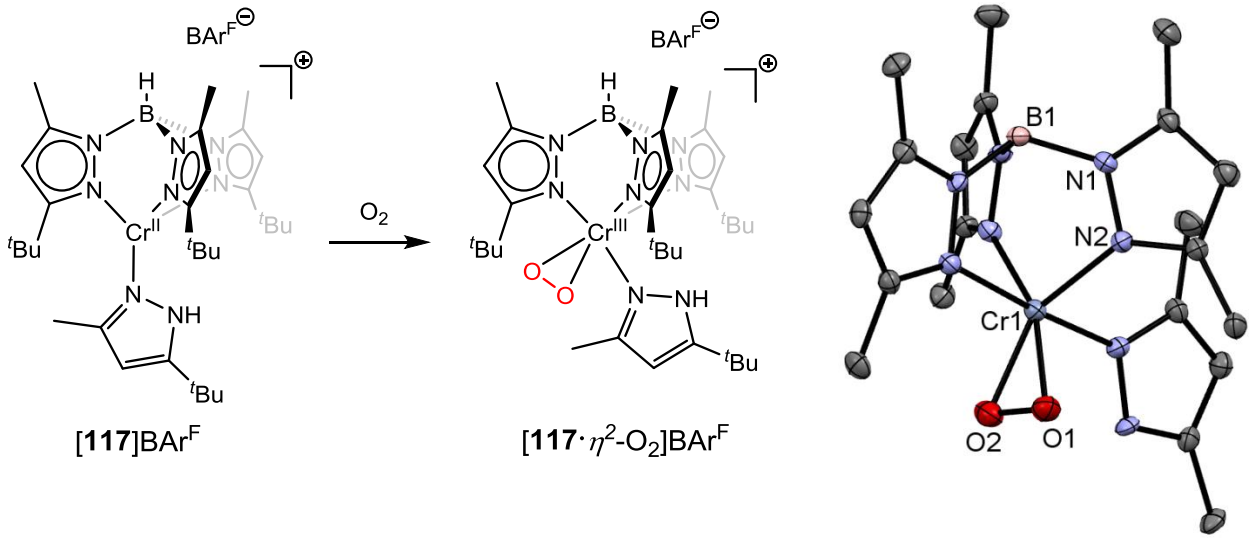

Figure 5.2: (*left*) Reaction of [**117**]BAr^{F} with dioxygen. (*right*) Molecular structure of [**117**$\cdot\eta^2$-O_2][BAr$^{f}_{4}$]. The [BAr$^{f}_{4}$] counterion, *tert*-butyl groups, dichloromethane solvate and hydrogen atoms omitted for clarity (red: oxygen, dark blue: chromium, blue: nitrogen, black: carbon, light pink: boron).

Finally several research groups have been engaged in mimicking the reactivity of metalloenzymes in order to better understand the catalytic cycles involved in *Photosystem II* or *haemoglobin*, for instance.[15] With such ideas in mind different sizes of the macrocyclic *N*-tetramethylated cyclams (TMC) have been extensively used to replace a porphyrin like ligand in the synthesis of a range of 3*d* metal peroxo complexes (Figure 5.3).

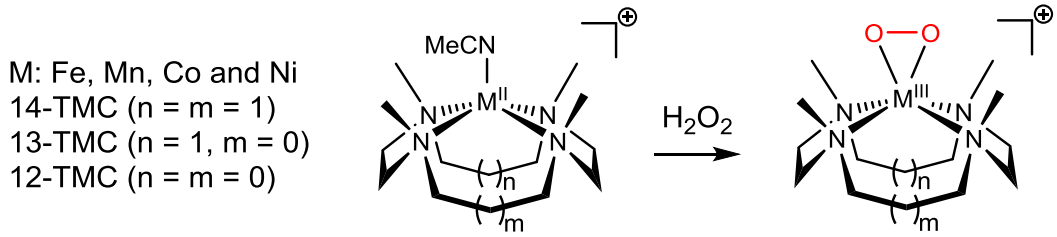

Figure 5.3: Synthetic route for metal-peroxo complexes (**118** – **125**) with hydrogen peroxide treatment.

While TMC complexes featuring Mn(II),[16] Fe(II),[17] Co(II)[18] and Ni(II)[19] do not react with O_2 to form the peroxo adduct, such systems can be obtained by using H_2O_2 as the oxygen source. The η^2-peroxo metal complexes **118** to **125**, have O—O distances ranging from 1.383(4) to 1.403(4) Å, depending on the metal ion and ring size (Table 5.1). A linear correlation can be established between the $\nu(^{16}O—^{16}O)$ vibrations (from 825 to 1131 cm^{-1}) and the O—O bond distance, consistent with the extent of reduction of the O_2 unit.

#	Compound	O—O distance [Å]	$\nu(^{16}O—^{16}O)$ ($\nu(^{18}O—^{18}O)$) [cm^{-1}]
118	$[Mn(13\text{-}TMC)O_2]^+$	1.410(4)	-
119	$[Mn(14\text{-}TMC)O_2]^+$	1.403(4)	-
120	$[Fe(13\text{-}TMC)O_2]^+$	1.463(6)	825(781)
121	$[Co(12\text{-}TMC)O_2]^+$	1.4389(17)	902(845)
122	$[Co(13\text{-}TMC)O_2]^+$	1.438(4)	902(846)
123	$[Ni(12\text{-}TMC)O_2]^+$	1.386(4)	1002(945)
124	$[Ni(13\text{-}TMC)O_2]^+$	1.383(4)	1008(950)
125	$[Ni(14\text{-}TMC)O_2]^+$	-	1131(1067)

Table 5.1: X-ray and Raman data for metal-peroxo and superoxo complexes **118** to **125**.

5.1.3 Group 13 compounds for the activation of oxygen

As early as 1907, sodium perborate (Na_2[**126**]) in combination with sodium silicate was used as a detergent and sold by Henkel under the brand name "Persil" (Figure 5.4).

Sodium perborate is isolated from the reaction of borax with hydrogen peroxide and sodium hydroxide (Figure 5.4); the chair-shaped 6-membered ring is composed of two boron atoms bridged with two peroxo units.

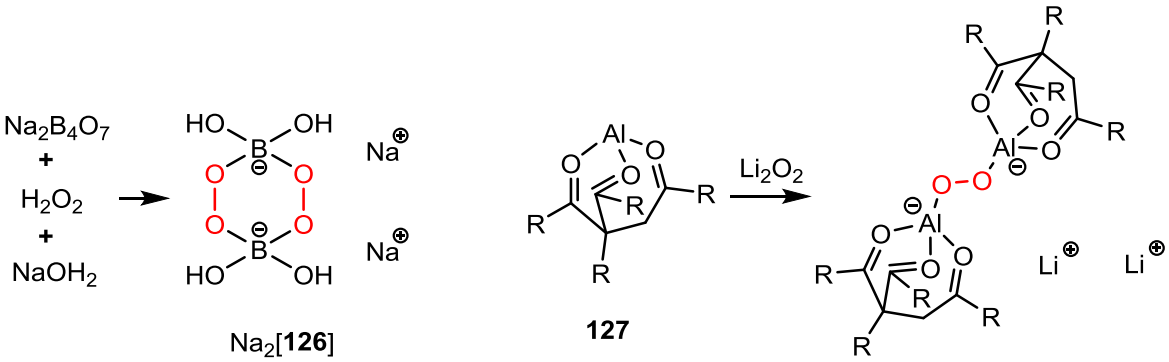

Figure 5.4: Formation of sodium perborate and Na_2[**126**] and reaction of **127** within a Li-battery.

More recently the use of aluminium and boron containing reagents has been employed in order to increase the solubility of certain anions (such as F^-, O^{2-}, O_2^{2-}, CN^-, N_3^- etc.) in aprotic polar solvents at lower temperatures without using costly complexing agents (*e.g.* crown-ethers or cryptands).[20] For instance, Li_2[(**127**)$_2$(μ_2-O_2)] can be obtained after treatment of **127** with lithium peroxide and can then be used in lithium-air batteries. The increased solubility at the cathode of the Li_2O_2 by-product in the presence of **127** limits the power loss between the charge and discharge phases of the Li-battery.[21]

The inherent mismatch between strongly reducing M—C bonds and highly oxidising peroxo group renders the isolation of peroxo complexes difficult.[22] Nonetheless a small number have been isolated after controlled exposure of organo-gallium or -indium compounds to oxygen.[23,24] Persistent alkyl-aluminium or gallium peroxides have been prepared, but only a limited number of alkyl-boron peroxides have been reported. First, in 2009, Piers *et al.* published a report of the reaction of dioxygen with a 9-boraanthracene derivative stabilized by an N-Heterocyclic carbenes (**128**).[25] Dioxygen is quantitatively added across the anthracene skeleton as shown by NMR spectroscopy and X-ray crystallography

(Figure 5.5). The O1—O2 bond distance of 1.456 Å is consistent with a endo-bound peroxo moiety.

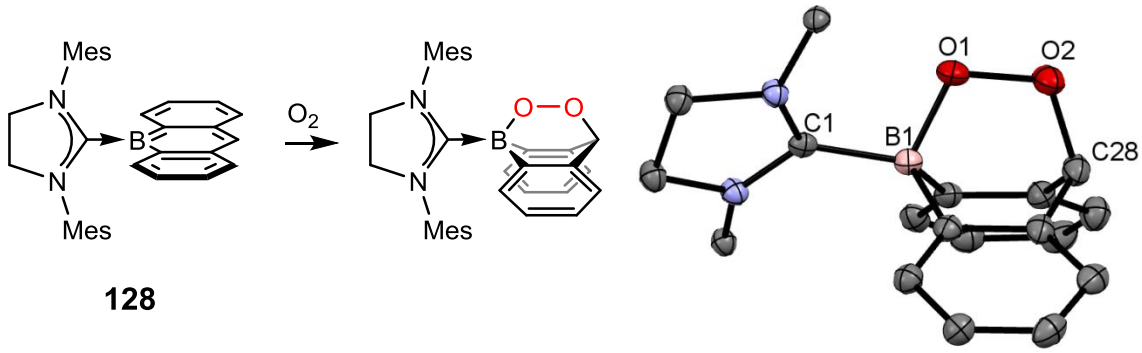

128

Figure 5.5: (*left*) reaction of **128** with molecular oxygen. (*right*) Molecular structure of **128** peroxo adduct. Mesityl ligand and hydrogen atoms have been omitted for clarity. Selected bond lengths [Å] and angles [°]: O1—O2 1.456(2), O1—B1 1.527(3), O2—C28 1.461(3), O2—O1—B1 112.54(14), O1—O2—C28 110.33(14).

5.2. Aims

Interest in sterically hindered Lewis acids and bases was renewed by Stephan's 2006 paper on the activation of small molecules by a "Frustrated Lewis Pair" (FLP).[26] Originally first observed by Brown in 1943 with 2,6-dimethyl pyridine and trimethyl borane, sterically crowded Lewis pairs can be prevented from forming a classical donor-acceptor adduct.[27] The unquenched reactivity of both moieties can be used for the cleavage or trapping of molecules such as CO_2 or N_2O.[28,29] The latter for example, can be trapped intact by a combination of tri-*tert*-butyl phosphine and the highly Lewis acidic tris(pentafluorobenzene)borane.[30] With the aim of developing a chemical detector for nitrous oxide, a ferrocene moiety was introduced into the borane component, and the Lewis acid **129** exploited in an FLP system with P^tBu_3 (Figure 5.6).[31] On exposure to N_2O the formation of a PNNOB linkage can be demonstrated unequivocally by the X-ray crystal structure for the solid state at least (Figure 5.7), and its generation in solution can be monitored by either UV-vis spectroscopy (Figure 5.6) or cyclic voltammetry.[31]

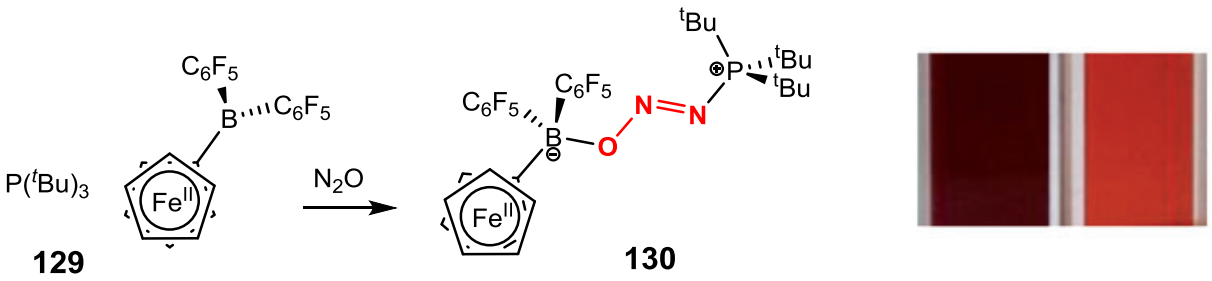

Figure 5.6: (*left*) Trapping of N_2O by the FLP system P(^{t}Bu)$_3$/**129** (*right*) colour before and after addition of N_2O.

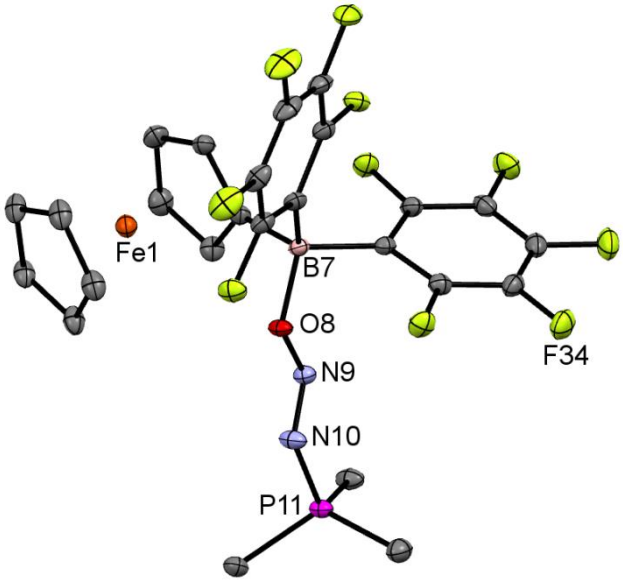

Figure 5.7: Molecular structure of **130**. Thermal ellipsoids set at the 50% probability level; hydrogen atoms, *tert*-butyl units and benzene solvent molecules are omitted for clarity (light pink: boron, yellow: fluoride; black: carbon; orange: iron; red: oxygen; blue: nitrogen; magenta: phosphorus).

The detection of other small molecules is important, and following the work conducted by Bourissou and co-workers, molecular oxygen was viewed as one of the target analytes. These authors used a phosphine-borane derivative (**131**) to trap O_2, although not through the formation of a simple adduct (Figure 5.8).[32] Instead, **132** was formed (as determined by multinuclear NMR spectra and X-ray crystallography) which features a P—O bond with the other oxygen atom inserted into a B—C(Mes) linkage.

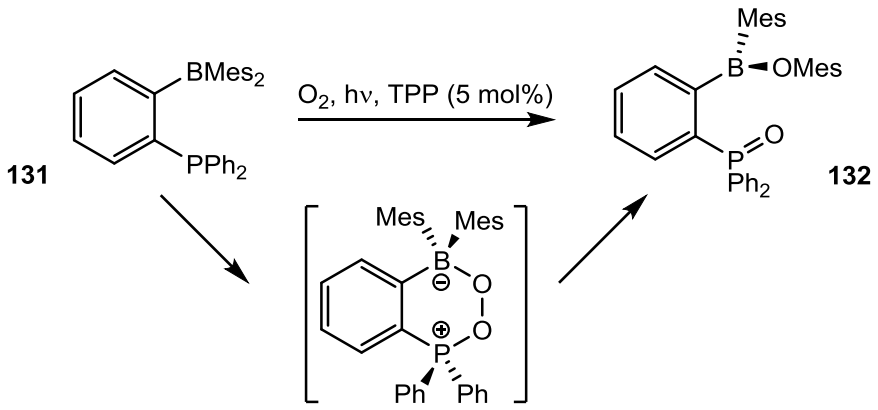

Figure 5.8: Fixation of $^1O_2$ by the phosphine borane **131**.

The Lewis acid **129** features the markedly more electron deficient C_6F_5 substituent at boron, and might therefore be less prone to aryl substituent migration than **131**. As such **129** might be exploited in the isolation of μ_2-O_2 containing moiety. However, during preliminary tests of the **129**/P(^{t}Bu)$_3$ system with oxygen, the formation of an unexpected B(μ_2-O_2)B containing product was observed instead (Figure 5.9).

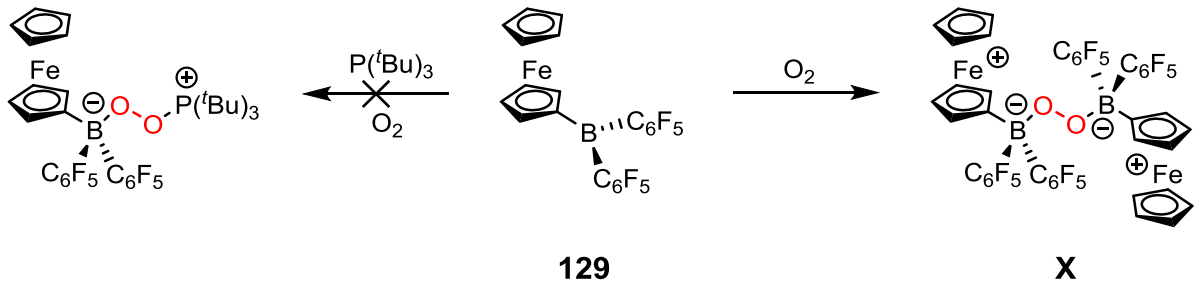

129 **X**

Figure 5.9: Formation of the B(μ_2-O_2)B derivative **X** on reaction of FcB(C_6F_5)$_2$ (**129**) with O_2.

5.3. Experimental

*FcB(C_6F_5)$_2$ (**129**)*

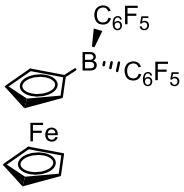

Following a procedure modified from that reported by Piers and co-workers,[33] ^{n}BuLi (17.5 mL of a 1.6 M solution in hexanes, 28 mmol) was added dropwise to a solution of 1-bromo-2,3,4,5,6-pentafluorobenzene (3.47 mL, 28 mmol) in hexane at -78˚C. The resulting mixture was stirred at -78˚C for a further 45 min and a solution of $FcBBr_2$ (5.00 g, 14 mmol) in hexane (150 mL) was then added dropwise at -78 ˚C. After warming to room temperature over a period of 12 h, volatiles were removed in vacuo and the residue was extracted with hexane. The combined organic extracts were concentrated in vacuo and the residue cooled to -20 ˚C to yield maroon crystals. Yield 4.80 g, 65%. ^{1}H, ^{11}B and ^{19}F NMR spectra were in agreement with literature data.[33]

*[(FcB(C$_6$F$_5$)$_2$)$_2$(μ$_2$-O$_2$)] (**X**)*

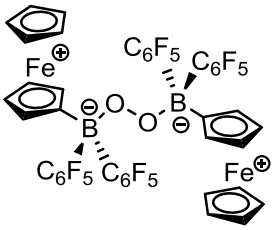

A solution of **129** (200 mg, 0.38 mmol) dissolved in benzene (50 mL), was freeze-pump-thaw degassed three times. The reaction vessel was then back-filled with oxygen (1 Bar) and the solution slowly changed colour from red to dark green. Crystals suitable for X-ray crystallography were obtained from a concentrated solution of benzene at room temperature. Yield: 337 mg, 81 %.

^{19}F NMR (282 MHz, thf-d$_8$, 25 °C): δ -157.4 (*b s*), -163.5 (*b s*), 168.5 (*b s*). ♦ ^{11}B{^{1}H} NMR (96 MHz, thf-d$_8$, 20˚C): -20. ♦ MS (EI+), *m*/*z* (%): 1114.9 ([M+Na]$^+$, 5%), accurate mass (calc. for [M+Na]$^+$, ^{54}Fe and ^{10}B isotopomer) 1114.9781 (meas.) 1114.9753, isotopic pattern correct for $C_{44}H_{18}B_2F_{20}Fe_2O_2$. ♦ Elemental analysis: calc. for $C_{44}H_{18}B_2F_{20}Fe_2O_2$, C 47.40%; H 1.60%; meas. C 47.29%; H 1.35%. ♦ UV-vis (thf): λ_{max} = 634 nm. ♦ Crystallographic data: $C_{68}H_{42}B_2F_{20}Fe_2O_2$, M_r = 1404.36, triclinic, *P-1*, *a* = 10.6265(2) Å, *b* = 11.7123(2) Å, *c* = 13.0807(3) Å, α =

84.5195(7)°, β = 79.0018(8)°, γ = 68.6912(8)°, V = 1488.27(5) Å^3, Z = 1, T = 150 K, λ = 0.71073 Å. 44062 reflections collected, 6651 independent [R(int) = 0.0737] used in all calculations, with 424 least-squares parameters, GOF on F^2 = 0.9419. R_1 = 0.0431, wR_2 = 0.0832 for observed unique reflections [I>2σ(I)] and R_1 = 0.0738, wR_2 = 0.1068 for all unique reflections. Max. and min. residual electron densities 0.62 and -0.70 e Å^{-3}.

$[CoCp_2]_2[(B(C_6F_5)_3)_2(\mu_2\text{-}O_2)]$ ***(XIc)***

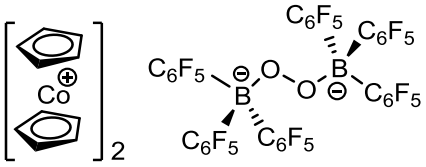

Cobaltocene (92 mg, 0.49 mmol) and tris(pentafluorobenzene)borane (250 mg, 0.49 mmol) were dissolved in dichloromethane (50 mL) solvent which had previously been saturated with oxygen. The solution changed colour from a dark orange to a pale yellow. The side product **XII** was filtered off, and the solvent removed in vacuo yield a yellow solid. Yield: 467 mg, 67 %.

^{1}H NMR (400 MHz, thf-d_8, 25 °C): δ 5.67 (*s*, 10H, Cp) ♦ ^{11}B NMR (128 MHz, thf-d_8, 25 °C): δ - 25. ♦ ^{19}F NMR (376 MHz, thf-d_8, 25 °C): δ – 168.7 (*t*, $^3J_{FF}$ = 20.40 Hz, 6F, *meta*-F of C_6F_5), - 166.1 (*t*, $^3J_{FF}$ = 19.60 Hz, 6F, *meta*-F of C_6F_5), -133.4 (*t*, $^3J_{FF}$ = 18.0 Hz, 6F, *meta*-F of C_6F_5). ♦ ^{13}C NMR (100 MHz, thf-d_8, 25 °C): δ 85.7 ($CoCp_2^+$), 126.9 (*b s*, *ipso*-C of C_6F_5 bound to B), 137.1 (*d*, $^1J_{CF}$ = 245 Hz, *meta*-C of C_6F_5), 138.6 (*d*, $^1J_{CF}$ = 242 Hz, *para*-C of C_6F_5), 149.2 (*d*, $^1J_{CF}$ = 227 Hz, *ortho*-C of C_6F_5).

$[CoCp_2(B(C_6F_5)_3)]$ ***(XII)***

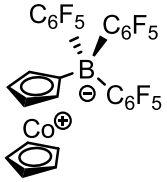

Cobaltocene (45 mg, 0.24 mmol) and tris(pentafluorobenzene)borane (125 mg, 0.24 mmol) were dissolved in benzene (20 mL). Crystals formed over 24 h, which were isolated by filtration and washed several times yielding a yellow solid. Yield: 52 mg, 31 %.

^{1}H NMR (400 MHz, $CDCl_3$, 25 °C): δ 5.19 (*s*, 5H, Cp), 5.39 and 5.47 (*s*, each 2H, C_5H_4), 7.26 ($CHCl_3$). ♦ ^{11}B NMR (128 MHz, $CDCl_3$, 25 °C): δ – 15. ♦ ^{19}F NMR (376 MHz, $CDCl_3$, 25 °C): δ – 164.7 (*t*, $^{3}J_{FF}$ = 23.4 Hz, 6F, *meta*-F of C_6F_5), - 159.5 (*t*, $^{3}J_{FF}$ = 20.7 Hz, 3F, *para*-F of C_6F_5), - 128.8 (*d*, $^{3}J_{FF}$ = 23.6 Hz, 6F, *ortho*-F of C_6F_5). ♦ ^{13}C NMR (100 MHz, $CDCl_3$, 25 °C): δ 81.4(C of C_5H_4), 83.5 (Cp), 84.6 (C of C_5H_4), 90.3 (quaternary C of C_5H_4 bound to B), 136.8 (*d*, $^{1}J_{CF}$ = 237 Hz, *meta*-C of C_6F_5), 138.9 (*d*, $^{1}J_{CF}$ = 240 Hz, *para*-C of C_6F_5), 148.4 (*d*, $^{1}J_{CF}$ = 237 Hz, *ortho*-C of C_6F_5), signal for quaternary C of C_6F_5 bound to B was not measured. ♦ Anal. calcd for $C_{28}H_9BCoF_{15}$•(chloroform)$_{0.1}$ C, 47.40%; H 1.29%. Found: C, 47.41%; H, 1.23%. ♦ MS (EI$^+$), *m/z* (%): 698.0 (100%), accurate mass (calc. for M^+, ^{10}B isotopomer) 697.9782 (meas.) 697.9847, isotopic pattern correct for $C_{28}H_9BCoF_{15}$. ♦ Crystallographic data: $C_{28}H_9BCoF_{15}$, M_r = 700.09, monoclinic, $P2_1/n$, a = 15.9483(4) Å, b = 10.0778(2) Å, c = 16.3340(4) Å, α =90°, β = 110.768(3)°, γ = 90°, V = 2454.68(11) Å^3, Z = 4, T = 150 K, λ = 1.54180 Å. 18330 reflections collected, 5130 independent [R(int) = 0.0404] used in all calculations, with 406 least-squares parameters, GOF on F^2 = 0.9880. R_1 = 0.0330, wR_2 = 0.0762 for observed unique reflections [I>2σ(I)] and R_1 = 0.0404, wR_2 = 0.0817 for all unique reflections. Max. and min. residual electron densities 0.36 and -0.46 e Å^{-3}.

*[TMPP][$(C_6F_5)OB(C_6F_5)_3$] ([TMPP]**XIII**)*

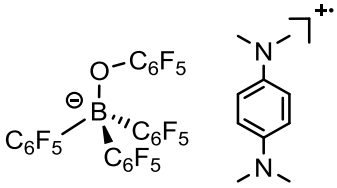

Tetramethyl-*p*-phenylenediamine (80 mg, 0.49 mmol) and tris(pentafluorophenyl)borane (250 mg, 0.49 mmol) were dissolved in dichloromethane (60 mL). The pale yellow solution was freeze-pump-thaw degassed three times and back-filled with oxygen. The resulting blue solution was concentrated to 15 mL and layered with heptane. After *ca*. 1 month a small number of red crystals of [TMPP]**XIII** suitable for X-ray crystallography were obtained.

MS (ESI-), *m/z* (%): 695.0 (100.0%), accurate mass (calc. for M-) 694.9733 (meas.) 694.9728, isotopic pattern correct for $C_{24}BF_{20}O$. ♦ MS (ESI-), *m/z* (%): 165.1 (100.0%). ♦ Crystallographic data: $C_{34}H_{16}BF_{20}N_2O$, M_r = 859.28, triclinic, *P-1*, *a* = 10.5963(2) Å, *b* = 18.2458(3) Å, *c* = 18.9346(4) Å, α = 111.7472(19)°, β = 93.9189(18)°, γ = 97.9516(15)°, *V* = 3338.96(12) Å^3, *Z* = 4, *T* = 150 K, λ = 1.54180 Å. 55033 reflections collected, 13967 independent [R(int) = 0.025] used in all calculations, with 1045 least-squares parameters, GOF on F^2 = 0.9994. R_1 = 0.0758, wR_2 = 0.2095 for observed unique reflections [I>2σ(I)] and R_1 = 0.0792, wR_2 = 0.2127 for all unique reflections. Max. and min. residual electron densities 1.76 and -0.58 e Å^{-3}.

*[TTF][$(C_6F_5)OB(C_6F_5)_3$] ([TTF]**XIII**)*

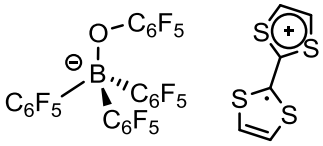

Tetrathiafulvalene (50 mg, 0.24 mmol) and tris(pentafluorophenyl)borane (125 mg, 0.24 mmol) were dissolved in dichloromethane (30 mL). The pale yellow solution was freeze-pump-thaw three degassed times and the reaction vessel back-filled with oxygen. The resulting dark orange solution was concentrated to 10 mL and layered with heptane. After *ca*. 1 month a small number of red crystals of [TTF]**XIII** suitable for X-ray crystallography were obtained.

Crystallographic data: $C_{30}H_4BF_{20}OS_4$, M_r = 899.40, triclinic, *P-1*, *a* = 9.9027(3) Å, *b* = 12.1839(4) Å, *c* = 13.4425(4) Å, α = 83.583(3)°, β = 81.596(3)°, γ = 79.910(2)°, *V* = 1573.46(9) Å^3, *Z* = 2, *T* = 150 K, λ = 1.54180 Å. 15579 reflections collected, 6480 independent [R(int) = 0.017] used in all calculations, with 505 least-squares parameters, GOF on F^2 = 1.0037. R_1 = 0.0415, wR_2 = 0.1079 for observed unique reflections [$I>2\sigma(I)$] and R_1 = 0.0428, wR_2 = 0.1090 for all unique reflections. Max. and min. residual electron densities 0.53 and -1.03 e Å^{-3}.

5.4. Results and discussion

5.4.1 Synthesis of $(FcB(C_6F_5)_2)_2(\mu_2\text{-}O_2)$

The Lewis acid **129** was synthesised *via* a modified literature procedure: treatment of ferrocene with boron tribromide yields $FcBBr_2$,[34] and the target compound was isolated after subsequent treatment with LiC_6F_5 at low temperature, and purified by recrystallization.[33] Exposure of a solution of **129** in benzene to an atmosphere of dry dioxygen is accompanied by a relatively slow change of colour of the solution from dark red (λ_{max} = 231 nm) to army green (λ_{max} = 634 nm), from which acicular crystals of the peroxo adduct **X** can be isolated. **X** was thus initially identified by X-ray crystallography (Figure 5.10), and shown to contain a centrosymmetric entity featuring two $FcB(C_6F_5)_2$ units bridged by an O_2 moiety. The boron atoms have evidently been pyramidalized during O_2 uptake ($\sum_{CBC}$ = 329.6°), with a slight elongation of the B—C bonds also accompanying this process (**144**: B—Cp 1.501(4) Å, B—C_6F_5 1.604(4) and 1.584(4) Å; **X**: B—Cp 1.624(4) Å, B—C_6F_5 1.662(4) and 1.669(4) Å).[33] The $FcB(C_6F_5)_2$ units are oriented trans to each other across the peroxo unit presumably on steric grounds (Figure 5.10). The O—O bond distance is 1.484(3) Å, which is consistent with the formation of a peroxide bridge, which together with the charge neutral nature of the overall species implies oxidation of both iron centres from Fe(II) to Fe(III).

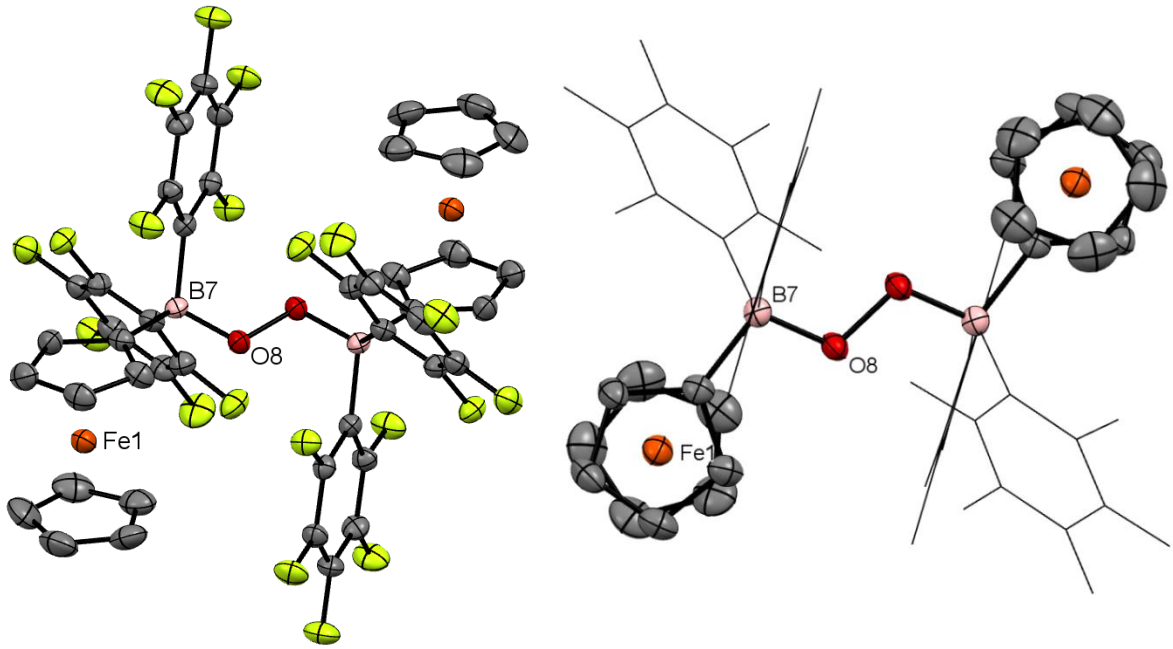

Figure 5.10: Molecular structure of **X**. Thermal ellipsoids set at the 50% probability level; hydrogen atoms and benzene solvent molecules omitted for clarity (light pink: boron, yellow: fluoride; black: carbon; orange: iron; red: oxygen). Selected bond lengths [Å] and angles [°]: B7—O8 1.467(3), B7—C9 1.662(4), B7—C20 1.669(4), B7—C3 1.624(4), O8—O8* 1.484(3), C3—B7—C9 112.2(2), C3—B7—C20 110.0(2), C9—B7—C20 107.4(2).

The formation of paramagnetic ferrocenium centres is consistent with the absence of any discernible peaks around δ_B 4 ppm in the ^{1}H NMR spectrum; nevertheless a clear shift was observed in the ^{11}B NMR spectrum from δ_B 53 ppm for **129** to δ_B -21 ppm for compound **X**. The corresponding ^{19}F NMR signals of the perfluorinated rings also feature large shifts upon fixation of the peroxide moiety (**129**: δ_F −127.9, −160.1 and −164.5 ppm; **X**: δ_F -157.4, -163.5 and 168.5 ppm).

The formation of the Fe(III) centres can be confirmed by EPR measurements: the g values ($g_\parallel$ = 4.2 and $g_\perp$ = 1.6) extrapolated from the data shown in Figure 5.11 are consistent with axial symmetry and fall within the range of known ferrocenium derivatives (*e.g.* ferrocenium, $g_\parallel$ = 4.6 and $g_\perp$ = 1.95; decamethylferrocenium, $g_\parallel$ = 4.43 and $g_\perp$ = 1.35).[35,36] Raman spectroscopy measurements in the solid state and in solution were attempted but unfortunately compound **X** was revealed to be too unstable under any excitation regime (λ_{laser}

= 1024, 785, 627 and 532 nm). Burn patterns are invariably observed when the laser beam was focused on the sample (even at λ_{laser} = 1024 nm) as shown in Figure 5.12.

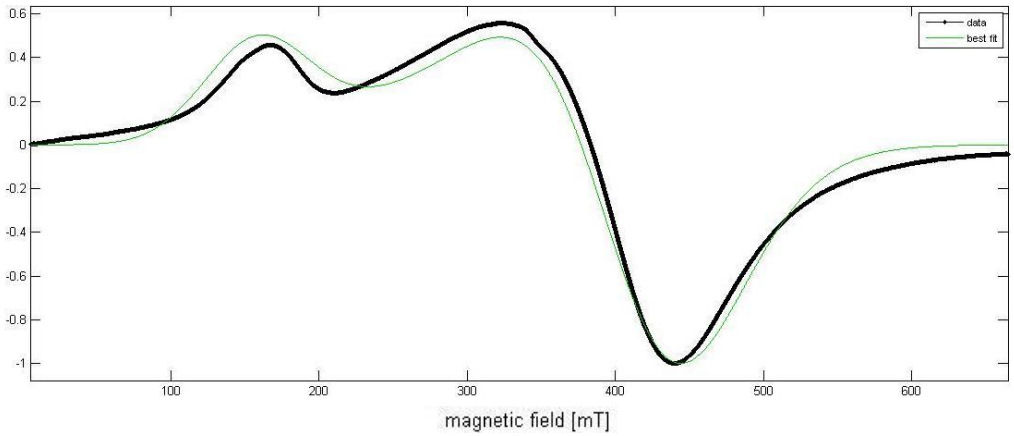

Figure 5.11: EPR spectrum of **X**: black curve correspond to the recorded data and green is the best fit.

Figure 5.12: Compound **X** under a 1064 nm laser for attempted solid-state resonance Raman spectroscopy measurements.

To obtain further evidence for a bisferrocenium peroxide formulation, DFT calculations were performed on compound **X**. In addition to reproducing closely the experimentally determined molecular geometry, the electronic structure of **X** was found to feature a HOMO (-5.15 eV, 49% *p*-character) which is the π^*(O—O) orbital lying out of the BO_2B plan, while a second π^*(O—O) orbital is stabilized by the interaction with the boron

atoms and thus lies lower in energy (HOMO-35, -5.65 eV, 57% *p*-character) (Figure 5.13). As such, these calculations are consistent with a formulation based on an O_2^{2-} bridge with a single bond between the two oxygen atoms.

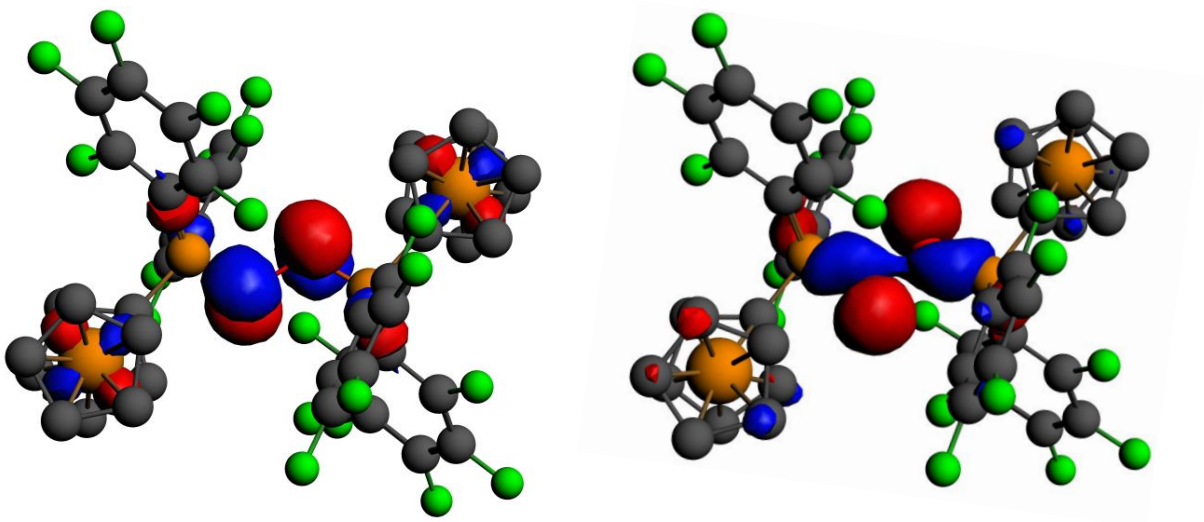

HOMO (-5.15 eV) HOMO-35 (-7.23 eV)

Figure 5.13: Representation of the filled π^*(O—O) orbitals in **X**: HOMO and HOMO-35 (density isovalues = 0.03).

A potential pathway leading to the formation of compound **X** is outlined in Figure 5.14. Unlike the boraanthracene system developed by Piers *et al.* where the formation of the peroxo unit could be achieved by thermal activation of singlet oxygen,[33] the formation of **X** is presumably intimately linked to the redox chemistry of the ferrocene centre. Molecular oxygen in close contact with the Lewis acidic boron centre in **129** could potentially be reduced to superoxide by the proximal iron centre, generating a superoxide ($O_2^{-\bullet}$) moiety with stronger Lewis basic donor properties that is captured by the borane. The process could be repeated with a second ferrocenyl borane molecule leading to the formation of **X**. In order to investigate the wider scope of such chemistry further experiments were conducted utilizing different metal centres and/or Lewis acidic boranes.

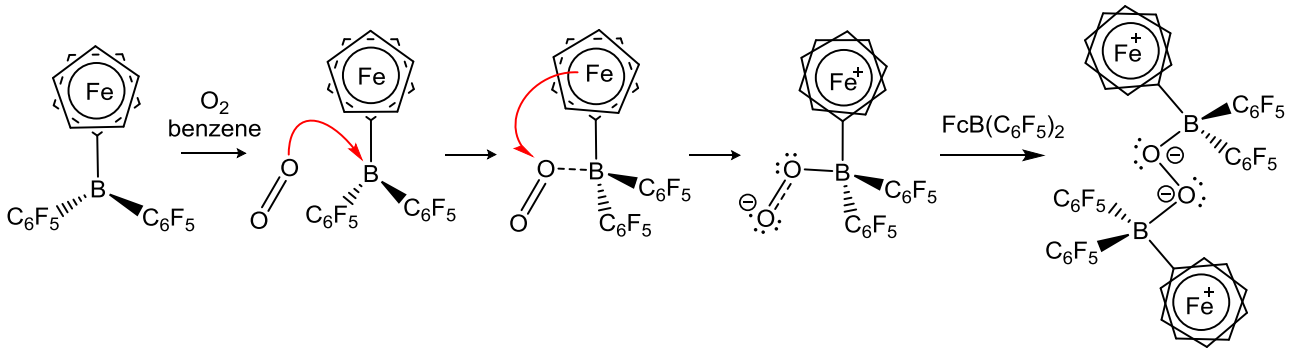

Figure 5.14: Proposed mechanism for the formation of compound **X.**

5.4.2 Studies of borane Lewis acidity and metallocene redox chemistry

The basic components of an oxygen reduction/capture system could be defined as a reducing metallocene and a Lewis acid. With regard to the former, ferrocene and cobaltocene were studied; ferrocene is conveniently air and moisture stable while cobaltocene was chosen for its strong reduction potential and its diamagnetic oxidized counterpart which, it was hoped, would facilitate characterisation of the product by NMR methods. Several Lewis acids were considered, from Krossing's Lewis superacid, $[Al(OC(CF_3)_3)_3]$, to tris(mesityl)borane, $BMes_3$. The synthesis of $[Fc]_2[(C_6F_5)_3B(\mu_2\text{-}O_2)B(C_6F_5)_3]$ (**XIa**) starting from ferrocene, tris(pentafluorobenzene)borane ($B(C_6F_5)_3$) was the first system to be probed. Multinuclear NMR spectroscopies reveal no visible change in either the ^{1}H, ^{19}F or ^{11}B NMR spectrum when both reactants are mixed together in the absence of O_2. Furthermore UV-vis spectroscopy shows no evidence of a shift in the absorption when compared to ferrocene (λ_{max} = 440 nm, Fe(III) *d-d* transitions).[37] On introduction of dioxygen into the system this band is red shifted to λ_{max} = 662 nm in a matter of seconds (Figure 5.15).

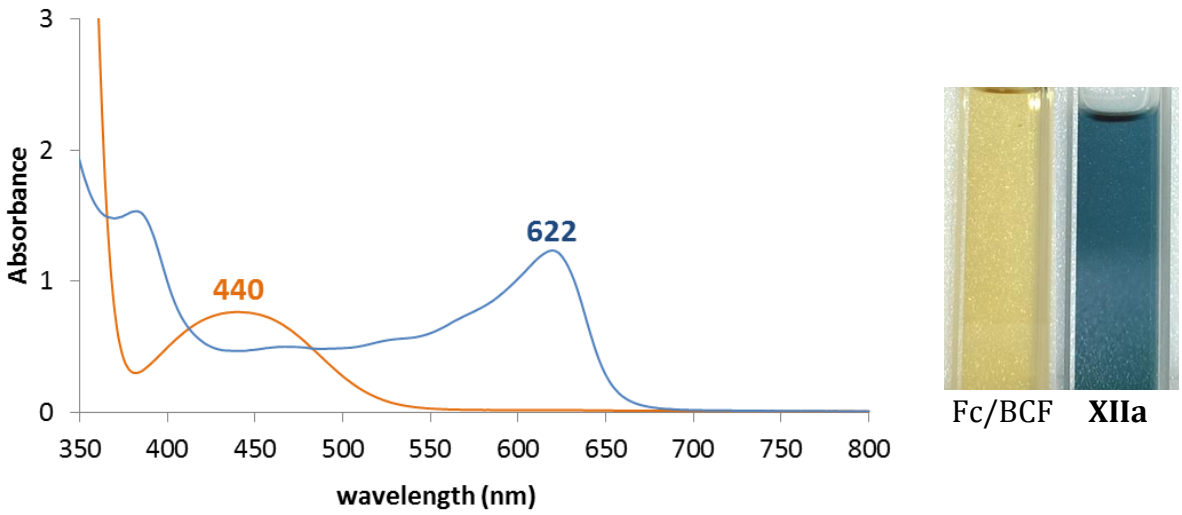

Figure 5.15: UV vis spectrum of ferrocene and tris(pentafluorobenzene)borane before (*orange curve*) and after (*blue curve*) exposure to one atmosphere of oxygen.

In addition, the reaction can be followed by either ^{19}F or ^{11}B NMR spectroscopy; the signal at δ_B 60 ppm shifts to δ_B -8 ppm (along with minor components at δ_B -3 and 2 ppm) consistent with the formation of borate species. Positive ion mass spectrometry reveals the presence of the ferrocenium ion (Figure 5.16), while the negative ion mode features several decomposition/fragmentation products, resulting either from splitting of the peroxo bridge or ligand scrambling (*e.g.* $(C_6F_5)O(B(C_6F_5)_3)$). Unfortunately Raman spectroscopy yielded similar results as found with compound **X**, in that the product burned before any data could be obtained, due to the absorption at λ = 622 nm (log ε = 4.1).

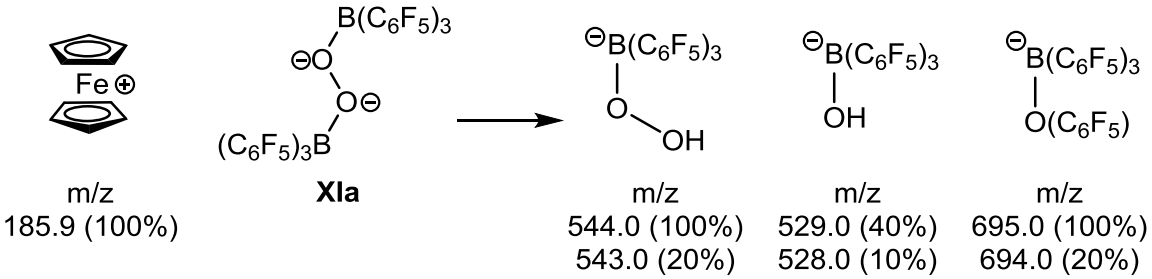

Figure 5.16: By-products of the formation of **XIa** identified by mass spectroscopy.

The control reactions shown in Figure 5.17 were conducted to insure that the formation of **XIa** arises from a cooperative interaction between ferrocene and $B(C_6F_5)_3$.

Oxygen was introduced to vessels containing ferrocene or $B(C_6F_5)_3$ and after 48 hours no reaction could be observed by NMR spectroscopy in any case. Thus the presence of both the metallocene and Lewis acid is necessary for O_2 reduction.

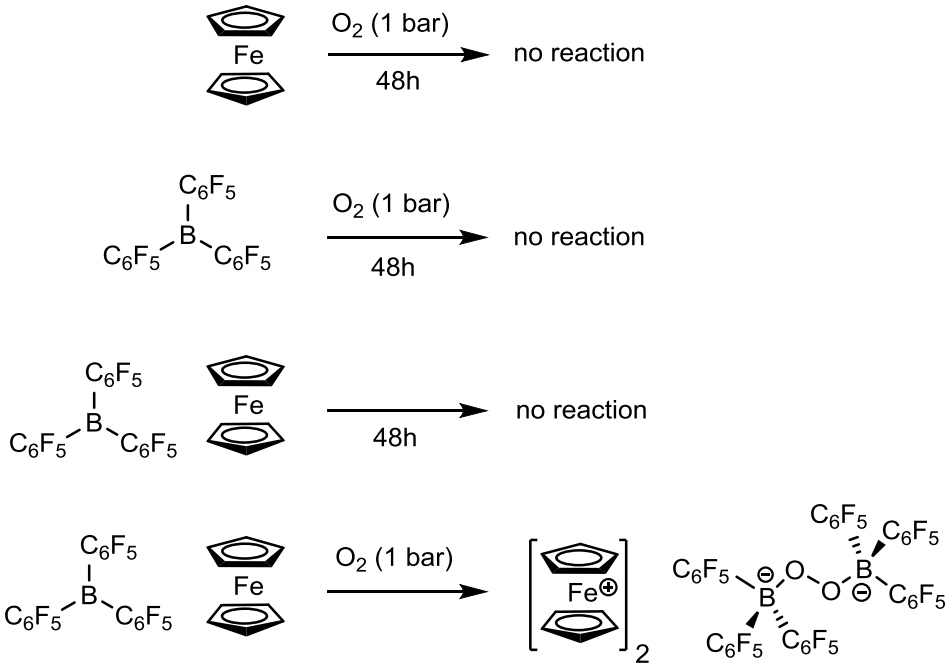

Figure 5.17: Control reactions and formation of compound **XIa**.

Although the formation of the radical anion $B(C_6F_5)^{-\bullet}$ has been reported in presence of the much more reducing metallocene decamethylcobaltocene, there is no evidence by EPR of the formation of the same radical anion with ferrocene.[38] Moreover, a one-electron transfer from ferrocene to $B(C_6F_5)_3$ appears incompatible with the relevant electrode potentials, *i.e.* $E°(B(C_6F_5)_3^{-\bullet}/B(C_6F_5)_3)$ = -1.18 V *vs* the ferrocene / ferrocenium couple in dichloromethane. In addition, a similar argument can be made concerning the one electron oxidation of ferrocene by molecular dioxygen ($E°(O_2^{-\bullet}/O_2)$ = -1.79 V *vs* the ferrocene / ferrocenium couple in DMSO.[39]

While this work was in progress, the formation of the peroxo compound $[Fc]_2[(C_6F_5)_3B(\mu_2\text{-}O_2)B(C_6F_5)_3]$ (**XIa**), was confirmed by X-ray crystallography by Agapie *et al.* (published in September 2014).[40] The authors also isolated single crystals of the analogous

compound **XIb** derived from decamethylferrocene (Fc*). The geometry and bond lengths in **XIa** and **XIb** around the boron centre are similar to that measured in the peroxo adduct **X**, moreover the O—O bond distance is about 1.48 Å for all three compounds (**X**: 1.484(3) Å, **XIa**: 1.488(7) Å, **XIb**: 1.4849(17) Å).

Agapie *et al.* draw attention on the fact that inner-sphere and outer-sphere activation of O_2 by ferrocenes has been proposed in the past. In the first case, the interaction of molecular oxygen with different organometallic complexes was explored by IR spectroscopy at very low temperatures (*i.e.* 16 K). Direct interaction between ferrocene and molecular oxygen is subjected to the pH of the environment, for instance ferrocenium salts can be isolated from the oxidation of ferrocene in concentrated sulphuric acid.[41] Bitterwolf and Campbelling proposed the protonation of the iron centre to be the first step in these reactions; followed by insertion of O_2 into the Fe—H bond leading to the loss of $HO_2^{\bullet}$ and formation of the stable ferrocenium cation.[42] However this process is unlikely to be applicable for the formation of **XI**.

An outer-sphere electron transfer between decamethyl-ferrocene and O_2 has been studied by Song *et al.* in ionic liquids.[43] These authors demonstrated the acceleration by imidazolium ionic liquids of the electron transfer from decamethyl-ferrocene and decamethyl-cobaltocene to dioxygen *via* the stabilization of the oxygen radical by an acidic C—H bond. Thus, a series of cyclic voltammograms were measured to assess the effect of the strong Lewis acid $B(C_6F_5)_3$ on electron transfer thermodynamics. The reduction of O_2 was monitored in dichloromethane with $[^nBu_4N][B(C_6F_5)_4]$ as a supporting electrolyte (Figure 5.18), and gives rise to an irreversible wave around -1.8 V vs the ferrocene / ferrocenium couple. Introduction of $B(C_6F_5)_3$ leads to the formation of two quasi reversible waves (at best); the first centred around -1.7 V is assigned to the $O_2^{-\bullet}/O_2$ reduction wave overlapping with the formation of the radical anion $B(C_6F_5)_3^{-\bullet}$. The second wave appears around -1.0 V, and can tentatively be

attributed to the reduction of dioxygen in close contact with the electron withdrawing borane. Furthermore measurements carried out at lower scan rates (under 0.1 mV sec^{-1}), did not feature the oxidation process of $O_2^{-\bullet}$ at -1.0 V as the radical $[B(C_6F_5)_3{\cdot}O_2]^{-\bullet}$ is likely to be very labile. This result is consistent with the experiments conducted by Qu and co-workers with $B(C_6F_5)_3$ and $O_2^{-\bullet}$.[44] The authors demonstrated that generation of $O_2^{-\bullet}$ in presence of $B(C_6F_5)_3$ will lead to the formation of the disproportionation products O_2 and O_2^{2-}, with the latter rapidly trapped by $B(C_6F_5)_3$ to form the peroxoborate adduct.[44]

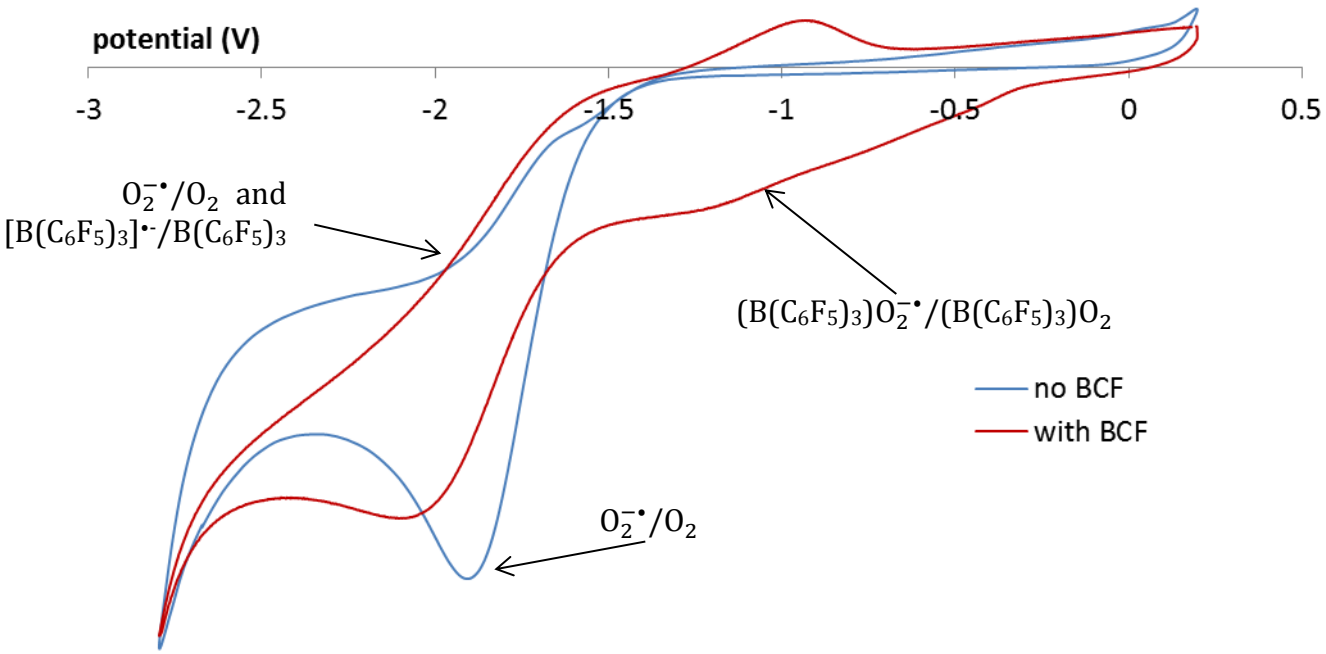

Figure 5.18: Cyclic voltammograms of dichloromethane saturated with oxygen (*blue curves*) and with tris(pentafluorobenzene)borane (*red curves*) with 0.1 M $[^nBu_4N][B(C_6F_5)_4]$ as a supporting electrolyte (scan rate 0.5 V s^{-1}) referenced *vs* ferrocene/ferrocenium.

The addition of $B(C_6F_5)_3$ to the electrochemical cell does not seem to affect the redox potential of ferrocene (Figure 5.19). Thus the reduction of $B(C_6F_5)_3$ under such conditions came in the same range to published results under similar conditions ($E°(B(C_6F_5)_3^{-\bullet}/B(C_6F_5)_3)$ = -1.97(0.1) V *vs* ferrocene/ferrocenium in dichloromethane with 0.1 M $[^nBu_4N][BAr^F{}_{24}]$).[39b]

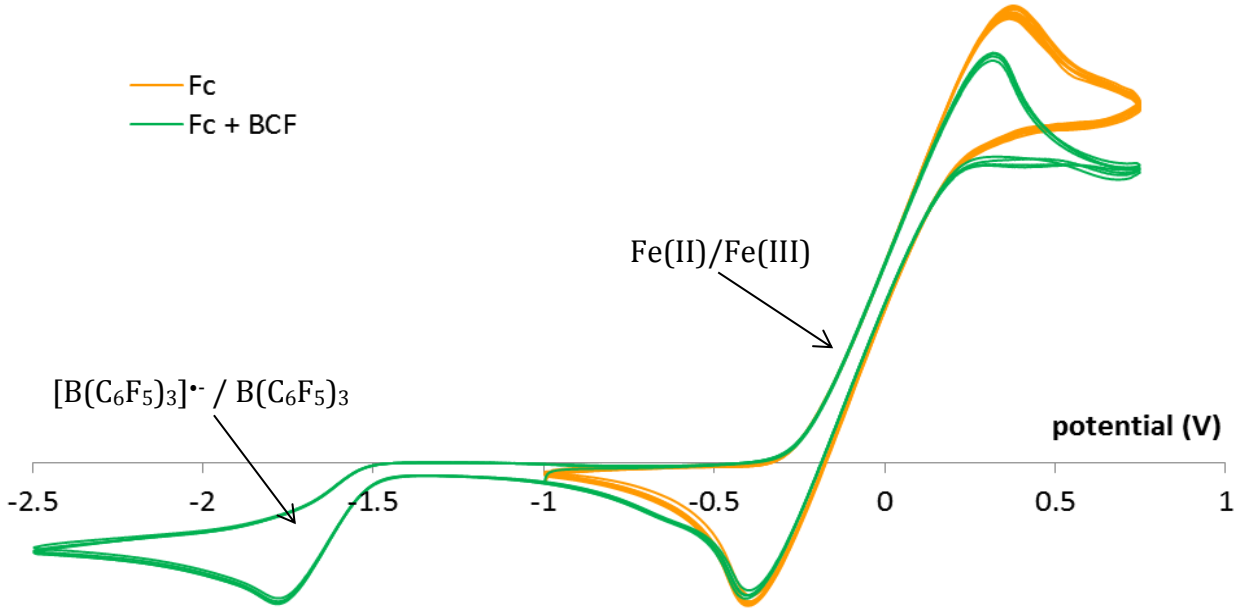

Figure 5.19: Cyclic voltammograms of ferrocene (*orange curves*) with and without tris-(pentafluorobenzene) borane (*green curves*) with 0.1 M [^{n}Bu$_4$N][B(C$_6$F$_5$)$_4$] as a supporting electrolyte in dichloromethane (scan rate 0.1 V s^{-1}) referenced *vs* ferrocene/ferrocenium.

From these results an alternative hypothesis can be envisioned for the formation of a peroxo adduct starting from ferrocene and B(C$_6$F$_5$)$_3$ (Figure 5.20). Starting with a two-body process, in which the oxygen and B(C$_6$F$_5$)$_3$ are in close contact to form {B(C$_6$F$_5$)$_3$·O$_2$}, a one-electron transfer then follows from the ferrocene reductant to the bound dioxygen. In accordance with the postulate of Qu *et al.*, the newly generated superoxide adduct, [B(C$_6$F$_5$)$_3$·O$_2$]$^{-\bullet}$, rapidly disproportionates into dioxygen gas and a peroxo dianion capped at both ends by a B(C$_6$F$_5$)$_3$ molecule (Figure 5.20).[44] The initial electron transfer step would be thermodynamically unfavourable but the overall reaction would be downhill due to the formation of the B—O bonds within the peroxoborate unit.

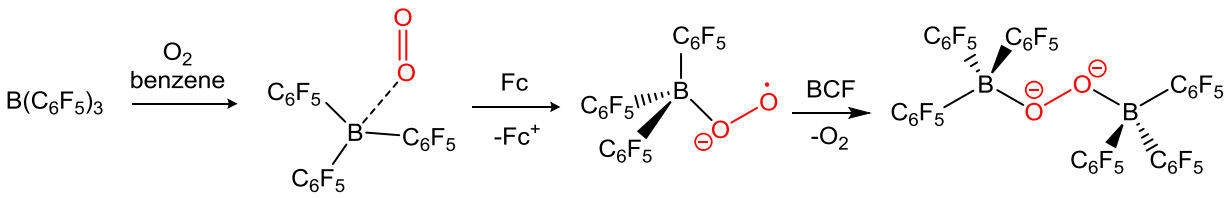

Figure 5.20: Proposed mechanism for the formation of **XIa**.

In the scheme presented above it seems likely that the limiting step is the transfer of an electron to the dioxygen/Lewis acid pair. In order to assess the influence of the Lewis acid on the rate of the reaction, different boranes were tested with varying strength of Lewis acidity: $B(C_6F_5)_3$, $MesB(C_6F_5)_2$, $Mes_2B(C_6F_5)$ and $BMes_3$.

The two weakest acids, $Mes_2B(C_6F_5)$ and $BMes_3$ in presence of ferrocene and dioxygen, did not yield any colour change or new products observable by ^{11}B or ^{19}F NMR spectroscopy; $MesB(C_6F_5)_2$, however, showed more promising results. The consumption of $MesB(C_6F_5)_2$ is much slower compared to the $B(C_6F_5)_3$/ferrocene/O_2 reaction under anhydrous conditions. ^{11}B NMR spectroscopy shows, at δ_B = -3 ppm, the presence of a small amount of what is thought to be the peroxoborate product $[(MesB(C_6F_5)_2)_2(\mu_2\text{-}O_2)]^{2-}$ after at least an hour after introduction of the oxygen into the vessel, and an extra 36 hours were necessary for the complete consumption of the starting materials. Since $MesB(C_6F_5)_2$ is a weaker Lewis acid than $B(C_6F_5)_3$ this could lead to a transition state higher in energy for the formation of the postulated superoxide adduct $[MesB(C_6F_5)_2\ O_2]^{-\bullet}$ thus slowing down the reduction process. However, attempts to isolate this peroxo adduct intact met little success, instead products resulting from the scrambling of the aryl substituents were obtained, as showed by the negative ion mass spectrometry results (Figure 5.21).

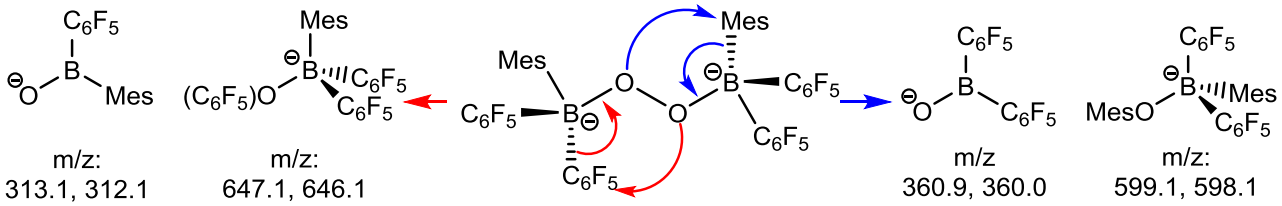

Figure 5.21: Proposed decomposition mechanism of by aryl substituent scrambling.

In addition, several other reductants were investigated in combination with $B(C_6F_5)_3$, in order to target a fully characterized (NMR, X-ray and Raman) peroxo adduct. The reducing agents listed in Table 5.2 were tested and all of them demonstrated activity; although it was

not always possible to definitely identify the products derived from the initial activation of oxygen.

Reductant	E^0 *vs.* SCE (V)	Solvent
$FeCp_2$	0.42	CH_2Cl_2
	0.38	MeCN
TMPD	0.37	CH_2Cl_2
TTF	0.12	CH_2Cl_2
$FeCp^*_2$	-0.012	DMF
	-0.105	CH_2Cl_2
$CoCp_2$	-0.86	DME
$CoCp^*_2$	-1.39	DMF

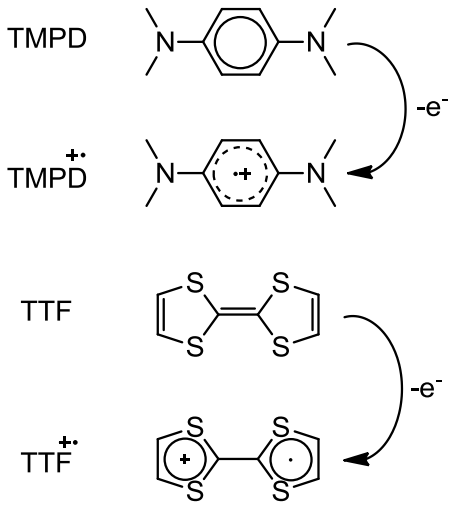

Table 5.2: (*left*) Formal redox potentials of different metallocenes[45] and organic reducing agents;[46] (*right*) one-electron oxidation reaction of TMPD and TTF.

From the metallocene family, the main focus was on cobaltocene ($CoCp_2$). Introduction of oxygen-saturated thf to a mixture of $Cp_2Co/B(C_6F_5)_3$ yielded the cobaltocenium peroxo adduct (**XIc**), as shown by the *in situ* ^1H NMR spectrum which shows only one sharp peak at δ_H = 5.67 ppm, an ^{11}B signal with an upfield shift at δ_B -25 ppm, and a positive ion mass spectrum which features the envelope of peaks for $CoCp_2^+$ (m/z : 188.9685).

The usual freeze-pump-thaw process for the introduction of O_2 was disregarded to limit the formation of the side product $CpCo(C_5H_4B(C_6F_5)_3)$ (**XII**) which results from the direct reaction of Cp_2Co and $B(C_6F_5)_3$. Electron transfer from cobalt is implied by the presence of a cobaltocenium type fragment within zwitterionic $CpCo(C_5H_4B(C_6F_5)_3)$, and while an anionic borate also results, the formation of **XII** is clearly a more complex process involving C—H activation in addition to simple electron transfer. The ^1H NMR spectrum of **XII** shows the expected pattern of signals for the substituted cyclopentadienyl ring; the sharp signal at δ_B -15 ppm in the ^{11}B NMR spectrum is also consistent with a borate product and the overall structure is confirmed by single X-ray crystallography (Figure 5.22). The redox pair

decamethylcobaltocene/$B(C_6F_5)_3$ was also examined in an attempt to circumvent the formation of **XII**, but it was revealed to be too unstable, rapidly evolving to $CoCp_2^{*+}$ and the unstable radical anion $B(C_6F_5)_3^{-\bullet}$.[39b]

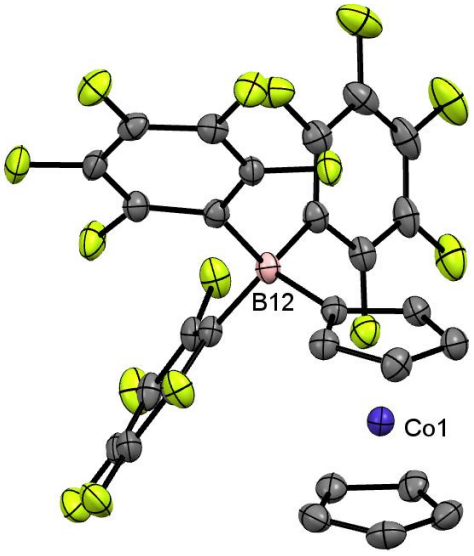

Figure 5.22: Molecular structure of **XII** with ORTEP ellipsoids set at the 50% probability level and hydrogen atoms omitted for clarity (light pink: boron, yellow: fluoride; black: carbon; dark blue: cobalt). Selected bond lengths [Å] and angles [°]:B12—C13 1.658(3), B12—C24 1.662(3), B12—C35 1.654(3), B12—C7 1.668(3), C7—B12—C13 105.88(15), C7—B12—C24 111.84(16), C13—B12—C24 109.12(14), C7—B12—C35 106.36(14), C13—B12—C35 112.40(16), C24—B12—C35 111.12(15).

Usefully, however, the photo-physical properties of **XIc** prove to be much more compatible with Raman studies (λ_{max} = 410 nm, logε = 4.10) than to the related ferrocenium species. Spectra measured for a thf solution (Figure 5.23, blue curve), feature a band at 843 cm^{-1} attributed to the ν(O—O) stretching vibration; this value is close to that of hydrogen peroxide in the same solvent (ν = 886 cm^{-1}; Figure 5.23). Furthermore, this band is in the same region as other main group peroxo adducts such as perborate ($[B_2(O_2)_2(OH)_4]^{2-}$, ν(O—O) = 883 cm^{-1}),[47], peroxodisulfate ($[S_2O_8]^{2-}$, ν(O—O) = 890 cm^{-1})[48] and peroxodiphosphate ($[P_2O_8]^{4-}$, ν(O—O) = 842 cm^{-1}).[49] In the solid-state Raman spectrum the ν(O—O) stretching band of **XIc** can be found at 840 cm^{-1} after excitation with a 1064 nm laser (Figure 5.24).

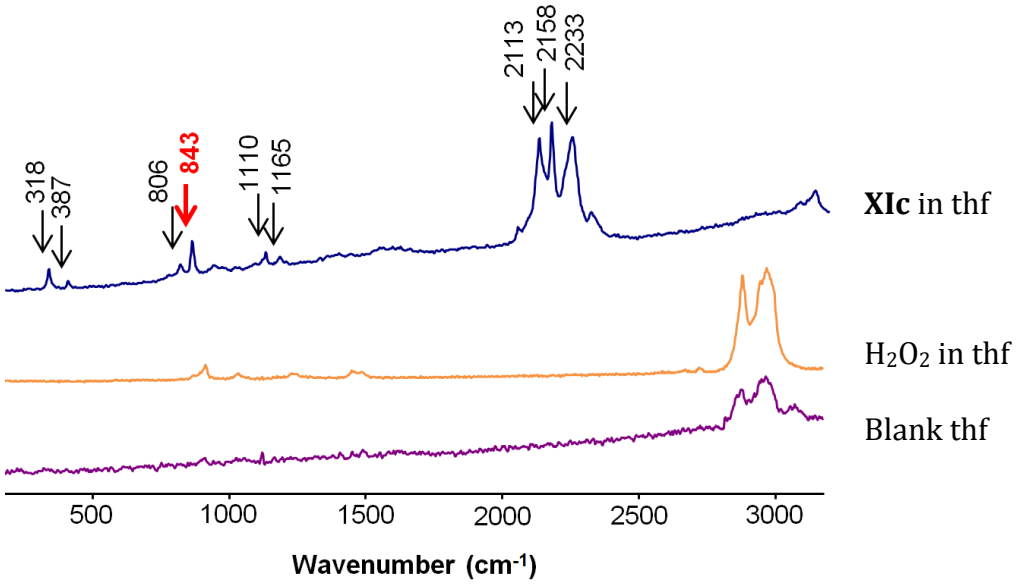

Figure 5.23: resonance Raman spectrum of **XIc**, hydrogen peroxide and blank thf after excitation with a 514 nm laser.

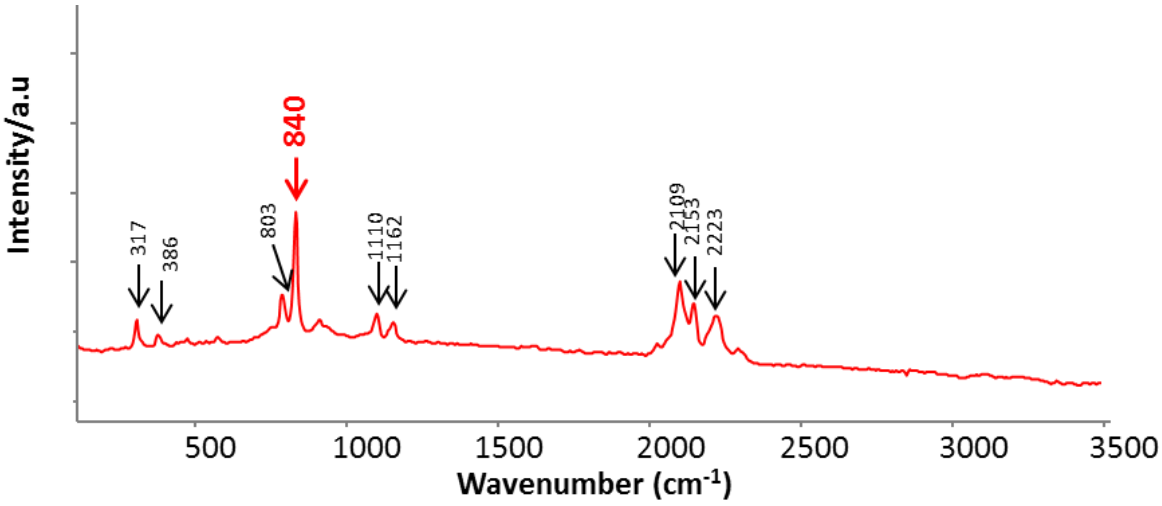

Figure 5.24: solid-state resonance Raman spectrum of **XIc** after excitation with a 1064 nm laser.

In order to assess the stability of the peroxoborate **XIc**, a sample was heated in thf at 60° C for a week and another sample in dichloromethane was subjected to radiation for 6 hours (Hg UV lamp). Both samples were monitored by ^{11}B and ^{19}F NMR spectroscopy. It appears that neither mild heat nor UV-irradiation affects the integrity of this species. Thus, **XII** is clearly not a by-product of the decomposition of the peroxoborate **XIc** (Figure 5.25), and it

seems most likely that these two species are formed *via* parallel reaction pathways, with or without the capture of the oxygen containing product.

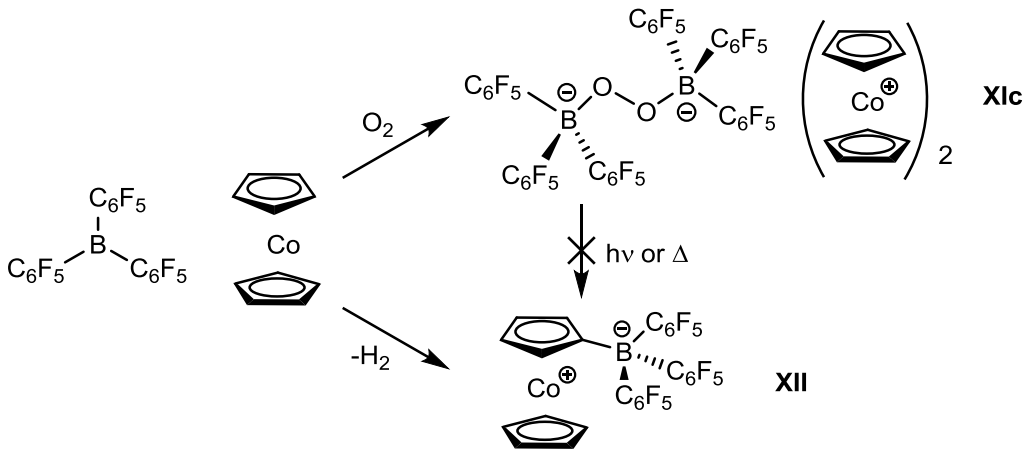

Figure 5.25: competitive reaction pathways for the formation of **XIc** and **XII**.

Organic reductants such as *N,N,N′,N′*-tetramethyl-*p*-phenylenediamine (TMPD, E^0 = 0.37 V *vs* SCE) and tetrathiafulvalene (TTF, E^0 = 0.12 V *vs* SCE) were also tested, targeting *metal-free* activation of molecular oxygen. In isolation, both TMPD and TTF are unaffected by the presence of dioxygen over a period of 24 hours, as deduced by ^{1}H NMR spectroscopy. The same observation was made with TMPD or TTF in the presence of $B(C_6F_5)_3$. However when the organic reductants and $B(C_6F_5)_3$ were placed in contact with dioxygen, the pale yellow solutions turn to intense orange with TTF (λ_{max} = 617 nm, logε = 4.0) or blue with TMPD (λ_{max} = 440 nm, logε = 4.2, Figure 5.26). The ^{11}B NMR spectra of both reaction mixtures exhibit a sharp resonance at δ_B -4 ppm consistent with the formation of a borate species.

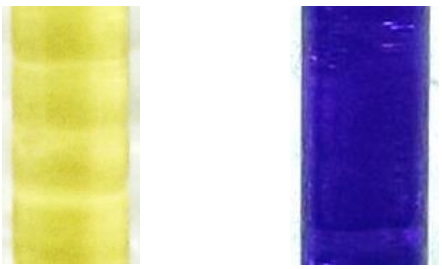

Figure 5.26: Colour change from $B(C_6F_5)_3$/TMPD on addition of O_2.

Single crystals of the targeted peroxoborate remained elusive, although evidence for the transient formation of O_2^{2-} bridge at least can be seen *via* through the solvation of the decomposition products [TTF][**XIII**] and [TMPD][**XIII**] presumably *via* a ligand scrambling process such as that highlighted in Figure 5.27.

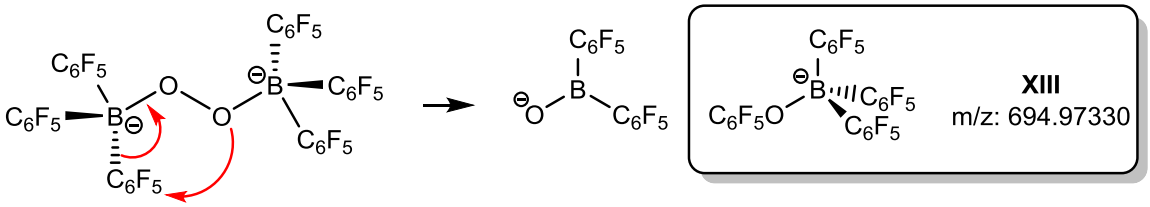

Figure 5.27: Aryl substituent scrambling mechanism for the formation of **XIII**$^-$.

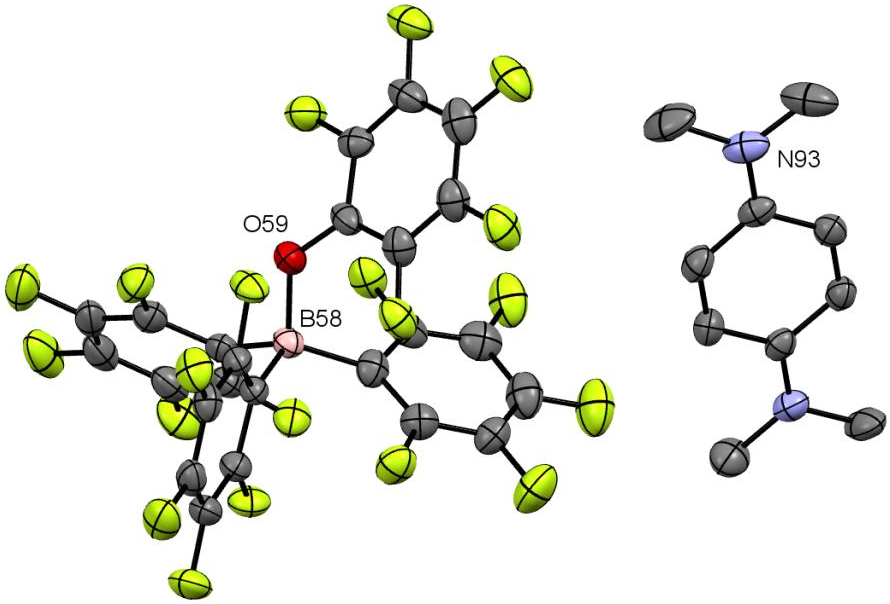

Figure 5.28: Molecular structure of [TMPD][**XIII**]. Thermal ellipsoids set at the 50% probability level; hydrogen atoms are omitted for clarity (light pink: boron, yellow: fluoride; black: carbon; red: oxygen, blue: nitrogen).

The crystal structures of [TMPD][**XIII**] (Figure 5.28) and [TTF][**XIII**] (Figure 5.29), both feature the tris-(pentafluorobenzene)(perfluorophenoxy)borate (**XIII**) with the corresponding radical cation $TMPD^{+\bullet}$ or $TTF^{+\bullet}$ as a counterion, and exhibit no extraordinary geometric features.

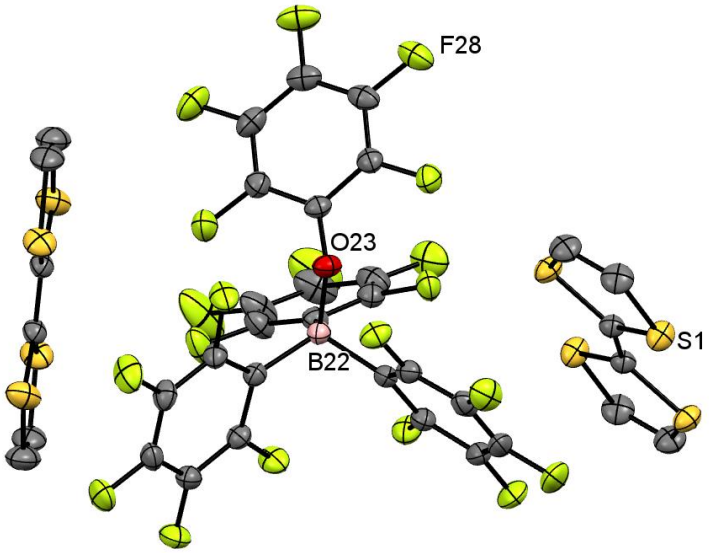

Figure 5.29: Molecular structure of [TTF][**XIII**]·TTF. Thermal ellipsoids set at the 50% probability level; hydrogen atoms are omitted for clarity (light pink: boron, yellow: fluoride; black: carbon; red: oxygen, gold: sulfur).

5.5. Conclusions

The highly Lewis acidic ferrocenylborane $FcB(C_6F_5)_2$ (**129**) has been used for the reduction of molecular oxygen to the peroxide $(FcB(C_6F_5)_2)_2(\mu_2\text{-}O_2)$ (**X**). The formation of a O_2^{2-} unit can be confirmed by X-ray crystallography and supported by DFT calculations with the accompanying ferrocenium centres being characterized by EPR spectroscopy.

The scope for the formation of related peroxides was probed *via* the reactions of chemically separate metallocenes/aryl boranes with dioxygen. Further investigation of the electronic effects of $B(C_6F_5)_3$ on the reduction potential of O_2 point towards the possible formation of a close contact pair between the Lewis acid and the dioxygen before one electron transfer from the ferrocene. The dismutation of the resulting superoxide borate into dioxygen and peroxide then could generate the observed peroxo borate following literature precedent.

A series of cobaltocenium derivatives were made in order to characterize the O_2^{2-} unit by Raman spectroscopy, and a ν(O—O) stretching vibration could be identified at 886 cm-1 in thf solution. Efforts to isolate a "metal-free" peroxoborate were attempted, with organic

reductants such as tetramethyl-*p*-phenylenediamine and tetrathiafulvalene being used, although only decomposition products of the target molecule could be isolated in these cases.

5.6. References

(1) L.J. Thenard, *Ann. Chim. Phys.*, **1818**, 8, 306.

(2) *Soyuz CSG User's Manual*, Arianespace, **June 2006**.

(3) Information retrieved from manufacturer websites: Akzo Nobel Pulp and Performance Chemicals, Arkema, Chang Chun Petrochemical Co., Evonik Industries AG, Hansol Chemicals.

(4) *Hydrogen Peroxide: A Global Strategic Business Report*, Global Industry Analysts Inc., **May 2014**.

(5) C. W. Jones, "*Applications of Hydrogen peroxide and derivatives*", RSC Clean technology monographs, Cambridge, UK, **1999**.

(6) Rust Frederick, "*Manufacture of hydrogen peroxide*", US 2871104 A, **27th January 1959**, Shell Development Corp.

(7) G. L. Semenza, *Science* **2007**, 318, 62.

(8) Z. Rappoport, J. F. Liebman, I. Marek and A. Greer, "*The chemistry of peroxides vol. 3*", Wiley & Sons, London, **2014**.

(9) H. Dau, C. Limberg, T. Reier, M. Risch, S. Roggan and P. Strasser, *Chem. Cat. Chem.* **2010**, 2, 724.

(10) L. M. Mirica, X. Ottenwaelder and T. D. P. Stack, *Chem. Rev.* **2004**, 114, 1013.

(11) S. Ferguson-Miller and G. T. Badcock, *Chem. Rev.* **1996**, 96, 2889.

(12) A. Albini and M. Fagnoni, "*Handbook of Synthetic Photochemistry*", chapter 11, Wiley-VCH Verlag, **2010**.

(13) (*a*) M. Selke and C. S. Foote, *J. Am. Chem. Soc.* **1993**, 115, 1166. (*b*) M. Selke, L. Rosenberg, J. L. Salvo and C. S. Foote, *Inorg. Chem.* **1995**, 34, 5715.

(14) K. Qin, C. D. Incarvito, A. L. Rheingold and K. H. Theopold, *Angew. Chem. Int. Ed.* **2002**, 41, 2333.

(15) J. Cho, R. Sarangi and W. Nam, *Acc. Chem. Res.* **2012**, 45, 1321

(16) (*a*) M. Sook Seo, J. Young Kim, J. Annaraj, Y. Kim, Y.-M. Lee, S.-J. Kim, J. Kim and W. Nam, *Angew. Chem. Int. Ed.* **2007**, 46, 377. (*b*) J. Annaraj, J. Cho, Y.-M. Lee, S. Yeon Kim, R. Latifi, S. P. de Visser and W. Nam, *Angew. Chem. Int. Ed.* **2009**, 48, 4150.

(17) J. Cho, S. Jeon, S. A. Wilson, L. V. Liu, E. A. Kang, J. J. Braymer, M. Hee Lim, B. Hedman, K. O. Hodgson, J. S. Valentine, E. I. Solomon and W. Nam, *Nature*, **2011**, 478, 502.

(18) J. Cho, R. Sarangi, H. Yeon Kang, J. Yoon Lee, M. Kubo, T. Ogura, E. I. Solomon and W. Nam, *J. Am. Chem. Soc.* **2010**, 132, 16977.

(19) (*a*) J. Cho, R Sarangi, J Annaraj, S Yeon Kim, M Kubo, T Ogura, E I. Solomon and W Nam, *Nat. Chem.* **2009**, 1, 568. (*b*) J. Cho, H. Yeon Kang, L. V. Liu, R. Sarangi, E. I. Solomon and W. Nam, *Chem. Sci.* **2013**, 4, 1502.

(20) M. Armand, J.-M. Tarascon, N. Recham, S. Grugeon, S. Laruelle and S. Devaraj, "*Boron or aluminium complexes*", WO 2009/122044 A2, **8th October 2009**.

(21) G. Girishkumar, B. McCloskey, A. C. Luntz, S. Swanson and W. Wilcke, *J. Phys. Chem. Lett.* **2010**, 1, 2193.

(22) S. Aldridge and A. J. Downs, "*the group 13 metals aluminium, gallium, indium and thallium*", John Wiley & Sons, Chichester, **2011**.

(23) M. B. Power, W. M. Cleaver, A. W. Apblett and W. R. Barron, *Polyhedron* **1992**, 4, 477.

(24) W. M. Cleaver and A. R. Barron, *J. Am. Chem. Soc.* **1989**, 111, 8967.

(25) T. K. Wood, W. E. Piers, B. A. Keay and M. Parvez, *Angew. Chem. Int. Ed.* **2009**, 48, 4009.

(26) (*a*) G. C. Welch and D. W. Stephan, *J. Am. Chem. Soc.* **2007**, 129, 1880. (*b*) G. C. Welch, R. R. S. Juan, J. D. Masuda and D. W. Stephan, *Science* **2006**, 314, 1124. (*c*) Review on FLP's: D. W. Stephan and G. Erker, *Angew. Chem. Int. Ed.* **2010**, 49, 46.

(27) H. C. Brown, H. I. Schlesinger and S. Z. Cardon, *J. Am. Chem. Soc.* **1942**, 64, 325

(28) (*a*) G. Ménard and D. W. Stephan, *J. Am. Chem. Soc.* **2010**, 132, 1796. (*b*) J. M. Farrell, J. A. Hatnean and D. W. Stephan, *J. Am. Chem. Soc.* **2012**, 134, 15728.

(29) (*a*) R. C. Neu, E. Otten, A. Lough and D. W. Stephan, *Chem. Sci.* **2011**, 2, 170. (*b*) G. Ménard, J. A. Hatnean, H. J. Cowley, A. J. Lough, J. A. Rawson and D. W. Stephan, *J. Am. Chem. Soc.* **2013**, 135, 6446.

(30) E. Otten, R. C. Neu and D. W. Stephan, *J. Am. Chem. Soc.* **2009**, 131, 9918.

(31) M. J. Kelly, J. Gilbert, R. Tirfoin, and S. Aldridge, *Angew. Chem. Int. Ed.* **2013**, 52, 14094.

(32) S. Porcel, G. Bouhadir, N. Saffon, L. Maron and D. Bourissou, *Angew. Chem. Int. Ed.* **2010**, 49, 6186.

(33) B. E. Carpenter, W. E. Piers, M. Parvez, G. P. A. Yap and S. J. Rettig, *Can. J. Chem.* **2001**, 79, 857.

(34) T. Renk, W. Ruf and W. Siebert, *J. Organomet. Chem*. **1976**, 120, 1.

(35) P. Zanello, A. Cinquantini, S. Mangani and G. Opromolla, L. Pardi, C. Janiak, M. D. Rausch, *J. Organomet. Chem.* **1994**, 471, 171.

(36) J. C. Gallucci, G. Opromolla, L. A. Paquette, L. Pardit, P. F. T. Schirch, M. R. Sivik, and P. Zanello, *Inorg. Chem.* **1993**, 32, 2292.

(37) A. V. Soudackov and K. Jug, *Int. J. Quant. Chem.* **1997**, 62, 403.

(38) R. J. Kwaan, C. J. Harlan and J. R. Norton, *Organometallics* **2001**, 20, 3818.

(39) (*a*) D. L. Maricle and W. G. Hodgson, *Anal. Chem.* **1965**, 37, 1562. (*b*) A. E. Ashley, T. J. Herrington, G. G. Wildgoose, H. Zaher, A. L. Thompson, N. H. Rees, T. Krämer and D. O'Hare, *J. Am. Chem. Soc.* **2011**, 133, 14727.

(40) J. T. Henthorn and T. Agapie, *Angew. Chem. Int. Ed.* **2014**, 53, 12893.

(41) W. L. Jolly, "*The Synthesis and Characterization of Inorganic Compounds*", Prentice-Hall, Englewood Cliffs (NJ), **1970**, p 487.

(42) T. E. Bitterwolf and A. C. Ling, *J. Organomet. Chem*. **1972**, 140, C29.

(43) D. Seong Choi, D. Hyun Kim, U. Sang Shin, R. R. Deshmukh, S.-g. Leeb and C. Eui Song, *Chem. Commun.* **2007**, 3467.

(44) D. Zheng, Q. Wang, H.-S. Lee, X.-Q. Yang and D. Qu, *Chem. Eur. J.* **2013**, 19, 8679.

(45) J. Ruiz Aranzaes, M.-C. Daniel and D. Astruc, *Can. J. Chem.* **2006**, 84: 288.

(46) S. V. Rosokha and J. K. Kochi, *J. Am. Chem. Soc.* **2007**, 129, 3683.

(47) J. Flanagan, W. P. Griffith, R. D. Powell and A. P. West, *Spectrochimica Acta* **1989**, 45A, 951.

(48) H. H. Eysel and G. Rosinger, *J. Raman Spectrosc.* **1987**, 18, 123.

(49) W. P. Griffith, R. D. Powell and A. C. Skapski, *Polyhedron* **1988**, 7, 1305.